THESIS

ELECTRONIC DENSITY OF STATES AND MAGNETIC PROPERTIES OF TRANSITION METAL ALLOYS

JUN-ICHIRO INOUE

Department of Applied Physics,

Nagoya University

1977

Contents

Chapter I. Introduction

The magnetic and thermal properties of transition metals have been well described by the itinerant electron model, i.e., the band model.[1,2] These properties of transition metals are closely connected with the electronic structure of d-electrons. The band-width of d-bands is rather narrow so that the exchange interaction among d-electrons is relatively large as compared to the kinetic energy. This exchange interaction is phenomenologically treated as an uniform molecular field in the band model. A microscopic foundation of this model has been given by the Hubbard Hamiltonian[3] represented by the sum of the kinetic energy and the intra-atomic Coulomb interaction which is treated in the Hartree-Fock approximation.

As for the magnetic transition metal alloys, there are two main theoretical approaches. One is the study for a metallic system with one magnetic impuriy by Friedel,[4] Anderson[5] and Wolff[6] using the Hartree-Fock approximation and the other is that for concentrated alloys using the band model and the rigid band approximation[7] which assumes that the band structure does not change by alloying. In the band model, the magnetic and thermal properties of transition metals and their alloys depend strongly on their density of states. Shimizu and co-workers[8] obtained an empirical density of states for transition metals and their alloys from the low temperature specific heat data by the rigid band approximation and theoretically studied the temperature and concentration dependences of their magnetic and thermal properties such as

the paramagnetic susceptibility, the magnetic moment and the specific heat in the band model using the rigid band approximation.

On the other hand, the electronic structure of a random system has been one of the important problems in statistical physics and has been studied extensively. Recently, an useful approximation called the coherent potential approximation (CPA)[9-14] was established within the single site approximation to calculate the density of states for alloys which contain random δ-function type potential at atomic sites. This approximation satisfies mathematical demands such as a sum rule and analyticity and gives satisfactory results in the dilute limit and atomic limit and well describes the concentration variation of the density of states for alloys. In addition, the local density of states for each constituent atom can be calculated by this approximation. Several calculations of the density of states for alloys have been carried out using this approximation.[14] These calculated results show that the density of states for alloys with a large random potential is greatly distorted as compared to that of the pure metal and depends on the concentration of the alloy.

The generalization of CPA has been developed in two directions. One is to include the effect of clusters[15,16] and the other is to include off-diagonal randomness.[17-19] In the former case, the calculated results for the density of states of one-dimensional alloys when the effect of clusters is taken into account show a fine structure which does not exist in that of pure metals and in the calculated densities

of states by the single site approximation. In the latter case, the transfer integrals between atomic sites depend on the atomic species at each site and are also random. The calculated results with off-diagonal randomness show that the density of states for alloys depends on the value of the transfer integrals.

In transition metal alloys, the atomic potentials differ from site to site and are relatively large as compared to the band-width. Furthermore the transfer integrals depend on the species of the constituent atoms because the band-widths of the transition metals are different from each other. Therefore, the density of states for the random alloy constituted from transition metals is expected to be much different from that of the pure transition metal. Consequently, to study the magnetic and thermal properties of transition metal alloys, it is necessary to know about their density of states itself. CPA instead of the rigid band approximation (which neglects the concentration variation of the density of states) is very useful and is a reasonable approximation to calculate the density of states of a realistic random alloy.

Several applications of CPA with diagonal randomness to transition metal alloys[20-24] have been carried out and the magnetic properties of these alloys have been studied by using a model with the Hubbard Hamiltonian and the Hartree-Fock approximation.[25-27] In this model, the exchange interaction varies from site to site and the magnetic moments for each constituent atom can be calculated. Furthermore, the dilute limit of this model gives the same results as those

obtained by the Wolff[6] and Anderson models.[5] These points are also an important improvement when compared to the rigid band approximation.

One of the purposes of this thesis is to calculate the density of states of transition metal alloys and to study the magnetic properties at 0 K and the thermal properties, i.e., the concentration dependences of the magnetic moment, paramagnetic susceptibility and low temperature specific heat coefficient, by using CPA and the Hartree-Fock approximation. In this study, special attention is paid to alloys which contain Ni atoms and show the transition between ferromagnetic and paramagnetic states at 0 K. The numerical calculations are carried out for Fe-Ni, Ni-Cu, Ni-Pd, Ni-Pt and Pd-Pt alloys. Another purpose is to study the temperature and concentration dependences of the spin susceptibility and electrical resistivity for paramagnetic V-Cr, Nb-Mo, Ta-W and Ni-Pt alloys.

The density of states and magnetic properties for Fe-Ni alloys have been calculated by Hasegawa and Kanamori[25] for both paramagnetic and ferromagnetic states. In their calculation, however, a simple shape is made use of as the density of states of the host band. In chapter II, a realistic density of states for Ni obtained by a band calculation is used as the density of states of the host band and the densities of states of fcc Fe-Ni alloys in the paramagnetic and ferromagnetic states are calculated. The average and local magnetic moments at 0 K and the low temperature specific heat coefficient are calculated from the calculated densities of states and these results are compared with experiment. The calculated

results of the magnetic moments and the low temperature specific heat coefficient agree well with experiment and are almost the same as those of Hasegawa and Kanamori.[25] It is found that these physical quantities are not so sensitive to the detailed structure of the density of states except near the Fermi level.

The same method as that used for Fe-Ni alloys in chapter II is used to calculate the density of states for ferromagnetic Ni-Cu alloys in chapter III. A simplified density of states for the host metal is used for simplicity of numerical calculation. The expression for the high-field spin susceptibility is obtained and its concentration dependence is calculated at 0 K. The values of the magnetic moments and the low temperature specific heat coefficient are also calculated. It is shown that these calculated results agree qualitatively with experiment except near the critical concentration where the ferromagnetism disappears. The origin of ferromagnetism in Ni-Cu alloys is discussed.

For Fe-Ni and Ni-Cu alloys, only the diagonal randomness which is the difference of potentials at each atomic site is taken into account. The off-diagonal randomness, i.e., the difference of the transfer integral between constituent atoms in an alloy is not so important as compared to the diagonal randomness in these alloys. However, it is necessary to include the off-diagonal randomness for alloys in which constituent atoms belong to the same column in the periodic table. Therefore, the densities of states for ferromagnetic or paramagnetic Ni-Pd, Ni-Pt and Pd-Pt alloys are calculated

by taking account of both the diagonal and off-diagonal randomnesses in chapter IV. The expression for the paramagnetic spin susceptibility generalized for alloys with off-diagonal randomness is obtained and its numerical values are calculated for these alloys. The concentration dependence of the magnetic moments and the low temperature specific heat coefficient are calculated and it is shown that the results are consistent with experiment.

In chapter V, the density of states for paramagnetic V-Cr, Nb-Mo and Ta-W alloys are calculated in CPA by making use of the densities of states for Cr, Nb and W which are obtained by the band calculation. The concentration variation of the temperature dependences of the paramagnetic spin susceptibility and the electrical resistivity is calculated and qualitative agreement with experiment is obtained. It is also shown that an enhancement of spin susceptibility due to exchange interactions should be taken into account for Cr rich V-Cr alloys.

The temperature variation of the paramagnetic spin susceptibility for Ni-Pt alloys is calculated in chapter VI. The densities of states for these alloys are calculated in CPA with off-diagonal randomness. In this calculation the exchange interaction between electrons is treated as a uniform molecular field. The calculated results are compared with experiment. In chapter VII, summary and conclusion of this thesis are given.

Chapter II. Density of States for FCC Fe-Ni Alloys

§1. Introduction

Experimental relation between magnetic moments and electron numbers per atom for ferromagnetic transition metal alloys at 0 K is represented by the well-known Slater-Pauling curve. Local magnetic moments for each constituent atom in alloys have been also measured by the neutron diffraction experiments. It is known from the Slater-Pauling curve that the saturation moment of fcc Fe-Ni alloys decreases rapidly near 70 at.% Fe. This is due to a first order transition and was explained by Shimizu and Hirooka[29] in the rigid band approximation by comparing the free energies in the ferromagnetic and paramagnetic states. However, the local moments of the Ni or Fe atoms cannot be discussed and the concentration variation of the densities of states cannot be taken into account in the rigid band approximation. These points can be improved by calculations using the coherent potential approximation (CPA).

CPA was first introduced to treat the excitation spectrum, for example the electronic density of states or the phonon spectrum etc., of disordered alloys by Soven,[9] Taylor,[10] Onodera and Toyozawa,[11] Yonezawa[12] and Leath.[13] A detailed explanation of CPA for a tight-binding model was given by Velicky et al.[14] Many applications to transition metal alloys have been carried out, e. g., calculations of the electronic density of states for paramagnetic Ni-Cu alloys by Kirkpatrick et al.[20], Stocks et al.[21] and Yamashita et al.[23], studies of magnetic properties of ferromagnetic transiton metal

alloys containing Ni or Fe atoms by Hasegawa and Kanamori[25] and for Ni-Cu alloys by Brouers and Vedyayev[26] and calculations of the paramagnetic spin susceptibility for Pt-Pd, Rh-Pd, Ni-Rh and Ni-Pd alloys by Levin et al.[27]

Hasegawa and Kanomori[25] calculated the concentration dependence of the density of states, average and local magnetic moments, the low temperature specific heat coefficient and the Curie temperature for Fe-Ni alloys in CPA and the Hartree-Fock approximation by use of a one band model with the Hubbard Hamiltonian. They obtained good agreement with experiment except the concentration dependence of the Curie temperature and the value of the local moments at Fe site for Ni rich Fe-Ni alloys.

They made use of a simple shape of the density of states for Ni as the host band. However, there are many calculations of the density of states for Ni. Therefore, we calculate the densities of states for the paramagnetic and ferromagnetic fcc Fe-Ni alloys making use of the realistic density of states for Ni calculated by Zornberg[29] and study the ferromagnetic properties of these alloys in this chapter. The model and formulation are explained in §2 and the calculated results are shown and compared with experiment in §3. Discussion and conclusion for the density of states and the magnetic properties of fcc Fe-Ni alloys are given in §4.

§2. Model and Formulation

The electronic structure of transition metals is complicated as the s- and d-bands are mixed with each other. However, in this calculation, only the d-bands are considered because the magnetic moment is almost carried by d-electrons. Furthermore the degeneracy of the d-bands is neglected in this study. The Hubbard Hamiltonian of a one band model is assumed and is given as follows, in the Wannier representation.

$$H = \sum_{i\sigma} \varepsilon_i a^+_{i\sigma} a_{i\sigma} + \sum_{ij\sigma} t_{ij} a^+_{i\sigma} a_{j\sigma} + \sum_i U_i a^+_{i+} a^+_{i+} a_{i-} a_{i-}, \qquad (2\text{-}1)$$

where $a^+_{i\sigma}$ or $a_{i\sigma}$ is a creation or annihilation operater of an electron with spin σ at i site. The value of σ is denoted as + or - according as the electron has a majority or minority spin. The ε_i is a δ-function type potential at i site, t_{ij} is a transfer integral between i and j sites and U_i is an intra-atomic Coulomb integral at i site, respectively. Appling the Hartree-Fock approximation to the last term in eq. (2-1), the Hamiltonian is written as,

$$H = \sum_{i\sigma} \varepsilon_{i\sigma} a^+_{i\sigma} a_{i\sigma} + \sum_{ij\sigma} t_{ij} a^+_{i\sigma} a_{j\sigma}, \qquad (2\text{-}2)$$

where

$$\varepsilon_{i\sigma} = \varepsilon_i + U_i n_{i-\sigma}. \qquad (2\text{-}3)$$

Here, $n_{i-\sigma}$ is the average number of d-electrons with spin $-\sigma$ at i site. For A-B alloys, the values of ε_i, U_i and $n_{i\sigma}$

are assumed to have one of two values, ε_A or ε_B, U_A or U_B and $n_{A\sigma}$ or $n_{B\sigma}$, respectively. The value of t_{ij} is assumed not to be changed by alloying in this chapter.

In CPA, a random alloy is considered as a one impurity system in a coherent potential Σ which will be determined self-consistently as a function of energy by an appropriate condition.[9,14] The value of Σ is spin dependent for ferromagnetic alloys and is denoted as Σ_σ. An effective Green's function for electrons with spin σ in ferromagnetic alloys was given by Velicky et al.[14] as,

$$G_\sigma(z) = N^{-1}\sum_k \{z - \varepsilon(k) - \Sigma_\sigma(z)\}^{-1} \tag{2-4}$$

$$= \int_{-\infty}^{\infty} \rho^o(\varepsilon)\{z - \varepsilon - \Sigma_\sigma(z)\}^{-1} d\varepsilon \tag{2-5}$$

where $\varepsilon(k)$ is the Fourier transform of t_{ij}, $z=E+i0$, $\rho^o(\varepsilon)$ is the paramagnetic density of states of a host metal whose energy-momentum relation is given by the $\varepsilon(k)$. The Green's function with spin σ at the atomic site i which is considered as one impurity in a coherent potential Σ_σ is given by

$$G_{i\sigma}(z) = G_\sigma(z)[1 - \{\varepsilon_{i\sigma} - \Sigma_\sigma(z)\}G_\sigma(z)]^{-1}, \quad i=A \text{ or } B. \tag{2-6}$$

The Σ_σ is determined by the following equation,

$$G_\sigma(z) = c_A G_{A\sigma}(z) + c_B G_{B\sigma}(z), \tag{2-7}$$

where c_A and c_B are the concentrations of A and B atoms, respectively. The eq. (2-7) is rewritten as,

$$\Sigma_\sigma(z) = c_A\varepsilon_{A\sigma} + c_B\varepsilon_{B\sigma} + \{\varepsilon_{A\sigma} - \Sigma_\sigma(z)\}G_\sigma(z) \times \{\varepsilon_{B\sigma} - \Sigma_\sigma(z)\}. \quad (2\text{-}8)$$

The values of $G_\sigma(z)$ and $\Sigma_\sigma(z)$ are obtained by solving eqs. (2-5) and (2-7) or (2-8) self-consistently. Details of the numerical calculation are shown in the Appendix.

The local and average densities of states of an alloy are given by

$$\rho_{i\sigma}(E) = -\pi^{-1}\mathrm{Im}\, G_{i\sigma}(E+i0), \quad i=A \text{ or } B, \quad (2\text{-}9)$$

$$\rho_\sigma(E) = c_A\rho_{A\sigma}(E) + c_B\rho_{B\sigma}(E). \quad (2\text{-}10)$$

In the paramagnetic states, $\rho_{i+}(E)=\rho_{i-}(E)=\rho_i(E)$ and $\rho_+(E)=\rho_-(E)=\rho(E)$. The local and average numbers of d-electrons with spin σ are given by

$$n_{i\sigma} = \int_{-\infty}^{\infty}\rho_{i\sigma}(E)f(E-\zeta)dE, \quad i=A \text{ or } B, \quad (2\text{-}11)$$

$$n_\sigma = c_A n_{A\sigma} + c_B n_{B\sigma}, \quad (2\text{-}12)$$

where $f(E-\zeta)$ is the Fermi distribution function and ζ is a chemical potential which is determined from the total number of d-electrons. The values of $n_{A\sigma}$ and $n_{B\sigma}$ are obtained by

solving eqs. (2-4)-(2-11) self-consistently. For ferromagnetic alloys, the local and average magnetic moments (μ_B per atom), m_i and m, are given by

$$m_i = n_{i+} - n_{i-}, \qquad i=A \text{ or } B, \tag{2-13}$$

$$m = c_A m_A + c_B m_B, \tag{2-14}$$

respectively. The low temperature specific heat coefficient γ is obtained from the value of the average density of states at the Fermi level as,

$$\gamma = \frac{1}{3}\pi^2 k_B^2 \{\rho_+(\zeta) + \rho_-(\zeta)\}, \tag{2-15}$$

where k_B is the Boltzmann constant. In the preceding formulation, A and B denote Fe and Ni, respectively.

The density of states for fcc Ni calculated by Zornberg[29] is used as that of the host metal. The broad s-band is subtracted from the whole density of states and its remaining part is shown in Fig. 2. Here and hereafter in this chapter the integrated number of states is normalized as 1 and the scale of the energy is reduced so that the band-width of Ni which is 5.08 eV equals to 2.

The number of d-holes in Ni is determined as 0.6 per atom from the fact that its saturation moment is about 0.6 μ_B per atom and that of fcc Fe is determined as 2.8 per atom because the exterpolated value to Fe of the saturation moment of fcc Fe-Ni alloys in the Slater-Pauling curve is about 2.8 μ_B per

atom. Parameters in the present calculations are $\delta_o=\varepsilon_{Fe}-\varepsilon_{Ni}$, U_{Fe} and U_{Ni}. The value of δ_o is determined as 0.603 so that the value of δ defined by

$$\delta = \delta_o + U_{Fe}n^o_{Fe} - U_{Ni}n^o_{Ni} \qquad (2\text{-}16)$$

becomes 0.317 which is the energy difference between the Fermi levels of Ni and Fe. Here $n^o_{Fe}=0.72$ and $n^o_{Ni}=0.94$ are the numbers of d-electrons per atom per spin of the paramagnetic Fe and Ni, respectively, in the one band model. The values of U_{Ni} and U_{Fe} are assumed to be the same U for simplicity and determined as U=1.3 so as to get a good agreement between the calculated and experimental values of the average magnetic moment.

§3. Calculated Results for FCC Fe-Ni Alloys

3-1 Density of states in the paramagnetic state

At first, by neglecting the Coulomb interaction terms in eqs. (2-3) and (2-16), the density of states for paramagnetic fcc Fe-Ni alloys is calculated. The value of δ is 0.317, which equals to δ_o. The calculated results are shown in Figs. 3-11. In the calculated results the density of states is smoothened as a whole and the peaks are flattened because of the imaginary part of the self-energy. This tendency is large for concentrated Fe-Ni alloys. The concentration variation of the shape of the peak at the top of the band is not symmetric with respect to the concentration of Fe and Ni atoms. This peak is most flattened for 30 at.% Fe-Ni alloy but it remains rather clearly in the Fe rich

alloys. As the value of δ_o is positive, Fe atoms contribute to the density of states in the high energy region. Therefore, the density of states increases in the high energy region and the upper peak is flattened with increasing Fe concentration as shown in Figs. 3 and 4. The Fermi level (denoted by a vertical line) moves to the lower energy region with increasing Fe concentration, i.e., on decreasing the total number of electrons.

3-2 Density of states in the ferromagnetic state

The density of states for ferromagnetic fcc Fe-Ni alloys is calculated by using the formulation and parameters explained in §2. The values of the parameters δ_o and U are 0.603 and 1.3, respectively. The numbers of electrons of each spin at each atomic site are calculated self-consistently. The calculated results of the density of states for ferromagnetic Fe-Ni alloys are shown in Figs. 12-21. The alloys with Fe concentration from 0 to 55 at.% are in the saturated ferromagnetic state. The number of electrons of each spin at each atomic site does not converge for ferromagnetic alloys with the concentration larger than 70 at.% Fe. This result seems to correspond to the fact that the ferromagnetic state becomes unstable around this concentration and the paramagnetic state becomes stable. This transition is considered to be a first order transition.[28] It is seen from Figs. 12-21 that the band-width of the minority spin band is broad and the density of states is smoothened but the density of states of the majority spin band is almost the same as that

of the host band. The reason is as follows. The value of $\delta_\sigma=\varepsilon_{Fe\sigma}-\varepsilon_{Ni\sigma}$ is large (about 0.6 for minority spin band) because $U_{Fe}=U_{Ni}$ and the values of n_{Fe+} and n_{Ni+} are nearly 1.0. However, δ_+ is nearly 0 because the value of $U(n_{Fe-}-n_{Ni-})$ cancels the value of δ_o. Another feature is the splitting of the minority spin band in the high energy region because of the large value of δ_-. In the sub-band which is splitted from the main band, the local density of states for the Fe atom is very large and this corresponds to a localized state at the Fe site.

3-3 Number of electrons

The calculated results of the number of electrons for each atom and for each spin are shown in Fig. 22. The numbers of electrons n_{Fe+}, n_{Ni-} and n_+ are 1 for alloys with the Fe concentration varying from 0 to 55 at.% because they are in the saturated ferromagnetic state. Above 55 at.% Fe, their values begin to decrease a little because the alloys are in the weak ferromagnetic state. The value of n_{Ni-} is larger than that of n_{Fe-}. This is due to the fact that the value of $\rho_{Ni-}(E)$ is larger in the low energy region than in the high energy region but that of $\rho_{Fe-}(E)$ is larger in the high energy region than in the low energy region because the atomic level of Ni is lower than that of Fe.

The value of n_{Fe-} increases with increasing Fe concentration but that of n_{Ni-} almost does not vary with the concentration. This fact is explained as follows. The value of $\rho_{Fe-}(E)$ is especially large for small Fe concentration in

the high energy region where the Fermi level is located and is rapidly decreases with increasing Fe concentration, but the value of $\rho_{Ni-}(E)$ is rather small in this region and does not vary so much with the concentration.

3-4 Magnetic moments

The calculated and experimental results of the average and local magnetic moments are shown in Fig. 23. The numerical values of these calculated results are shown in Table I. The calculated result for the average moment is $5\times(2.0-1.44\times c_{Fe}-1.88\times c_{Ni})$ μ_B per atom for saturated ferromagnetic alloys and agrees with the Slater-Pauling curve. In the weak ferromagnetic state, as the value of n_+ begins to decrease, the calculated result for m begins to deviate from the Slater-Pauling curve.

The calculated results for m_{Ni} agree well with experiment,[30,31] but those for m_{Fe} are slightly larger than the experimental values in the low Fe concentration. If charge neutrality is demanded, the value of m_{Fe} should become 2.8 μ_B per atom but the calculated result is larger than that. This is because the value of $\rho_{Fe-}(E)$ is large in the high energy region as mentioned above. It has been shown that this disagreement at $c_{Fe}\simeq 0.1$ is improved a little by taking into account the degeneracy of the d-band.[25]

3-5 Low temperature specific heat coefficient

The low temperature specific heat coefficient γ is obtained from eq. (2-15). The calculated and experimental[32]

results are shown in Fig. 24. The numerical values of the calculated results for γ are shown in Table I. The concentration variation of the calculated results agrees qualitatively with that of experiment, although the experimental values are 1.5-2.0 times as large as the calculated results because the electron-phonon enhancement is neglected in the calculation. The value of γ is large for Fe dilute alloys because the Fermi level locates at the peak of the density of states. With increasing Fe concentration, the value of γ decreases because the $\rho_{-}(E)$ is smoothened by a large random potential. The rapid increase of γ at higher concentration than 55 at.% Fe is due to the fact that the Fermi level begins to touch the majority spin band.

§4. Discussion and Conclusion

The present calculated results for the density of states and the magnetic moments differ very little from those obtained by Hasegawa and Kanamori[25] using a simple shape of the density of states as that of the host metal. This is because only the shape of the density of states near the Fermi level contributes to the electronic properties in alloys and the fine structure is smoothed by the random potential.

In the single site approximation, the potential at one site is treated exactly and the other atomic potentials are replaced by a coherent potential. Therefore, the configuration of the surrounding atoms is neglected. If the effect of the surrounding atoms on the density of states or on the magnetic properties is large, the single site approximation

cannot be applied. However, as the local magnetic moments in Fe-Ni alloys obtained experimentally do not change much with concentration, the neglection of the fluctuation of the random potential may be a good approximation.

In the calculation presented in this chapter, the difference between the band-widths of Ni and Fe is neglected. This may not be realistic. Some improvements[17-19] of this point have been carried out and its application to magnetic alloys is treated in chapter IV.

The instability of the ferromagnetic state can be understood as the electrons with majority spin can easily transfer to the state of minority spin because the Fermi level locates near the upper edge of the majority spin band. However, it could not be made clear at which concentration this instability occurs, because of an ambiguity in the numerical calculation.

There is an explanation that the rapid increase of the value of γ with increasing Fe concentration around 55 at.% Fe is due to a spin fluctuation. However, this explanation is not so clear at present because it has not been clarified whether the transition from the ferromagnetic state is to the paramagnetic or antiferromagnetic state.

The charge neutrality condition is not satisfied in the ferromagnetic state. This is due to the neglection of the screening among electrons. It may be necessary to include the screening effect to satisfy charge neutrality and this is a problem to be investigated.

In conclusion, the observed results for the concentration

variations of the magnetic moments at 0 K and of γ for fcc Fe-Ni alloys are in good agreement with the calculated results in CPA and in the Hartree-Fock approximation and this fact justifies the calculated densities of states for these alloys. However, the magnetic properties around the concentration where the ferromagnetism disappears has not been clarified by the present calculations.

Chapter III. Ferromagnetic Properties of Ni-Cu Alloys

§1. Introduction

The magnetic moment of ferromagnetic Ni-Cu alloys decreases linearly from the value of 0.606 μ_B per atom for pure Ni with increasing Cu concentration. It begins to deviate from linearity at about 40 at.% Cu and goes to zero at about 60 at.% Cu.[33] Local magnetic moments have also been measured by neutron diffraction experiments.[34-36] From these experimental results it was shown that Cu atoms do not have local magnetic moments, only the Ni atoms have magnetic moments and there exists spatially uniform negative polarization. The concentration variation of magnetic moments for ferromagnetic Ni-Cu alloys have been discussed by many people[36-38] in the Jaccarino-Walker model.[39] In Ni-Cu alloys, the low temperature specific heat coefficient γ shows a peak around the critical concentration where the ferromagnetism disappears. To explain this fact there are two models, i.e., one is due to the cluster effect and the other is due to the paramagnon effect. According to the experimental results obtained for the low temperature specific heat by Gupta et al.[40] and for the magnetic properties by Robbins et al.[41], the former effect is important, Measurements of high-field susceptibility by Acher and Huguenin[42] also showed that the cluster effect is large around the critical concentration.

Shimizu and Hirooka[28] calculated the Curie temperature, high-field spin susceptibility and bulk magnetic moment for ferromagnetic Ni-Cu alloys in the rigid band model. They

made use of the empirical density of states curve determined from the low temperature specific heat data for Ni alloys. Their calculated results agreed well with the observed ones for Ni-Cu alloys.

Recently, however, an electronic structure of random system has been extensively studied by the coherent potential approximation (CPA).[9,14] For paramagnetic Ni-Cu alloys, Kirkpatrick et al.[20] and Stocks et al.[21] calculated the density of states using that of pure Ni or pure Cu obtained from their band calculations. Their calculated results were consistent with the experimental results of photo-emission, soft X-ray experiments and measurements of γ for paramagnetic Ni-Cu alloys. For Ni rich ferromagnetic Ni-Cu alloys, Brouers and Vedyayev[26] calculated the bulk magnetic moment in a simple two band model by CPA, but they did not calculate local quantities. Using CPA and the Hartree-Fock approximation for electron interaction, Hasegawa and Kanamori[25] calculated the density of states, low temperature specific heat coefficient γ and local moments for many ferromagnetic Fe and Ni alloys except Ni-Cu alloys.

In this chapter the density of states for ferromagnetic Ni-Cu alloys is calculated by CPA and the magnetic properties of these alloys are studied by the same method as that of Hasegawa and Kanamori.[25] Furthermore, the high-field spin susceptibility is calculated in CPA for ferromagnetic Ni-Cu alloys. The concentration where the high-field spin susceptibility diverges is determined as the critical concentration. From the calculated density of states the bulk and

local magnetic moments and γ are calculated for ferromagnetic Ni-Cu alloys including the region of critical concentration. The cluster effect which is large near the critical concentration may be small for Ni rich Ni-Cu alloys. Therefore, it is meaningful to apply CPA to the Ni rich Ni-Cu alloys, as CPA is a single site approximation. The difference between band structures of Ni and Cu metals and also cluster effects are neglected in this chapter. Moreover, the degeneracy of the d-bands is neglected and whole density of states of the d- and s-bands is treated as one band.

Recently, an investigation similar to this chapter was reported by Ghosh and Bhattacharyya.[43] They made use of the density of states calculated by Callaway and Wang[44] for pure Ni and subtracted from it the contribution due to conduction electrons assuming one d-hole per atom. However, their calculated results for magnetic moments did not explain the experimental results well and the values of magnetic moments near the critical concentration are not clear in their calculations. In addition they did not discuss the high-field spin susceptibility.

In §2, the formulation and parameters used in this chapter are explained. In §3, high-field spin susceptibility at 0 K is calculated. In §4, the calculated results are shown and compared with experiment. In §5, discussion and conclusion of this chapter are given.

§2. Model for Ni-Cu Alloys

In ferromagnetic Ni-Cu alloys, magnetic moments are carried by almost d-like electrons. However, the conduction band cannot be ignored, because the contribution to high-field spin susceptibility from conduction electrons is large. The whole density of states for d- and s-bands of Ni is treated as one band.

The one-electron Hamiltonian H with the Hartree-Fock approximation for Coulomb interactions is given in the Wannier representation as follows,

$$H = \sum_{i\sigma} (\varepsilon_i + U_i n_{i-\sigma}) a^+_{i\sigma} a_{i\sigma} + \sum_{ij\sigma} t_{ij} a^+_{i\sigma} a_{j\sigma}, \qquad (3\text{-}1)$$

where all notations are the same as those in eq. (2-1).

The formulation for CPA has been already explained in §2, chap. II. The local and the average densities of states for Ni-Cu alloys are calculated by eqs. (2-9) and (2-10), respectively. The number of electrons for each atom and for each spin is calculated from eq. (2-11). The local and the average magnetic moments are given by eqs. (2-13) and (2-14), respectively. The low temperature specific heat coefficient is given by eq. (2-15). In this chapter A and B denote Ni and Cu atoms, respectively.

The calculated density of states by Wakoh and Yamashita[45] for paramagnetic Ni, which is shown in Fig. 25, is made use of as the density of states for the host Ni metal, as our calculation is carried out for Ni rich alloys.

The intra-atomic Coulomb integrals for Ni and Cu atoms

are assumed to be equal to U. The value of U is determined as 0.635 eV so that the ferromagnetic Ni has a magnetic moment of 0.557 μ_B per atom. The value of U may be too large for Cu atoms, but it makes Cu still paramagnetic because of the small value of the density of states at the Fermi level. The value of the Bohr magneton number of Ni is determined from the observed magnetic moment by considering the g-factor.[46] The position of the Fermi level of the majority spin band for ferromagnetic Ni is determined so that it becomes higher than the upper edge of the d-band by 0.04 eV.[47]

The $\varepsilon_A-\varepsilon_B$ is the difference between potentials at Ni and Cu atoms. In order to exclude the term due to Coulomb interaction from the ε_A and ε_B for pure metals in the Hartree-Fock approximation, we define the difference between the potentials at the Ni and Cu atoms as $\varepsilon_A-\varepsilon_B+(n_B^\circ-n_A^\circ)U\equiv\delta$, where n_A° and n_B° are the number of electrons per atom per spin for paramagnetic Ni and Cu, respectively. The value of δ is determined as 2.353 eV so as to find the critical concentration at 53 at.% Cu. From the values of δ and U determined above, the value of $\varepsilon_A-\varepsilon_B$ becomes 2.040 eV which is similar to the value of 1.822 eV obtained in the band calculation by Stocks et al.[21] and used for their calculation of the density of states for paramagnetic Ni-Cu alloys.

§3. High-Field Spin Susceptibility

Uniform static paramagnetic spin susceptibility for alloys has been calculated by Hasegawa and Kanamori[25] and Levin et al.[27] Their formulation is generalized to ferromagnetic alloys.

When an external field h is applied, the Zeeman energy is added to the Hamiltonian (3-1) and the local Green's function $G_{i\sigma}(Z)$ given in eq. (2-6), the number of electron for each atom and each spin $n_{i\sigma}$ given in eq. (2-11), and the Fermi distribution function f become dependent on h. The average spin susceptibility χ_s is defined by

$$\chi_s = c_A\chi_A + c_B\chi_B \tag{3-2}$$

with

$$\chi_i = \mu_B\{\partial n_{i+}(h)/\partial h - \partial n_{i-}(h)/\partial h\}_{h\to 0}, \quad i=A \text{ or } B, \tag{3-3}$$

$$n_{i\sigma}(h) = \int_{-\infty}^{\infty} dE f(E-\zeta(h)-\sigma\mu_B h)\rho_{i\sigma}(E,h) \tag{3-4}$$

where μ_B is a Bohr magneton and $\zeta(h)$ is a chemical potential under h. The $\partial n_{i\sigma}(h)/\partial h$ at 0 K in the limit of h=0 is obtained as follows,

$$\frac{\partial n_{i\sigma}}{\partial h} = \rho_{i\sigma}(\zeta)\{\frac{\partial\zeta(h)}{h} + \sigma\mu_B\} + f_\sigma^{ii}U\frac{\partial n_{i-\sigma}}{\partial h} + f_\sigma^{ij}U\frac{\partial n_{j-\sigma}}{\partial h}, \tag{3-5}$$

where ζ is the chemical potential without h and i or j means A or B. The term $\lim_{h\to 0}\{\partial n_{i\sigma}(h)/\partial h\}$ is expressed as $\partial n_{i\sigma}/\partial h$ for abbreviation. The f_σ^{ij}'s in eq. (3-5), which are the same expression as that given by Levin et al.[27] for para-

magnetic alloys, are written as

$$f_\sigma^{ij} = -\pi^{-1}\mathrm{Im}\int_{-\infty}^{\infty} dE\ f(E-\zeta)\{1-(\varepsilon_{i\sigma}-\Sigma_\sigma)G_\sigma\}^{-2}$$

$$\times \frac{\partial G_\sigma}{\partial \Sigma_\sigma}\frac{\partial \Sigma_\sigma}{\partial \varepsilon_{j\sigma}} + G^2(\delta_{ij} - \frac{\partial \Sigma_\sigma}{\partial \varepsilon_{j\sigma}})\} \qquad (3\text{-}6)$$

with

$$\frac{\partial G_\sigma}{\partial \Sigma_\sigma} = \int_{-\infty}^{\infty} d\varepsilon \rho^{o}(\varepsilon)(E+i0-\Sigma_\sigma-\varepsilon)^{-2} \qquad (3\text{-}7)$$

and

$$\partial\Sigma_\sigma/\partial\varepsilon_{i\sigma} = \{c_i - G_\sigma(\varepsilon_{j\sigma}-\Sigma_\sigma)\}\{1-(\varepsilon_{i\sigma}+\varepsilon_{j\sigma}-2\Sigma_\sigma)G_\sigma$$

$$+ (\varepsilon_{i\sigma}-\Sigma_\sigma)(\varepsilon_{j\sigma}-\Sigma_\sigma)\partial G_\sigma/\partial\Sigma_\sigma\}^{-1}. \qquad (3\text{-}8)$$

The energy dependence of G_σ and Σ_σ are omitted in eqs. (3-6), (3-7) and (3-8) for abbreviation. The $\partial\zeta(h)/\partial h$ is given in the limit of h=0 by

$$\partial\zeta(h)/\partial h = -\rho_F^{-1}[\mu_B\{\rho_+(\zeta)-\rho_-(\zeta)\} + c_A(Q_{A+} + Q_{A-})$$

$$+ c_B(Q_{B+} + Q_{B-})] \qquad (3\text{-}9)$$

where

$$Q_{i\sigma} = f_\sigma^{ii}U\partial n_{i-\sigma}/\partial h + f_\sigma^{ij}U\partial n_{j-\sigma}/\partial h \qquad (3\text{-}10)$$

$$\rho_\sigma(E) = c_A\rho_{A\sigma}(E) + c_B\rho_{B\sigma}(E) \tag{3-11}$$

$$\rho_F = \rho_+(\zeta) + \rho_-(\zeta). \tag{3-12}$$

From eqs. (3-5), (3-9) and (3-10), four simultaneous equations for $\partial n_{i\sigma}/\partial h$ (i=A and B and $\sigma=\pm1$) are obtained as follows,

$$(\rho_{i\sigma}R_{i-\sigma}U+\rho_F)\partial n_{i\sigma}/\partial h + (\rho_{i\sigma}R_{i\sigma}-\rho_F f_\sigma^{ii})U\partial n_{i-\sigma}/\partial h$$

$$+ \rho_{i\sigma}R_{j-\sigma}U\partial n_{j\sigma}/\partial h + (\rho_{i\sigma}R_{j\sigma}-\rho_F f_\sigma^{ij})U\partial n_{j-\sigma}/\partial h$$

$$= \sigma\mu_B\rho_{i\sigma}\rho_{-\sigma} \tag{3-13}$$

with

$$R_{i\sigma} = c_i f_\sigma^{ii} + c_j f_\sigma^{ji}$$

for j=B when i=A and j=A when i=B, where $\rho_{i\sigma}$ and ρ_σ are the values of the local and average densities of states with spin σ at the Fermi level, respectively. The values of $\partial n_{i\sigma}/\partial h$'s are obtained numerically from eq. (3-13) and χ_s and χ_i are calculated from eqs. (3-2) and (3-3). In the paramagnetic state eq. (3-13) coincides with the formulae obtained by Hasegawa and Kanamori[25] and Levin et at.[27]

§4. Calculated Results and Comparison with Experiment

4-1 Density of states

The electronic density of states for ferromagnetic Ni-Cu alloys with 90, 80, 70, 65, 60, 55 and 50 at.% Ni are calculated and the results are shown in Figs. 26-32. The density of states for paramagnetic Ni-Cu alloys with 47, 45, 40, 35, 30 and 20 at.% Ni are also calculated and these results are shown in Figs. 33-38. In Figs. 26-38, curves 1 is the average density of states for each spin and curves 2 and 3 are the local densities of states of Ni and Cu atoms. The important feature of the density of states for Ni $\rho_{Ni\sigma}(E)$ is the existence of a peak at the Fermi level. This peak remains in the average density of states $\rho_{\sigma}(E)$ for Ni rich alloys. However, this peak is flattened at large Cu concentration and it almost disappears at 50 at.% Cu. This result is due to a large value of δ for electrons of both spins.

The $\rho_{\sigma}(E)$ at high energy is almost completely contributed to by Ni atoms and the one at low energy is contributed to by Cu atoms because of the large value of δ. The local density of states of Cu atoms $\rho_{Cu\sigma}(E)$ is very different from the density of states of the host metal at all concentrations, but $\rho_{Ni\sigma}(E)$ always shows a peak similar to that of pure Ni. The fact that the Fermi level occurs in the neighbourhood of the peak in $\rho_{Ni\sigma}(E)$ is considered as the origin of the ferromagnetism in Ni-Cu alloys, even if the corresponding peak in $\rho_{\sigma}(E)$ is flattened. The $\rho_{Cu\sigma}(E)$ at the Fermi level is very small and Cu atoms do not contribute to the magnetic moment and γ. As the Cu concentration increases, the density

of states near the upper edge of the d-band is smoothened by the conduction band.

4-2 Magnetic moment

The observed magnetic moment mg/2 of pure Ni is 0.606 Bohr magneton per atom and the g-factor is 2.18.[46] Then the observed value of m for pure Ni is 0.557 μ_B per atom. As the magnetic moment of Cu atom is almost zero as shown below, the value of the g-factor for Ni-Cu alloys is assumed to be the same as that of pure Ni.[46]

The calculated results for mg/2 for Ni-Cu alloys are shown in Fig. 39 with the experimental results.[33-36] The numerical values of the calculated results for magnetic moment are shown in Table II. The calculated value of the average magnetic moment decreases almost linearly until 50 at.% Cu with increasing Cu concentration as shown by curve 1 in Fig. 39. This agrees with experiment but the rate of decrease of the calculated result is slightly smaller than the observed one. Near the critical concentration, the calculated magnetic moment decreases rapidly and this is different from the observed results. This difference may be due to the cluster effect which has not been taken into account sufficiently in CPA.

As shown by curves 2 and 3 in Fig. 39, the calculated value of the local magnetic moment of Ni atoms is large and that of Cu atoms is almost zero. This result is explained by the calculated results of the local density of states $\rho_{i\sigma}(E)$ as mentioned above. The experimental value of the local magnetic moment is the sum of the magnetic moment localized

at each atom and the spatially uniform negative polarization. The calculated values of the local magnetic moment of Ni atoms agree with the experimental values.[34-36] The experimental values of the local magnetic moment of Cu atom are negative and are about -0.1 μ_B per atom.[34-36] These values were determined from the assumption that Cu atoms have no localized moment and they have only spatially uniform negative polarization. Mook[48] also concluded by neutron diffraction experiment that a uniform negative polarization exists in Ni. This negative polarization could not be obtained in our calculation because it is impossible to distinguish the fairly localized moment and the uniform negative polarization in a one band model.

4-3 Low temperature specific heat coefficient

Low temperature specific heat coefficient γ can be estimated from the value of the density of states at the Fermi level by eq. (2-15). The calculated result of γ is shown in Fig. 40. The numerical values of the calculated results for γ are shown in Table II. The value of γ obtained by Wakoh and Yamashita[45] for ferromagnetic Ni is 14.1×10^{-4} cal/mol deg^2. For ferromagnetic alloys, the calculated value of γ decreases almost linearly with increasing Cu concentration. This is explained in the following way. First, the peak of $\rho_{\downarrow}(E)$ in the neighbourhood of the Fermi level is flattened as the Cu concentration increases. The peak remains clearly in the 90 at.% Ni alloy as shown in Fig. 26, but it almost disappears in the 50 at.% Ni alloy as shown in Fig. 32. Secondly, the Fermi level moves to the region of low density

of states as the average number of electrons per atom increases with increasing Cu concentration. The contribution from the majority (up) spin band to γ is small, although it increases a little with increasing Cu concentration. The density of states at the Fermi level of minority (down) spin band decreases rapidly and as a whole γ decreases with increasing Cu concentration.

The observed values of γ[41,49,50] for ferromagnetic alloys are larger than the calculated ones, but they decrease almost linearly until 35 at.% Cu and this qualitatively coincides with the calculated results as shown in Fig. 40. The difference between the observed and calculated values of γ will be explained by the enhancement due to electron-phonon interactions. The observed values of γ show a broad peak around the critical concentration. This anomaly may be explained by the cluster effect or paramagnon effect. At present we cannot assert which effect is correct. The calculated values of γ for paramagnetic Ni-Cu alloys are also shown in Fig. 40, but they are larger than the experimental values for concentrations lower than 40 at.% Ni.

Curve 2 in Fig. 40 shows the values of γ calculated by making use of the calculated density of states of Zornberg[29] for Ni and by neglecting the part of the density of states due to the conduction band. This result apparently shows a concentration dependence of γ similar to the observed one near the critical concentration. This is explained by the fact that Ni rich alloys are in the saturated ferromagnetic state below 35 at.% Cu and become weakly ferromagnetic above

35 at.% Cu and so the value of the density of states at the Fermi level of the majority (up) spin band increases with increasing Cu concentration until the critical concentration. However this result is not correct because the large effect of s-d hybridization in a real transition metal is neglected in this case.

Curve 3 in Fig. 40 is the calculated result by Stocks et al.[21] for paramagnetic Ni-Cu alloys and it roughly agrees with experiment for Cu rich alloys, but their result cannot be compared with the observed concentration dependence of γ for ferromagnetic Ni rich alloys.

4-4 High-field spin susceptibility

The calculated result of the high-field spin susceptibility χ_s at 0 K and in the limit of h=0 is shown in Fig. 41 together with the experimental results.[42,51-53] The numerical values of the calculated results for χ_s are shown in Table II. The value of δ is determined above so that χ_s diverges at 53 at.% Cu. The broken curve is the result calculated in the rigid band model by Shimizu and Hirooka[28] using an empirical density of states obtained from low temperature specific heat data for Ni alloys. Experimental values in Fig. 41 are the sum of spin and orbital susceptibilities.

For pure Ni, χ_s is estimated as 0.748×10^{-4} emu/mol from the density of states calculated by Wakoh and Yamashita.[45] The orbital susceptibility for Ni was estimated as 0.232×10^{-4} emu/mol by Hirooka and Shimizu.[54] Therefore, the total susceptibility is 0.980×10^{-4} emu/mol and this agrees reasonably with the observed values of 1.13×10^{-4} emu/mol by Foner et at.[51]

and 1.11×10^{-4} emu/mol by Acher and Huguenin.[42] The calculated result of Hirooka and Shimizu[54] was 1.04×10^{-4} emu/mol. The experimental values are smaller than the calculated values near the critical concentration as shown in Fig. 41, because of the high magnetic field applied in the experiments. Therefore, the agreement between the calculated and observed results is not so unsatisfactory.

§5. Discussion and Conclusion

The value of the difference between potentials at Ni and Cu atoms δ used in this chapter is large and consequently Ni atoms contribute to the density of states in the high energy region and Cu atoms contribute to it in the low energy region. The peak in $\rho_{Ni\sigma}(E)$ remains even when the corresponding peak in $\rho_{\sigma}(E)$ disappears in concentrated alloys. Then the ferromagnetism in concentrated alloys is maintained by the peak in $\rho_{Ni\sigma}(E)$ and the magnetic moment is carried almost completely by the Ni atoms. It is seen that the local electronic structure is important in determining the magnetic properties of Ni-Cu alloys. The calculated values of γ decrease linearly with increasing Cu concentration because of the smoothing of the peak in $\rho_{\sigma}(E)$.

In the calculated results by Ghosh and Bhattacharyya[43] for the density of states for ferromagnetic Ni-Cu alloy with 50 at.% Cu, the Fermi level is located at the position where the density of states is very low. On the contrary, in our calculation, as shown in §4, the Fermi level is located in the d-band. Their calculated result for the concentration vari-

ation of the average number of d-electrons per atom in the majority spin band shows a minimum, while in our calculation it changes monotonically with Cu concentration. Their calculated results for the magnetic moments did not agree with experiment.

For paramagnetic Ni-Cu alloys the calculated values of γ are larger than the experimental ones as shown in Fig. 40. This is because the mixing between d- and s-bands is overestimated in our one band model, so that the value of the density of states at the Fermi level is large. In real transition metals, the d-electrons transfer to the s-band through the s-d hybridization and vice versa, but in the one band model, s- and d-electrons similarly transfer to the same band. It will be necessary to treat the s-d hybridization correctly in the calculation of the density of states for paramagnetic Ni-Cu alloys.

Lang and Ehrenreich[55] proposed the minimum polarity model and Kirkpatrick et al.[56] applied it to ferromagnetic Ni-Cu alloys. They assumed that each local density of states for an alloy is the same as the density of states of pure metal and postulated charge neutrality. For Ni-Cu alloys they assumed that the density of states at the Fermi level is contributed to only by Ni atoms and that the states due to Cu occur far below the Fermi level. Their model is qualitatively consistent with the calculated results by CPA. However, it may be a shortcoming that their model does not include the energy and concentration dependences of the local density of states which are important in calculating the

magnetic moment and χ_s of alloys. In the present results, the numbers of electrons per atom at each atomic site of Ni and Cu are about 9.95 and 11.47 at 10 at.% Cu and 9.61 and 11.39 at 50 at.% Cu, respectively. Then the charge neutrality at each site is not satisfied in the present calculations. This result may be due to neglecting the screening of the impurity potential in these alloys.

The disagreement between the calculated and experimental results for m, γ and χ_s near the critical concentration will be due to the clustering of atoms and spin fluctuations. It may be considered that the Hartree-Fock approximation is not appropriate to take into account spin fluctuations near the critical concentration. The spatially uniform negative polarization, which are found in neutron diffraction experiments for ferromagnetic Ni-Cu alloys, could not be explained by the simple model in this chapter. It will require a more precise model and complicated calculations.

Finally, it is concluded that the magnetic properties of ferromagnetic Ni-Cu alloys are qualitatively explained by the density of states obtained by CPA with a large value of δ except in the critical region.

Chapter IV. Magnetic Properties of Ni-Pd, Ni-Pt and Pd-Pt Alloys

§1. Introduction

The electronic structure of random systems has been extensively studied by the coherent potential approximation (CPA)[9-14] which has also been applied to study the magnetic properties of alloys of transition metals.[25-27] The generalization of CPA has been carried out in two directions. One is to take account of clusters, and the other is to include the off-diagonal randomness. As for the former many studies were carried out.[15,16] The latter was developed by Blackman et al.[17] and Shiba[18] within the single site approximation.

In usual calculations in CPA only diagonal randomness is taken into account and the band structures of the component metals in an alloy are assumed to be the same. However, actually the band structures of pure metals are different from each other and this difference is important for alloys of elements which are in the same column in the periodic table. For example, according to the band calculation, the band-width of Pt is about 1.8 times as large as that of Ni. This accounts for the difference between the values of the density of states at the Fermi level, although these metals have nearly the same number of d-electrons.

Calculations of the magnetic properties of binary alloys among Ni, Pd and Pt were carried out by Levin et al.[27], Harris and Zuckermann[57], Kato and Shimizu[58] and Alben and Wohlfarth.[59] Levin et al.[27] calculated the paramagnetic

spin susceptibility for Ni-Pd and Pd-Pt alloys using the Hartree-Fock approximation and CPA and assuming the same band structure for pure Ni, Pd and Pt. The values of the intra-atomic Coulomb interaction was determined for pure metals and the concentration variation of the susceptibility was accounted for the change in the density of states and the local density of states at the Fermi level. On the other hand, Harris and Zuckermann[57] and Kato and Shimizu[58] applied CPA to the calculation of $\chi(q, \omega)$ obtained in the random phase approximation and calculated the concentration variation of the susceptibility which is produced by the change of the effective value of the intra-atomic Coulomb integral in alloys. In their calculations the variation of the density of states of the alloys was neglected. Alben and Wohlfarth[59] calculated the magnetic moment and the low temperature specific heat coefficient γ for Ni-Pt alloys in CPA, but they did not take account of the difference between the band-widths of pure Ni and Pt.

In this chapter, by taking account of the difference between the band-widths of component metals which was neglected in the previous works, the density of states, the paramagnetic spin susceptibility χ, magnetic moments and γ are calculated for Ni-Pd, Ni-Pt and Pd-Pt alloys. The method proposed by Shiba[18] is made use of to include the off-diagonal randomness. The effect of clustering which may cause the spatial fluctuation of the magnetic moment near the critical concentration where the ferromagnetism disappears is neglected. This spatial fluctuation may give tailing of the magnetic moment into the paramagnetic region. This tailing of the magnetic moment

is large in Ni-Cu alloys, for example, but very small in Ni-Pd or Ni-Pt alloys.

In §2, the model and the formulation of Shiba's method are explained briefly and the formulations of χ generalized for the alloys with off-diagonal randomness are presented. The parameters used in this calculation are explained in §3. In §4, the calculated results are shown and compared with the experimental results. Discussion and conclusion are given in §5.

§2. Density of States in CPA with Off-Diagonal Randomness

In one band Hubbard model with the Hartree-Fock approximation, the Hamiltonian is given by

$$H = \sum_{i\sigma} (\varepsilon_i + U_i n_{i-\sigma}) a^+_{i\sigma} a_{i\sigma} + \sum_{ij\sigma} t_{ij} a^+_{i\sigma} a_{j\sigma}, \qquad (4\text{-}1)$$

where all notations are the same as those in eq. (2-1). The values of ε_i, U_i and $n_{i\sigma}$ are assumed to take one of only two values, ε_A or ε_B, U_A or U_B and $n_{A\sigma}$ or $n_{B\sigma}$, respectively, according as the i site is occupied by A or B atoms.

The method developed by Shiba[18] is briefly explained as follows. By assuming a relation among transfer integrals, i.e., $t^2_{AB}=t_{AA}t_{BB}$, the Green's function for an alloy is expanded by locators

$$\mathcal{L}^{-1}_{i\sigma}(z) = W_i (z - \varepsilon_{i\sigma})^{-1}, \qquad (4\text{-}2)$$

where $z=E+i0$, $\varepsilon_{i\sigma}=\varepsilon_i+U_i n_{i-\sigma}$ and W_i represents the ratio of

the band-width of A or B metal to that of the host metal. The effective Green's function $F_\sigma(z)$ of the alloy is given by

$$F_\sigma(z) = \int dE \rho^o(E) \{\mathcal{L}_\sigma(z) - E\}^{-1}, \tag{4-3}$$

where $\rho^o(E)$ is the density of states of the host metal and $\mathcal{L}_\sigma^{-1}(z)$ is a coherent locator determined by the following equation

$$(\mathcal{L}_{A\sigma} - \mathcal{L}_\sigma)(\mathcal{L}_{B\sigma} - \mathcal{L}_\sigma)F_\sigma - \mathcal{L}_\sigma + c_A\mathcal{L}_{A\sigma} + c_B\mathcal{L}_{B\sigma} = 0, \tag{4-4}$$

where the argument z is neglected for abbreviation and c_A or c_B is the concentration of A or B atoms. The local density of states with spin σ for A or B atom $\rho_{A\sigma}(E)$ or $\rho_{B\sigma}(E)$ and the average density of states $\rho_\sigma(E)$ with spin σ are given as,

$$\rho_{i\sigma}(E) = -\pi^{-1}\mathrm{Im}\ \{W_i^{-1}(\mathcal{L}_{i\sigma} - \mathcal{L}_\sigma + F_\sigma^{-1})^{-1}\},\ i=A \text{ or } B \tag{4-5}$$

$$\rho_\sigma(E) = c_A\rho_{A\sigma}(E) + c_B\rho_{B\sigma}(E).$$

The $F_\sigma(z)$ and $\mathcal{L}_\sigma(z)$ must be solved self-consistently by eqs. (4-3) and (4-4). Eqs. (4-3)-(4-6) are the results obtained by Shiba.[18)]

The average number of d-electrons $n_{i-\sigma}$ appeared in the expression of $\varepsilon_{i\sigma}$ is obtained from

$$n_{i-\sigma} = \int_{-\infty}^{\infty} dE f(E-\zeta)\rho_{i-\sigma}(E), \tag{4-7}$$

where $f(E-\zeta)$ is the Fermi distribution function and ζ is a chemical potential. This value of n_{i-} should be calculated self-consistently from eqs. (4-5) and (4-7). The local and average magnetic moments are given by $m_i=n_{i+}-n_{i-}$ and $m=c_Am_A+c_Bm_B$, respectively. Instead of m_i and m, the values given by $m_i^*=m_ig_i/2$ and $m^*=c_Am_A^*+c_Bm_B^*$ are used to compare with the experimental values, where g_i is the g-factor of i (A or B) metal. The paramagnetic spin susceptibility χ is given as

$$\chi = c_A\chi_A + c_B\chi_B, \tag{4-8}$$

$$\chi_A = \frac{2\mu_B^2\{\rho_A(\zeta)(1+f_{BB}U_B) - \rho_B(\zeta)f_{AB}U_B\}}{(1+f_{AA}U_A)(1+f_{BB}U_B) - f_{AB}f_{BA}U_AU_B}, \tag{4-9}$$

where $\rho_{i\sigma}(\zeta)=\rho_{i-\sigma}(\zeta)=\rho_i(\zeta)$ with i=A or B and χ_B is obtained by exchanging the suffixes A and B in eq. (4-9). Above expressions are the same as those obtained by Levin et al.[27], but the equations for the f_{ij}'s, where i or j is A or B are different from theirs because the off-diagonal randomness is included in the present case and are given as follows,

$$f_{ij} = -\pi^{-1}\mathrm{Im}\int_{-\infty}^{\infty} dEf(E-\zeta)\frac{\partial F_i}{\partial \varepsilon_j}, \tag{4-10}$$

$$F_i = W_i^{-1}(\mathcal{L}_i - \mathcal{L} + F^{-1})^{-1}, \tag{4-11}$$

$$\frac{\partial F_i}{\partial \varepsilon_j} = W_i^{-1}(\mathcal{L}_i - \mathcal{L} + F^{-1})^{-2}\{W_i^{-1}\delta_{ij} + (F^{-2}\frac{\partial F}{\partial \mathcal{L}} + 1)\frac{\partial \mathcal{L}}{\partial \varepsilon_j}\}, \tag{4-12}$$

$$\frac{\partial \mathcal{L}}{\partial \epsilon_j} = [W_A^{-1}\delta_{Aj}\{(\mathcal{L}_B - \mathcal{L})F + c_A\} + W_B^{-1}\delta_{Bj}$$

$$\times \{(\mathcal{L}_A - \mathcal{L})F + c_B\}] \times \{(\mathcal{L}_A - \mathcal{L})(\mathcal{L}_B - \mathcal{L})\frac{\partial F}{\partial \mathcal{L}}$$

$$+ (2\mathcal{L} - \mathcal{L}_A - \mathcal{L}_B)F - 1\}^{-1}, \qquad (4\text{-}13)$$

$$\frac{\partial F}{\partial \mathcal{L}} = -\int dE\rho^o(E)(\mathcal{L} - E)^{-2}, \qquad (4\text{-}14)$$

where the spin suffix σ is dropped because the alloy is in the paramagnetic state and the argument z of F, F_i, $\mathcal{L}$ and $\mathcal{L}_i$ are also dropped for abbreviation. By replacing $\mathcal{L}$ by $z-\Sigma$ and W_i by 1, these equations are reduced to the equations obtained by the original CPA.

§3. Simple Models for Ni, Pd and Pt

The values of several parameters, such as the number of d-holes of each metal, U_i, W_i and ϵ_i where i is Ni, Pd or Pt, are determined for each pure metal except the value of $\delta_o = \epsilon_A - \epsilon_B$. In this chapter, A means Ni in Ni-Pd and Ni-Pt alloys or Pd in Pd-Pt alloys. The number of d-holes in Ni is determined as 0.56 per atom by considering that the value of g-factor is 2.18[46] and those of Pd and Pt are determined as 0.36 and 0.3 per atom, respectively, from the de Haas-van Alphen experiments.[60] Knapp and Jones[61] estimated the electron phonon enhancement factor of Pd and Pt metal as 1.7 ±0.1 and 1.6±0.1, respectively. For simplicity the electron phonon enhancement factors of Ni, Pd and Pt are assumed to be

the same and equal to 1.6. The values of the density of states at the Fermi level for each metal are determined from the electron phonon enhancement factor and the experimental values of γ which are 7.1, 9.53 and 6.57 mJ/mol·K^2 for Ni,[49] Pd and Pt,[62] respectively.

The intra-atomic Coulomb integrals U_{Pd} and U_{Pt} are determined as 0.704 and 0.849 eV from the values of the density of states at the Fermi level and the observed values[63] of χ, 7.36 and 2.16×10^{-4} emu/mol for Pd and Pt, respectively. The observed values of χ for Pd and Pt are assumed to be only due to spin, because the contributions from orbital and diamagnetic susceptibilities are almost cancelled out. The g-factors for Pd and Pt are assumed to be 2.0. The value of U_{Ni} is determined as 0.745 eV from the fact that the Fermi level of the ferromagnetic Ni metal locates at the position higher than the upper edge of the majority spin band by 0.04 eV.[47]

The heights of the density of states at the peak near the Fermi level for Ni[45] and Pt[64] are 5.0 and 2.67 eV^{-1} per atom, respectively, and the ratio between these values 1.873 is assumed to be equal to the ratio W_{Pt} between the band-width of Pt and Ni, whose band-width is 4.45 eV.[45] A simple shape of $\rho^{o}(E)$ as shown in Fig. 42 is used for d-electrons in paramagnetic Ni and the shape of the density of states for d-electrons in pure Pd and Pt is similar to that of Ni. The band-width for Pd is determined uniquely from the simplified density of states, the number of d-holes and the fixed value of the density of states at the Fermi level.

Thus the value of W_{Pd} is fixed as 1.414.

The values of δ_o which is the only adjustable parameter for the alloys are determined as 0.849, 1.977 and 0.890 eV for Ni-Pd, Ni-Pt and Pd-Pt alloys, respectively, so that the critical concentrations occur at 2.3 at.% Ni for Ni-Pd alloys and at 42 at.% Ni for Ni-Pt alloys and the calculated values of γ for Pd-Pt alloys agree well with experiment.

§4. Calculated Results and Comparison with Experiment

The average and local densities of states, average and local magnetic moments, susceptibility and low temperature specific heat coefficient are numerically calculated by the formulae given in §2 and the numerical values of the parameters given in §3. At first, to demonstrate the concentration variation of the density of states for alloys with off-diagonal randomness, the calculated results of the average and local densities of states $\rho(E)$ and $\rho_i(E)$ for paramagnetic Ni-Pt alloys are shown in Figs. 43-51. In these figures curves 1, 2 and 3 are the average and local densities of states of Ni and Pt atoms, respectively. Here and hereafter in this chapter the band-width of pure Ni is normalized as 2 and the density of states is scaled so as to normalize the total number of states as 1. The higher band edge shifts to lower energy with increasing Pt concentration. As the band-width increases, the height of $\rho(E)$ decreases. The peak in $\rho(E)$ is not smeared out at any concentration, and this result differs from the results obtained for Ni-Fe alloys[25] and Ni-Cu alloys as shown in chapters II and III.

The peak in $\rho_{Ni}(E)$ or $\rho_{Pt}(E)$ is similar to that of each pure metal and $\rho_{Pt}(E)$ is high at lower energy region in alloys of low Pt concentration.

The reason why the peak near the Fermi level remains as sharp even in concentrated alloys is explained by the fact that the scattering potential for electrons is effectively small in this energy region. This may be due to the model made use of in taking account of the off-diagonal randomness. Blackman et al.[17] have discussed that their approximation is exact for the first four moments of the density of states whereas CPA theory with only diagonal randomness is correct up to the eighth moments.

The variation of $\rho(E)$ and $\rho_i(E)$ for A_{60}-B_{40} alloy with the change of W_B is demonstrated in Fig. 52. The value of δ_o is 0.3 times the band-width of A metal and the values of U_A and U_B are 0. Note that the peak in $\rho(E)$ is smoothened when W_B=1.0 but remains clearly with increasing value of W_B up to 1.8 and it is smoothened again when W_B=2.2 The Ni-Pt alloys correspond to the case W_B=1.8.

4-1 Ni-Pd alloys

The calculated results of $\rho_\sigma(E)$ and $\rho_{i\sigma}(E)$ for ferromagnetic Ni-Pd alloys are shown in Figs. 53-61. Curves 1, 2 and 3 in these figures are the average density of states and local densities of states of Ni and Pd atoms, respectively. The $\rho_\sigma(E)$ and $\rho_{i\sigma}(E)$ for each spin shows a concentration variation similar to that of Ni-Pt alloys. The Ni rich Ni-Pd alloys are saturated ferromagnets up to 60 at.% Ni. It should be noted that the value of $\rho_{Ni-}(E)$ at the peak increases with

increasing Pd concentration. Therefore the number of d-holes with minority spin at the Ni atoms increases with increasing Pd concentration. The $\rho(E)$, $\rho_{Ni}(E)$ and $\rho_{Pd}(E)$ for paramagnetic 1 at.% Ni-Pd alloy are shown in Fig. 62. The $\rho_{Pd}(E)$ almost overlaps with the $\rho(E)$. In this alloy, the peak of $\rho_{Ni}(E)$ is also high.

The concentration variation of the calculated and observed[65-69] values of m^*, m^*_{Ni} and m^*_{Pd} for Ni-Pd alloys are shown by curves 1, 2 and 3, respectively, in Fig. 63. The calculated values of m^* agree qualitatively with experiment and they decrease rapidly with increasing Pd concentration near the critical concentration, which is similar to the result obtained by classical Landau theory.[70] The calculated values of m^* decrease linearly with increasing Pd concentration from pure Ni to 60 at.% Ni as these alloys are saturated ferromagnets. The experimental decrement is a little smaller than that of the calculated result. This difference between the experimental and calculated results may be explained by the transfer of d-electrons to the s-band rather than by a value of the number of d-holes in pure Pd larger than 0.36 per atom. By taking account of the transfer of d-electrons to the s-band, a residual resistivity of Ni-Pd alloys was calculated by Kimura et al.[71] and a good agreement with experiment was obtained.

The calculated values of m^*_{Ni} increase with increasing Pd concentration up to about 80 at.% Pd and decrease rapidly near the critical concentration. As for the fact that they increase with increasing Pd concentration, the calculated

results agree qualitatively with the results of neutron diffraction experiments[69] but there is a large quantitative discrepancy between them. In the Ni rich alloys, this discrepancy is due to a spatially uniform negative polarization about -0.1 μ_B per atom[48], but the reason for the difference in the Pd rich alloys is not clear at present. Even if the off-diagonal randomness does not exist, the increase of m^*_{Ni} with increasing Pd concentration also occurs as long as the critical concentration is at 2.3 at.% Ni. However, if the critical concentration is moved to the region of higher Ni concentration by changing the value of δ_o, the value of m^*_{Ni} turns out to decrease with increasing Pd concentration. The reason why the value of m^*_{Ni} increases with increasing Pd concentration is that the $\rho_{Ni}(E)$ near the Fermi level increases with increasing Pd concentration as shown in Figs. 53-61. The large value of the $\rho_{Ni}(E)$ at the Fermi level as shown in Fig. 62 is also related to the occurrence of ferromagnetism at low Ni concentration. The calculated value of m^*_{Pd} agrees well with the experimental values[69] except for Ni rich alloys.

The calculated and experimental[63,65,72,73] values of the paramagnetic susceptibility are shown in Fig. 64. The calculated values agree well with experiment except in the critical region where the observed values do not tend to zero at the critical concentration because of high applied magnetic field.

The calculated values for γ and the experimental ones[49,62,65,72-74] are shown in Fig. 65. The calculated values are multiplied by the electron phonon enhancement

factor 1.6. Near the critical concentration the calculated values considerably differ from the experimental values and this difference may be due to the effect of spin fluctuations. The calculated values of γ decrease slighly from the value for Ni with increasing Pd concentration because Ni rich alloys are saturated ferromagnets and the $\rho_{-}(E)$ at the Fermi level decreases with the increasing band-width of the alloys. The agreement between the calculated and experimental values is not so unsatisfactory except in the case of Pd rich alloys.

The numerical values of the calculated results for the average and local magnetic moments, γ and paramagnetic spin susceptibility for Ni-Pd alloys are shown in Table III.

4-2 Ni-Pt alloys

The calculated results of $\rho(E)$ and $\rho_i(E)$ for paramagnetic Ni-Pt alloys are shown in Figs. 43-51. $\rho_\sigma(E)$ and $\rho_{i\sigma}(E)$ for the ferromagnetic state are shown in Figs. 66-70. The curves 1, 2 and 3 in these figures are average density of states and local densities of states of Ni and Pt atoms, respectively. The $\rho_{i\sigma}(E)$ for majority and minority spins are similar to those obtained by splitting the $\rho_i(E)$ in the paramagnetic state at the same concentration. This is due the fact that the magnetic moments in these alloys are so small that the difference between potentials in the majority and minority spin states is not so different from that in the paramagnetic state at the same concentration.

The calculated and experimental[75-80] values for the concentration variation of m^*, m^*_{Ni}, m^*_{Pt} and χ^{-1} are shown as curves 1, 2, 3 and 4, respectively, in Fig. 71. The

alloys whose Ni concentration is larger than about 90 at.% are saturated ferromagnets. The values of m* decrease monotonically with increasing Pt concentration and agree qualitatively with the experiments. The concentration dependence near the critical concentration is the same as that of Ni-Pd alloys. The values of m^*_{Pt} are fairly large in Ni rich region and this is due to a large value of U_{Pt}. For a smaller value of U_{Pt} than that adopted in this calculation for Ni-Pt alloys, the values of m^*_{Pt} become smaller than those in Fig. 71. The concentration variation of the calculated values of χ^{-1} agrees qualitatively with the experimental results. However, the calculated values of χ^{-1} are somewhat larger than the experimental values near 20 at.% Ni and the origin of this difference between the calculated and experimental values is not clear at present.

The calculated and experimental[49,62,79,81,82] values of γ are shown in Fig. 72. The calculated values are multiplied by the electron phonon enhancement factor 1.6. The value of γ increases almost linearly with increasing Ni concentration as does the experimental value in the paramagnetic state, but the rate of increase of the experimental value is much larger than that of the calculated value. Our calculated results are similar to those obtained by Alben and Wohlfarth,[59] but in their results the values calculated in the ordinary CPA were modified by taking into account the difference between the densities of states of pure Ni and Pt. The difference between the calculated and experimental value of γ may be due to the effects of spin fluctuations or clusters.

The numerical values of the calculated results for m^*, m^*_{Ni}, m^*_{Pt}, γ and χ for Ni-Pt alloys are shown in Table IV.

4-3 Pd-Pt alloys

The calculated results for $\rho(E)$ and $\rho_i(E)$ are shown in Figs. 73-81. In these figures curves 1, 2 and 3 are the average density of states and local densities of states of Pd and Pt atoms, respectively. The whole feature is similar to that of the paramagnetic Ni-Pt alloys except that the difference between band-widths of pure Pd and Pt is not so large and that the peak in the density of states is rounded a little as compared with that of Ni-Pt alloys. The calculated results for γ multiplied by the phonon enhancement factor 1.6 and the experimental values[62] are shown in Fig. 82 and good agreement between them is obtained. The difference between the values of γ of pure Pd and Pt is mainly due to the difference between their band-widths because the difference between the numbers of d-holes in Pd and Pt is small.

The calculated and experimental[62,63] values of χ are shown in Fig. 83. The calculated values with U_{Pt}=0.849 eV shown by the solid curve in Fig. 83 do not agree well with the experimental values and this may be due to a relatively large value of U_{Pt}. If we take a smaller value U_{Pt}=0.774 eV and the value of δ_o as 0.534 eV, better agreement between the calculated and experimental results is obtained as shown by broken curve in Fig. 83. However, the calculated result with U_{Pt}=0.774 eV differs a little in Pt rich alloys and this disagreement may be attributed to the concentration variation of U corresponding to the concentration variation of the

band-width. The calculated values of γ for U_{Pt}=0.774 eV also agree well with the experimental results. The numerical values of the calculated results for γ and χ are shown in Table V.

§5. Discussion and Conclusion

The values defined as $\delta=\delta_o+n_A^oU_A-n_B^oU_B$, where n_A^o and n_B^o are the numbers of d-electrons in the pure paramagnetic metals and A means Ni in Ni-Pd and Ni-Pt alloys or Pd in Pd-Pt alloys, are 1.02, 1.38 and 0.17 eV for Ni-Pd, Ni-Pt and Pd-Pt alloys, respectively. These values are reasonable, as the atomic potentials of Ni, Pd and Pt atoms become deeper in this order.

The concentration variation obtained in the present calculations for the number of d-holes per atom for Ni-Pd, Ni-Pt and Pd-Pt alloys are shown in Fig. 84. The condition of charge neutrality is not satisfied in all these alloys. This is due to neglecting the screening of the potential by electrons. However, the number of d-holes at the Pt site in Pd rich Pd-Pt alloys is rather large because the value of δ in Pd-Pt alloys is small. The value of δ for U_{Pt}=0.774 eV is almost the same as that for U_{Pt}=0.849 eV. The fact that one cannot obtain a value of δ which explains the experimental values of γ and χ and at the same time satisfies charge neutrality may be due to the following two reasons. One is that the values of U_i and $\rho(E)$ obtained for pure Pd and Pt may be inappropriate because of the uncertainty in the value of the electron mass enhancement factor. The other is that the $\rho(E)$ and $\rho_i(E)$ for alloys near the peak may not be obtained correctly because CPA with off-diagonal randomness is not so good as mentioned

in the beginning of §4. Thus the results obtained in §4 may not be quantitatively correct, but the qualitative feature may be correct.

It should be noted that the concentration variation of the number of d-holes of Ni atom in Ni-Pd alloys differs from that in Ni-Pt alloys. This difference will be related to the difference between the critical concentration of Ni-Pd and Ni-Pt alloys.

We now discuss the dependence of the number of d-electrons on the strength of the diagonal and off-diagonal randomnesses. If we consider the alloy with only diagonal randomness, the electrons are piled up at the atomic site, the potential of which is deeper than the other atomic site because the transfer of electrons does not depend on the atomic species. As the numbers of d-electrons in pure Ni, Pd and Pt are similar to each another, the charge neutrality in Ni-Pd, Ni-Pt and Pd-Pt alloys is approximately satisfied when the potential difference is very small. Then the shape of the local densities of states of A and B atoms are similar to each other and the charge density may be considered to be uniform. This case corresponds to the rigid band approximation.

If the off-diagonal randomness is included and if B metal has a deeper potential and a wider band-width than A metal, the electrons are not so much piled up at the B site because the probability of transfering from the B site to another site is larger than that from the A site. Therefore, the numbers of electrons at the A site and the B site can be nearly equal when there are both the diagonal and off-diagonal randomnesses. Even if these numbers of electrons are equal, the shape of $\rho_A(E)$

and $\rho_B(E)$ are in general different from each other.

The situation described above is shown in Fig. 85 where the relation between the potential difference $\delta_o=\varepsilon_A-\varepsilon_B$ and the band-width W_B for A_{60}-B_{40} alloys is indicated. The value of W_A is taken as 1.0. The numbers of d-electrons of the A and B metals are taken as those of Ni and Pt, respectively. As this calculation has been carried out for $U_A=U_B=0$, the value of δ_o equals to that of δ. In Fig. 85(a) the dependence on δ_o and W_B of the numbers of electrons per atom at A and B sites is shown. For each value of δ_o, the value of n_A increases with increasing value of W_B whereas that of n_B decreases. This is because the top of the band of the B metal becomes higher than that of the A metal with increasing values of W_B. The change in the densities of states for $\delta_o=0.6$ with respect to the change of W_B is shown in Fig. 52. The value of n_A becomes equal to that of n_B at the value of W_B where the curve of n_A crosses that of n_B for each value δ_o in Fig. 85(a). It is found that with increasing value of W_B, the relation that n_A is equal to n_B can be satisfied at a larger value of δ_o. This fact is clearly shown in Fig. 85(b) where the solid line is the case where $n_A=n_B$ and the broken line is the case where $n_A=n_A^o$ and $n_B=n_B^o$. As the value of W_B approaches 1, the value of δ_o approaches 0.

In the calculations of this thesis, it is assumed that the values of U_i do not change in alloys. However, these values must change by alloying because of the change of the band-width and the electron correlation.[57,58,83] If the change of the value of U on alloying is included, better

agreement will be obtained. As mentioned already, the approximation used to take account of the off-diagonal randomness is not so satisfactory and this is a possible reason for the fact that the peak in the density of states remains very sharp even in concentrated alloys. So it may be necessary to study the concentration variation of the density of states by a better approximation such as the cluster approximation for the off-diagonal randomness.

Next, we discuss the differences between the calculated results obtained by Levin et al.[27] and those in this chapter. Almost the same results for χ as those in this chapter were obtained by them for Ni-Pd alloys. They also found that the Ni atoms are responsible for the occurrence of the ferromagnetic states in Ni-Pd alloys. However, there is a difference between the values of δ used by Levin et al. and in this chapter. Their value of δ was 0.38 eV but ours is 1.02 eV which may be more reasonable than the former as the corresponding value was obtained as 1.86 eV by Hodges et al.[84] For Pd-Pt alloys, Levin et al. obtained good agreement between the calculated results and experiment for χ. As they assumed that Pd and Pt have the same numbers of d-electrons and the same band-width, the values of the density of states at the Fermi level for Pd and Pt are the same. Therefore, their calculated results of γ for Pd and Pt were the same and the concentration variation of γ showed a shallow minimum which does not agree with experiment because the contribution from spin fluctuations may be small in these alloys.

The calculated results for γ for Ni-Pd and Ni-Pt alloys

in this chapter could not explain the experimental values satisfactorily. Recently, Jacobs and Zaman[85] calculated the concentration variation of γ for Ni-Pt alloys by including the effect of clusters and obtained good agreement with experiment in the paramagnetic state. It may be necessary to include the effect of clusters for Ni-Pt alloys. The quantitative disagreement between the calculated values in this chapter and experimental ones for m^* and χ^{-1} may also be explained by the effect of clusters.

The merits of the calculations including the off-diagonal randomness are as follows. First, it can consistently treat the alloys with any concentration of atoms with different band-width. Therefore, for example, the magnetic properties of Ni-Pt alloys in the ferromagnetic and paramagnetic states can be calculated consistently. Secondly, as mentioned at the beginning of this section, this calculation including the off-diagonal randomness is better than the corresponding calculation in the ordinary CPA when the numbers of electrons of the constituent atoms are the same. Finally, the concentration variation of γ can be well explained in Pd-Pt alloys.

It is concluded that by taking account of the off-diagonal randomness, the concentration variation of m^*, m_A^*, m_B^*, γ and χ can be explained satisfactorily, at least qualitatively, for Ni-Pd, Ni-Pt and Pd-Pt alloys except for the value of γ in Pd rich Ni-Pd alloys and Ni-Pt alloys, where the effect of spin fluctuations or clusters may be important.

Chapter V. Temperature Dependences of Electrical Resistivity and Magnetic Susceptibility for V-Cr, Nb-Mo and Ta-W Alloys at High Temperature

§1. Introduction

It is well-known that in certain transition metals the paramagnetic susceptibility χ increases with increasing temperatures, whereas in others it decreases with increasing temperatures. In the former metals the electrical resistivity R at high temperature increases more rapidly than the linear dependence on T with increasing temperature and in the latter ones less rapidly than T. The former and the latter metals were defined as "plus group" and "minus group", respectively, by Shimizu.[8] Temperature dependences of R and χ at high temperature for many transition metals were theoretically studied in detail by the band picture.[8,86,87] It was shown that these temperature dependences were strongly dependent on the shape of the density of states $\rho(E)$ for d-electrons and on the position of the Fermi level E_F.

The relation between the temperature variation of R or the unenhanced paramagnetic spin susceptibility χ_o and the shape of $\rho(E)$ and the position of E_F was explained in the following way. At low temperature as compared with the degeneracy temperature of d-electrons, R/T and χ_o can be expanded as power series of T up to T^2 term as[8]

$$(R/T)/(R/T)_o = 1 - (\pi k_B T)^2 (3\nu_1^2 - \nu_2)/6 \ , \qquad (5\text{-}1)$$

$$\chi_o = 2\mu_B^2\rho(E_F)\{1 - (\pi k_B T)^2(\nu_1^2-\nu_2)/6\} , \qquad (5\text{-}2)$$

where

$$\nu_n = (d^n\rho(E_F)/dE_F^n)/\rho(E_F) , \qquad (5\text{-}3)$$

$(R/T)_o$ is the value of R/T at a reference temperature and μ_B is the Bohr magneton. In the plus group metals, as E_F occurs in the neighbourhood of a minimum of $\rho(E)$, $\nu_2>\nu_1^2\simeq 0$ and $A=3\nu_1^2-\nu_2$ and $B=\nu_1^2-\nu_2$ are negative, R/T and χ_o increase with increasing temperature. On the other hand, in the minus group metals, as E_F occurs in the neighbourhood of a maximum of $\rho(E)$, $\nu_2<0$ and A and B are positive, R/T and χ_o decrease with increasing temperature. From the measured temperature variations of χ for V-Cr, Nb-Mo and Ta-W alloys,[88,89] it is seen that these alloys are in the minus or plus group with large or small concentration of V, Nb and Ta. The theoretical study of the temperature dependence of χ for these alloys was carried out by Shimizu et al.[8] using the rigid band approximation and qualitative agreement between the calculated and observed results was obtained. Recently, the R for V-Cr[90] and Ta-W[91] alloys was measured at high temperature and it was shown that the values of A for these alloys change from positive values to negative values with increasing Cr or W concentration.

The purpose of this chapter is to calculate the temperature dependences of χ_o and R/T for V-Cr, Nb-Mo and Ta-W alloys by using eqs. (5-1)-(5-3) and to investigate their

dependence on the shape of $\rho(E)$. As these alloys become the minus or plus group according to the concentration of alloys the relation between the temperature dependences of χ_o and R/T and the shape of $\rho(E)$ can be more clearly understood than for pure metals.

By making use of the calculated $\rho(E)$ for pure metals the $\rho(E)$ for alloys can be calculated in the coherent potential approximation (CPA).[9-14] In §2, $\rho(E)$'s for V-Cr, Nb-Mo and Ta-W alloys are calculated in CPA. In §3, the calculated values of A and B are shown and compared with experiment. In §4, the molecular field is taken into account to compare the calculated value of χ with experiment for Cr and Cr rich V-Cr alloys. Discussion and conclusion are given in §5.

§2. Density of States for Alloys

The densities of states $\rho(E)$ for paramagnetic V-Cr, Nb-Mo and Ta-W alloys are calculated in CPA using the formulation explained in §2, chap. II. The degeneracy of the d-bands is neglected and the whole density of states is treated as one band. The calculated $\rho(E)$ by Connolly[92] for Cr, by Mattheiss[93] for Nb and by Petroff and Viswanathan[94] for W are used to calculate $\rho(E)$ for V-Cr, Nb-Mo and Ta-W alloys, respectively. In numerical calculations, the fictitious bumps in the histogram of the calculated $\rho(E)$ for Nb and W are smoothened.

The molecular field coefficients for V, Cr, Nb, Mo, Ta and W are estimated previously and they were found to be zero or small except for W.[8] Therefore, the molecular field coefficients in V-Cr, Nb-Mo and Ta-W alloys are neglected in

this section, i.e., the Coulomb interaction terms in eqs. (2-3) and (2-16) are neglected. The potential difference between the constituent atoms of the alloys is determined so that charge neutrality is nearly satisfied, i.e., the number of d-electrons on V, Nb and Ta atoms is about 5 per atom and that on Cr, Mo and W atoms is about 6 per atom. The values of the potential difference for the V-Cr, Nb-Mo and Ta-W alloys determined as above are 0.05, 0.052 and 0.06 Ryd, respectively. The calculated results of $\rho(E)$ for these alloys are shown in Figs. 86-88.

The whole shape of the calculated $\rho(E)$ for an alloy is similar to that of the pure metal, but the height of the peaks in the alloys is lower than that of the pure metals, as shown in Figs. 86-88. The minimum in $\rho(E)$ of the pure metals does not disappear by alloying, because the potential difference between constituent atoms is small compared with the band-width for alloys. From this fact it may be said that the rigid band approximation is not so bad for these alloys.

§3. Temperature Dependence of R and χ

The coefficients A and B of T^2 terms in the series expansion of R/T and χ_0 with respect to T^2 in eqs. (5-1) and (5-2) are numerically calculated. The $\rho(E)$ calculated for alloys in §2 are made use of and the energy derivatives of $\rho(E)$ at E_F are calculated numerically. The calculated results of A for R/T and B for χ_0 are shown in Figs. 89 and 90. The experimental values of A for V-Cr[90] and Ta-W[91] and those of B for V-Cr, Nb-Mo and Ta-W alloys are also shown in the same figures.

These values change their sign from positive to negative with increasing values of the electron per atom ratio e/a. The experimental values of B are estimated from the observed results of χ[88,89] at T>1000 K by the formula $\chi=a-\mu_B^2\rho(E_F)\times(\pi k_B T)^2 B/3$ where a is a constant. The values of B for Cr and V_{25}-Cr_{75} alloy were found to be so large (-67.7 and -57.4 eV^{-2}, respectively) that these values are not plotted in Fig. 90.

The calculated values of A and B for V-Cr and Ta-W alloys are positive for the V or Ta rich region and negative for the Cr or W rich region. Although the dependences on the concentration of the calculated values are not very smooth, they agree qualitatively with the experimental results. These results are explained from the shape of $\rho(E)$ and the position of E_F in the following way. For V or Ta alloys, as E_F occurs near the maximum of $\rho(E)$, ν_2 is negative and A or B is positive. With increasing value of e/a, ν_2 becomes negative and $|\nu_1|$ becomes small, so that A or B of these alloys becomes negative.

The reason why the calculated values of A and B for V or Ta rich alloys are larger than the experimental ones is that the peak in $\rho(E)$ near E_F is very sharp and the value of $|\nu_2|$ is very large in these alloys. Other calculated values of A and B for V-Cr and Ta-W alloys, where the calculated $\rho(E)$ for pure V[94] and Ta[95] instead of Cr and W are made use of, are also shown in Figs. 89 and 90. These values at the V and Ta rich regions are small because the values of $|\nu_2|$ are small. These calculated values of A and B may be more adequate than those shown by the thick curves in Figs. 89 and 90 in comparing with experiment, because the calculated density

of states for pure metals of high concentration is used. To explain a large difference between the calculated and experimental values of B for Cr and Cr rich V-Cr alloys, it is necessary to take into account the enhancement of B by the molecular field, as discussed in the next section.

For Mo rich Nb-Mo alloys the calculated values of A and B are negative and those of B agree qualitatively with experiment as shown in Figs. 89 and 90. However, for Nb rich alloys the values of A and B are also negative and this is in contradiction to the experimental results for χ. This result is due to the fact that the value of ν_2 at E_F is largely positive in pure Nb because of a rapid change of the calculated $\rho(E)$ near E_F. When the concentration of Mo atom becomes larger than 20 at.%, the value of ν_2 becomes positive and consequently A and B become positive and this is in agreement with experiment.

The value of A for V-Cr alloys are somewhat larger than those of Nb-Mo and Ta-W alloys. This fact is attributed to the fact that the d-band of Cr is narrower than that of Nb or W. The error in the numerical calculation of $d^2\rho(E_F)/dE_F^2$ is somewhat large and this is one of the reasons that the curves of A and B in Figs. 89 and 90 are not so smooth. Therefore, the numerical values of A and B themselves are not so important, but the qualitative feature of the concentration variation of A and B will be correct.

§4. Temperature Dependence of χ for Cr

As discussed in §3, the calculated value of B for Cr

differs considerably from the experimental values. This difference can be explained by the enhancement due to the molecular field. To see this, the full temperature dependence of χ_o for Cr is calculated at first by using the $\rho(E)$ calculated by Connolly[92] and using the well-known method.[8,86,87] The calculated value of χ given by $\chi=\chi_o(1-\alpha\chi_o)^{-1}+\chi_c$, where α is a molecular field coefficient and χ_c a temperature independent susceptibility, and the experimental data for Cr are shown in Fig. 91. The numerical values of the calculated results for χ are shown in Table VI. The values of α and χ_c are determined as 2.552×10^{4} mol/emu and 0.864×10^{-4} emu/mol, respectively, so that the calculated values coincide with the experimental ones at 400 K and 1500 K. The calculated results agree well with experiment above the Néel temperature.

The value of the Stoner enhancement factor $I=(1-\alpha\chi_o)^{-1}$ is obtained as 3.05 at 0 K for Cr. This value is similar to the value of 2.53 obtained by Oh et al.[97], but is larger than the value of 1.69 obtained by the method given above from the empirical density of states shown in reference 8. The disagreement between the values of I obtained here and before is attributed to the difference between the band-widths in $\rho(E)$ used to calculate χ_o.

By including the enhancement factor, χ is expanded as power series of T as

$$\chi = 2\mu_B^2\rho(E_F)\ I\{1-(\pi k_B T)^2(\nu_1^2-\nu_2)I/6\} + \chi_c\ . \qquad (5\text{-}4)$$

The coefficient of T^2 term in eq. (5-4) is proportional to I^2,

so that the absolute value of the coefficient of T^2 for Cr becomes about 9 times as large as that obtained without α. Therefore the value of B estimated from experiment becomes the same order as the calculated value. This fact is also true for Cr rich V-Cr alloys.

§5. Discussion and Conclusion

In eq. (5-1) only the scattering of electrons due to the electron phonon interaction is taken into account and it is assumed that the random potential only contributes to the residual resistivity which is not so dependent on the temperature. This assumption may not be unreasonable because the temperature in question is much higher than the Debye temperature so that the scattering of electrons by phonons is much greater than by the random potential.

It is concluded that the concentration variations of the temperature coefficients of R/T and χ for V-Cr, Nb-Mo and Ta-W alloys at high temperature are strongly dependent on the shape of the density of states near E_F. Furthermore it is found that α is important for the temperature dependence of χ for Cr and Cr rich V-Cr alloys. In these alloys, E_F moves from the position near the peak to the broad bottom of $\rho(E)$ with increasing value of e/a and consequently the value of ν_1 changes from a negative value to a positive one. The value of ν_2 has a large negative or a positive value when E_F occurs in the neighbourhood of a peak or a minimum of $\rho(E)$. The fact that the concentration variations of A and B obtained as above for V-Cr, Nb-Mo and Ta-W alloys agree qualitatively with

experiment may be considered as the appropriateness of the shape of the calculated density of states for these alloys and of the band model.

Chapter VI. Temperature Variation of Spin Susceptibility for Ni-Pt Alloys

§1. Introduction

The temperature variation of paramagnetic spin susceptibility $\chi(T)$ for alloys is in general enhanced locally and affected by the change of the density of states with temperature because the random potential in an alloy varies with temperature. However, with regard to the first point it has been shown that the susceptibility at 0 K can be approximately represented by the uniform enhancement model for Pd-Pt and Ni-Rh alloys[27] and for the Ni-Pt alloy as will be found from the results in chap. IV. The second effect will be quite small. Therefore, $\chi(T)$ for Ni-Pt alloys can be calculated by the usual method as for pure metal in the band model.

§2. Calculated Results, Discussion and Conclusion

The densities of states for Ni-Pt alloys are calculated by CPA including the diagonal and off-diagonal randomnesses.[18] The formulation is explained in chap. IV. The Coulomb interaction term in the Hamiltonian given by eq. (4-1) is neglected. The density of states for Pt calculated by Mueller et al.[64], which is shown in Fig. 92, is used as that of the host metal. The height of the peak near the Fermi level in the density of states for Ni calculated by Zornberg[29] is 4.87 eV^{-1} per atom and that of Pt[64] is 2.67 eV^{-1} per atom and the inverse of the ratio between these values is taken as the ratio between the band-widths of Ni and Pt. The

difference between the atomic potentials of Ni and Pt is determined as 2.0 eV so as to nearly satisfy charge neutrality at 42.9 at.% Ni. The calculated densities of states for Ni-Pt alloys are shown in Figs. 93-96. The height of the density of states increases and the band-width decreases with increasing Ni concentration. The shape of the density of states is smoothened except near the Fermi level and the peak near the Fermi level becomes high and narrow with increasing Ni concentration.

The calculated results and experimental values[88,98-101] of $1/\chi(T)=1/\chi_o(T)-\alpha$ for Pt, Ni and Ni-Pt alloys are shown in Fig. 97, where $\chi_o(T)$ is the Pauli spin susceptibility and α is a molecular field coefficient. The numerical values of $\chi(T)$ calculated using the density of states for Pt[64] are shown in Table VIII. The solid curves are the calculated results for Pt and Ni-Pt alloys. The values of $\chi_o(T)$ for Pt is calculated from the density of states calculated for Pt by Mueller et al.[64] However, the Fermi level must be located 0.09 eV lower than the position obtained in the a priori calculation by Mueller et al. to get a good agreement with experiment. Therefore, the number of electrons decreases by 0.20 per atom and the value of the density of states at the Fermi level becomes 2.65 eV^{-1} per atom. The agreement between the calculated and experimental values of $1/\chi(T)$ for Pt is satisfactory except below 200 K. The value of α for Pt is 0.687×10^4 mol/emu. The $\chi_o(T)$ are calculated for 24.1, 32.6, 42.9 and 90.9 at.% Ni and the values of α are 0.919, 0.912, 0.885 and 0.858×10^4 mol/emu, respectively. The value of α is treated

as an adjustable parameter and the concentration variation of α for these alloys cannot be explained at present. The calculated results for these alloys show good agreement with experiment. However, they do not agree below 100 K because the calculated results show a T^2 dependence but the experimental values show a almost linear dependence on T very near to 0 K. The slope of the calculated $1/\chi(T)$ is independent of concentration and is found to be rather insensitive to the value of the potential difference in the alloys above about 500 K. It is also insensitive to the position of the Fermi level at high temperature in so far as it is located near the peak, but its value at low temperature is sensitive to the position of the Fermi level. It should be noted that the calculated results of $1/\chi(T)$ show a weak downwards bend at high temperature, as is observed in Pt.[88] Although the calculations of $1/\chi(T)$ have been carried out for only four alloys, similar results will be obtained for other concentrations.

The broken curves in Fig. 97 are the calculated results for a 90.9 at.% Ni alloy and pure Ni using the density of states obtained by Shimizu and Hirooka[28]. The result for Ni is that reported by them[54] before, where α is 0.783×10^{4} mol/emu and the value of the temperature independent susceptibility χ_c is 0.594×10^{-4} emu/mol. These calculated results are in good agreement with experiment.[100,101] For Pt and Ni-Pt alloys, χ_c is not included but it may be necessary for Ni rich alloys.

In conclusion, the calculated results of $\chi(T)$ for Pt

and Ni-Pt alloys agree well with experiment except at very low temperature. The slope of $1/\chi(T)$ at high temperature does not perceptibly change with concentration and is relatively insensitive to the position of the Fermi level. It would be interesting to measure the temperature variation of $\chi(T)$ at high temperature for Ni-Pt alloys.

Chapter VII. Summary and Conclusion

In this thesis, CPA was applied to calculate the density of states for some transition metal alloys and to explain the magnetic and thermal properties for these alloys in the band model. This work is divided into two parts. One is a study for alloys in the ground state and the other is that for alloys at finite temperature.

In the first point, CPA and the Hartree-Fock approximation for the electron interaction have been combined and the numerical calculation on the density of states and the magnetic and thermal properties have been carried out for Fe-Ni, Ni-Cu, Ni-Pd, Ni-Pt and Pd-Pt alloys. Both the diagonal and off-diagonal randomnesses have been taken into account for Ni-Pd, Ni-Pt and Pd-Pt alloys. The density of states and the concentration variation of the low temperature specific heat coefficient have been calculated for all these alloys and the average and local magnetic moments have been calculated except for Pd-Pt alloys which are paramagnetic at all compositions. The concentration variation of the high-field spin susceptibility for the ferromagnetic Ni-Cu alloys and that of the paramagnetic spin susceptibility for Ni-Pd, Ni-Pt and Pd-Pt alloys have been also calculated.

In the second point, the densities of states for alloys have been calculated by CPA neglecting the electron interaction which is treated as an uniform molecular field. These calculations have been carried out for V-Cr, Nb-Mo, Ta-W and Ni-Pt alloys. The temperature coefficients of the T^2

term in the series expansion of the paramagnetic spin susceptibility and the electrical resistivity have been calculated for V-Cr, Nb-Mo and Ta-W alloys and the temperature variation of the paramagnetic spin susceptibility for Ni-Pt alloys has been calculated. A realistic shape of the density of states for the host metal has been taken into account for these alloys.

The comparison with experiment and the conclusions are summarized as follows. Ferromagnetic Fe-Ni and Ni-Cu alloys are treated in chapter II and chapter III, respectively. The calculated densities of states for these alloys are in general considerably smoothened except those for the majority spin band for Fe-Ni alloys. The difference between the shapes of the density of states for majority and minority spin bands for Fe-Ni alloys is large but that for Ni-Cu alloys is small. The smallness of this difference for Ni-Cu alloys is due to the smallness of the magnetic moment. The calculated results of the average and local magnetic moments and the low temperature specific heat coefficient are in agreement with experiment qualitatively except near the critical concentration where the ferromagnetism disappears. For Fe-Ni alloys, difficulty in the numerical calculations prevents comparison with experiment at the critical concentration. As for the Ni-Cu alloys, the enhancement of the low temperature specific heat coefficient and the tailing of the magnetic moments which were observed near critical concentration are not explained well by the present calculated results. These phenomena may be due to clusters or spin fluctuations which are not included in this thesis. The calculated result of the high-field

spin susceptibility for Ni-Cu alloys agrees qualitatively with experiment.

In chapter IV, the ferromagnetic or paramagnetic Ni-Pd, Ni-Pt and Pd-Pt alloys have been treated. The off-diagonal randomness has been taken into account. The shapes of the calculated densities of states are similar to each other but their band-width and height change with concentration. The agreement between the calculated results and the experiments for the average and local magnetic moments and the paramagnetic spin susceptibility are satisfactory. However, the calculated results for the low temperature specific heat coefficient are considerably different from the experimental values at the critical concentration and in the paramagnetic region for Ni-Pd and Ni-Pt alloys. This fact may be due to spin fluctuations or clusters.

In chapter V, the densities of states for V-Cr, Nb-Mo and Ta-W alloys have been calculated in CPA and it has been found that their calculated results do not differ much from that of the host metal and consequently the rigid band approximation is not so bad for these alloys. By making use of the calculated results of the densities of states for these alloys, the temperature coefficients of the T^2 term in the series expansion of the paramagnetic spin susceptibility, and the electrical resistivity have been calculated. It has been found that these coefficients depend strongly on the shape of the density of states at the Fermi level and the qualitative agreement between their calculated results and the experimental values shows the validity of the band model.

It has also been found that to explain the observed temperature variation of the magnetic susceptibility the molecular field should be taken into account in Cr rich alloys. By taking into account the molecular field and the temperature independent susceptibility, the temperature variation of the spin susceptibility for Cr has been calculated and a very good agreement with experiment has been obtained.

In chapter VI, the densities of states for Ni-Pt alloys have been calculated in CPA using the realistic density of states of Pt as that of the host metal and the temperature variation of the paramagnetic spin susceptibility has been calculated by assuming a uniform molecular field. The agreement between the calculated results and the observed data for Pt is satisfactory but the agreement for the alloys is qualitatively satisfactory except at very low temperature. It has been found that the slope of the calculated spin susceptibility with respect to temperature is almost independent of the concentration.

It is concluded that qualitative agreement between the calculated and experimental results for the magnetic and thermal properties of these alloys except the critical concentration indicates the validity of the model and of the approximation to treat the randomness for concentrated alloys except in the critical region.

Acknowledgements

The author would like to express his sincere thanks to Professor M. Shimizu for obliging guidance and valuable discussions throughout the course of the present study. He also expresses his thanks to Dr. T. Kato, Dr. I. Takahashi and Dr. Y. Takahashi for their enlightening discussions and constant encouragements.

Appendix. Method of Numerical Calculation of the Green's Function

A numerical method to solve the eqs. (2-5) and (2-8) self-consistently and its program are explained in this Appendix.

The function $\rho^{o}(\varepsilon)$ is approximated by a linear interpolation connecting the points $\rho^{o}(\varepsilon_i)$. Then, the integration in eq. (2-5) is carried out to obtain

$$G(z) = \sum_{i=2}^{n-1} \left(\frac{\rho^{o}_{i+1}-\rho^{o}_{i}}{\varepsilon_{i+1}-\varepsilon_{i}} - \frac{\rho^{o}_{i}-\rho^{o}_{i-1}}{\varepsilon_{i}-\varepsilon_{i-1}} \right) \{z-\Sigma(z)-\varepsilon_i\} \times \ln\{z-\Sigma(z)-\varepsilon_i\}, \qquad (A\text{-}1)$$

where ρ^{o}_{i} is the value of the density of states at ε_i, and ε_2 and ε_{n-1} represent the lowest and highest energy in $\rho^{o}(\varepsilon)$, respectively. The suffix σ is neglected for simplicity. The value G(z) is put into eq. (2-8), which is solved by the Newton Raphson method as follows. The eqs. (2-8) and (A-1) are considered as functions of Σ for each z and a function $f(\Sigma)$ is defined as,

$$f(\Sigma) = \{\Sigma^2-(\varepsilon_A+\varepsilon_B)+\varepsilon_A\varepsilon_B\}G(\Sigma) + \Sigma - (c_A\varepsilon_A+c_B\varepsilon_B). \qquad (A\text{-}2)$$

For an initial value of Σ, the final value of Σ represented as Σ_f is given by

$$\Sigma_f = \Sigma - f(\Sigma)/\frac{df(\Sigma)}{d\Sigma}. \qquad (A\text{-}3)$$

The value of Σ for each z is calculated by iterating eqs. (A-2) and (A-3) using eq. (A-1) and its derivative with respect to Σ until the desired accuracy is obtained. These equations are first solved at an energy sufficiently below the band by using $c_A\varepsilon_A+c_B\varepsilon_B$ as the initial value of Σ to obtain a good first approximation for Σ for successive procedures. At each step, the value of Σ obtained by the proceeding step is used as the initial value for a given value of z. In the program, the procedure to determine the Fermi level is also included.

List of the name for the physical quantities.

A	Value of the density of states for the host band: $\rho^o(\varepsilon)$.
DE	Energy point for the host band: ε.
NDE	Number of energy points: n.
ENA	Electron numbers of pure A metal: n_A^o.
ENB	Electron numbers of pure B metal: n_B^o
DELTA	Potential difference: δ.
CA	Atomic concentration of A metal: c_A.
CB	Atomic concentration of B metal: c_B.
VA	Potential value at A site: ε_A.
VB	Potential value at B site: ε_B.
EL	Lowest energy edge of the host band.
EH	Highest energy edge of the host band.
VV	Average value of the potentials.
H	Energy mesh.
Z	Energy value: z.

EN Average value of the electron numbers.

SC Self-energy: Σ.

GC Green's function: G(z).

DS Average density of states for alloys: $\rho(E)$.

DSA Local density of states for A atom: $\rho_A(E)$.

DSB Local density of states for B atom: $\rho_B(E)$.

ZFE Fermi energy: E_F.

DSFE Value of the density of states at the Fermi level.

ANE Electron numbers of A atom in alloys: n_A.

BNE Electron numbers of B atom in alloys: n_B.

```
      COMPLEX   SC,GC, DG,ZC, SPC,SQC, SRC, SSC
      DIMENSION A(500),DE(500), Z(500),DS(500),DSA(500),DSB(500)
      PAI=3.14159265
      DATA H, ENA,ENB,NDE/0.01,0.86,0,96,7/
      READ(5,100)(A(I),DE(I),I=1,NDE)
  100 FORMAT(6F12.0)
      DELTA=0.5
      CA=0.3
      CB=1-CA
      VA=0
      VB=-DELTA
      VV=CA*VA+CB*VB
      EL=DE(2)
      EH=DE(NDE-1)
      JEL=(0.5*(VA+VB-ABS(VA-VB))+EL)/H
      JEH=(0.5*(VA+VB+ABS(VA-VB))+EH)/H
      JMX=JEH-JEL+10
      DO 5000 J=1,JMX
      Z(J)=(JEL+J-5)*H
      IF(J-1) 10,10,20
   10 SC=VV
      GO TO 30
   20 ZCRT=Z(J)-REAL(SC)
      IF(ZCRT.GE.EL-5*H.AND.ZCRT.LT.EL+5*H) SC=CMPLX(REAL(SC),
     *-0.005)
   30 M=1
   40 CONTINUE
      GC=DG=(0.0,0.0)
      DO 1000 I=2,NDE-1
      ZC=Z(J)-SC-DE(I)
      AH=(A(I+1)-A(I))/(DE(I+1)-DE(I))-(A(I)-A(I-1))/(DE(I)-
     *DE(I-1))
```

```
      GC=GC+AH*ZC*CLOG(ZC)
      DG=DG-AH*CLOG(ZC)
 1000 CONTINUE
      SPC=SC**2-(VA+VB)*SC+VA*VB
      SQC=SPC*GC+SC-VV
      SRC=SPC*DG+(2.0*SC-VA-VB)*GC+1.0
      SSC=SQC/SRC
      SA=ABS(REAL(SSC))
      IF(ABS(REAL(SC)).GE.1.0E-5) SA=ABS(REAL(SSC)/REAL(SC))
      SB=ABS(AIMAG(SSC))
      IF(ABS(AIMAG(SC)).GE.1.0E-5) SB=ABS(AIMAG(SSC)/AIMAG(SC))
      IF(SA.LT.1.0E-5.AND.SB.LT.1.0E-5) GO TO 60
      SC=SC-SSC
      M=M+1
      IF(M-10) 40,40,50
   50 WRITE(6,200)
  200 FORMAT(1H+,125X,3HILL)
   60 CONTINUE
      DSA(J)=-AIMAG(GC/(1.0-(VA-SC)*GC))/PAI
      DSB(J)=-AIMAG(GC/(1.0-(VB-SC)*GC))/PAI
      DS(J)=CA*DSA(J)+CB*DSB(J)
      JM=J-(J/50)*50
      IF(JM) 80,70,80
   70 WRITE(6,300)
  300 FORMAT(1H1,/,5X1HZ12X2HDS11X3HDSA11X3HDSB24X2HGC24X2HSC)
   80 WRITE(6,400) Z(J),DS(J),DSA(J),DSB(J),GC,SC
  400 FORMAT(1H ,4F12.4,2X,2(2F12.5,2X))
 5000 CONTINUE
      EN=CA*ENA+CB*ENB
      SDS=0
      DO 6000 J=2,JMX
      SDSS=SDS+(DS(J)+DS(J-1))*H/2
      IF(SDS.LE.EN AND.SDSS.GE.EN) GO TO 90
      SDS=SDSS
 6000 CONTINUE
   90 CONTINUE
      JF=J
      JFE=J-1
      SSS=EN-SDS
      DDD=DS(JF)-DS(JFE)
      ZZZ=(SQRT((H*DS(JFE))**2+2*DDD*H*SSS)-H*DS(JFE))/DDD
      ZFE=Z(JFE)+ZZZ
      DSFE=DS(JFE)+DDD/H*ZZZ
      AEN=(DSA(1)+DSA(JFE))
      BEN=(DSB(1)+DSB(JFE))
      DO 7000 J=2,JFE-1
      AEN=AEN+DSA(J)
      BEN=BEN+DSB(J)
 7000 CONTINUE
      AEN=AEN*H+DSA(JFE)*ZZZ+0.5*(DSA(JF)-DSA(JFE))*ZZZ**2/H
      BEN=BEN*H+DSB(JFE)*ZZZ+0.5*(DSB(JF)-DSB(JFE))*ZZZ**2/H
      WRITE(6,500) DSFE,AEN,BEN,ZFE
  500 FORMAT(1H ,/,4F12.6,/)
      STOP
      END
```

References

1) J. C. Slater: Phys. Rev. 49 (1936) 537, 931.

2) E. C. Stoner: Proc. Roy. Soc. A165 (1938) 372, A169 (1939) 339.

3) J. Hubbard: Proc. Roy. Soc. A276 (1963) 238, A277 (1964) 237, A281 (1964) 401.

4) J. Friedel: Nuovo Cimento 2 (1958) 287.

5) P. W. Anderson: Phys. Rev. 124 (1961) 41.

6) P. A. Wolff: Phys. Rev. 124 (1961) 1030.

7) N. F. Mott and H. Jones: The Theory of the Properties of Metals and Alloys (Dover, New York 1936).

8) M. Shimizu: Proc. 3rd. IMR Symposium, Electronic Density of States, NBS Spec. Publ. 323 (1970) 685. This paper contains references of a series of papers.

9) P. Soven: Phys. Rev. 156 (1967) 809.

10) D. W. Taylor: Phys. Rev. 156 (1967) 1017.

11) Y. Onodera and Y. Toyozawa: J. Phys. Soc. Japan 24 (1968) 341.

12) F. Yonezawa: Prog. Theor. Phys. 40 (1968) 734.

13) P. L. Leath: Phys. Rev. 171 (1968) 725.

14) B. Velicky, S. Kirkpatrick and H. Ehrenreich: Phys. Rev. 175 (1968) 747.

15) M. Tsukada: J. Phys. Soc. Japan 26 (1969) 684, 32 (1972) 1475, K. F. Freed and M. H. Cohen: Phys. Rev. B3 (1971) 3400, B. G. Nickel and J. A. Krumhansel: Phys. Rev. B4 (1971) 4354, W. H. Butler: Phys. Rev. B8 (1973) 4499, I. Takahashi and M. Shimizu: Phys.

Letters 33A (1970) 441, Prog. Theor. Phys. 51 (1974) 1678, 53 (1975) 41.

16) R. J. Elliott, J. A. Krumhansel and P. L. Leath: Rev. Mod. Phys. 46 (1974) 465.

17) J. A. Blackman, D. M. Esterling and N. F. Berk: Phys. Rev. B4 (1971) 2412.

18) H. Shiba: Prog. Theor. Phys. 46 (1971) 77.

19) F. Brouers: Solid State Commun. 10 (1972) 757.

20) S. Kirkpatrick, B. Velicky and H. Ehrenreich: Phys. Rev. B1 (1970) 3250.

21) G. M. Stocks, R. W. Williams and J. Faulkner: Phys. Rev. B4 (1971) 4390.

22) G. M. Stocks, R. W. Williams and J. Faulkner: J. Phys. F: Metal Phys. 3 (1973) 1688.

23) J. Yamashita, S. Wakoh and S. Asano: J. Phys. Soc. Japan 31 (1971) 1620.

24) J. Yamashita, S. Asano and S. Wakoh: Prog. Theor. Phys. 47 (1972) 774.

25) H. Hasegawa and J. Kanamori: J. Phys. Soc. Japan 31 (1971) 382, 33 (1972) 1599, 1607.

26) F. Brouers and A. V. Vedyayev: Phys. Letters 40A (1972) 77.

27) K. Levin, R. Bass and K. H. Bennemann: Phys. Rev. B6 (1972) 1865.

28) M. Shimizu and S. Hirooka: Phys. Letters 27A (1968) 530.

29) E. I. Zornberg: Phys. Rev. B1 (1970) 244.

30) C. G. Shull and M. K. Wilkinson: Phys. Rev. 97 (1955) 304.

31) M. F. Collins, R. V. Jones and R. D. Lowde: J. Phys. Soc. Japan 17 B-III (1962) 19.

32) K. P. Gupta, C. H. Cheng and P. A. Beck: J. Phys. Chem. Solid 25 (1964) 73.

33) S. A. Ahern, M. J. C. Martin and W. Sucksmith: Proc. Roy. Soc. A248 (1958) 145.

34) A. T. Aldred, B. D. Rainford, T. J. Hicks and J. S. Kouvel: Phys. Rev. B7 (1973) 218.

35) Y. Ito and J. Akimitsu: J. Phys. Soc. Japan 35 (1973) 1000.

36) J. W. Cable, E. O. Wollan and H. R. Child: Phys. Rev. Letters 22 (1969) 1256.

37) C. G. Robbins, H. Claus and P. A. Beck: Phys. Rev. Letters 22 (1969) 1307.

38) J. P. Perrier, B. Tissier and R. Tournier: Phys. Rev. Letters 24 (1970) 313.

39) V. Jaccarino and L. R. Walker: Phys. Rev. Letters 15 (1965) 258.

40) K. P. Gupta, C. H. Cheng and P. A. Beck: Phys. Rev. 133 (1964) A203.

41) C. G. Robbins, H. Claus and P. A. Beck: J. Appl. Phys. 40 (1969) 2269.

42) F. Acher and R. Huguenin: Phys. Letters 38A (1972) 343.

43) D. K. Ghosh and P. Bhattacharyya: Phys. Rev. B11 (1975) 2642.

44) J. Callaway and C. S. Wang: Phys. Rev. B7 (1973) 1096.

45) S. Wakoh and J. Yamashita: J. Phys. Soc. Japan 19 (1964) 1342.

46) A. J. P. Meyer and G. Asch: J. Appl. Phys. 32 (1961) 330S.

47) E. P. Wohlfarth: Proc. Int. Conf. Mag. Nottingham (1964) 51.

48) H. A. Mook: Phys. Rev. 148 (1966) 495.

49) F. Heiniger, E. Bucher and J. Muller: Phys. kondens. Materie 5 (1966) 243.

50) M. Dixson, F. E. Hoare and T. M. Holden: Proc. Roy. Soc. A303 (1968) 339.

51) S. Foner, A. J. Freeman, N. A. Blum, R. B. Frankel, E. J. McNiff, Jr. and H. C. Praddaude: Phys. Rev. 181 (1969) 863.

52) F. Acher: private communication to M. S.

53) V. E. Rode, A. Blyushke, S. A. Finkel'berg and A. I. Leichenko: Soviet. Physics. JETP 35 (1972) 568.

54) S. Hirooka and M. Shimizu: Phys. Letters 46A (1973) 209.

55) N. D. Lang and H. Ehrenreich: Phys. Rev. 168 (1968) 605.

56) S. Kirkpatrick, B. Velicky, N. D. Lang and H. Ehrenreich: J. Appl. Phys. 40 (1969) 1283.

57) R. Harris and M. J. Zuckermann: Phys. Rev. B5 (1972) 101.

58) T. Kato and M. Shimizu: J. Phys. Soc. Japan 33 (1972) 363.

59) R. Alben and E. P. Wohlfarth: Phys. Letters 49A (1974) 271.

60) J. J. Vuilleman and M. G. Priestly: Phys. Rev. Letters

14 (1965) 307.

61) G. S. Knapp and R. W. Jones: Phys. Rev. B6 (1972) 1761.

62) M. Gibson, D. E. Moody and R. Stevens: J. de Phys. suppl. 32 (1971) C1-990

63) S. Kobayashi, H. Launois, P. Lederer, C. Froideaux, W. Treutmann and E. Vogt: Solid State Commun. 6 (1968) 265.

64) F. M. Mueller, J. W. Garland, M. H. Cohen and K. H. Bennemann: Ann. Phys. 67 (1971) 19.

65) G. Chouteau, R. Fourneaux, K. Gobrecht and R. Tournier: Phys. Rev. Letters 20 (1968) 193.

66) G. Fischer, A. Herr and A. J. P. Meyer: J. Appl. Phys. 39 (1968) 545.

67) C. Sadron: Ann. Phys. (paris) 17 (1932) 371.

68) J. Crangle and W. R. Scott: J. Appl. Phys. 36 (1965) 921.

69) J. W. Cable and H. R. Child: Phys. Rev. B1 (1970) 3809.

70) E. P. Wohlfarth: J. de Phys. suppl. 32 (1971) C1-636.

71) H. Kimura, A. Katsuki and M. Shimizu: J. Phys. Soc. Japan 21 (1966) 307.

72) A. I. Schindler and C. A. Mackliet: Phys. Rev. Letters 20 (1968) 15.

73) D. Shaltiel, J. H. Wernick, H. J. Williams and M. Peter: Phys. Rev. 135 (1964) A1346.

74) C. A. Mackliet and A. I. Schindler: J. Phys. Chem. Solids. 24 (1963) 1639.

75) V. Marian: Ann. Phys. 7 (1973) 514.

76) G. Fisher and M. J. Besnus: Solid State Commun. 7 (1969)

1527.

77) M. J. Besnus and A. Herr: Phys. Letters 39A (1972) 83.

78) H. L. Alberts, J. Beille, D. Bloch and E. P. Wohlfarth: Phys. Rev. B9 (1974) 2233.

79) D. J. Gillespie, C. A. Mackliet and A. I. Schindler: Boulder conf. Low Temp. Phys. (1972).

80) G. Chouteau: Thesis, University of Grenoble (1973).

81) C. A. Mackliet, A. I. Schindler and D. J. Gillespie: Phys. Rev. B1 (1970) 3283.

82) J. Beille, D. Bloch and R. Kuentzler: Solid State Commun. 14 (1974) 963.

83) J. Kanamori: Prog. Theor. Phys. 30 (1963) 275.

84) L. Hodges, R. E. Watson and H. Ehrenreich: Phys. Rev. B5 (1972) 3953.

85) R. J. Jacobs and N. Zaman: ICM, Amsterdam (1976).

86) T. Aisaka and M. Shimizu: J. Phys. Soc. Japan 28 (1970) 646.

87) M. Shimizu and M. Sakoh: J. Phys. Soc. Japan 36 (1974) 1000.

88) H. Kojima, R. S. Tebble and D. E. G. Williams: Proc. Roy. Soc. A260 (1961) 237.

89) S. Taniguchi, R. S. Tebble and D. E. G. Williams: Proc. Roy. Soc. A265 (1962) 502.

90) J. C. H. Chiu: Phys. Rev. B13 (1976) No. 4. 1507.

91) L. Thomas: Z. Metallkunde 56 (1968) 127.

92) J. W. Connolly: Proc. 3rd. IMR Symposium, Electronic Density of States, NBS Spec. Publ. 323 (1970) 27.

93) L. F. Mattheiss: Phys. Rev. B1 (1970) 373.

94) I. Petroff and C. R. Viswanathan: Proc. 3rd. IMR Symposium, Electronic Density of States, NBS Spec. Publ. 323 (1970) 53.

95) D. A. Papaconstantopouls, J. R. Anderson and J. W. McCaffrey: Phys. Rev. B5 (1972) 1214.

96) V. W. D. Weiss and R. Kohlhaas: Z. Naturforschg. 19a (1964) 1631.

97) K. H. Oh, B. N. Harman, S. H. Liu and S. K. Sinha: Phys. Rev. B14 (1976) 1283.

98) J. Beille, D. Bloch and M. J. Besnus: J. Phys. F: Metal Phys. 4 (1974) 1.

99) D. W. Budworth, F. E. Hoare and J. Preston: Proc. Roy. Soc. A257 (1960) 250.

100) C. Manders: Ann. Phys. Paris 11 (1936) 167.

101) S. Arajs and R. V. Colvin: J. Phys. Chem. Solids 24 (1963) 1233.

Table I. Calculated values of average and local magnetic moments and low temperature specific heat coefficient for Fe-Ni alloys.

concen. Ni at.%	m μ_B/Atom	m_{Fe} μ_B/Atom	m_{Ni} μ_B/Atom	$10^4\gamma$ cal/mol K^2
100	0.60	——	0.60	10.44
95	0.72	3.25	0.58	9.35
90	0.84	3.22	0.56	9.25
80	1.09	3.13	0.53	6.05
70	1.26	2.96	0.55	5.32
60	1.49	2.84	0.58	5.58
50	1.71	2.78	0.62	5.97
45	1.81	2.78	0.65	6.60
40	1.92	2.75	0.65	8.94
35	1.99	2.71	0.66	11.33
30	2.03	2.61	0.64	14.42

Table II. Calculated values of average and local magnetic moments, low temperature specific heat coefficient and high-field spin susceptibility for ferromagnetic Ni-Cu alloys. g=2.18

concen. Ni at.%	mg/2 μ_B/Atom	$m_{Ni}g/2$ μ_B/Atom	$m_{Cu}g/2$ μ_B/Atom	$10^4\chi_s$ emu/mol	$10^4\gamma$ cal/mol K^2
100	0.606	0.606	———	0.748	14.10
90	0.499	0.554	0.0052	0.933	13.34
80	0.399	0.496	0.0112	1.260	12.42
70	0.295	0.419	0.0064	1.860	11.71
65	0.244	0.371	0.0059	2.494	11.25
60	0.190	0.314	0.0035	3.629	10.87
55	0.133	0.240	0.0028	6.518	10.45
50	0.072	0.143	0.0013	16.879	9.86

Table III. Calculated values of average and local magnetic moments, low temperature specific heat coefficient and paramagnetic spin susceptibility for Ni-Pd alloys.

$g_{Ni}=2.18$, $g_{Pd}=2.0$

concen. Ni at.%	$\langle mg/2 \rangle$ μ_B/Atom	$m_{Ni}g_{Ni}/2$ μ_B/Atom	$m_{Pd}g_{Pd}/2$ μ_B/Atom	γ mJ/mol K^2	$10^4\chi$ emu/mol
100	0.606	0.606	——	7.1	——
90	0.586	0.621	0.273	7.06	——
80	0.562	0.634	0.274	6.99	——
70	0.538	0.650	0.276	6.90	——
60	0.513	0.669	0.279	6.84	——
50	0.487	0.692	0.282	7.08	——
40	0.455	0.714	0.282	7.39	——
30	0.415	0.735	0.278	7.80	——
20	0.357	0.744	0.261	8.35	——
15	0.315	0.733	0.241	8.72	——
10	0.255	0.696	0.206	9.11	——
5	0.152	0.555	0.130	9.51	——
2	——	——	——	9.68	74.49
1.5	——	——	——	9.64	25.02
1.0	——	——	——	9.60	14.54
0.5	——	——	——	9.57	9.95
0.0	——	——	——	9.53	7.36

Table IV. Calculated values of average and local magnetic moments, low temperature specific heat coefficient and paramagnetic spin susceptibility for Ni-Pt alloys.

$g_{Ni}=2.18$, $g_{Pt}=2.0$

concen. Ni at.%	$\langle mg/2 \rangle$ μ_B/Atom	$m_{Ni}g_{Ni}/2$ μ_B/Atom	$m_{Pt}g_{Pt}/2$ μ_B/Atom	γ mJ/mol K^2	$10^4\chi$ emu/mol
100	0.606	0.606	——	7.1	——
90	0.578	0.596	0.423	7.06	——
80	0.541	0.572	0.416	7.66	——
70	0.484	0.525	0.390	8.37	——
60	0.405	0.447	0.340	8.98	——
50	0.284	0.319	0.249	9.48	——
45	0.177	0.199	0.158	9.47	——
40	——	——	——	9.24	51.49
35	——	——	——	8.83	14.24
30	——	——	——	8.44	8.22
25	——	——	——	8.08	5.75
20	——	——	——	7.74	4.39
15	——	——	——	7.42	3.53
10	——	——	——	7.12	2.94
5	——	——	——	6.84	2.50
0	——	——	——	6.57	2.16

Table V. Calculated values of low temperature specific heat coefficient and paramagnetic spin susceptibility for Pd-Pt alloys.

concen. Pd at.%	γ mJ/mol K^2	$10^4\chi^*$ emu/mol	$10^4\chi^{**}$ emu/mol
0	6.57	2.16	1.73
10	6.62	2.44	1.89
20	6.65	2.72	2.06
30	6.68	3.04	2.23
40	6.72	3.37	2.41
50	6.80	3.72	2.62
60	6.95	4.21	2.89
70	7.21	4.88	3.31
80	7.64	5.77	3.94
90	8.34	6.92	5.07
100	9.53	7.36	7.36

* U_{Pt}=0.849eV

** U_{Pt}=0.774eV

Table VI. Calculated values of $\chi(T)$ for Cr, where the molecular field coefficient $\alpha=2.5518\times10^{4}$ mol/emu and the temperature independent susceptibility $\chi_c=0.8678\times10^{-4}$ emu/mol are assumed.

T K	$10^4\chi(T)$ emu/mol	T K	$10^4\chi(T)$ emu/mol
0	1.6727	1000	1.8680
100	1.6696	1100	1.9053
200	1.6707	1200	1.9447
300	1.6785	1300	1.9863
400	1.6940	1400	2.0298
500	1.7149	1500	2.0755
600	1.7402	1600	2.1232
700	1.7685	1700	2.1729
800	1.7995	1800	2.2247
900	1.8327	1900	2.2780
		2000	2.3330

Table VII. Calculated values of $1/\chi_o(T)-\alpha$ (10^2 mol/emu) for Ni-Pt alloys.

T K \ concen. Ni at.%	0.0	24.1	32.6	42.9	90.9
0	48.00	7.38	2.78	——	——
100	50.62	9.80	5.20	2.08	——
200	54.10	13.06	8.46	5.35	——
300	57.53	16.48	11.91	8.85	——
400	61.12	20.11	15.57	12.54	——
500	64.83	23.82	19.28	16.24	——
600	68.56	27.48	22.91	19.84	2.00
700	72.24	31.04	26.43	23.30	5.21
800	75.82	34.48	29.82	26.63	8.29
900	79.30	37.80	33.09	29.84	11.26
1000	82.68	41.02	36.25	32.95	14.15
1100	85.96	44.14	39.33	35.97	16.98
1200	89.15	47.18	42.33	38.92	19.75
1300	92.26	50.16	45.27	41.82	22.47
1400	95.32	53.09	48.16	44.66	25.15
1500	98.32	55.98	51.01	47.47	27.79
1600	101.29	58.83	53.83	50.25	30.40
1700	104.23	61.66	56.62	53.01	32.97
1800	107.14	64.48	59.40	55.75	35.52
1900	110.04	67.28	62.17	58.48	38.04
2000	112.94	70.08	64.94	61.20	40.53

Figure Captions

Fig. 1. Slater-Pauling curve. The dependence of the saturated moment on the number of electrons per atom is shown.

▼ Ni-Zn, □ Ni-Co, ○ Ni-Fe, △ Ni-Cu,
○ Ni-Mn, ◇ Ni-Cr, ▽ Ni-V, ● Co-Fe,
0 Co-Mn, ▲ Co-Cr, + Fe-Cr, ● Fe-V,
⊗ pure metal.

Fig. 2. Density of states for Ni taken as that of the host band. The density of states for s-band is cut off. The density of states is scaled so that the whole number of states is normalized as 1 and the band-width is reduced as 2. The vertical line shows the Fermi level for the paramagnetic state.

Figs. 3-11. Calculated results of the densities of states for the paramagnetic fcc Fe-Ni alloys. The value of x denotes the atomic concentration of Fe. In this calculation, the Coulomb interaction is neglected and the value of δ_0 is 0.32. Each vertical line shows the Fermi level.

Figs. 12-21. Calculated results of the densities of states for the ferromagnetic fcc Fe-Ni alloys. The values of δ and U are 0.603 and 1.3, respectively. The value of x denotes the atomic concentration of Fe. Majority and minority spin states are indicated by $\uparrow$ and $\downarrow$, respectively.

Fig. 22. Calculated results of the concentration variations of the average and local numbers of electrons for each spin per atom per band.

Fig. 23. Calculated results (solid curves) of the average and local magnetic moments per atom for the ferromagnetic fcc Fe-Ni alloys. The experimental values are shown by ○ [30] and △ [31].

Fig. 24. Concentration variation of the low temperature specific heat coefficient γ. A solid curve is the calculated result and a broken curve is the experimental one. [32]

Fig. 25. Density of states for pure Ni. The histogram is the calculated result of Wakoh and Yamashita [45] and the solid curve is the simplified density of states used in the calculation for Ni-Cu alloys. The broken line denotes the Fermi level in the paramagnetic state and the chained lines denote that in the ferromagnetic state.

Figs. 26-32. Densities of states for the ferromagnetic Ni-Cu alloys. Curve 1 is the average density of states and curves 2 and 3 are the local densities of states for Ni and Cu atoms, respectively. The vertical line shows the Fermi level. Majority and minority spin states are indicated by $\uparrow$ and $\downarrow$, respectively.

Figs. 33-38. Densities of states for paramagnetic Ni-Cu alloys. Curve 1 is the average density of states and curve 2 and 3 are the local densities of states for Ni and Cu atoms, respectively. The vertical line shows the Fermi level.

Fig. 39. Magnetic moments for Ni-Cu alloys. Curve 1, 2 and 3 are the calculated results of average magnetic moment and local magnetic moments of Ni and Cu atoms. ●,[33] ○,[34] △,[35] and □[36] are the experimental data.

Fig. 40. Low temperature specific heat coefficient of Ni-Cu alloys. Curve 1 is the calculated result from the density of states with the conduction band and curve 2 is that from the density of states without the conduction band. Curve 3 is the calculated result by Stocks et al.[21] ○,[41] ●[49] and □[50] are the experimental data.

Fig. 41. High-field spin susceptibility of Ni-Cu alloys. Solid curve is the calculated result by CPA and broken curve is the calculated result by the rigid band model[54] and ○,[42] □,[52] ◇[51] and ●[53] are the experimental data.

Fig. 42. Density of states used as that of the host band in the calculation for Ni-Pd, Ni-Pt and Pd-Pt alloys. The band-width is reduced as 2 and the density of states is scaled so as to normalize the total numbers of state as 1.

Figs. 43-51. Average (curve 1) and local (curve 2 for Ni and curve 3 for Pt) densities of states for paramagnetic Ni-Pt alloys. The vertical line shows the Fermi level.

Fig. 52. Dependence of the average (solid curves) and local (broken curves for A atom and chained curves for B atom) densities of states for A_{60}-B_{40} alloys on the ratio of the band-width W_B to that of A metal. The band-width of A (Ni) metal is reduced to 2. The value of δ_o is 0.3 times the band-width of Ni.

Figs. 53-61. Average (curve 1) and local (curve 2 for Ni and curve 3 for Pd) densities of states for ferromagnetic Ni-Pd alloys. Majority and minority spin states are indicated by $\uparrow$ and $\downarrow$, respectively. The vertical line shows the Fermi level.

Fig. 62. Average (curve 1) and local (curve 2 for Ni and curve 3 for Pd) densities of states for a paramagnetic Ni-Pd alloy. The vertical line shows the Fermi level.

Fig. 63. Calculated results of the average (curve 1) and local (curve 2 for Ni and curve 3 for Pd) magnetic moments for Ni-Pd alloys. The experimental data of the average moments are indicated by ●,[66] ■,[67] ▲,[68] ▼,[65] and ◇.[69] Those[69] of the local moments are indicated by ○, □ for Ni and ▽, △ for Pd. The data indicated by ○ and △ are obtained by neutron diffuse scattering and □ and ▽ by

neutron Bragg scattering.

Fig. 64. Calculated result (solid curve) and the experimental data (□,[63] ●,[65] ○[72] and △[73]) of the inverse of the paramagnetic spin susceptibility for Ni-Pd alloys.

Fig. 65. Calculated result (solid curve) and the experimental data (◇,[62] □,[49] ●,[72] □,[73] ○[74] and △[65]) of γ for Ni-Pd alloys.

Figs. 66-70. Average (curve 1) and local (curve 2 for Ni and curve 3 for Pt) densities of states for ferromagnetic Ni-Pt alloys. Majority and minority spin states are indicated by $\uparrow$ and $\downarrow$. The vertical line shows the Fermi level.

Fig. 71. Calculated results of the average (curve 1) and local magnetic moments (curve 2 for Ni and curve 3 for Pt) and the inverse of the paramagnetic spin susceptibility (curve 4) for Ni-Pt alloys. △,[75] ○,[76] □[77] and ◇[78] are the experimental data of m and ▲,[77] ■[79] and ●[80] are those of χ^{-1}.

Fig. 72. Calculated results (solid curve) and the experimental data (○,[79] ●,[81] □,[82] ■[49] and △[62]) of γ for Ni-Pt alloys.

Figs. 73-81. Average (curve 1) and local (curve 2 for Pd and curve 3 for Pt) densities of states for Pd-Pt alloys.

The vertical line shows the Fermi level.

Fig. 82. Calculated result (solid curve) for U_{Pt}=0.849 eV and the experimental data ●[62] of γ for Pd-Pt alloys.

Fig. 83. Calculated results (solid curve for U_{Pt}=0.849 eV and broken curve for U_{Pt}=0.774 eV) and the experimental data (●[62] and ○[63]) of χ for Pd-Pt alloys.

Fig. 84. Calculated results for the concentration variation of the number of d-holes at A or B atom in A-B alloys, for Ni-Pd (solid curves), Ni-Pt (chained curves) and Pd-Pt (broken curves).

Fig. 85. (a); Dependences of the numbers of electrons at A and B sites, n_A (broken curves) and n_B (solid curves), on the potential difference δ_o and on the ratio of the band-width W_B to that of A metal. (b); Relation between W_B and δ_o when n_A=n_B (solid line) and n_A=9.44 and n_B=9.7 (broken line).

Fig. 86. Densities of states for pure Cr and V-Cr alloys. The vertical line shows the Fermi level.

Fig. 87. Densities of states for pure Nb and Nb-Mo alloys. The vertical line shows the Fermi level.

Fig. 88. Densities of states for pure W and Ta-W alloys. The vertical line shows the Fermi level.

Fig. 89. Calculated and experimental values of $A=3\nu_1^2-\nu_2$. Thick solid, chained and broken curves are the calculated results for Cr based V-Cr, Nb based Nb-Mo and W base Ta-W alloys, respectively, and fine solid and broken curves for V based V-Cr and Ta base Ta-W alloys, respectively. Small circles and squares are the experimental values for V-Cr,[90] and Ta-W[91] alloys, respectively.

Fig. 90. Calculated and experimental values of $B=\nu_1^2-\nu_2$. The notation for five curves is the same as that shown in Fig. 89. Small cicles, triangles and squares are the experimental values[88,89] for V-Cr, Nb-Mo and Ta-W alloys, respectively.

Fig. 91. Temperature dependence of X for Cr. Solid curve is the calculated result and small circles are the observed values.[96]

Fig. 92. Calculated density of states by Mueller et al.[64] for Pt. A vertical solid line shows the Fermi level obtained a priori calculation by Mueller et al. and a chained line is that used in chapter VII.

Figs. 93-96. Average (curve 1) and local (curve 2 for Ni and curve 3 for Pt) densities of states for paramagnetic

Ni-Pt alloys. The density of states for Pt shown in Fig. 92 was used as that of the host band.

Fig. 97. Calculated (solid and broken curves) and observed ($\circ$,[98] $\bullet$,[99] $\square$,[88] $\blacktriangle$,[100] $\triangle$[101]) temperature variation of 1/X(T) for Pt, Ni and Ni-Pt alloys. Solid curves 1, 2, 3, 4 and 5 are the calculated results for Pt, 24.1, 32.6, 42.9, and 90.9 at.% Ni-Pt, and broken curves 6 and 7 are the ones for 90.9 at.% Ni-Pt and Ni, respectively. Insert is the enlargement of the low temperature results.

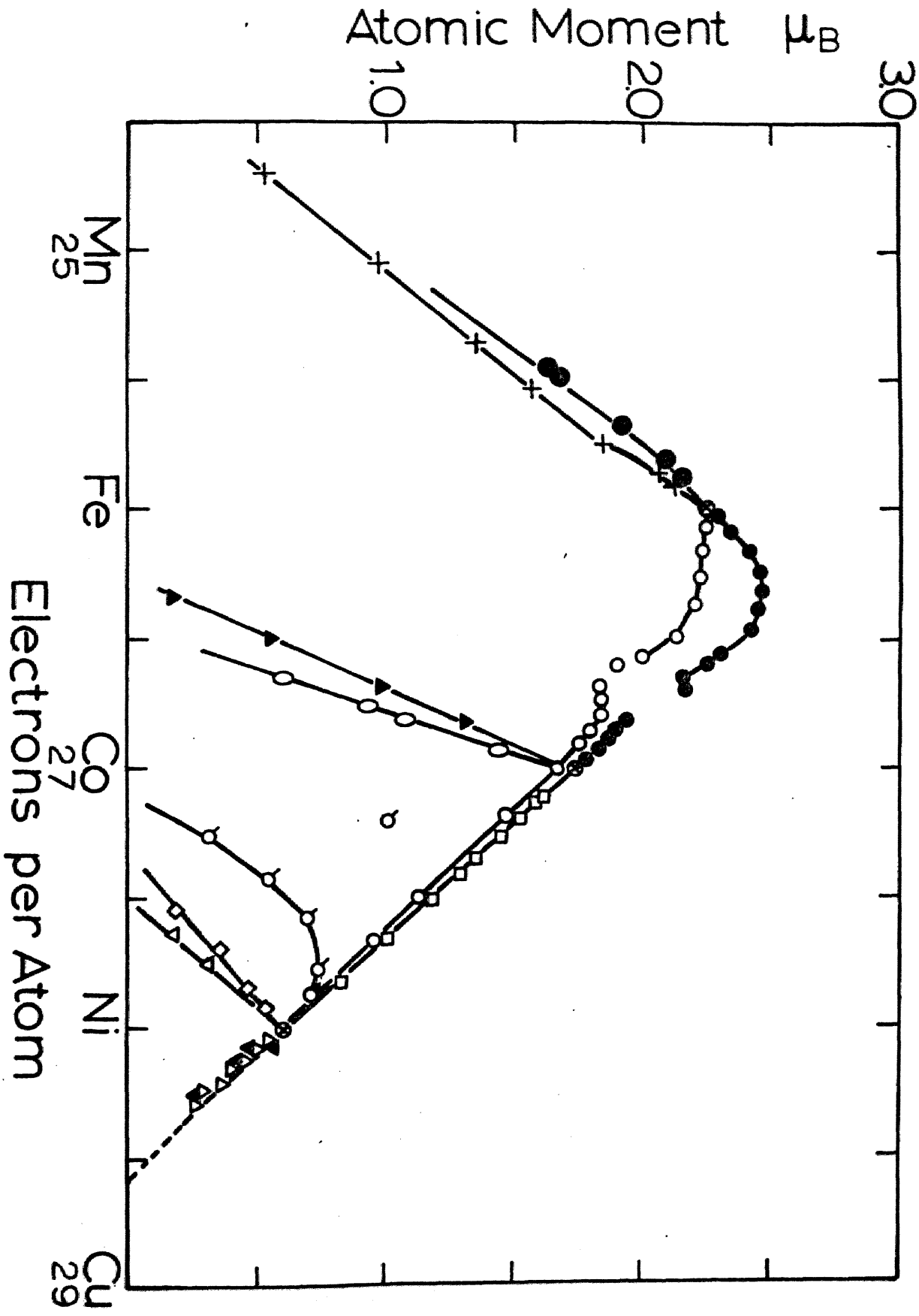
Atomic Moment μ_B
1.0
2.0
3.0
Mn
25
Fe
Co
27
Ni
Cu
29
Electrons per Atom

Fig. 1

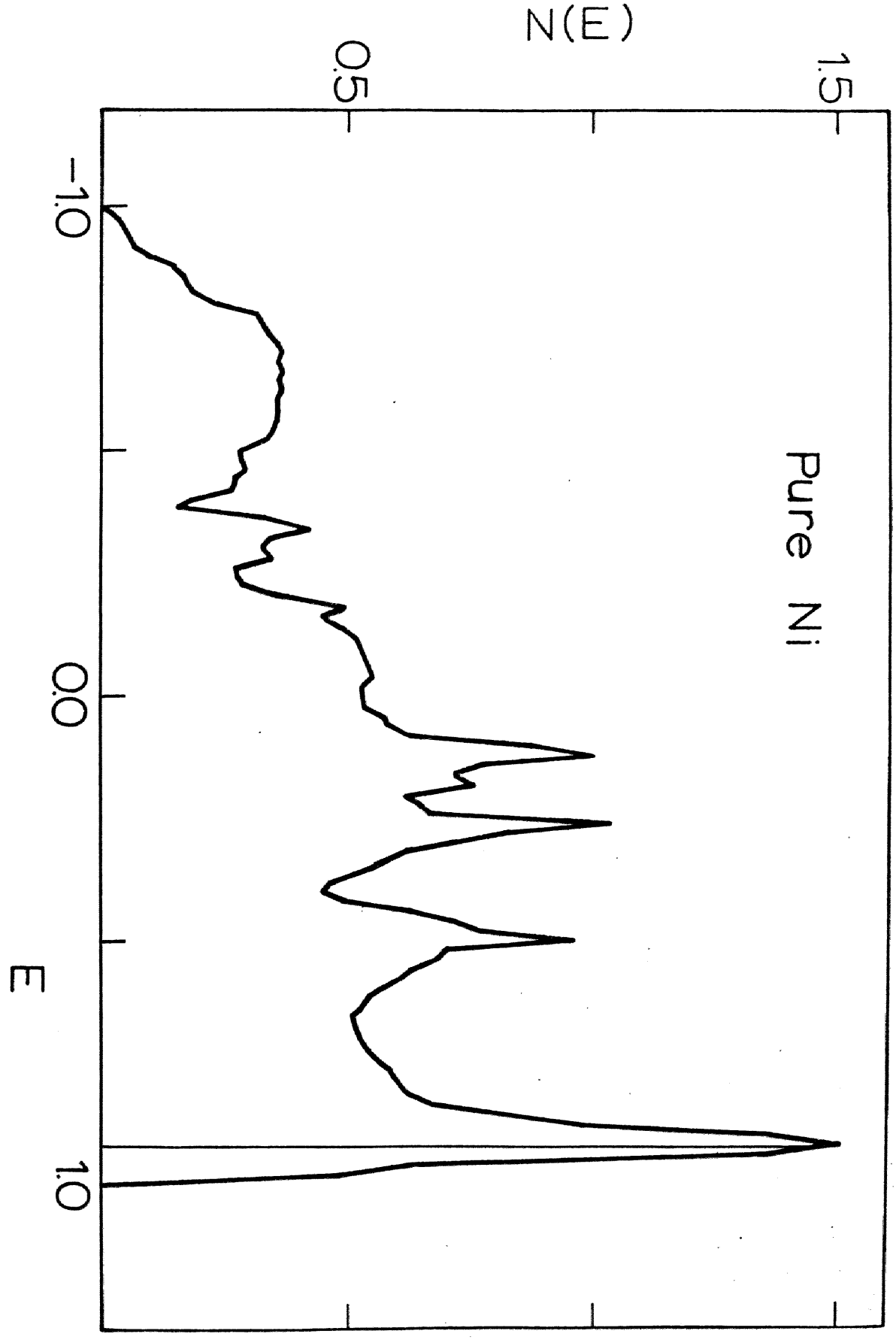

Fig. 2

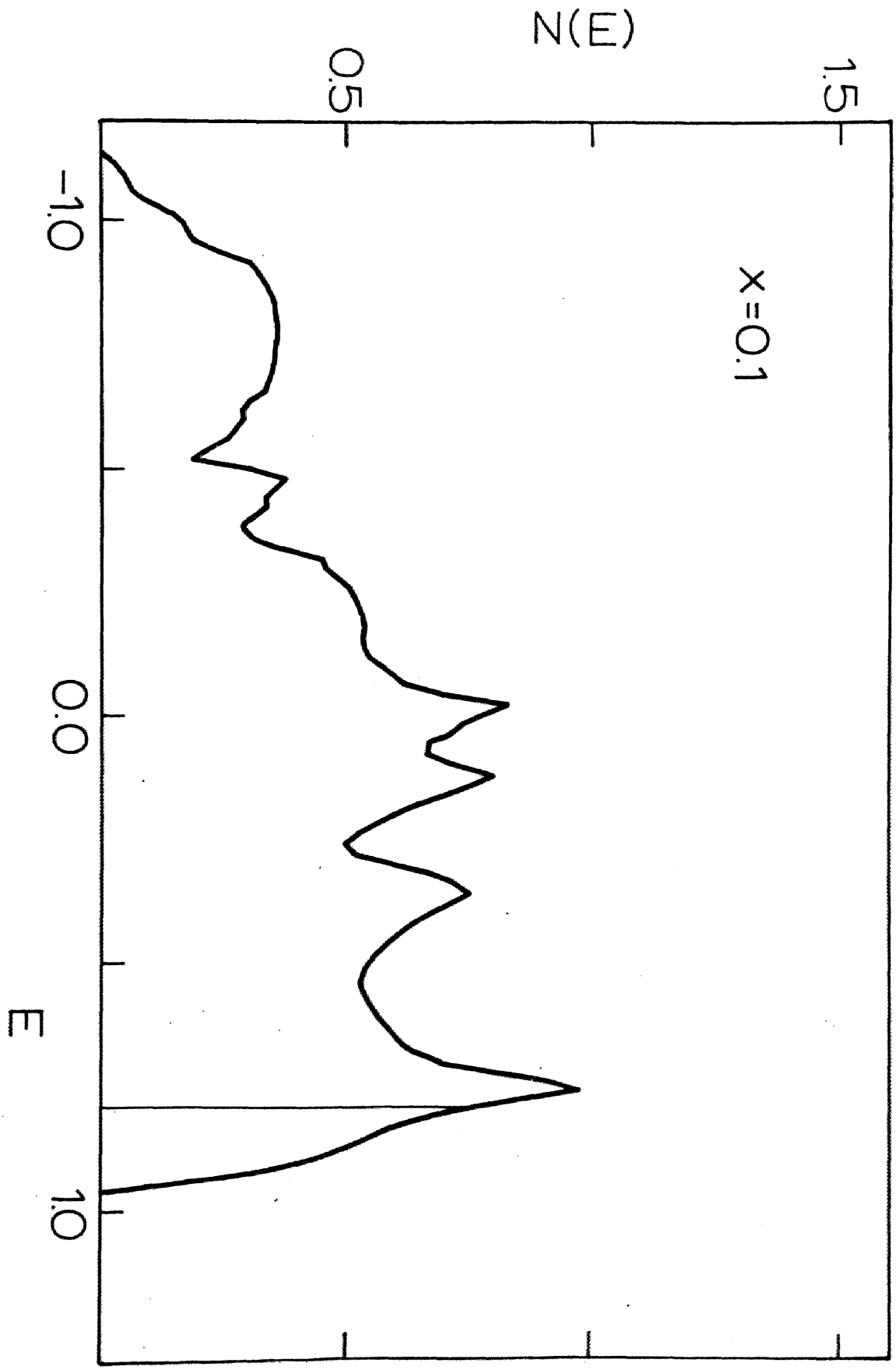

Fig. 3

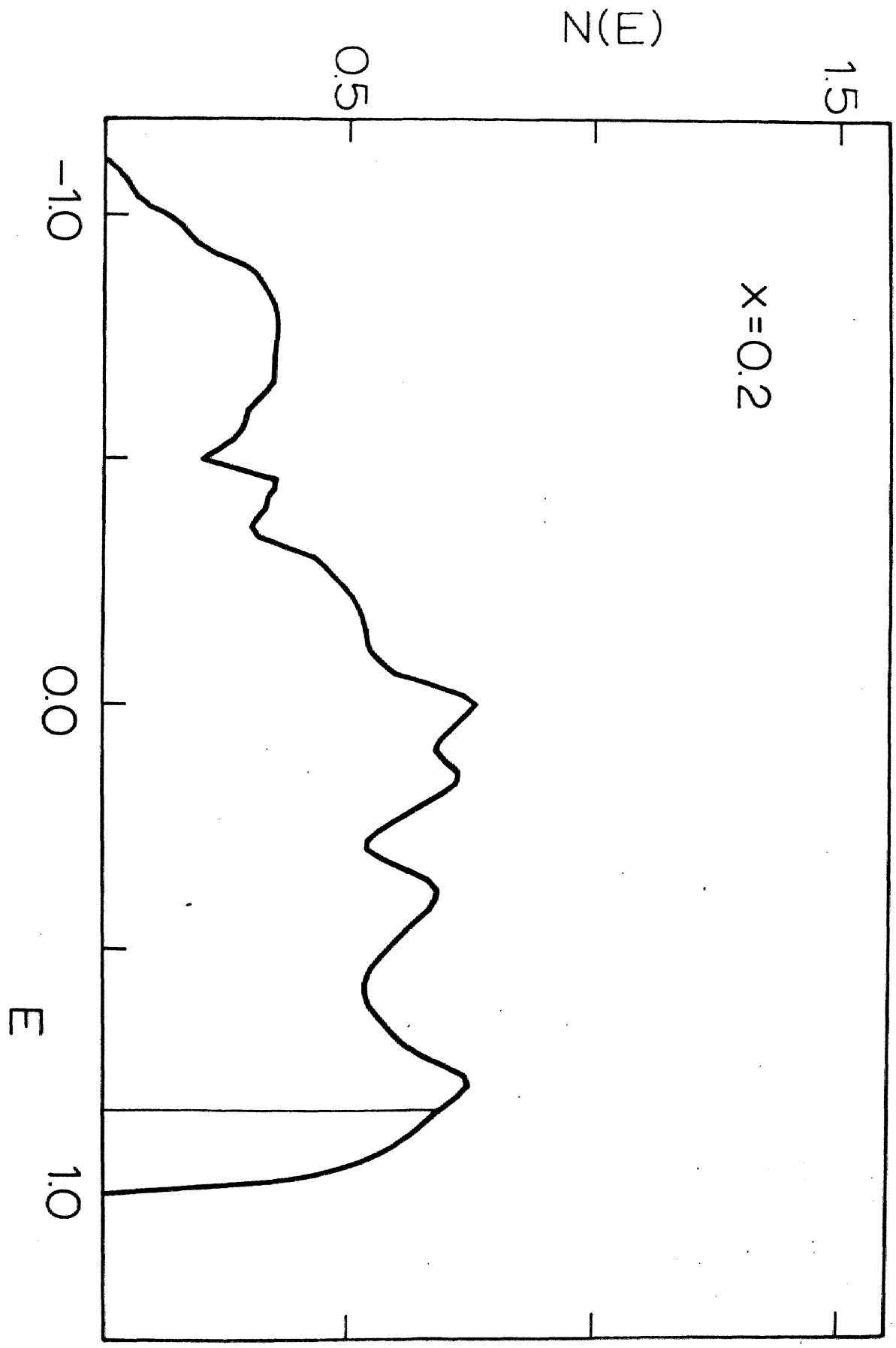

Fig. 4

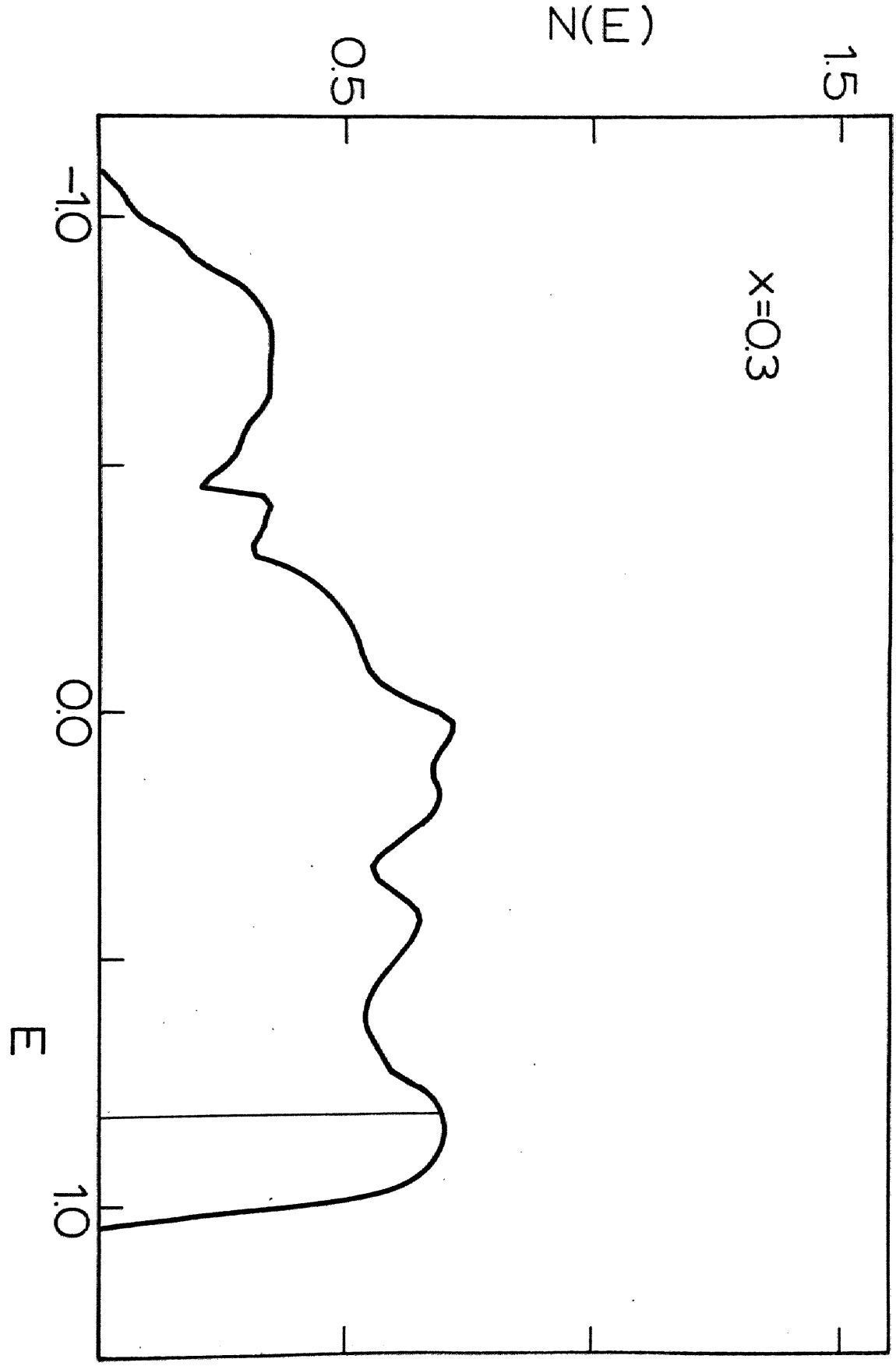

Fig. 5

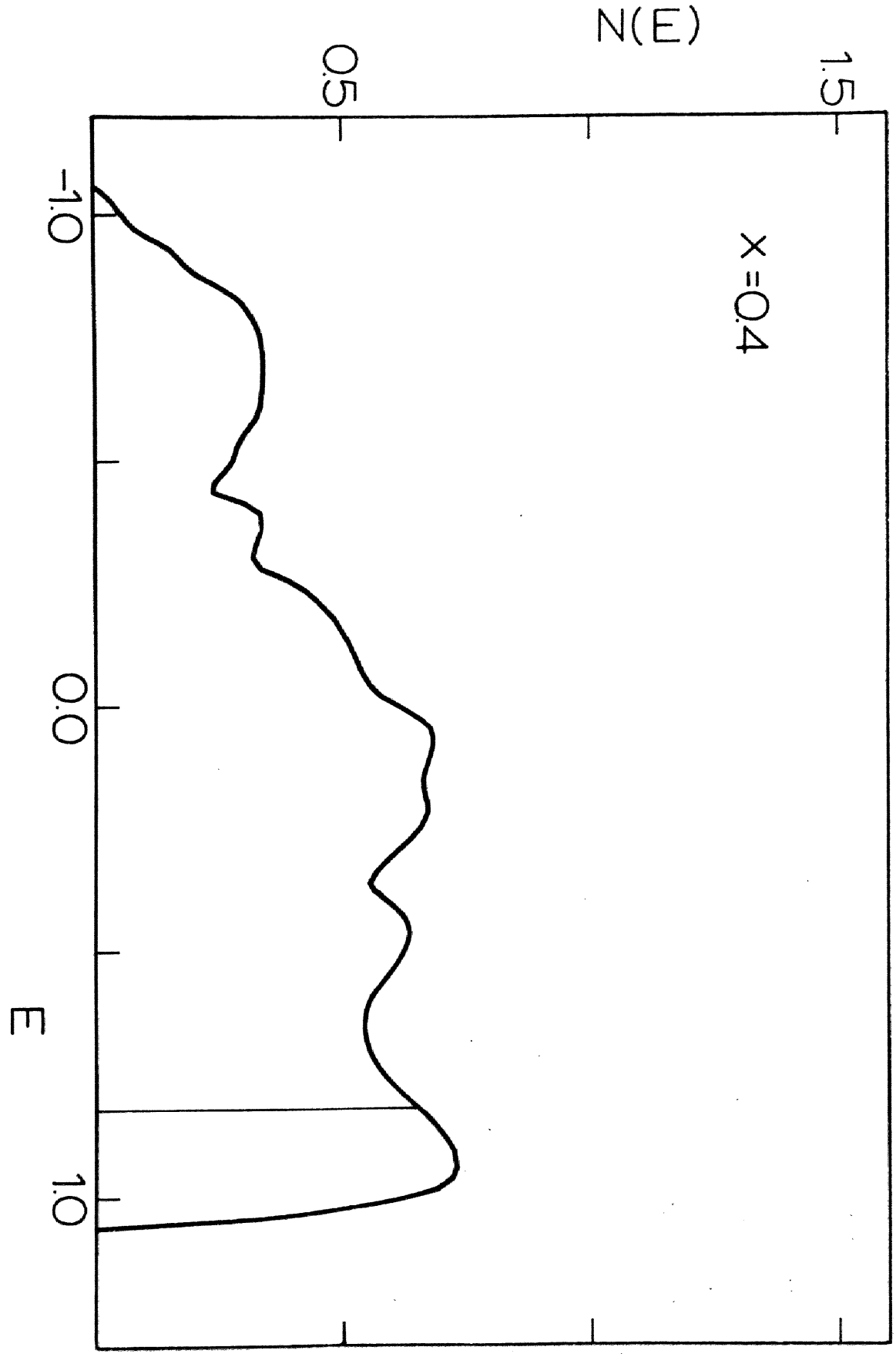

Fig. 6

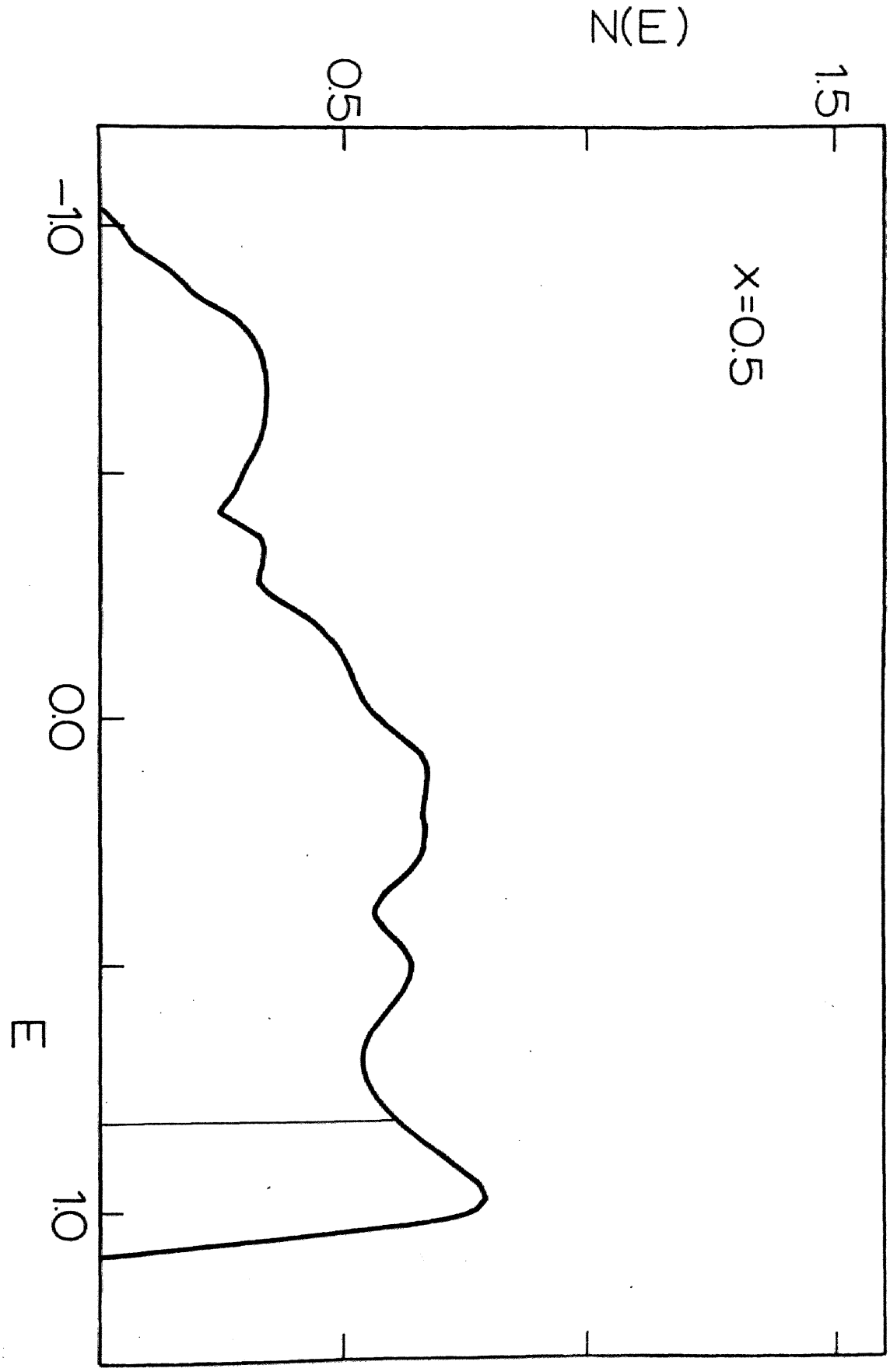

Fig. 7

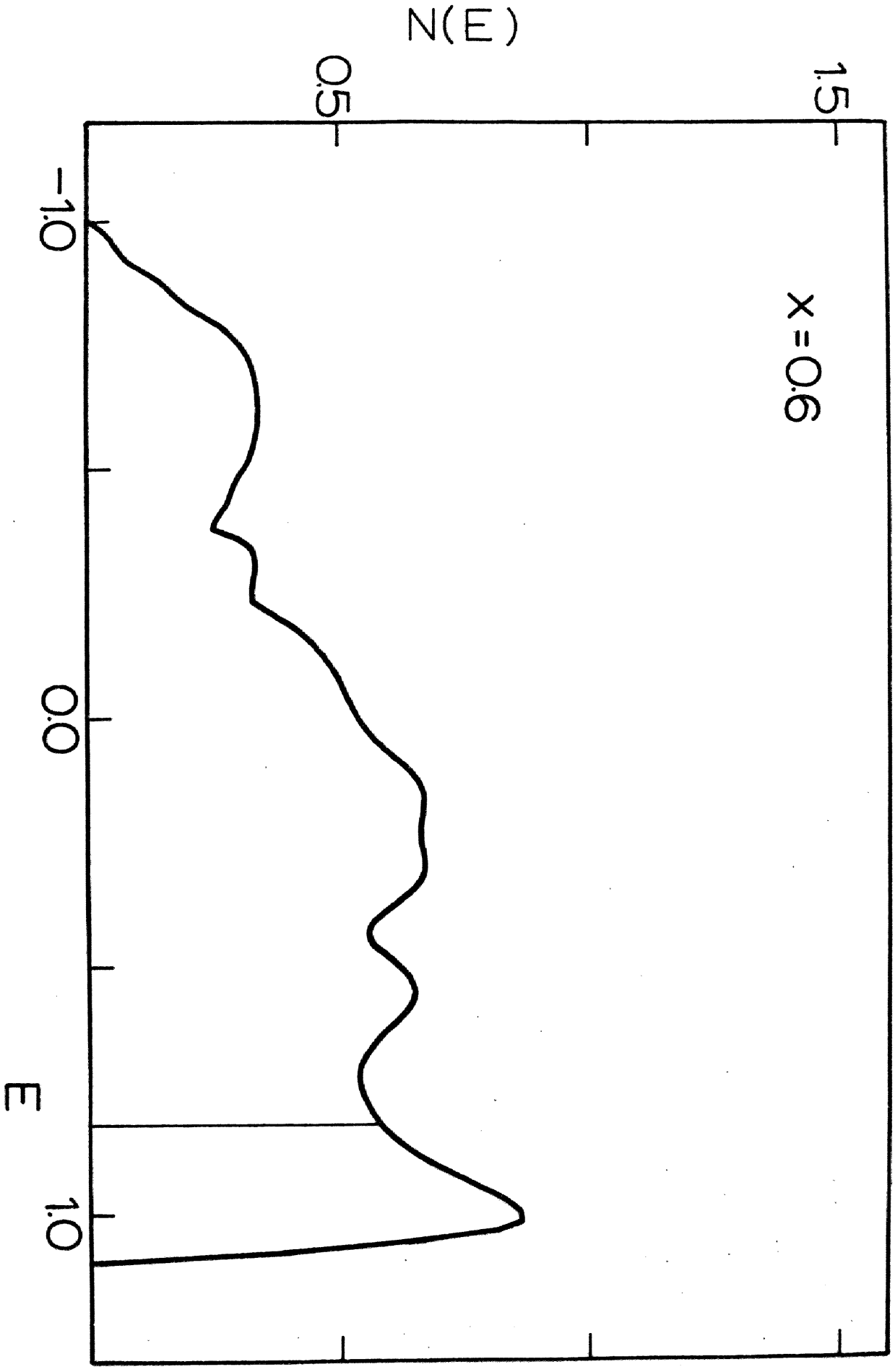

Fig. 8

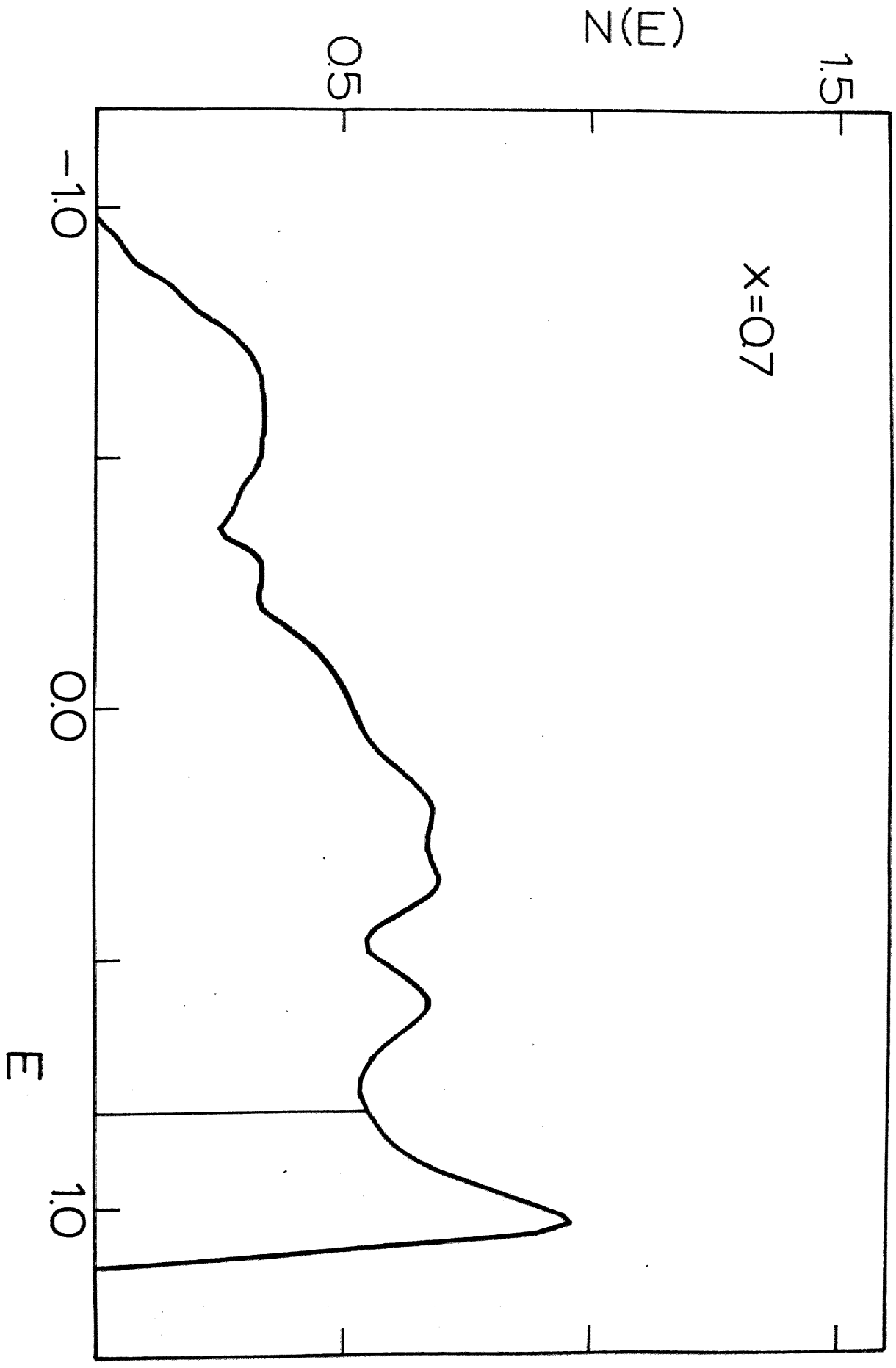

Fig. 9

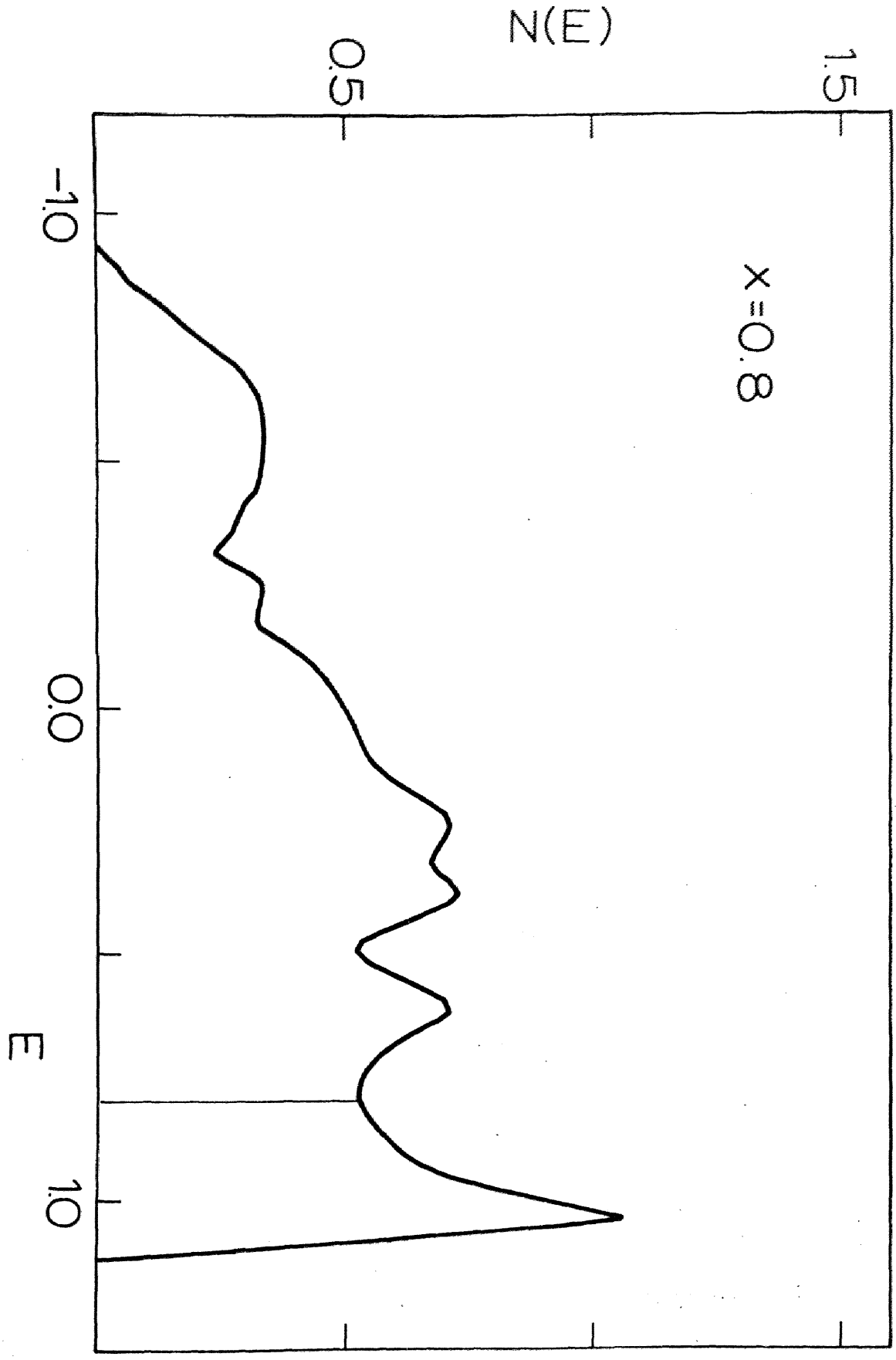

Fig.10

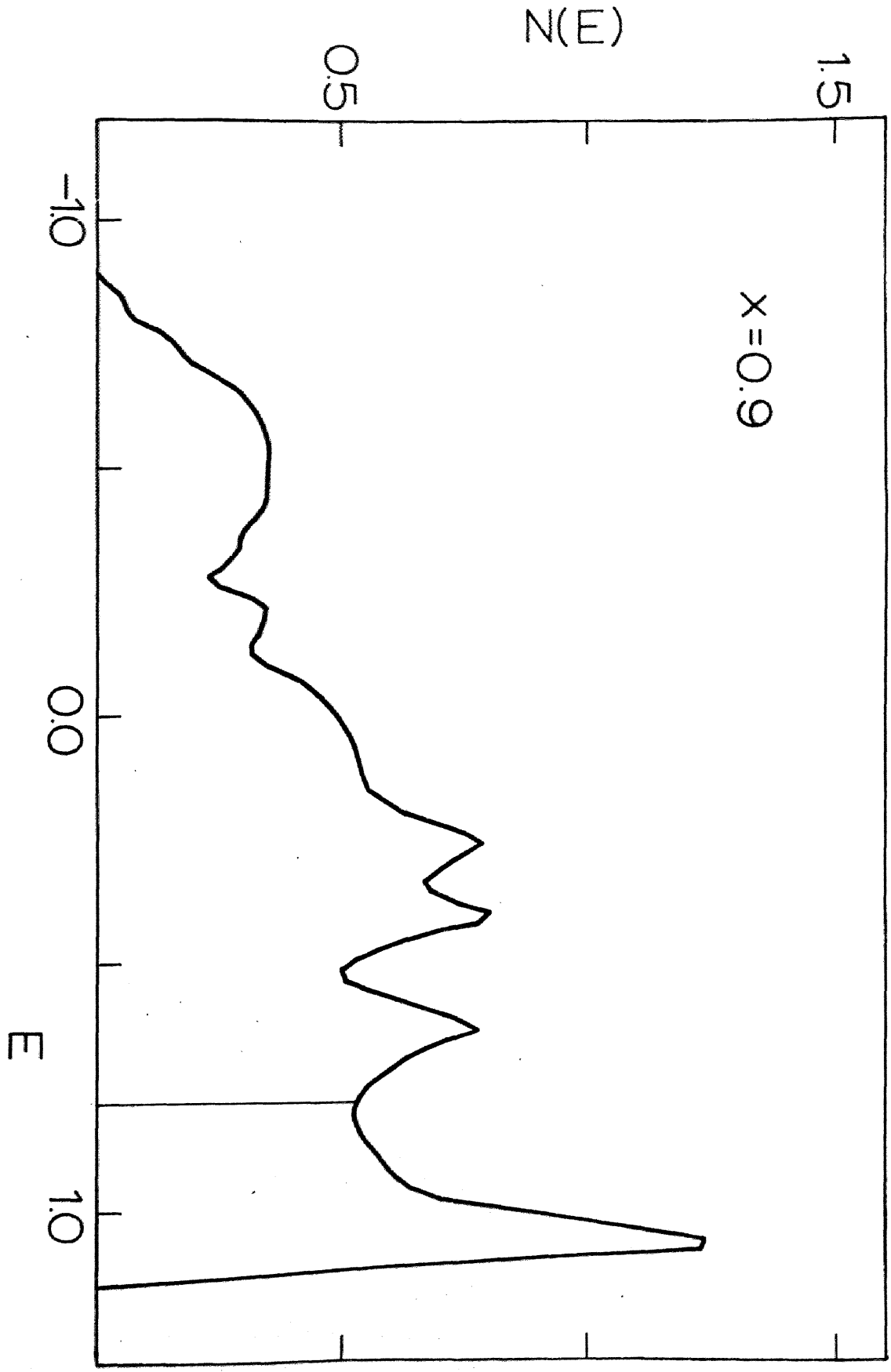

Fig.11

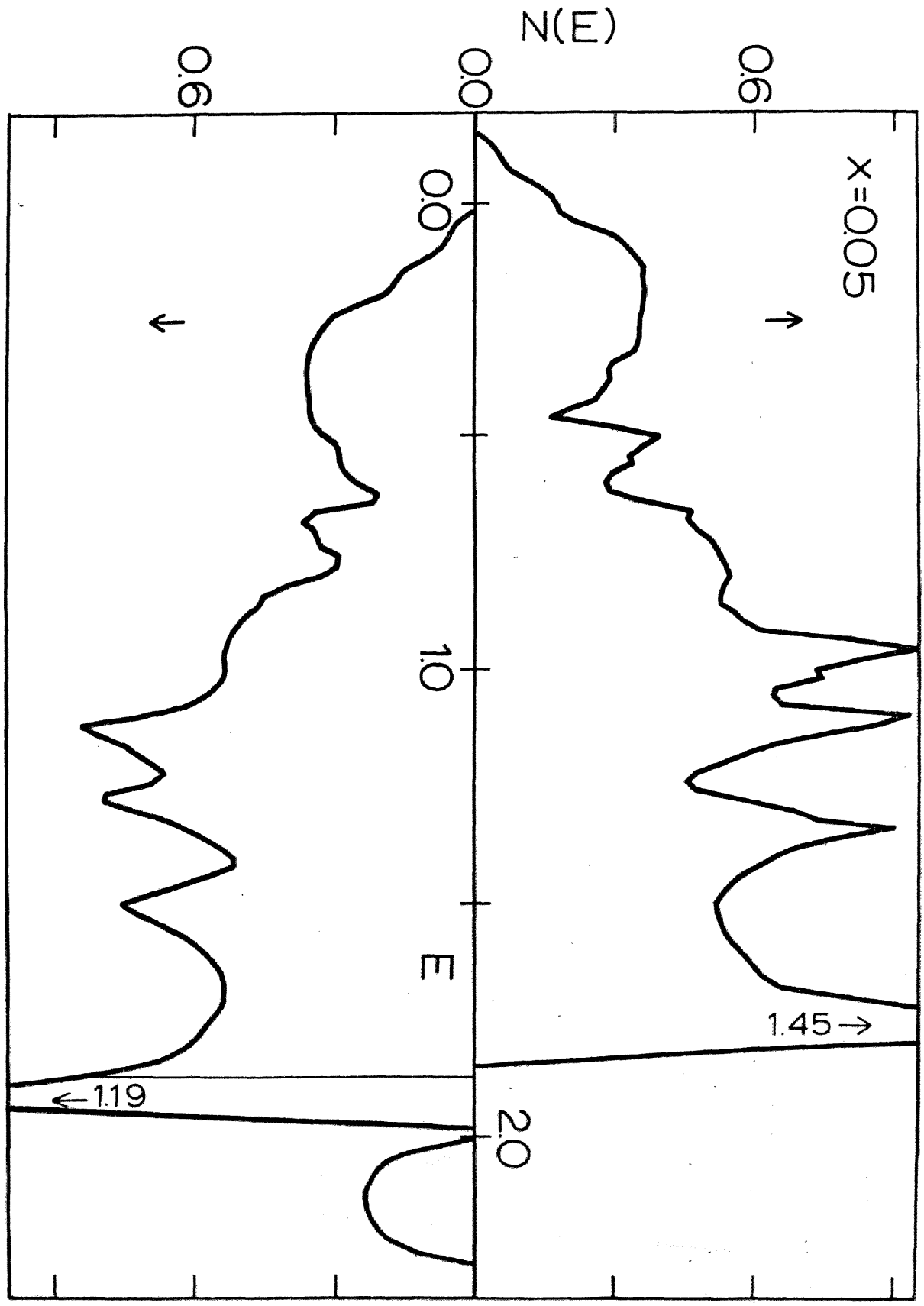

Fig. 12

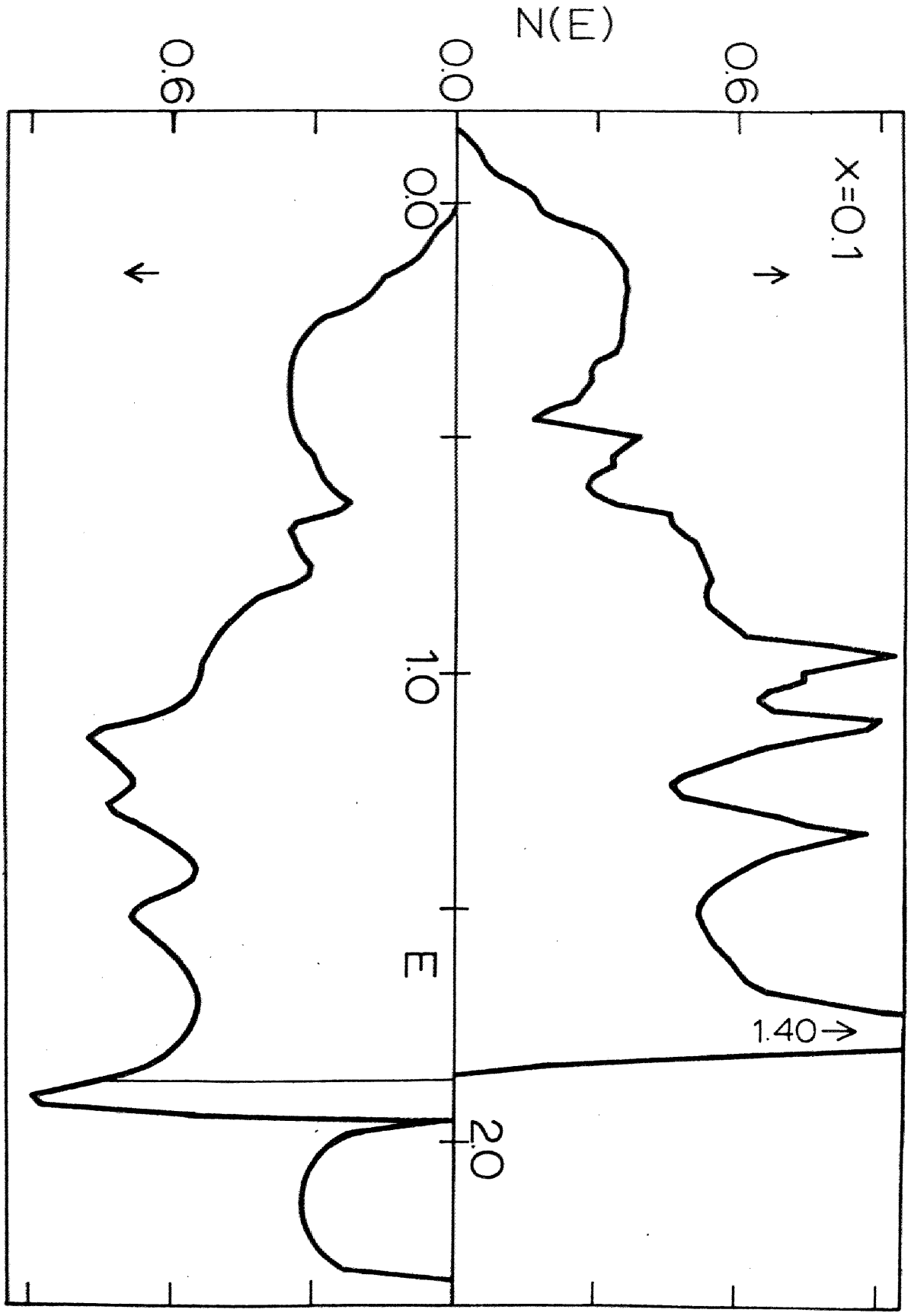

Fig. 13

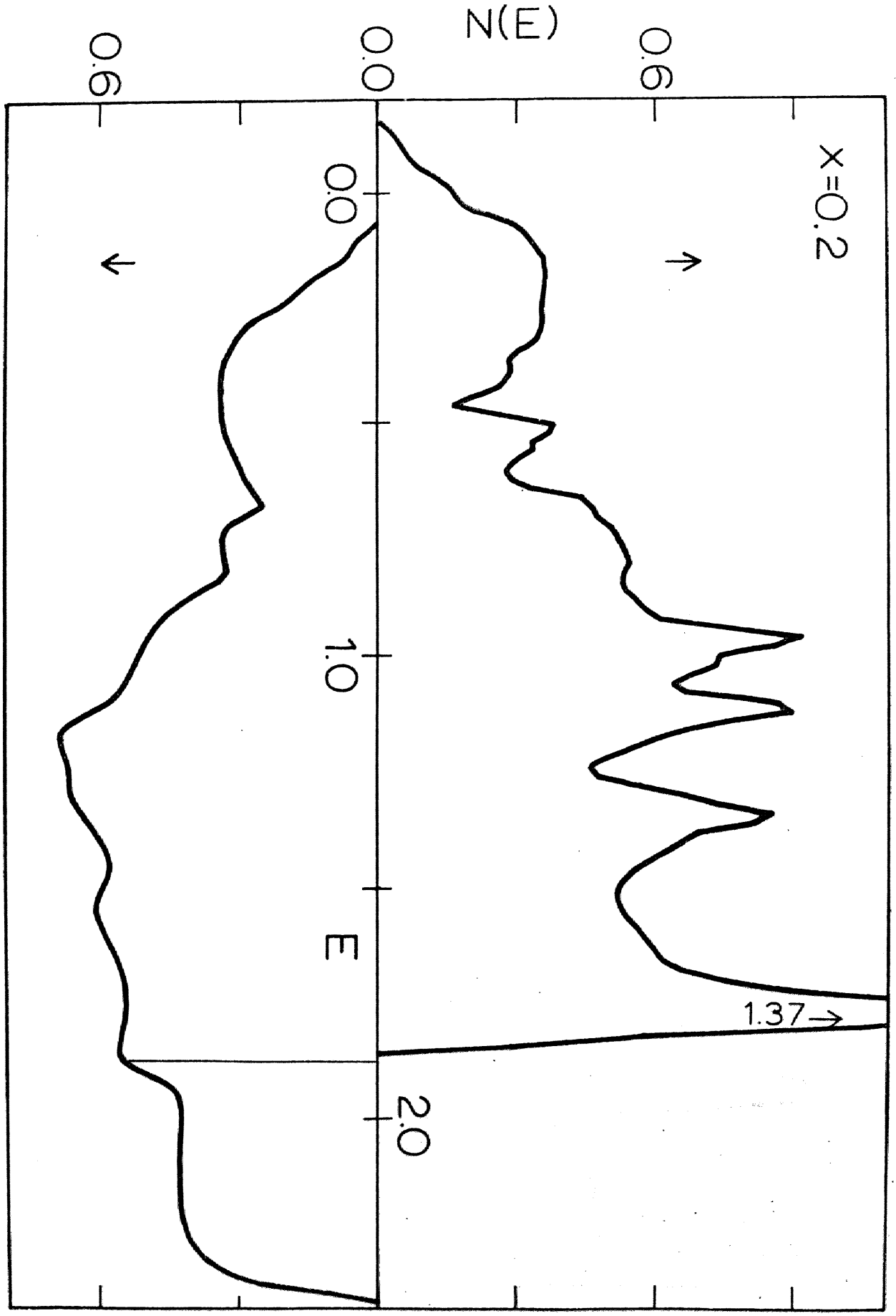

Fig.14

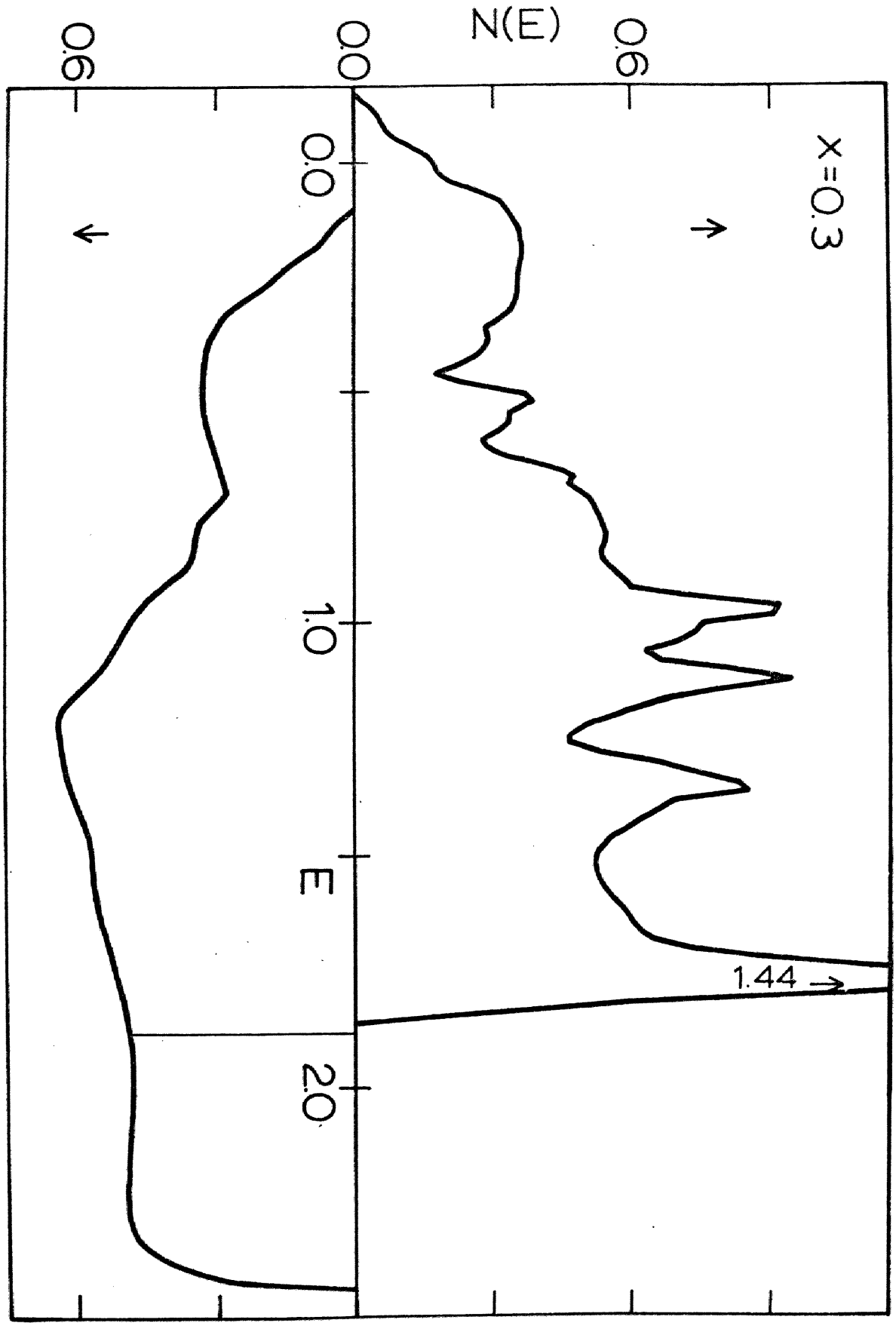

Fig.15

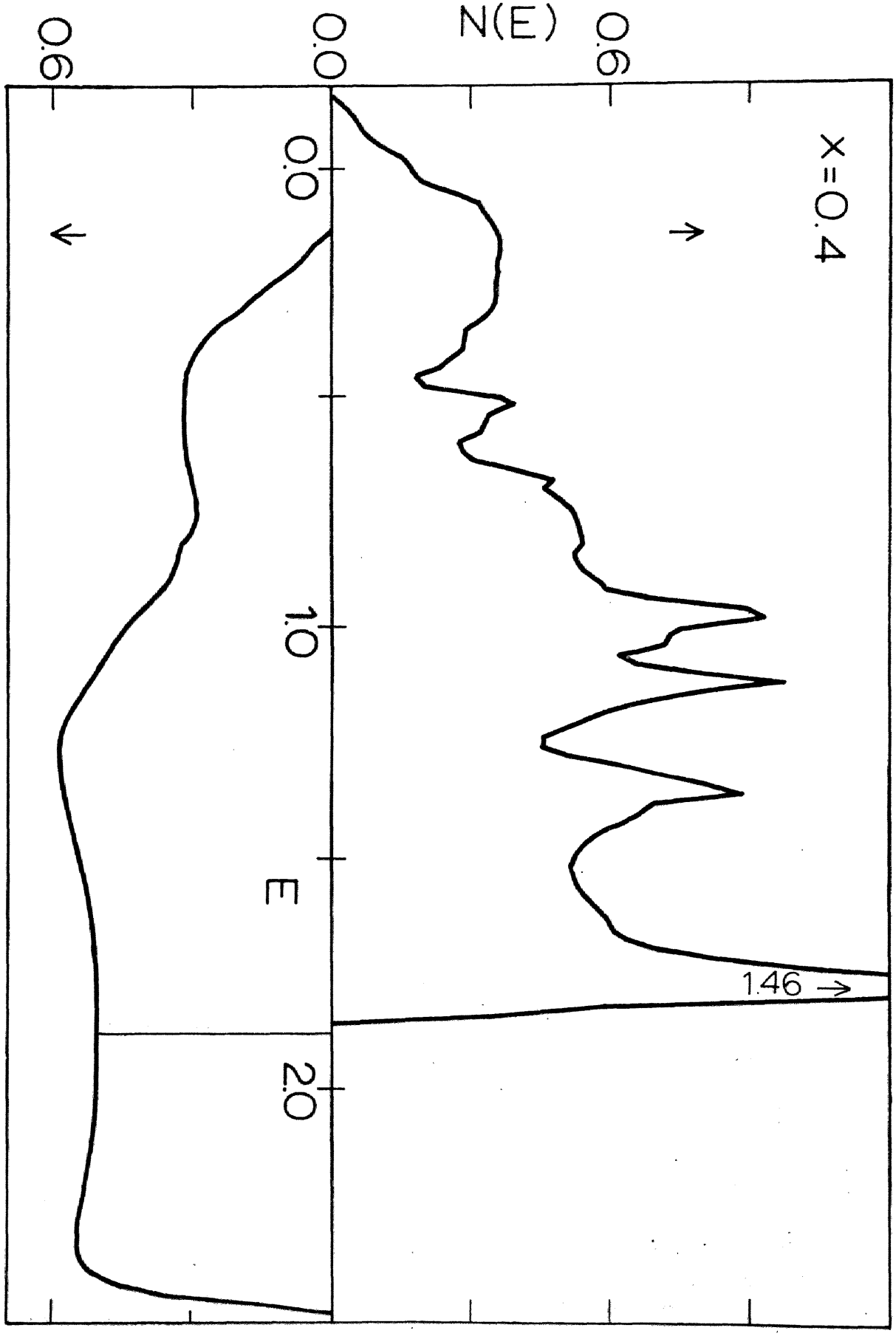

Fig.16

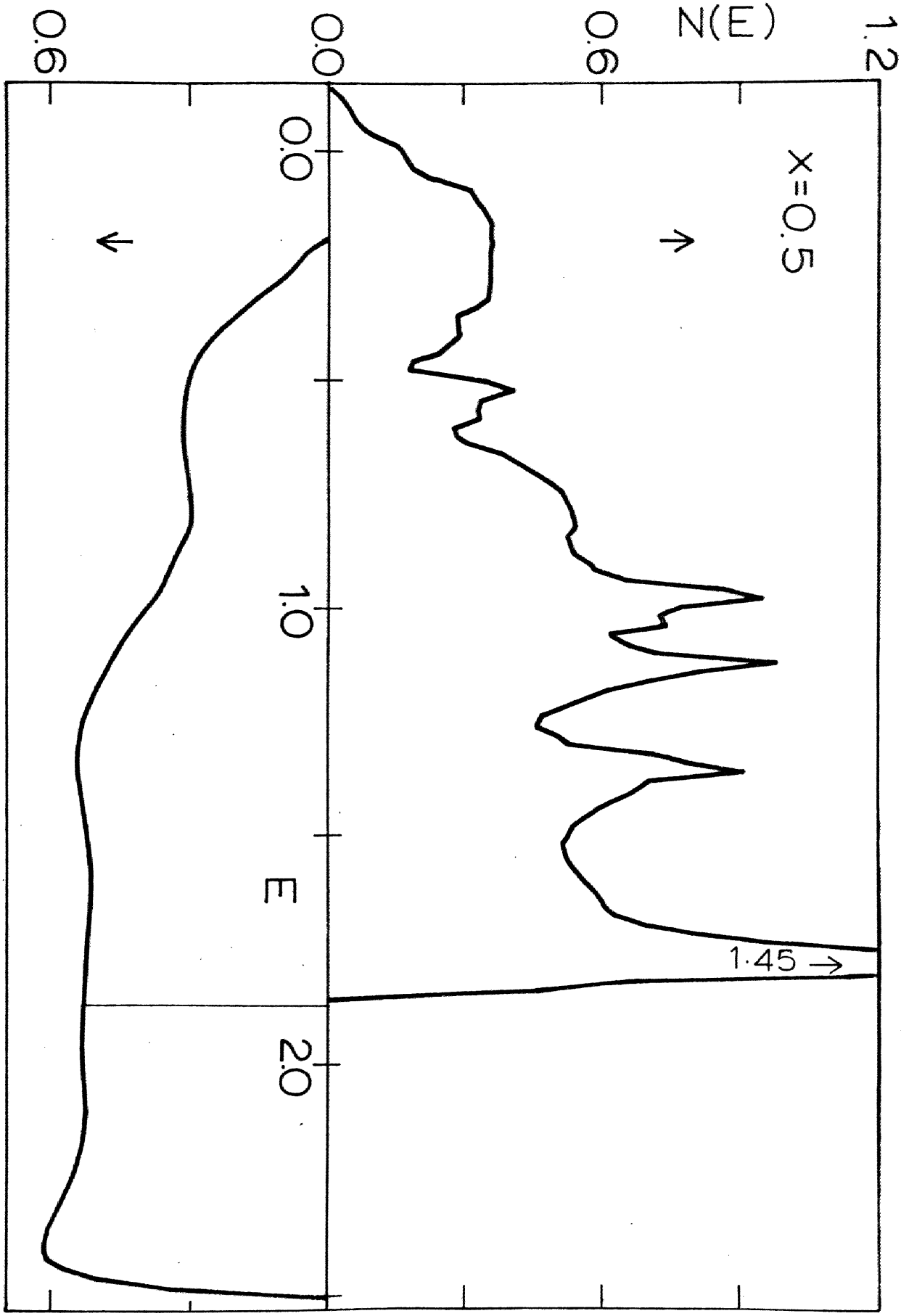

Fig.17

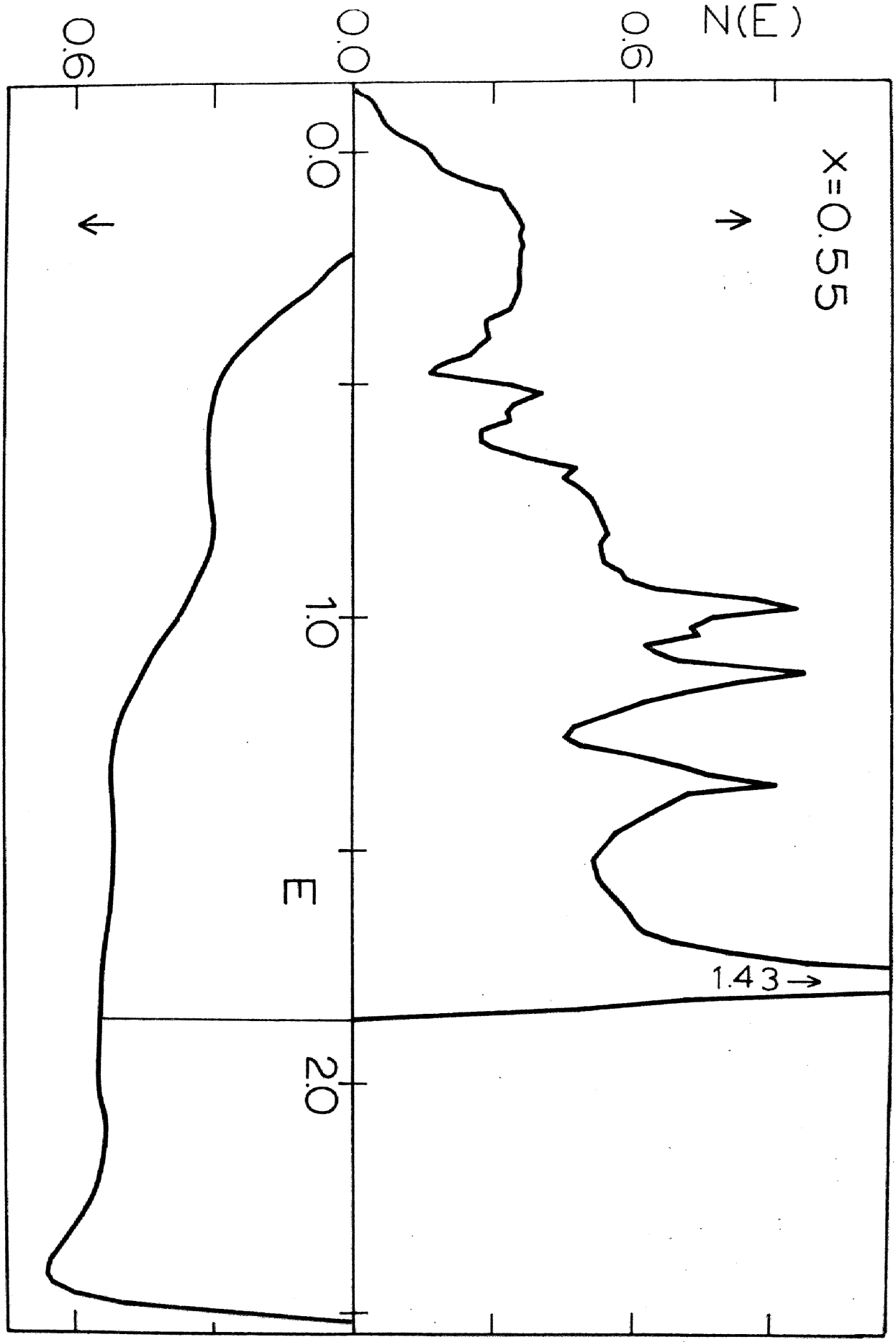

Fig. 18

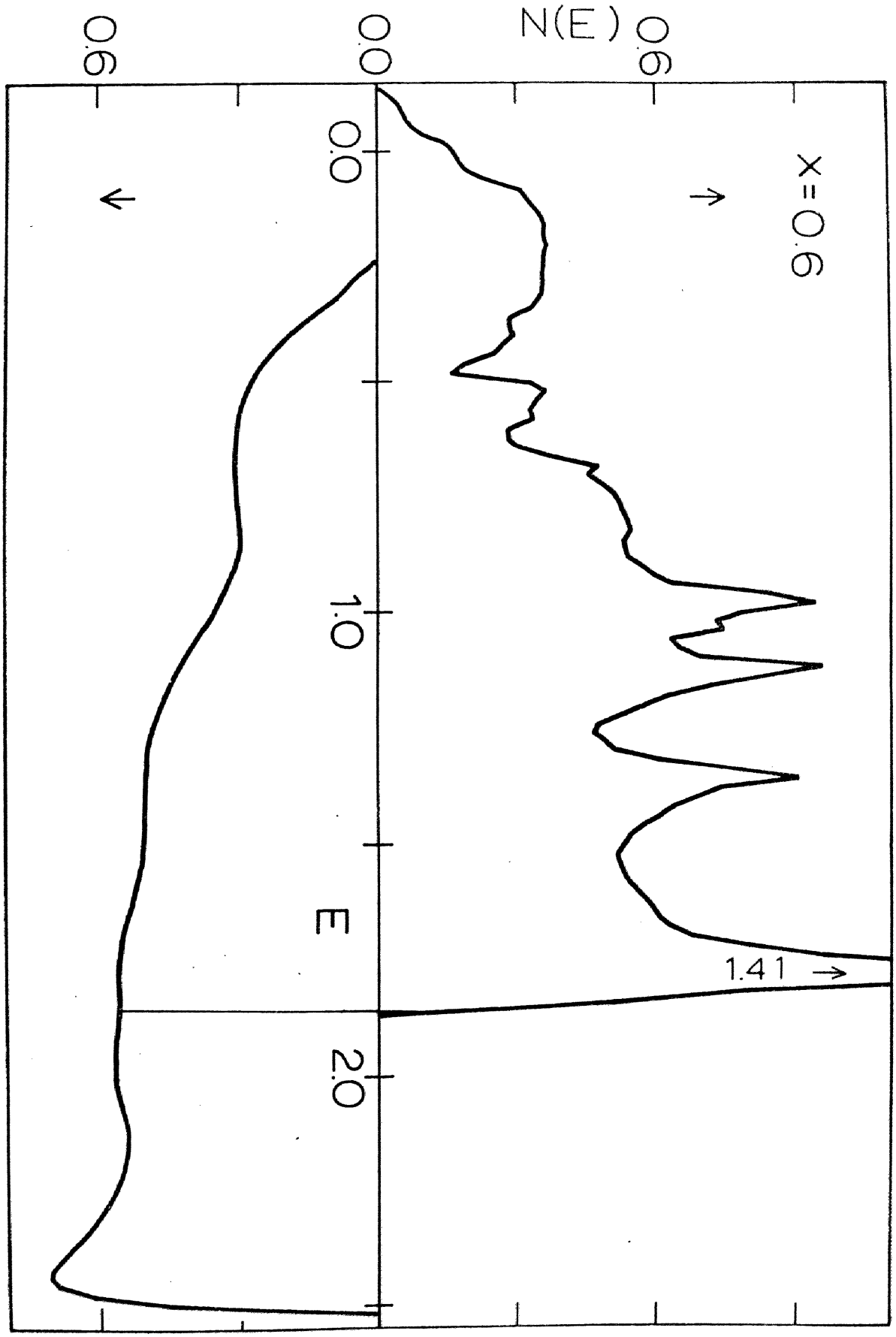

Fig.19

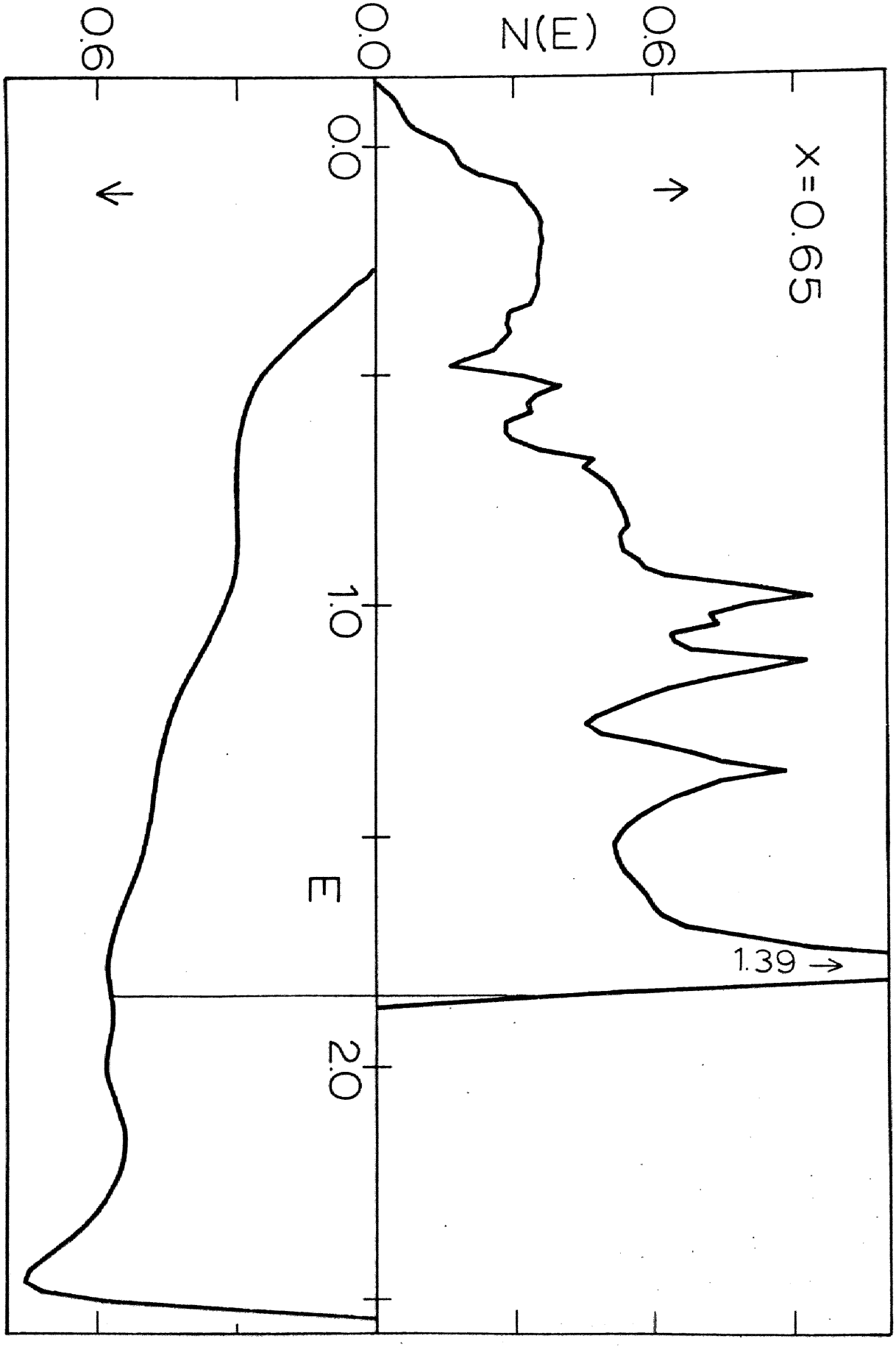

Fig. 20

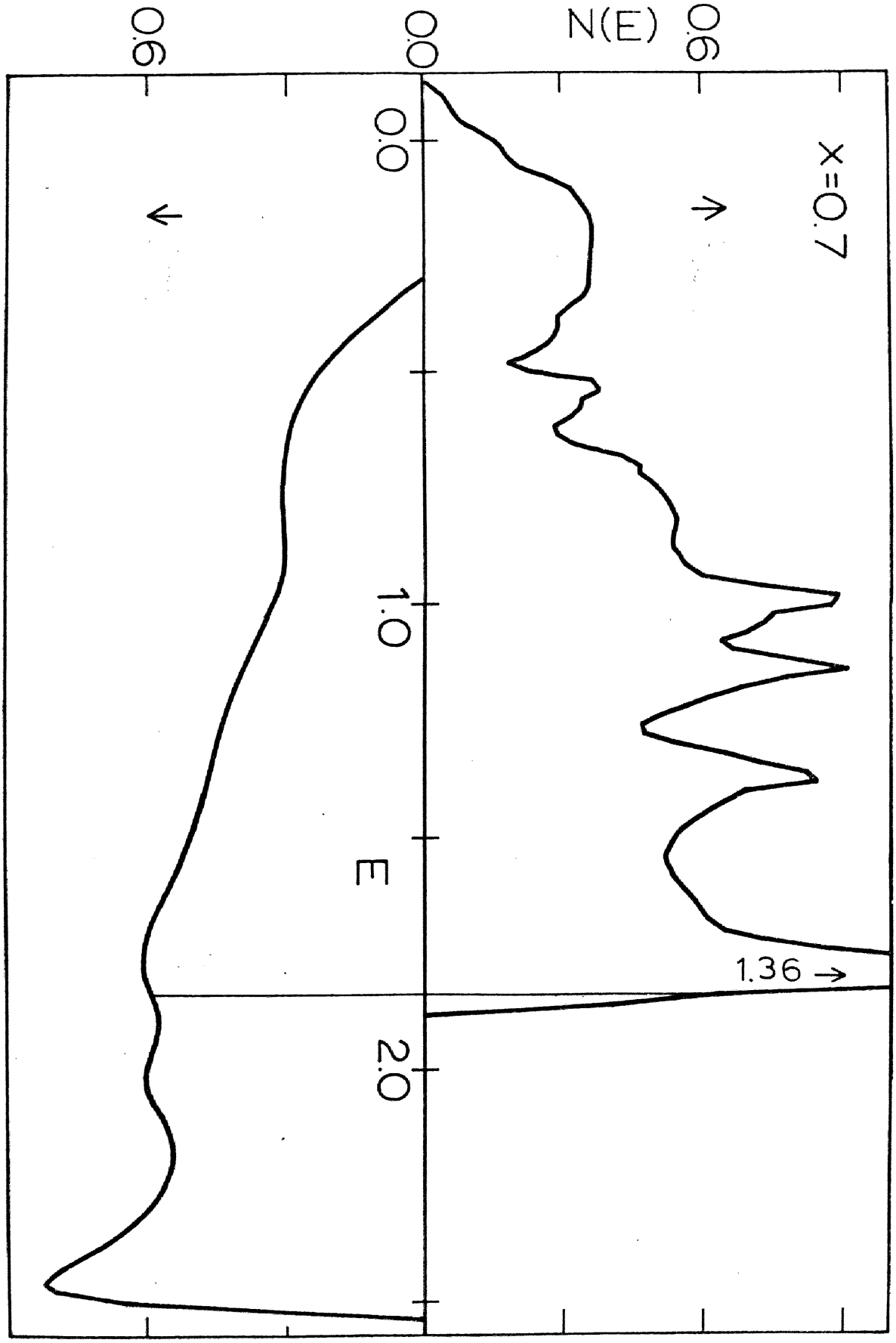

Fig. 21

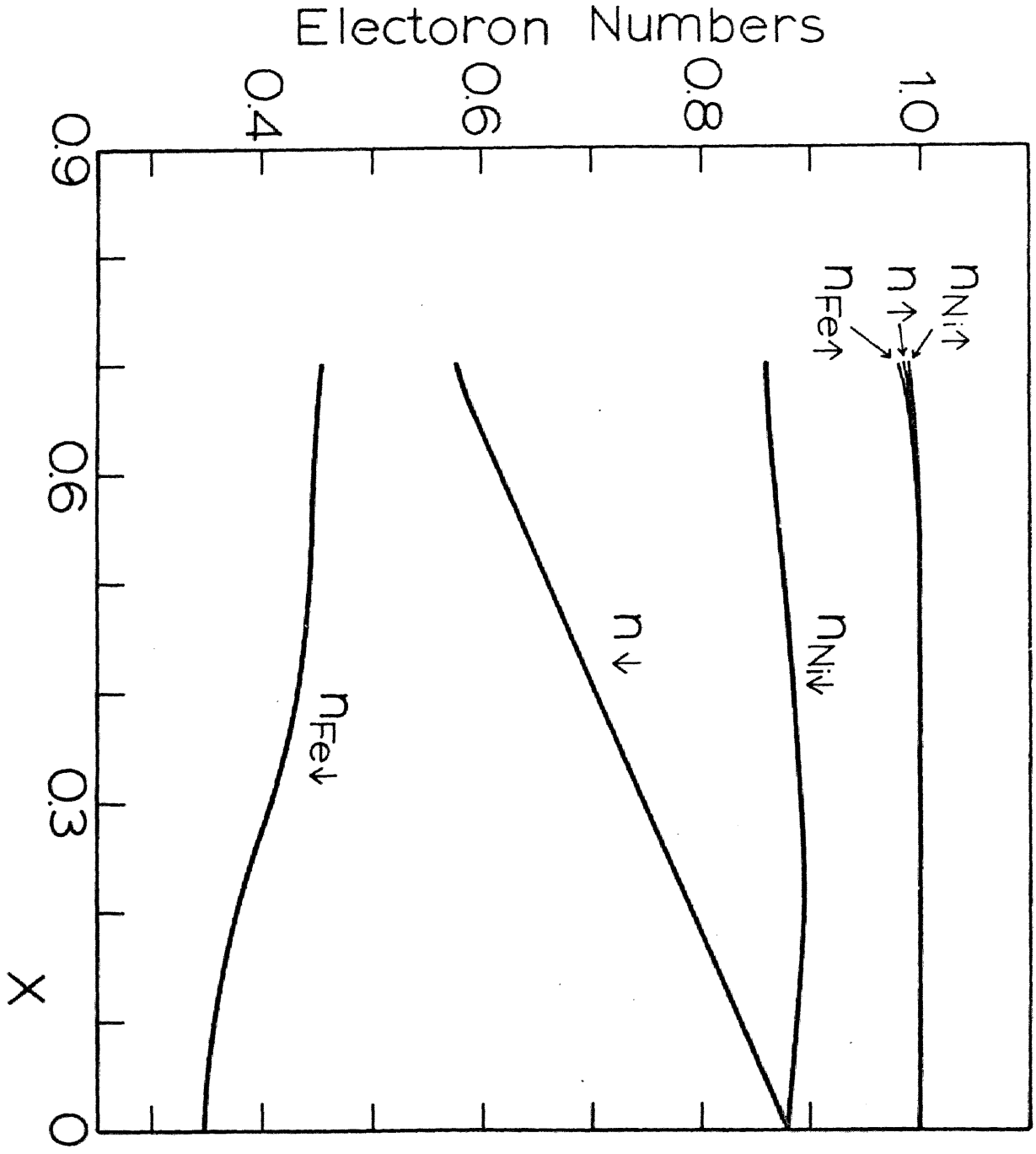
Electoron Numbers
0.4
0.6
0.8
1.0
0.9
0.6
0.3
0
X
$n_{Fe\uparrow}$
$n_{\uparrow}$
$n_{Ni\uparrow}$
$n_{Fe\downarrow}$
$n_{\downarrow}$
$n_{Ni\downarrow}$

Fig. 22

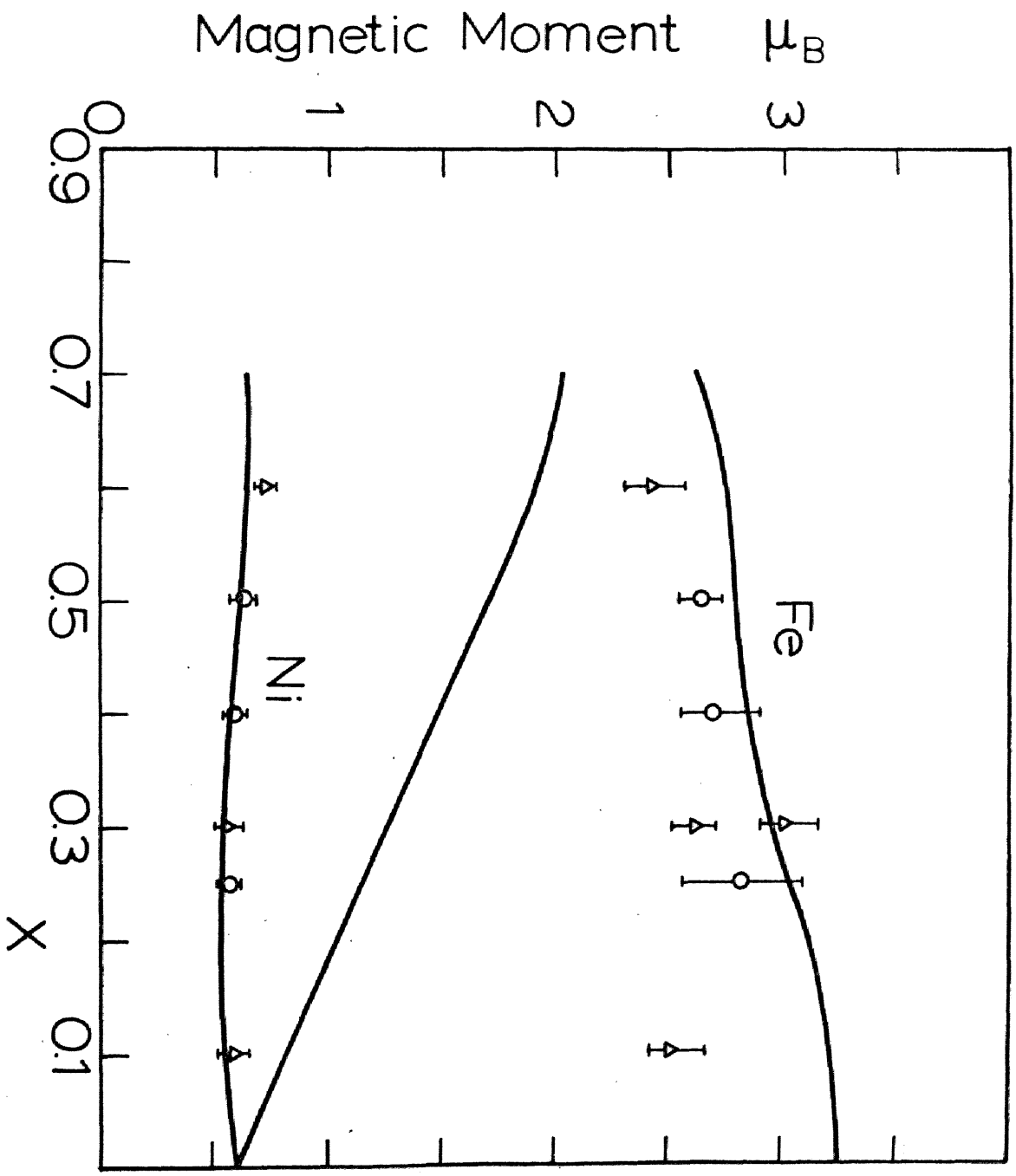

Fig. 23

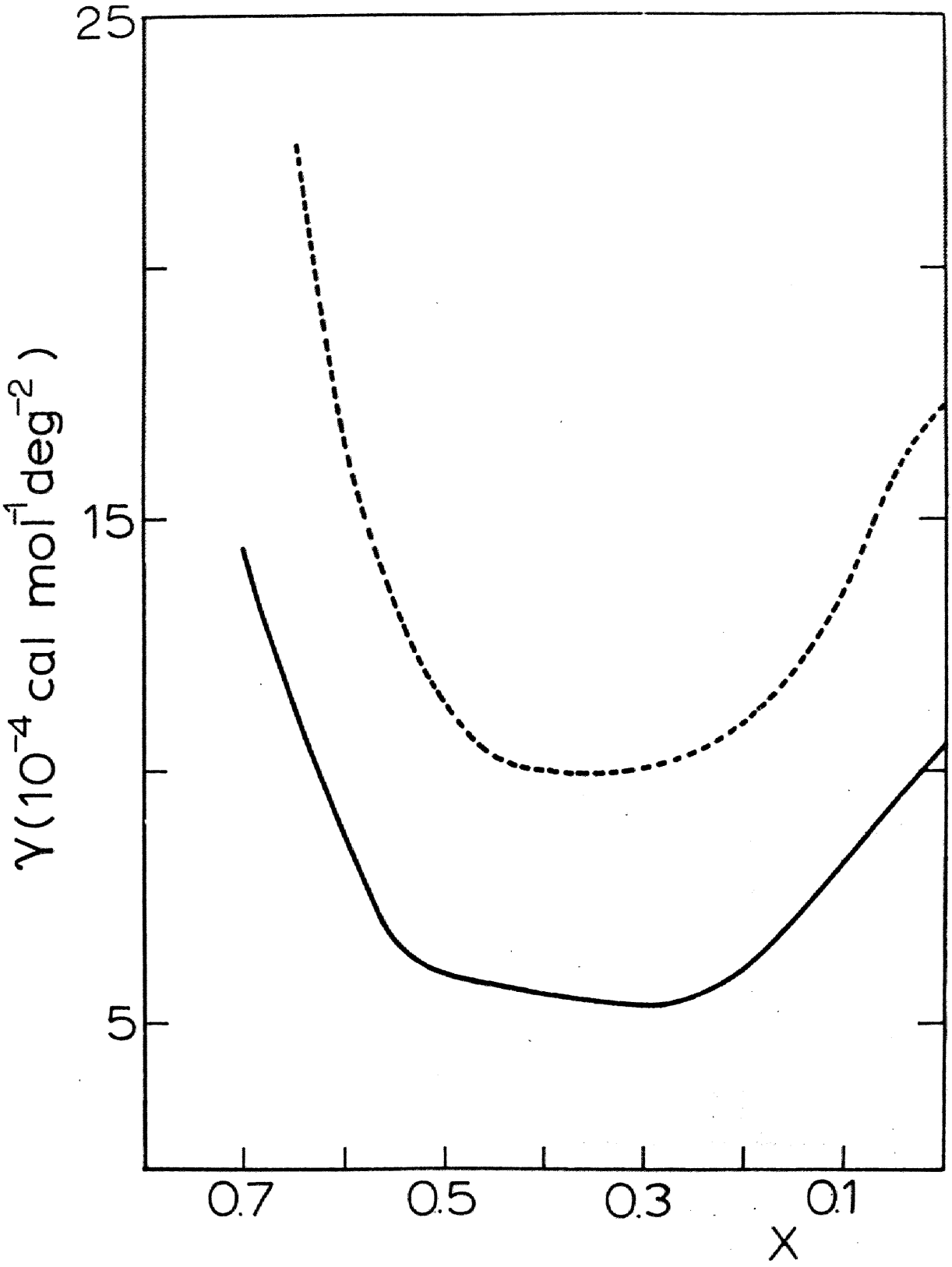

Fig. 24

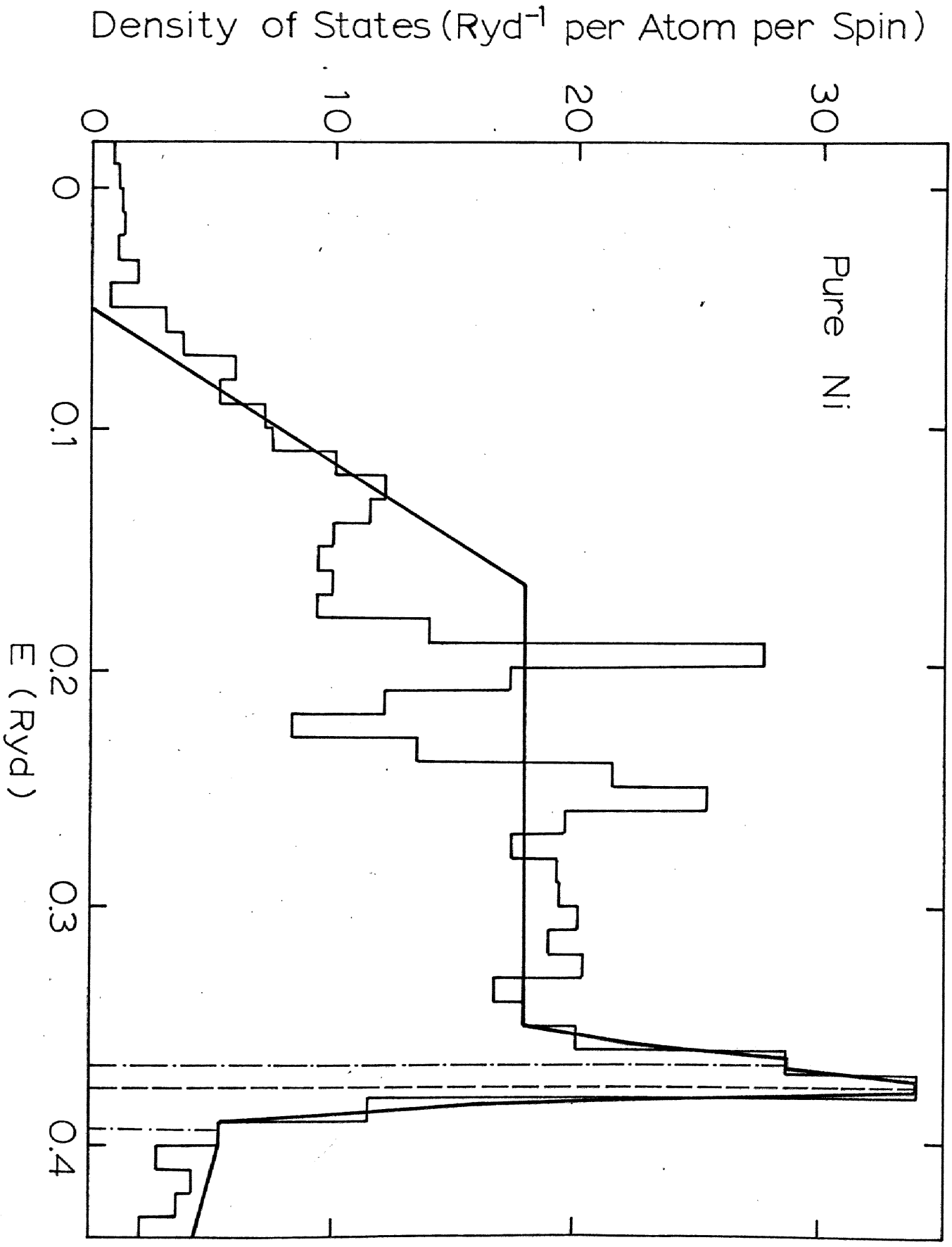
Density of States (Ryd^{-1} per Atom per Spin)
0
10
20
30
0
0.1
0.2
0.3
0.4
E (Ryd)
Pure Ni

Fig. 25

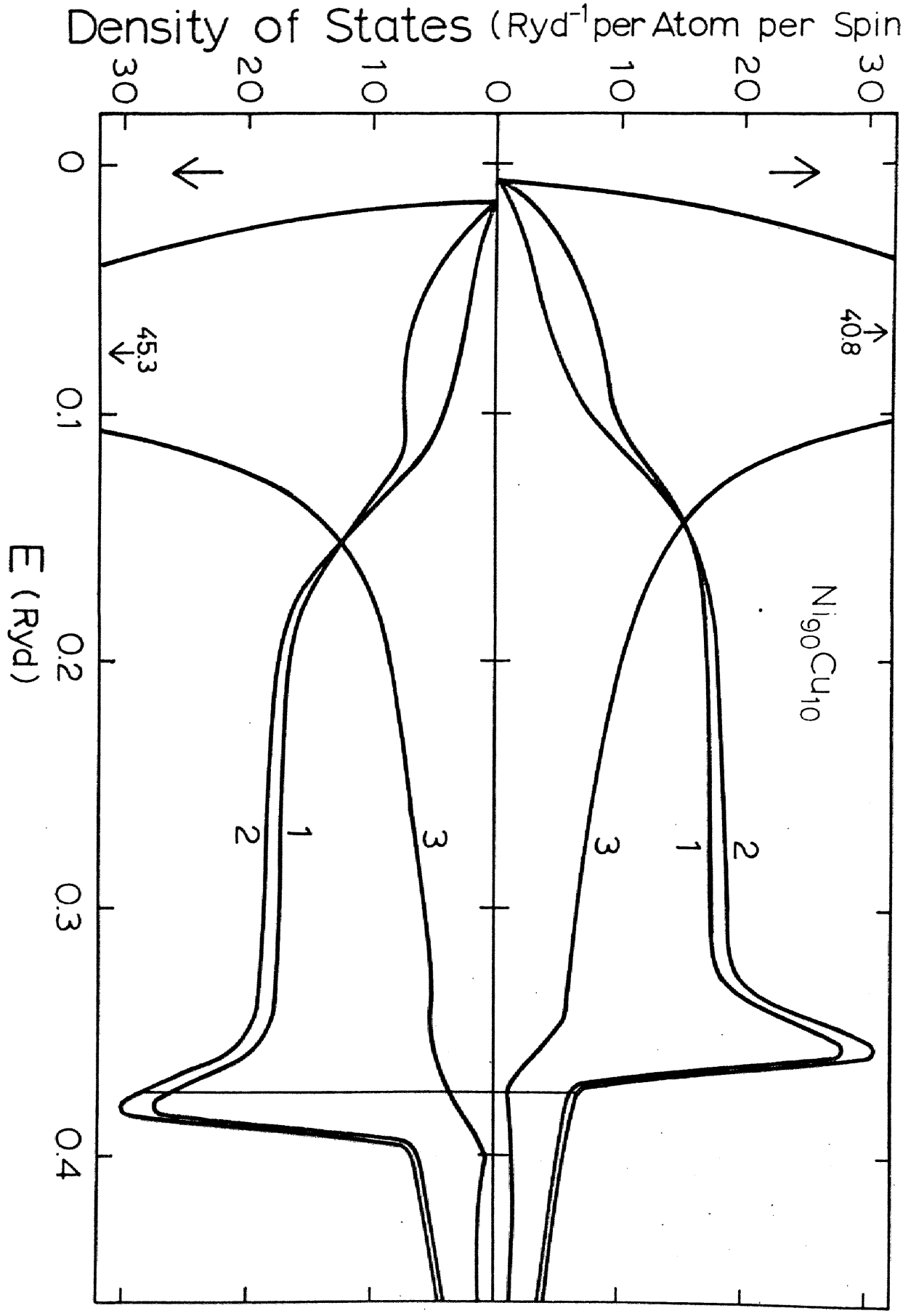
Density of States (Ryd⁻¹ per Atom per Spin)
30
20
10
0
10
20
30
0
0.1
0.2
0.3
0.4
E (Ryd)
45.3
40.8
Ni90Cu10
1
2
3
3
1
2

Fig. 26

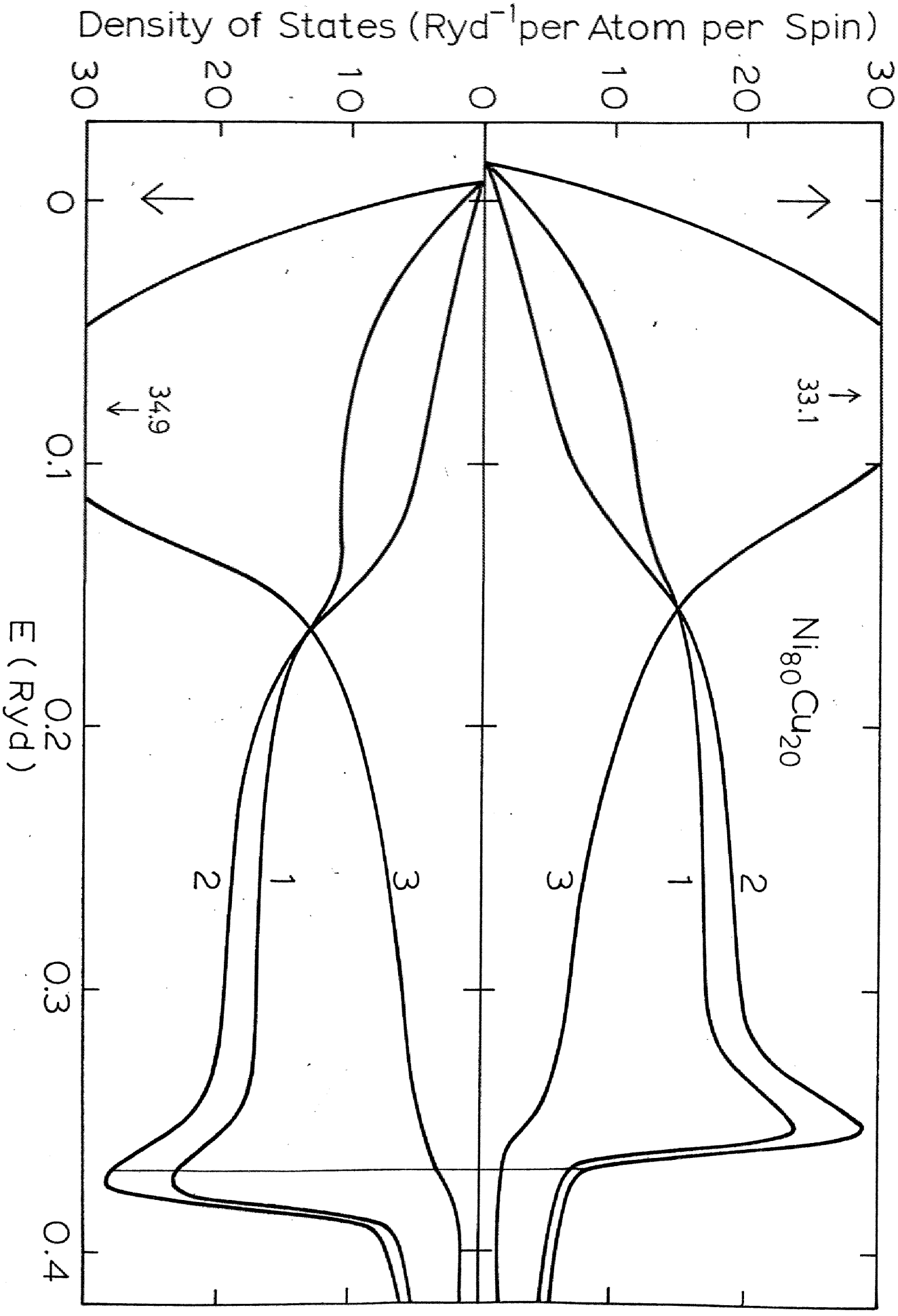
Density of States (Ryd^{-1} per Atom per Spin)
30
20
10
0
10
20
30
0
0.1
0.2
0.3
0.4
E (Ryd)
34.9
33.1
1
2
3
3
1
2
$Ni_{80}Cu_{20}$

Fig. 27

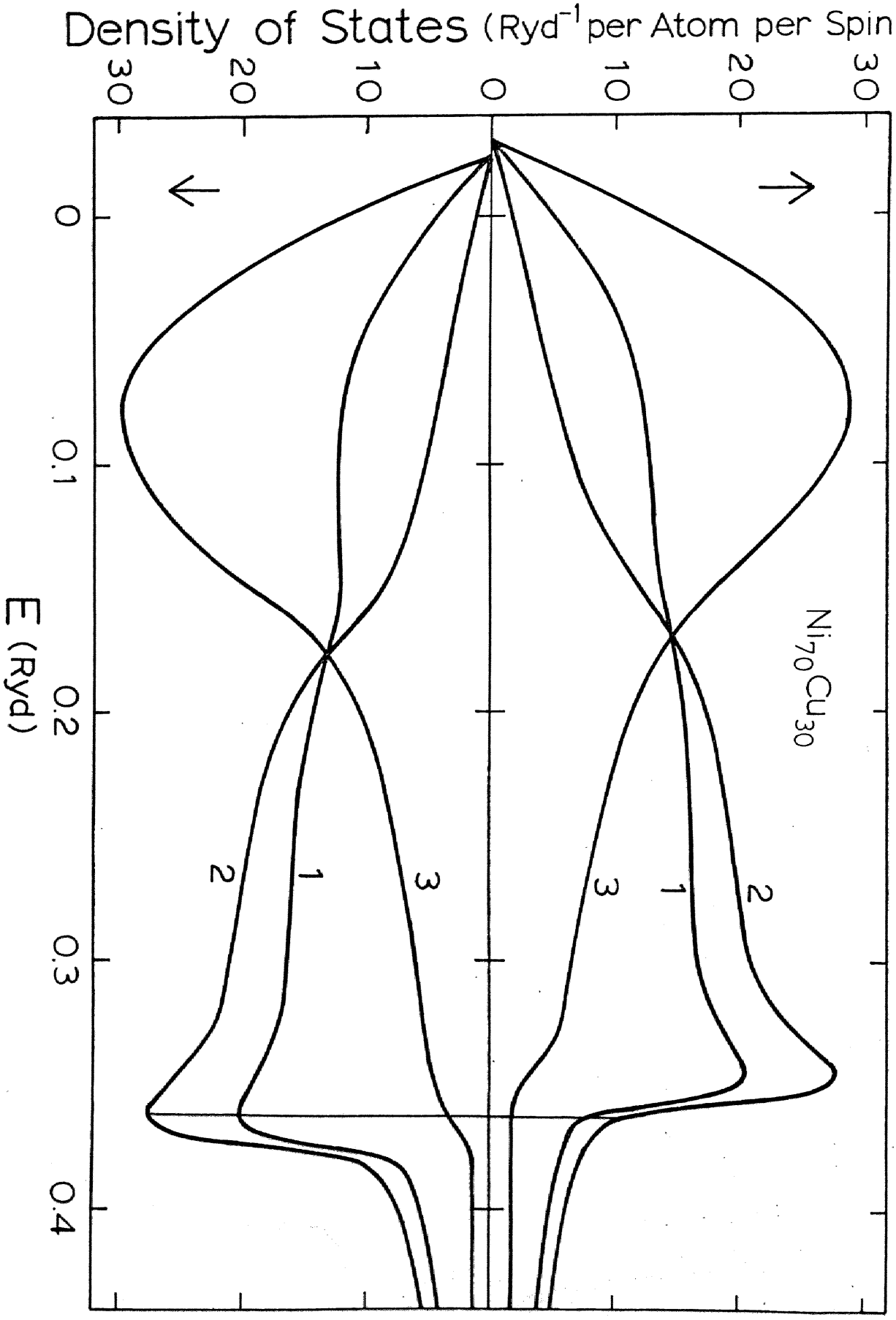
Density of States (Ryd^{-1} per Atom per Spin)
30
20
10
0
10
20
30
0
0.1
0.2
0.3
0.4
E (Ryd)
Ni$_{70}$Cu$_{30}$
1
2
3
3
1
2

Fig. 28

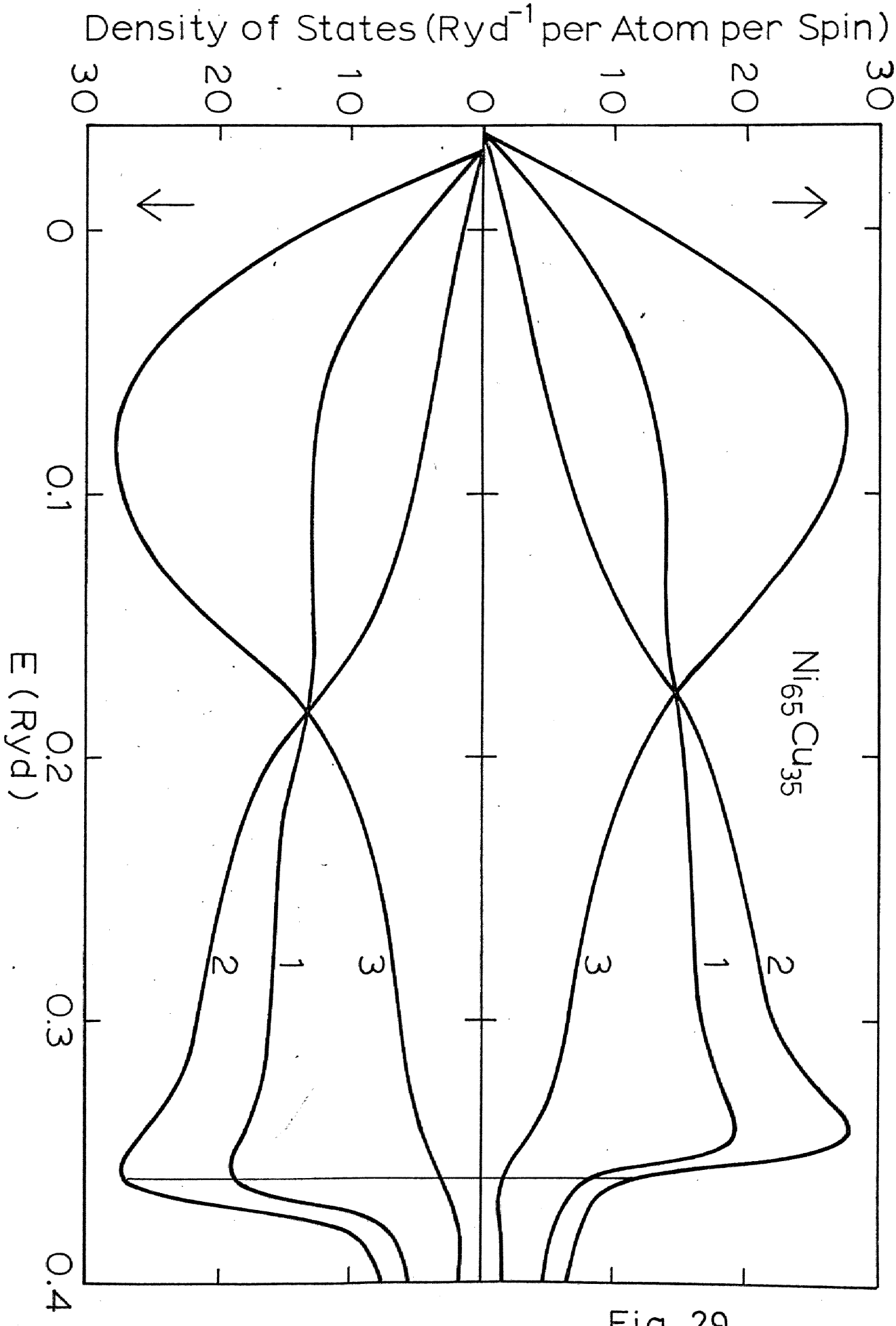
Density of States (Ryd^{-1} per Atom per Spin)
30
20
10
0
10
20
30
0
0.1
0.2
0.3
0.4
E (Ryd)
$Ni_{65}Cu_{35}$
1
2
3
3
1
2

Fig. 29

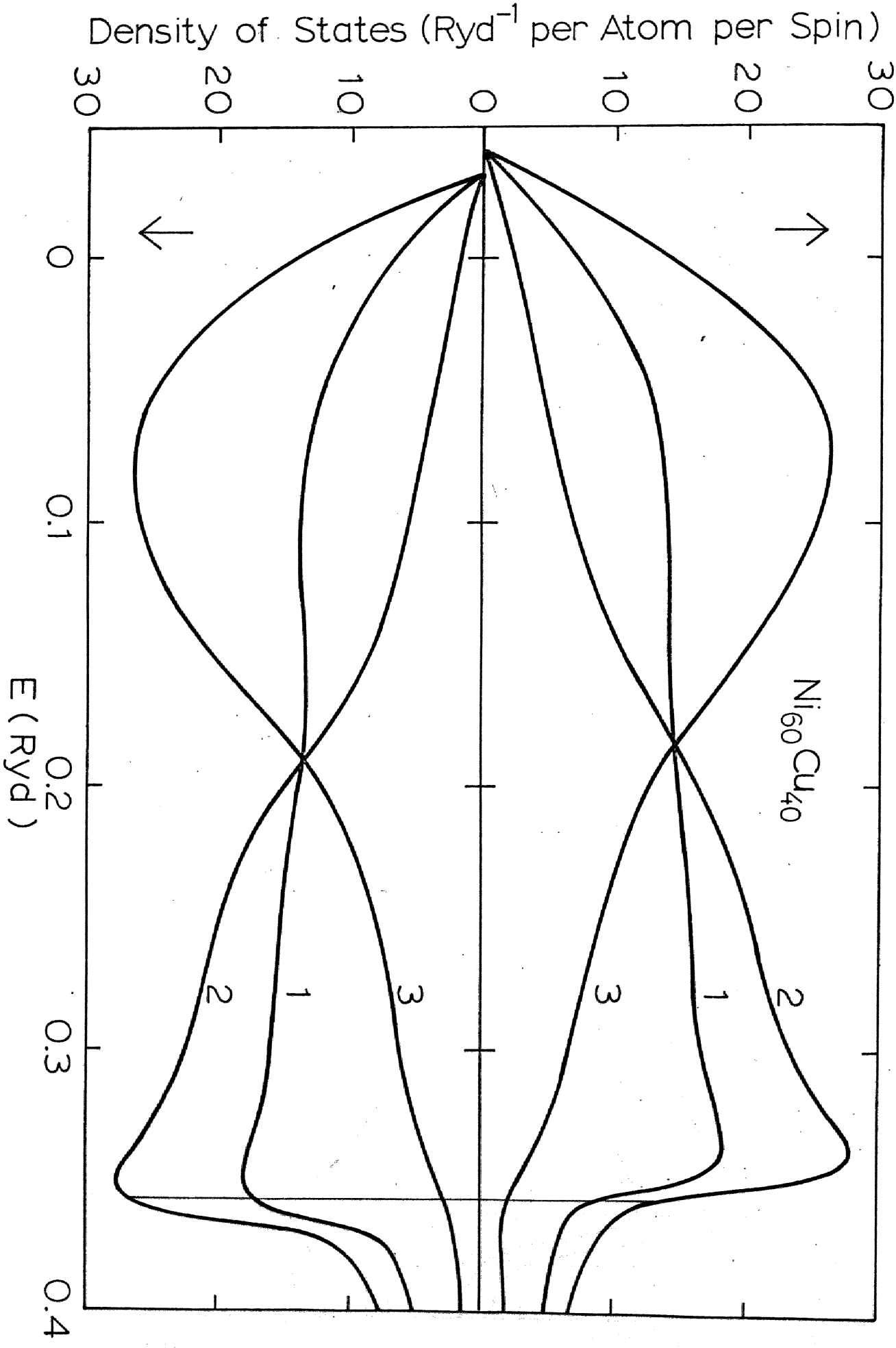
Density of States (Ryd^{-1} per Atom per Spin)
30
20
10
0
10
20
30
0
0.1
0.2
0.3
0.4
E (Ryd)
$Ni_{60}Cu_{40}$
1
2
3
3
1
2

Fig. 30

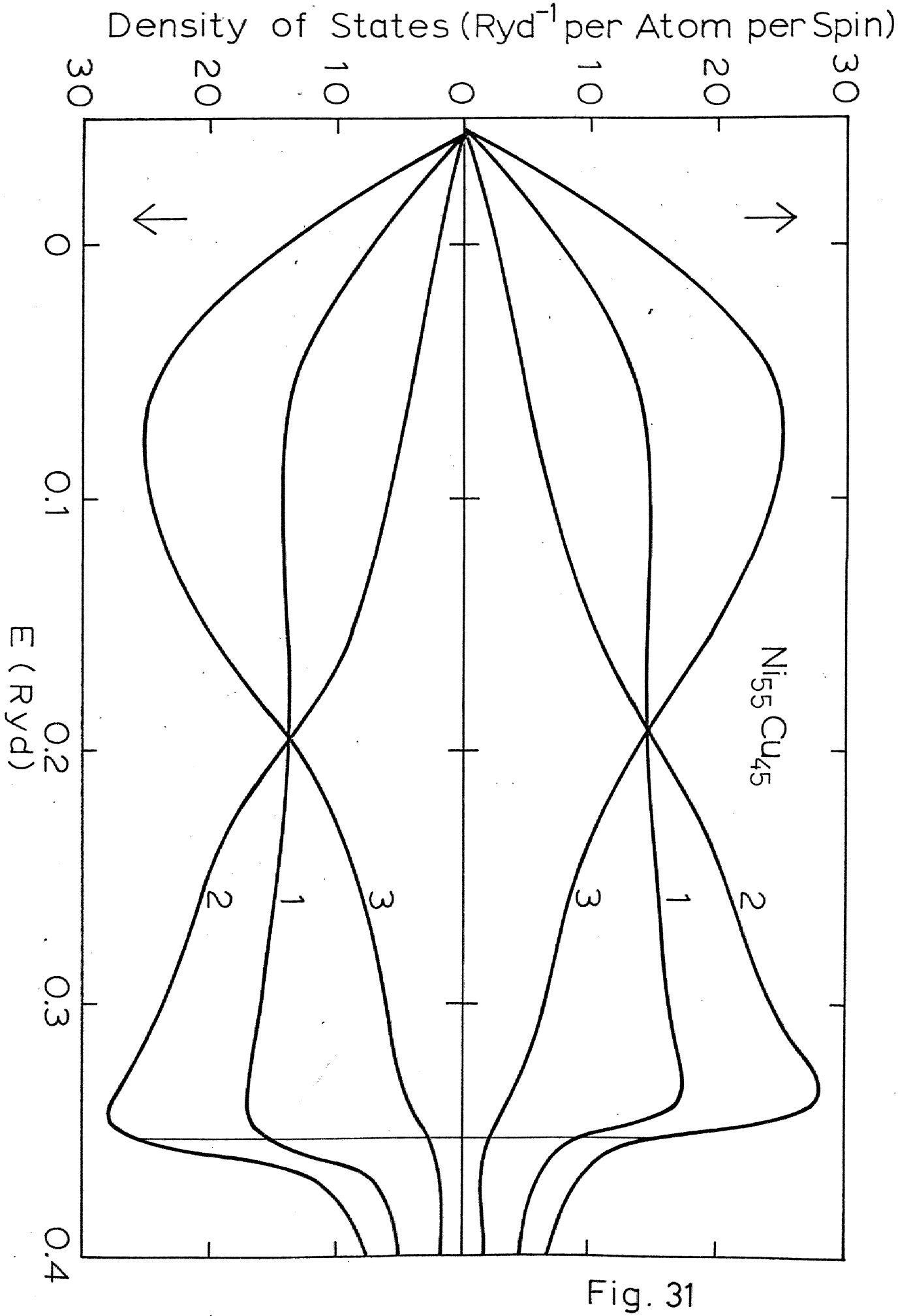
Density of States (Ryd^{-1} per Atom per Spin)
30
20
10
0
10
20
30
0
0.1
0.2
0.3
0.4
E (Ryd)
$Ni_{55}Cu_{45}$
1
2
3
3
1
2

Fig. 31

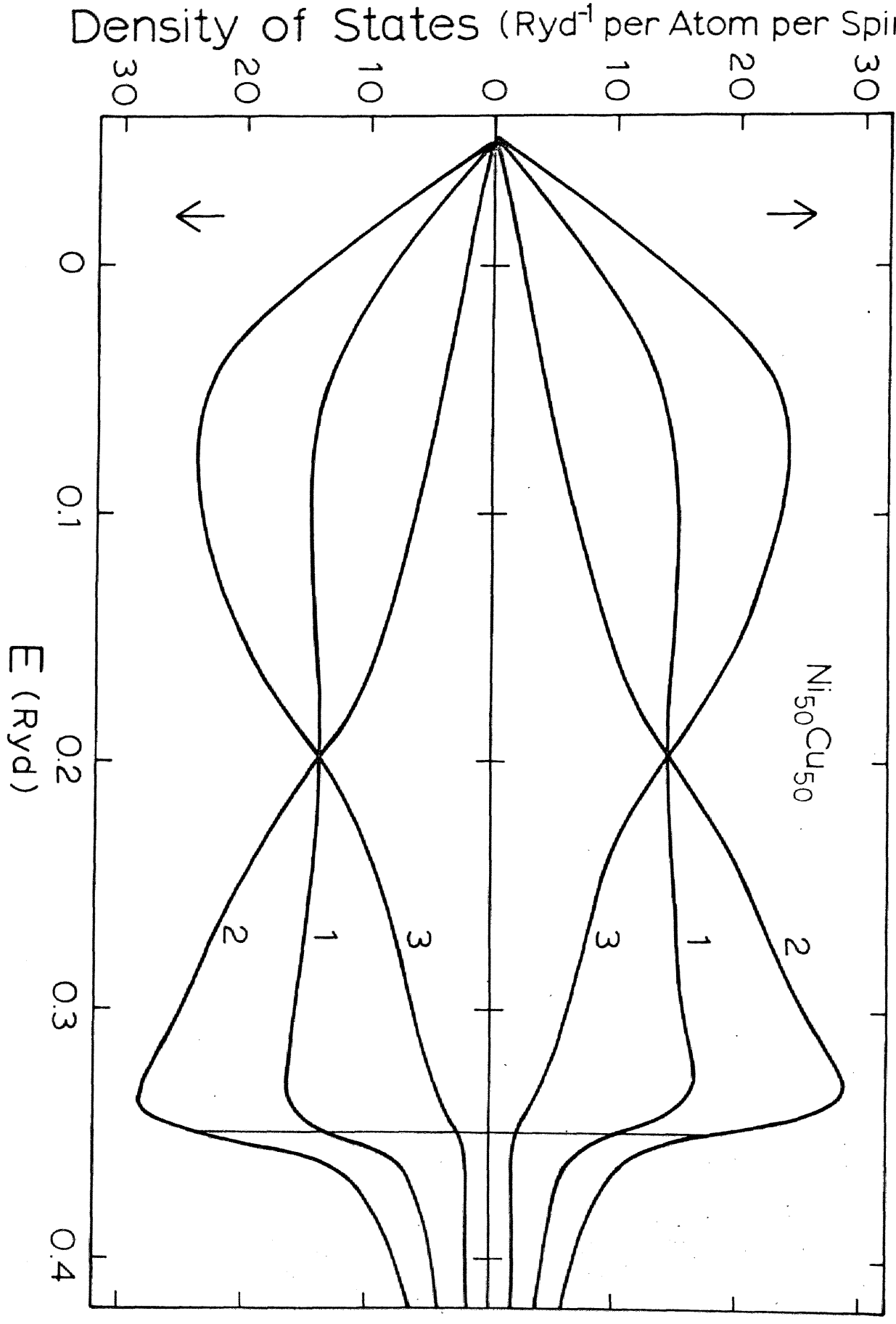
Density of States (Ryd^{-1} per Atom per Spin)
30
20
10
0
10
20
30
0
0.1
0.2
0.3
0.4
E (Ryd)
$Ni_{50}Cu_{50}$
1
2
3
3
1
2

Fig. 32

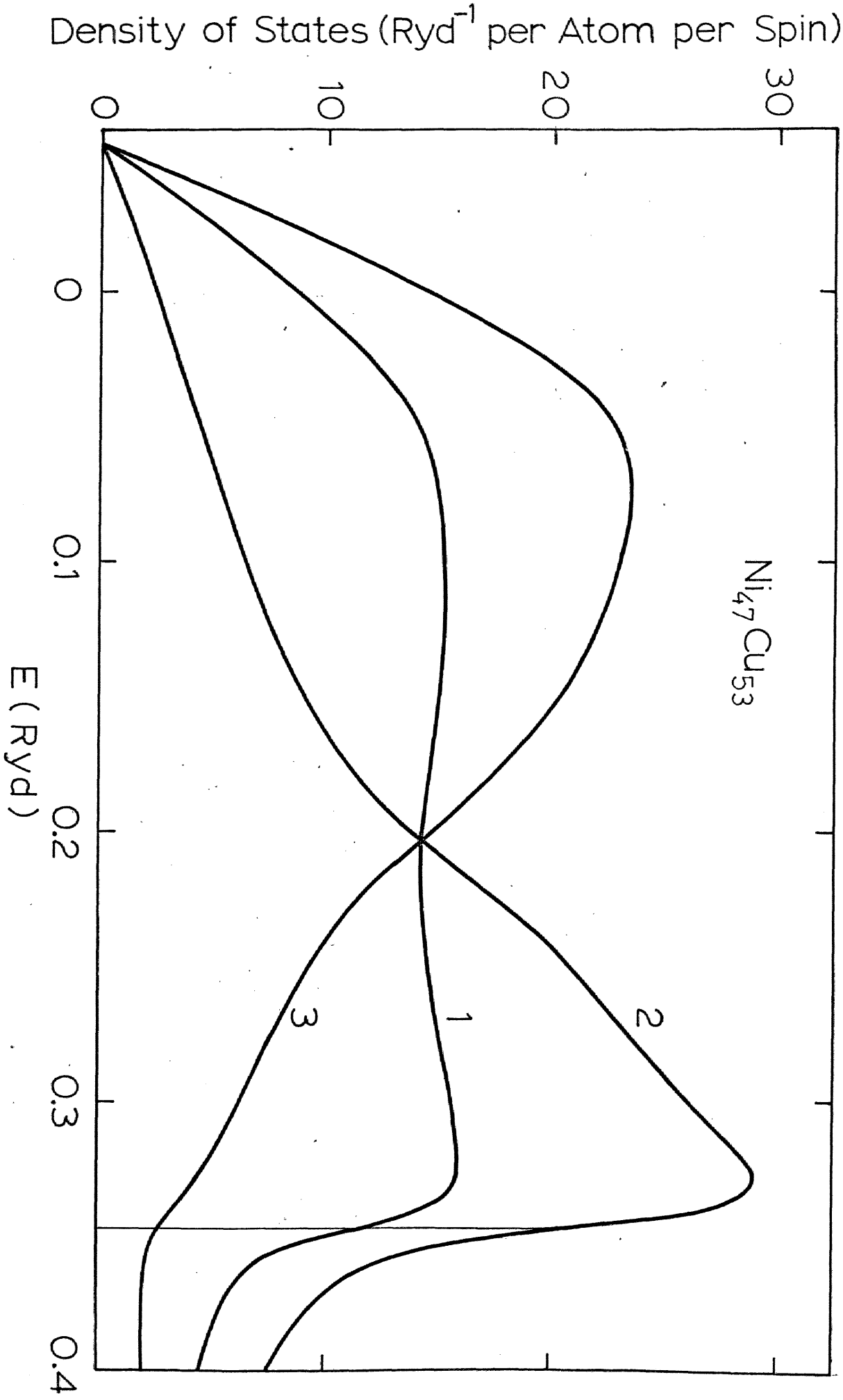
Density of States (Ryd^{-1} per Atom per Spin)
0
10
20
30
0
0.1
0.2
0.3
0.4
E (Ryd)
$Ni_{47}Cu_{53}$
1
2
3

Fig. 33

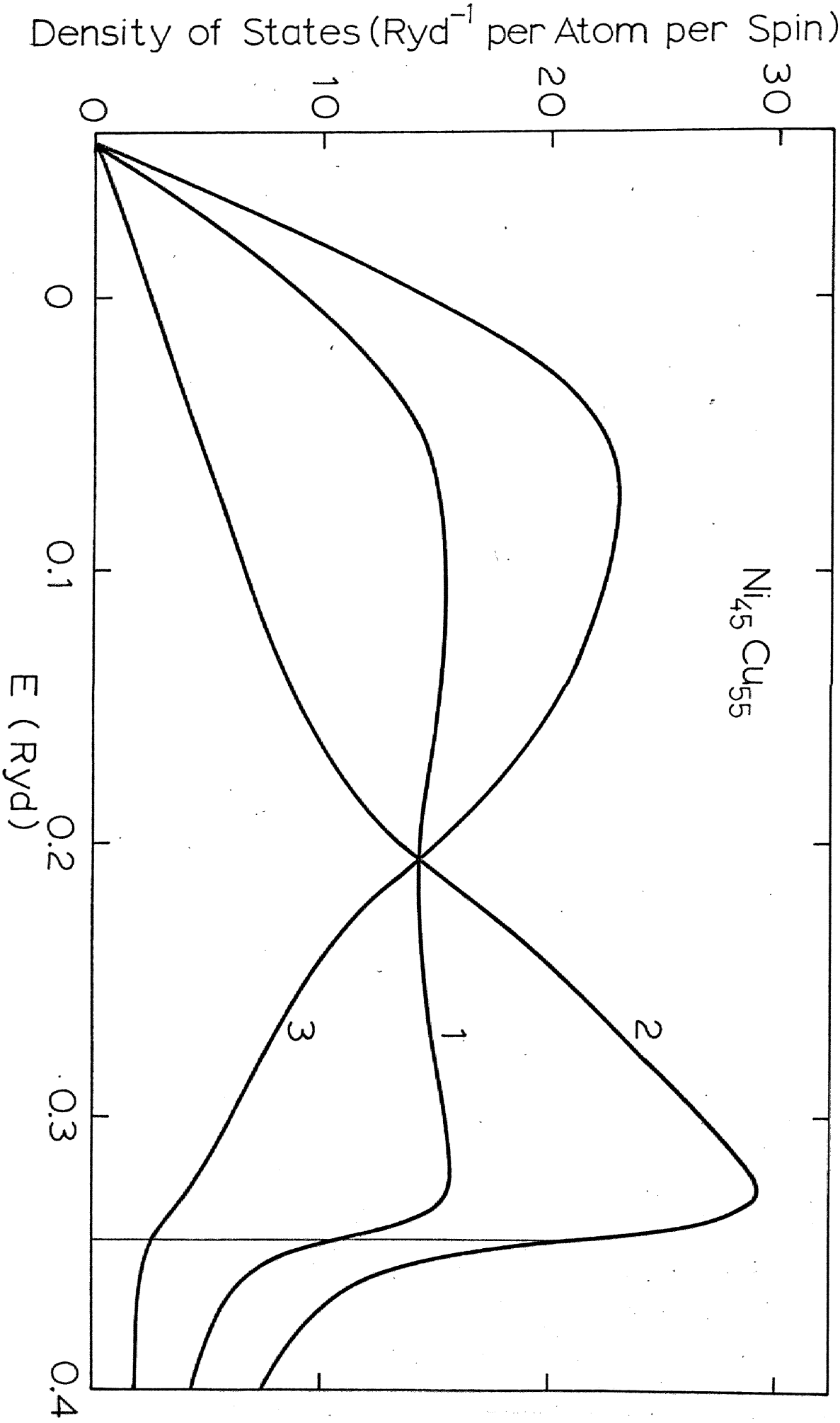
Density of States (Ryd^{-1} per Atom per Spin)
0
10
20
30
0
0.1
0.2
0.3
0.4
E (Ryd)
$Ni_{45}Cu_{55}$
1
2
3

Fig. 34

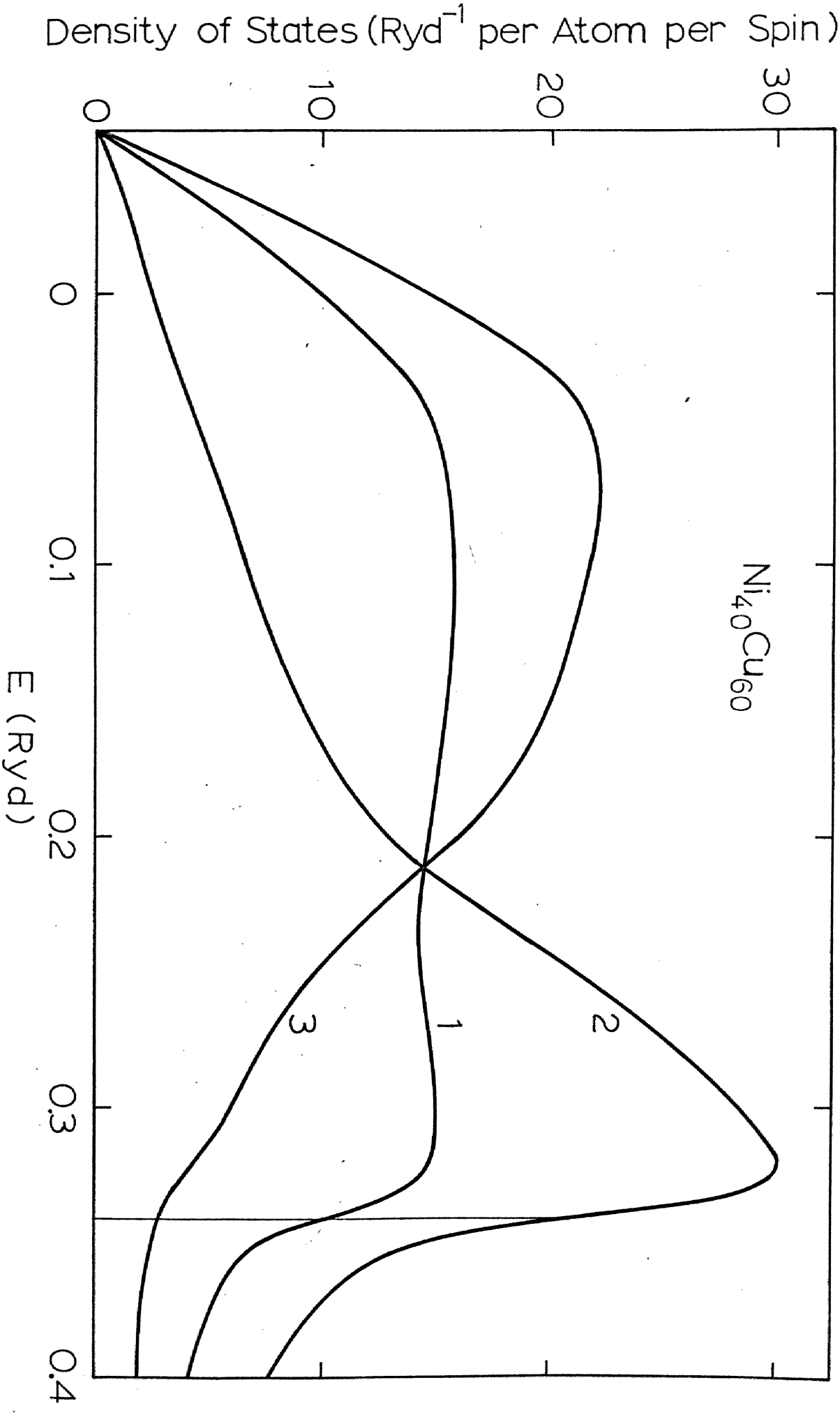
Density of States (Ryd^{-1} per Atom per Spin)
0
10
20
30
E (Ryd)
0
0.1
0.2
0.3
0.4
$Ni_{40}Cu_{60}$
1
2
3

Fig. 35

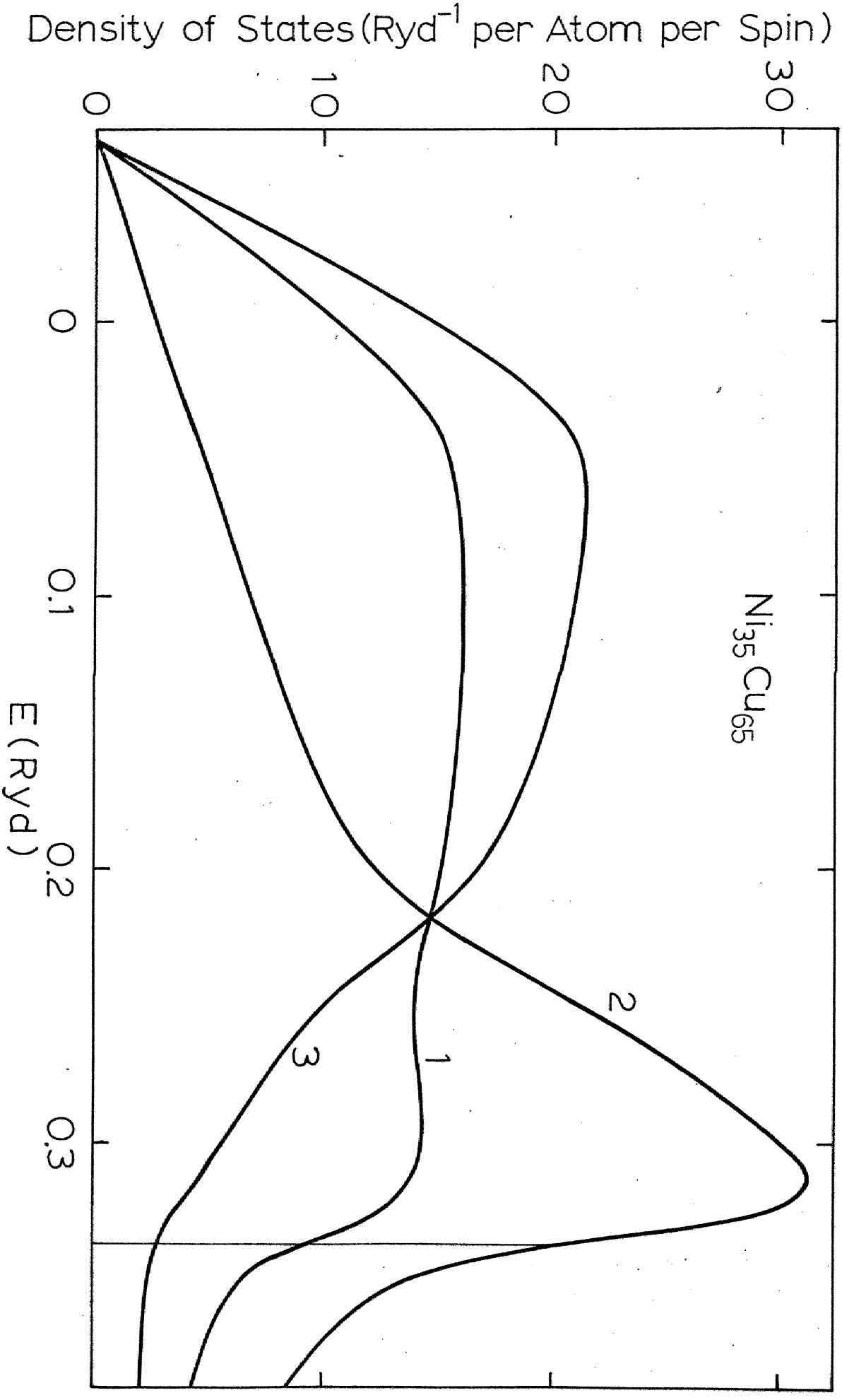
Density of States (Ryd^{-1} per Atom per Spin)
0
10
20
30
0
0.1
0.2
0.3
E (Ryd)
$Ni_{35}Cu_{65}$
1
2
3

Fig. 36

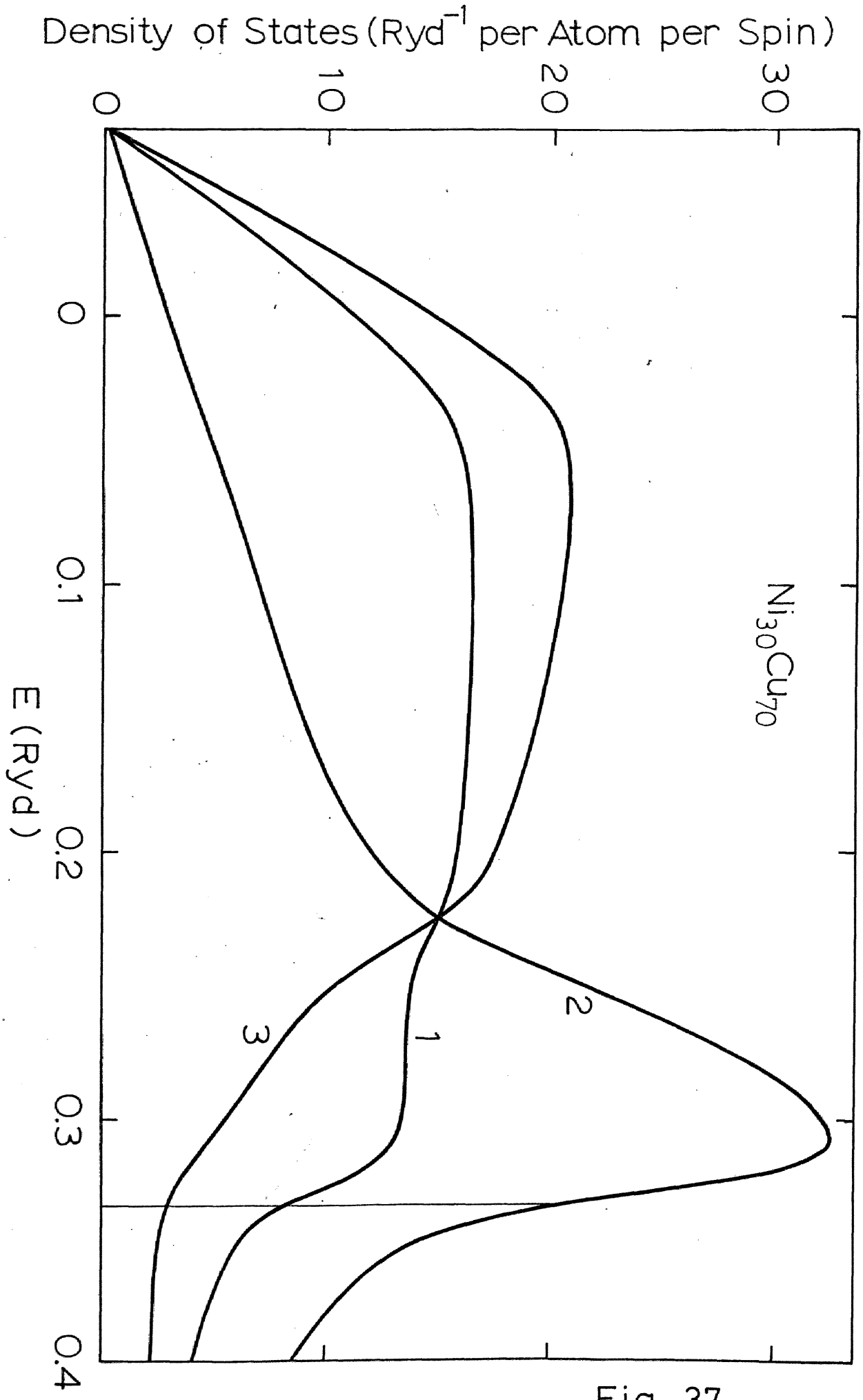
Density of States (Ryd^{-1} per Atom per Spin)
0
10
20
30
E (Ryd)
0
0.1
0.2
0.3
0.4
$Ni_{30}Cu_{70}$
1
2
3

Fig. 37

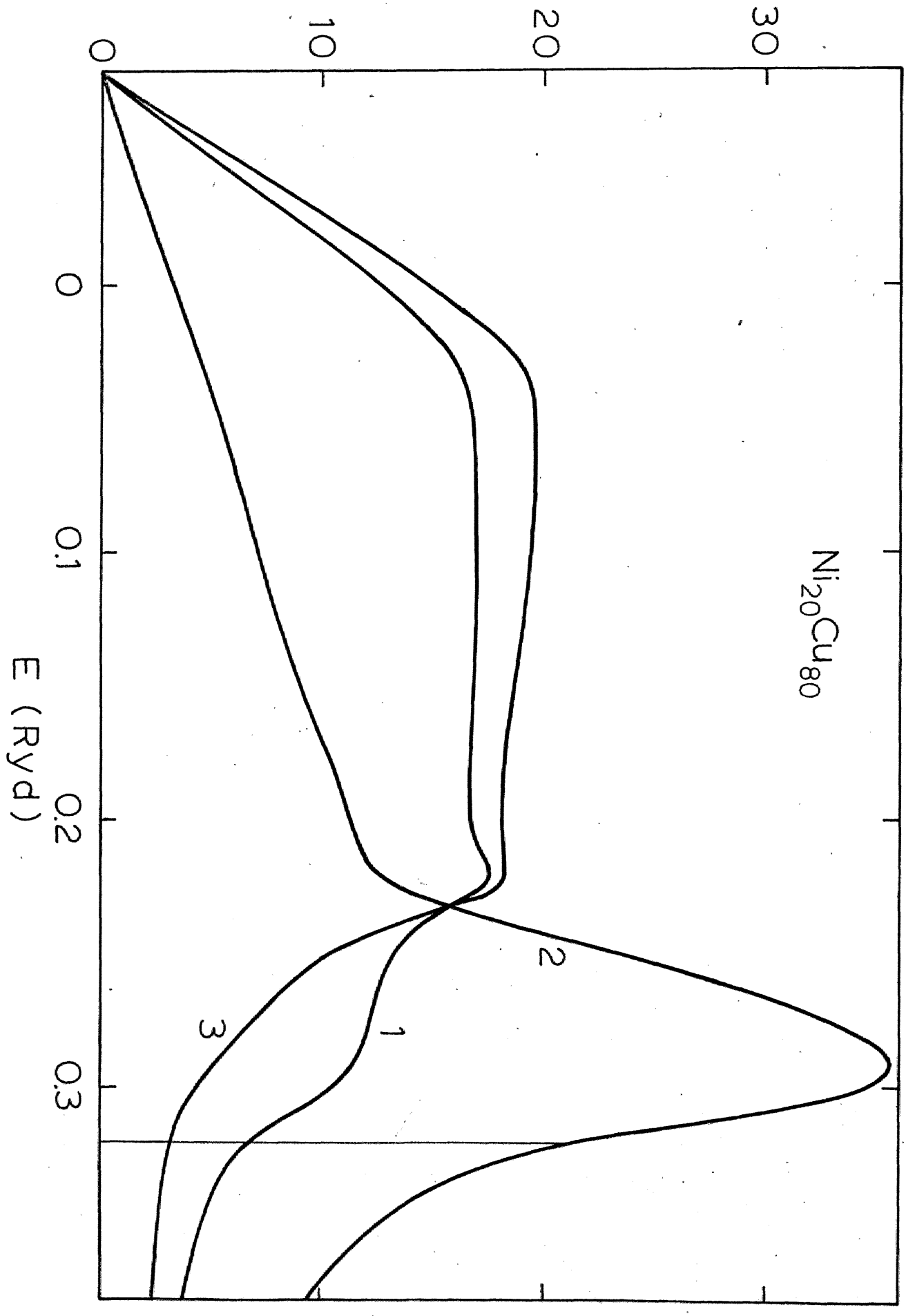
Density of States (Ryd^{-1} per Atom per Spin)
0
10
20
30
0
0.1
0.2
0.3
E (Ryd)
$Ni_{20}Cu_{80}$
1
2
3

Fig. 38

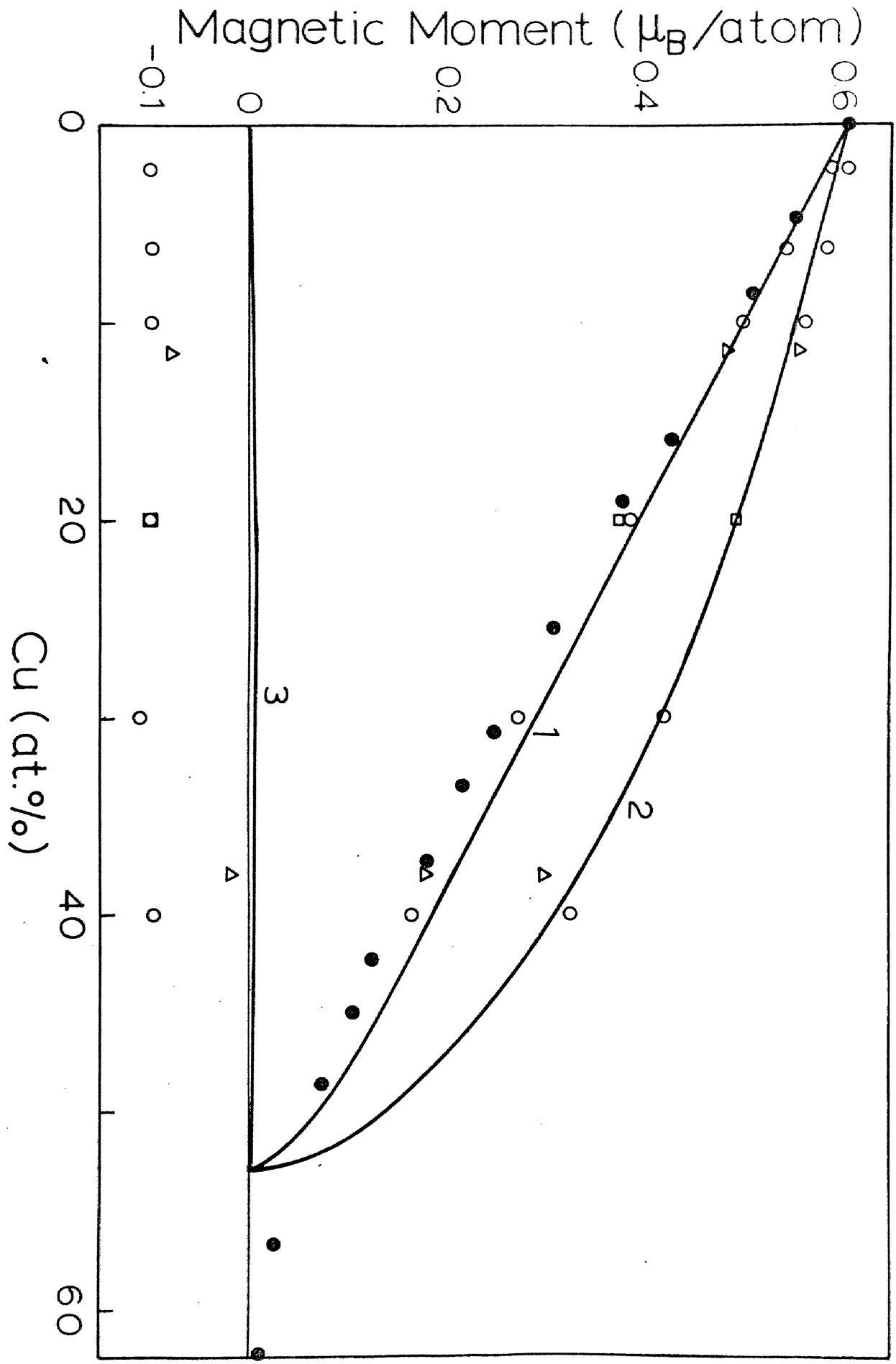

Fig. 39

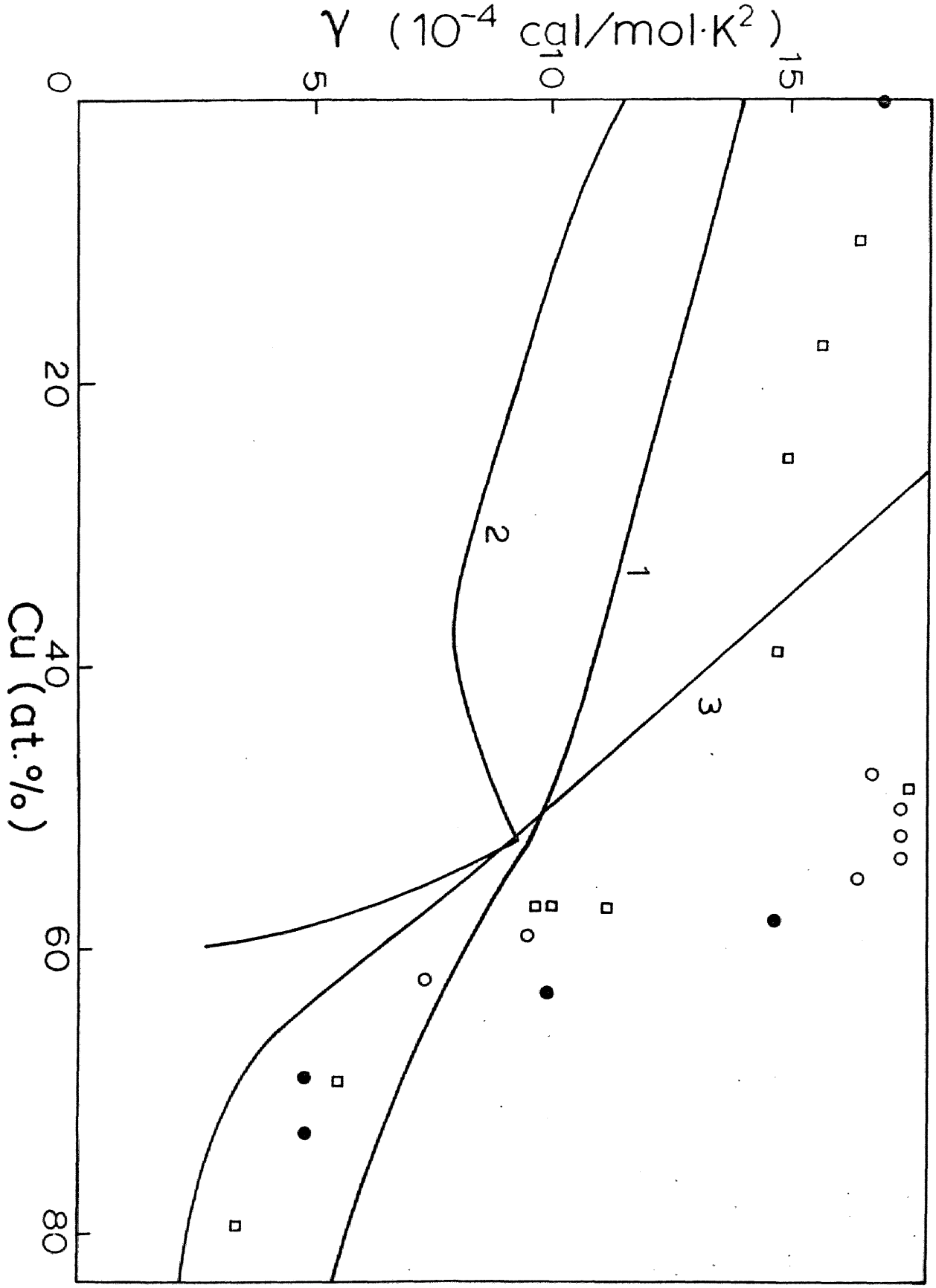

Fig. 40

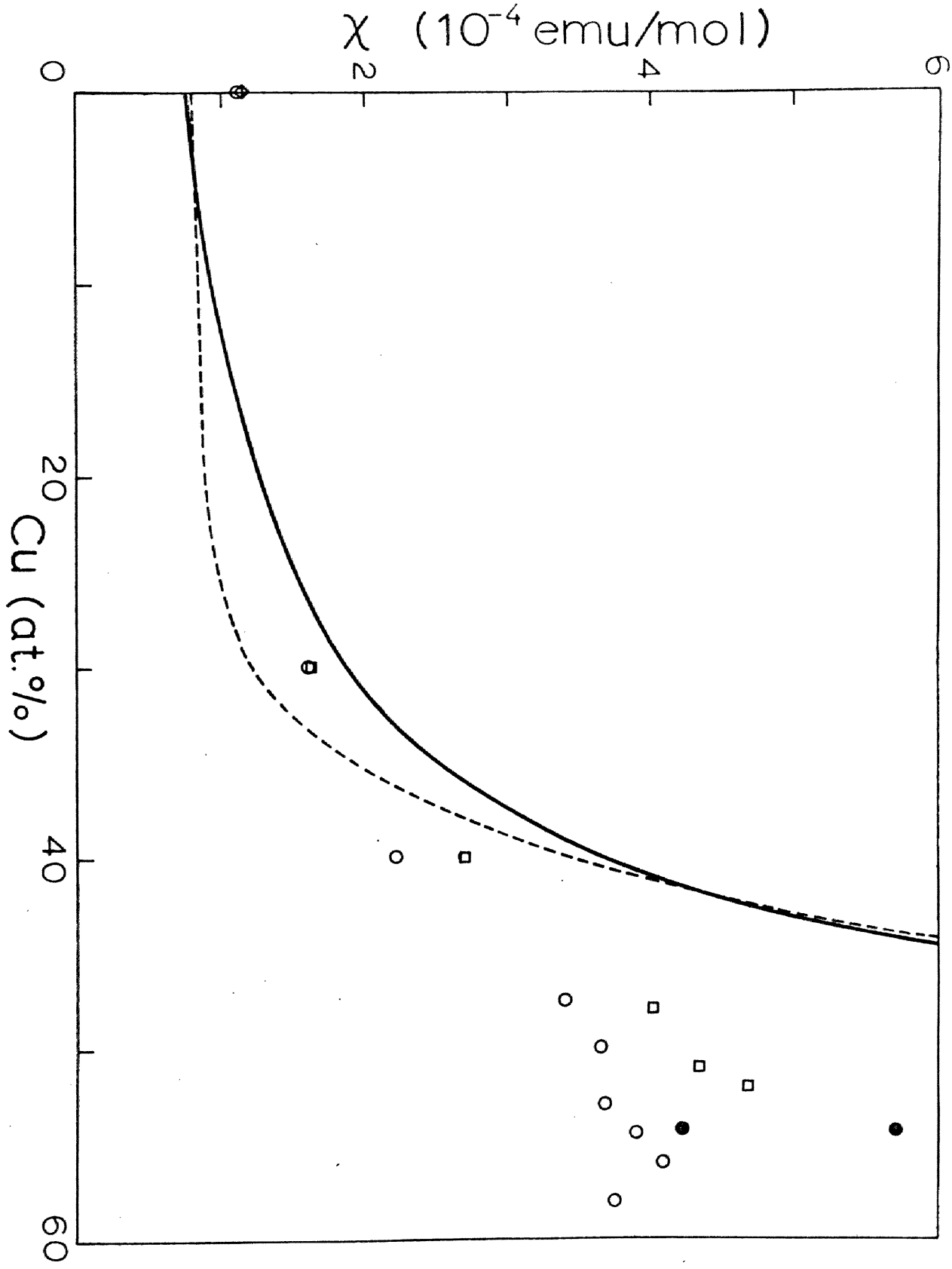

Fig. 41

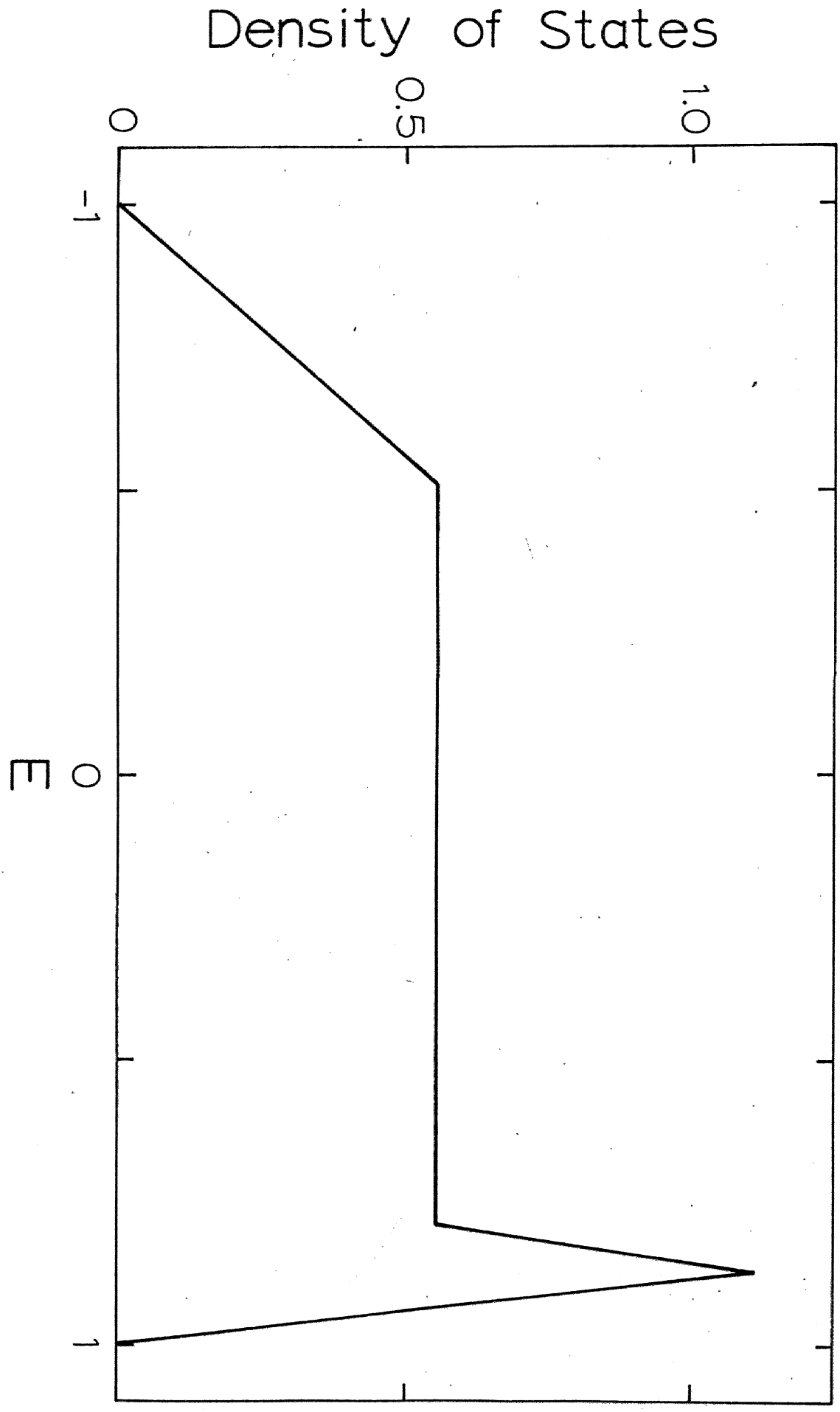

Fig. 42

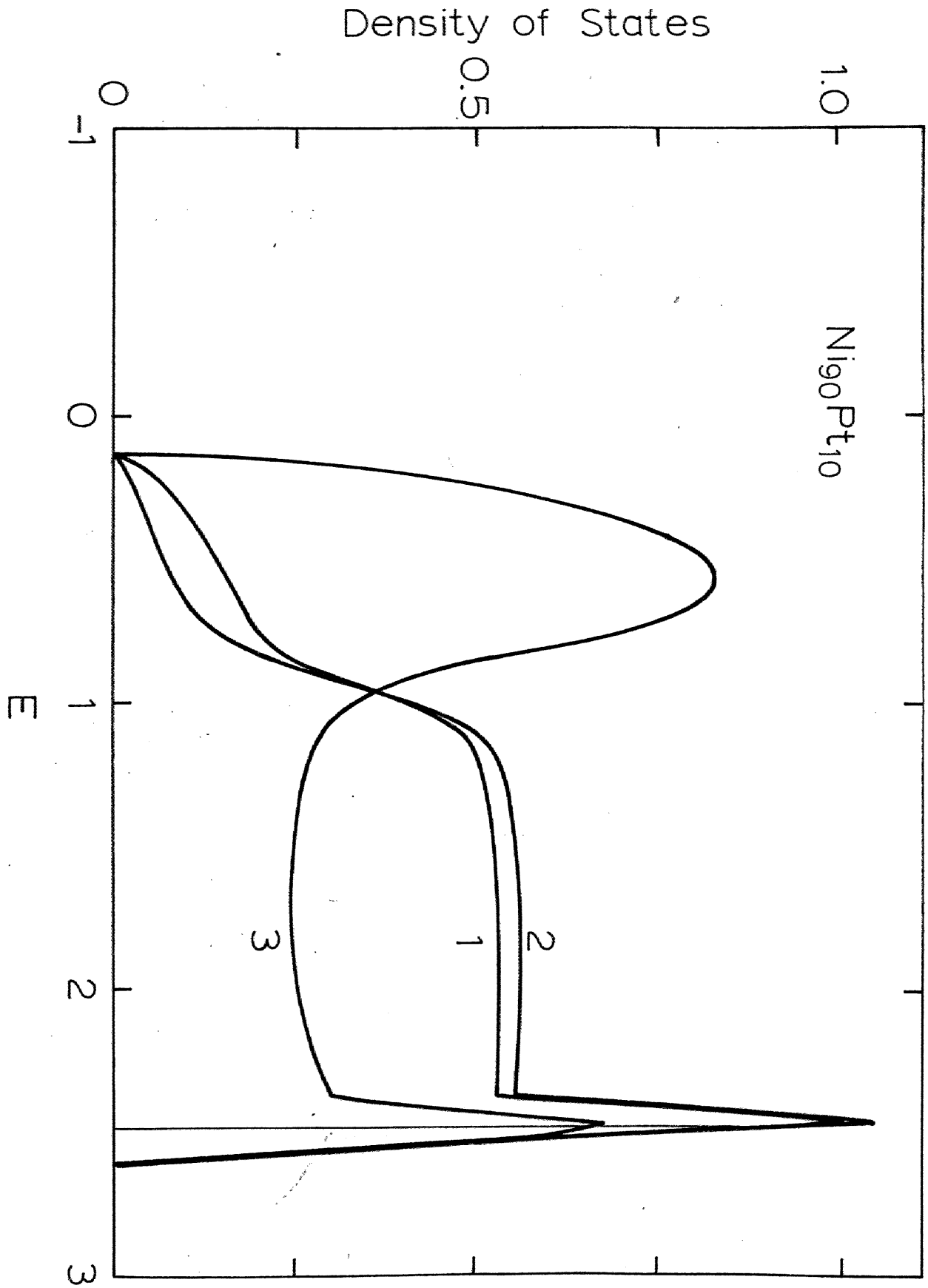

Fig. 43

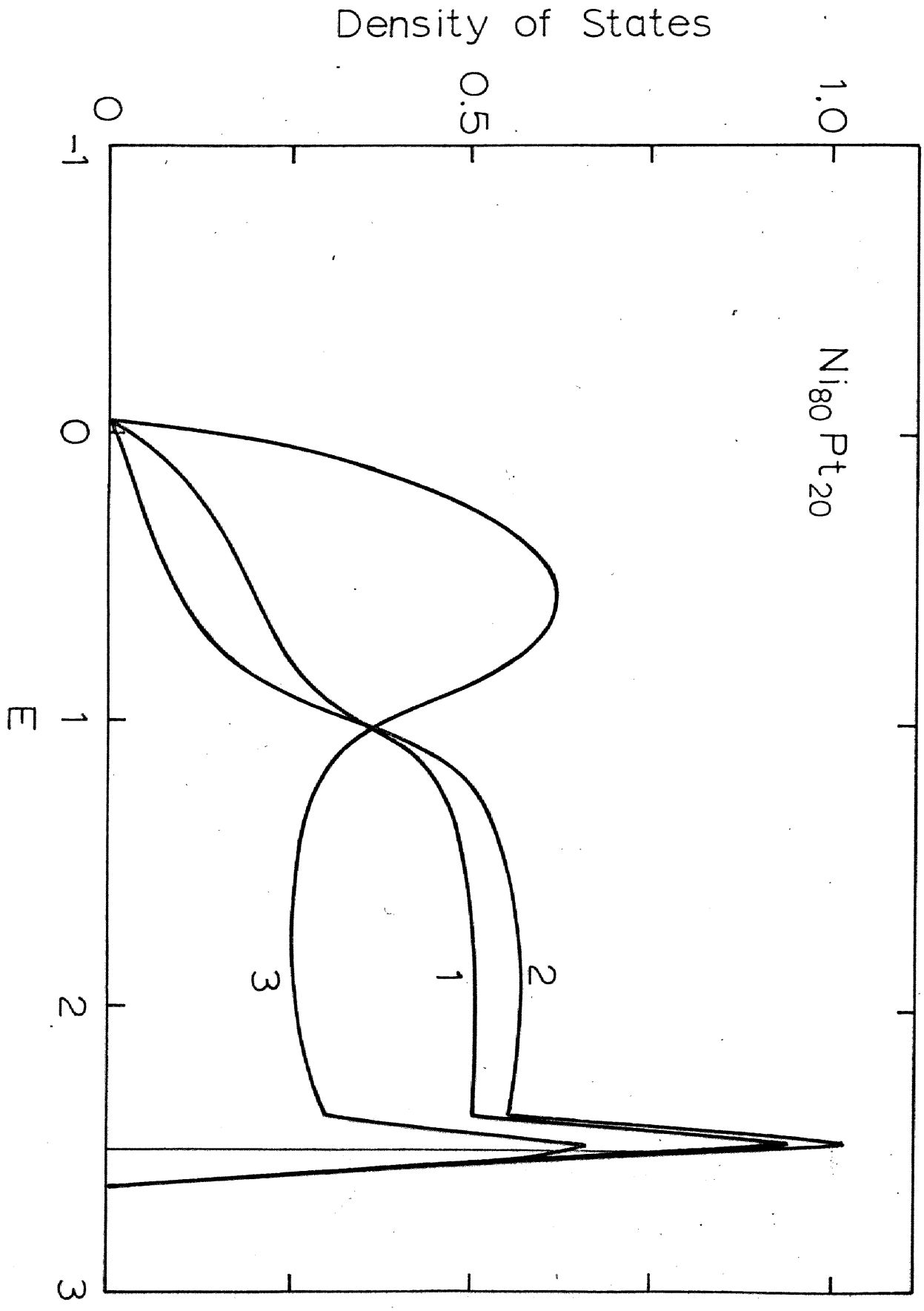

Fig.44

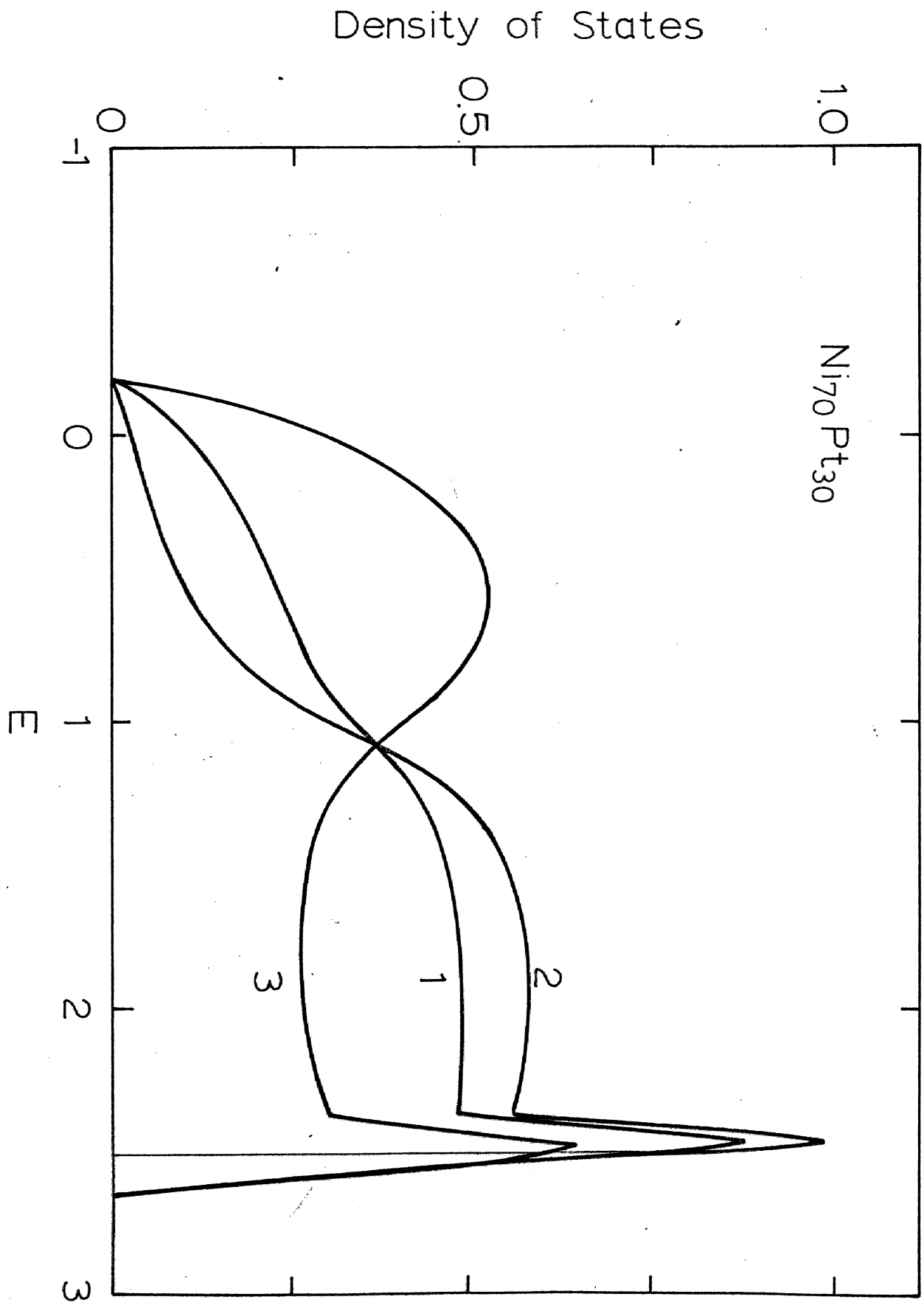

Fig. 45

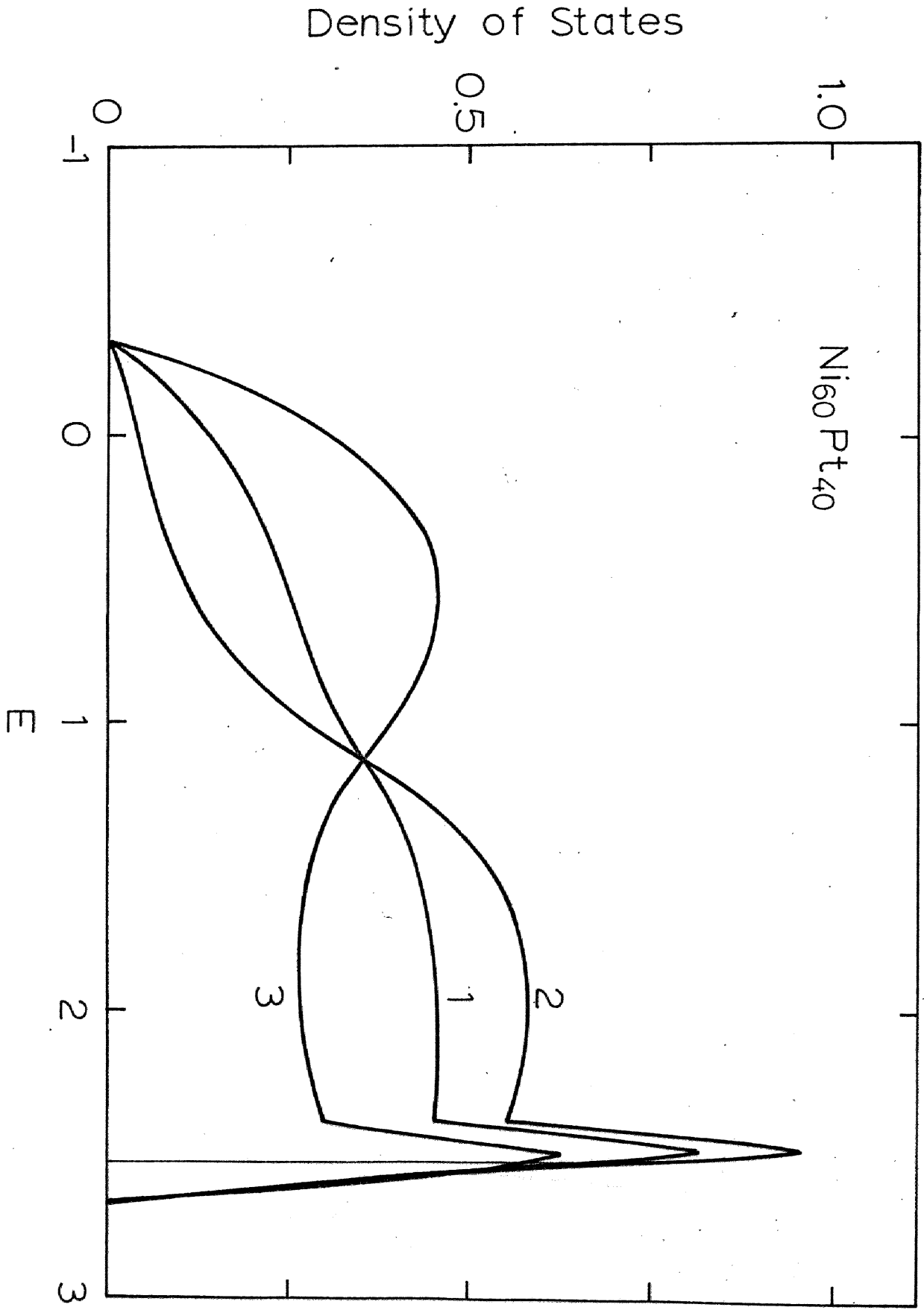

Fig. 46

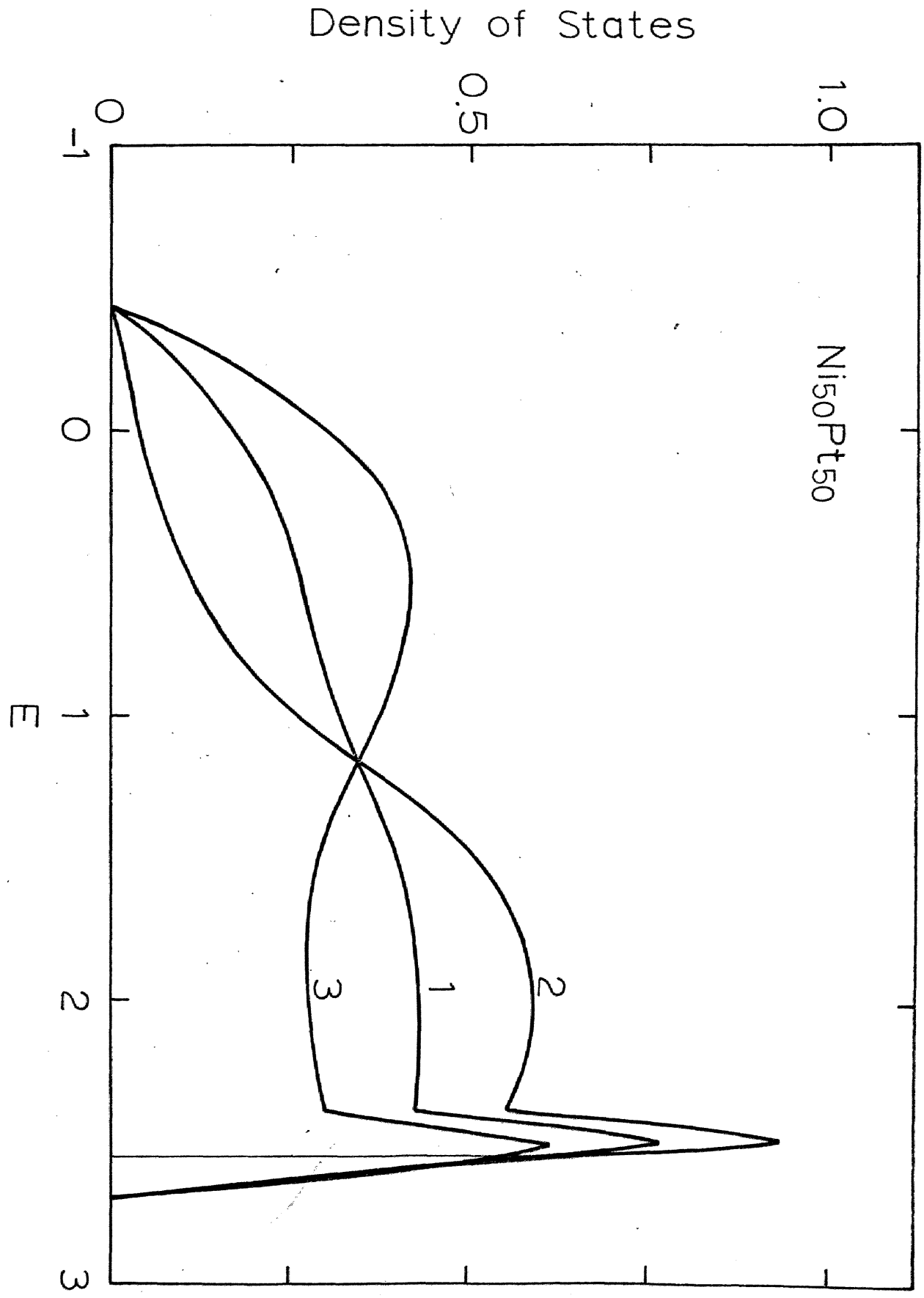

Fig. 47

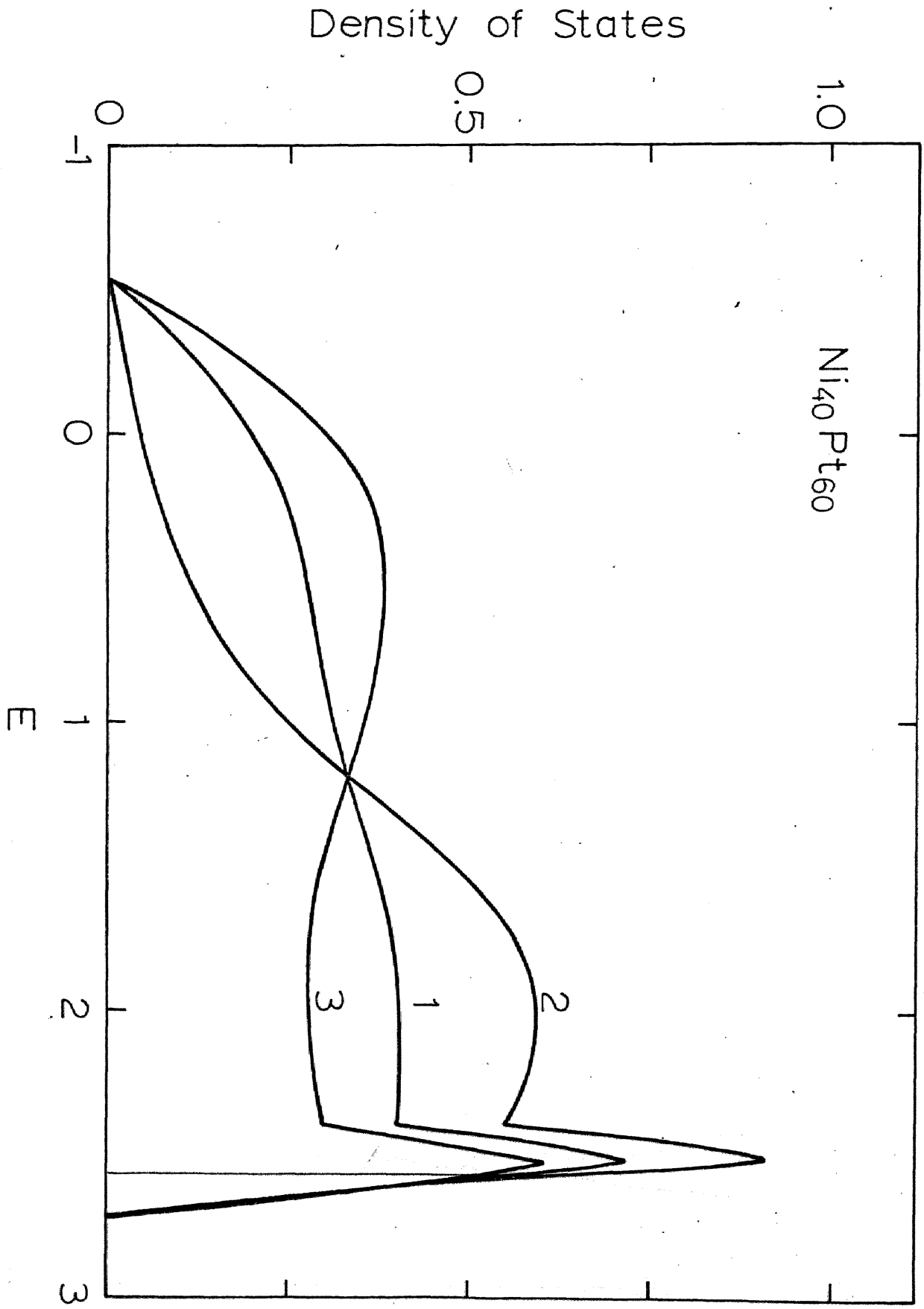

Fig. 48

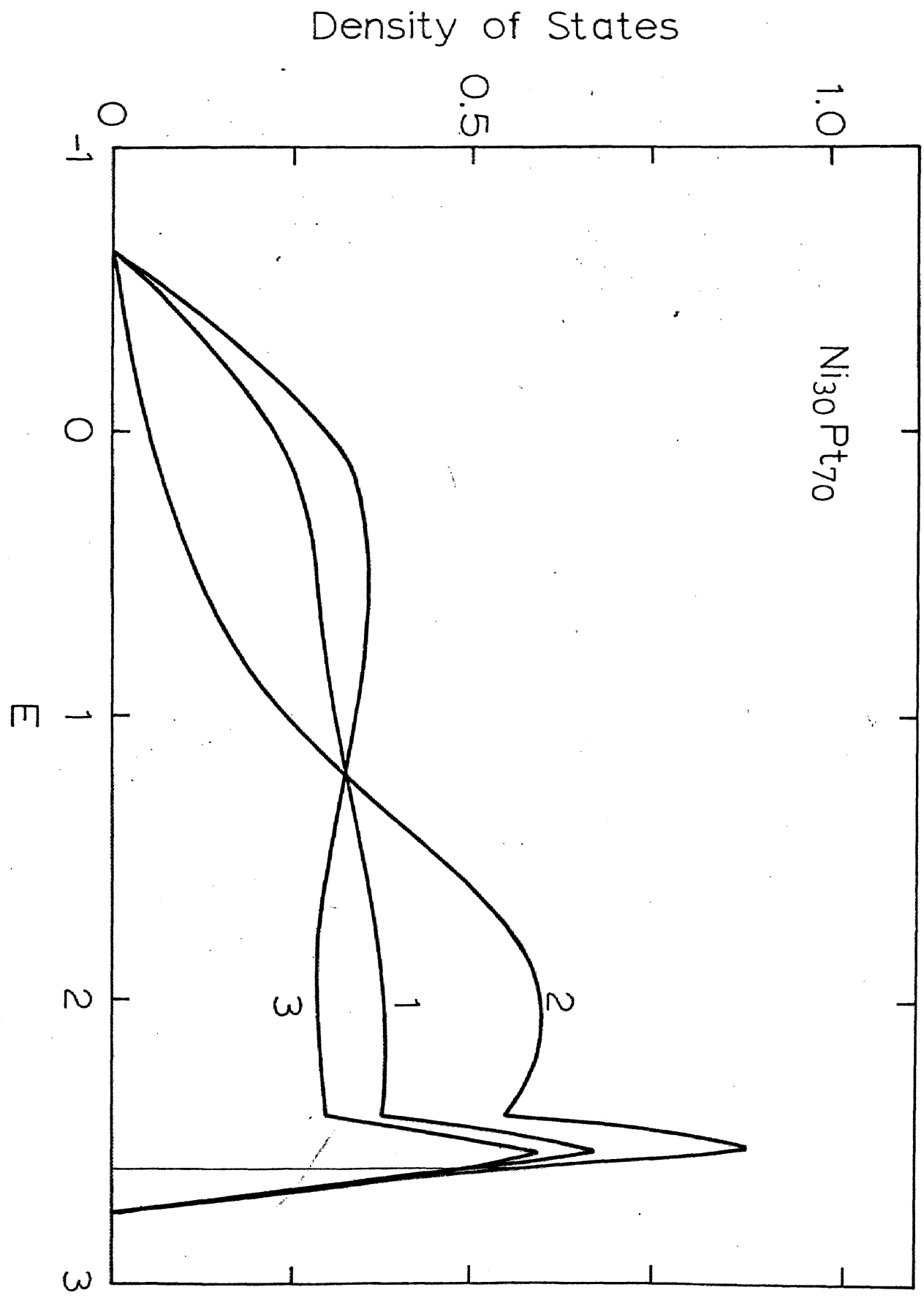

Fig. 49

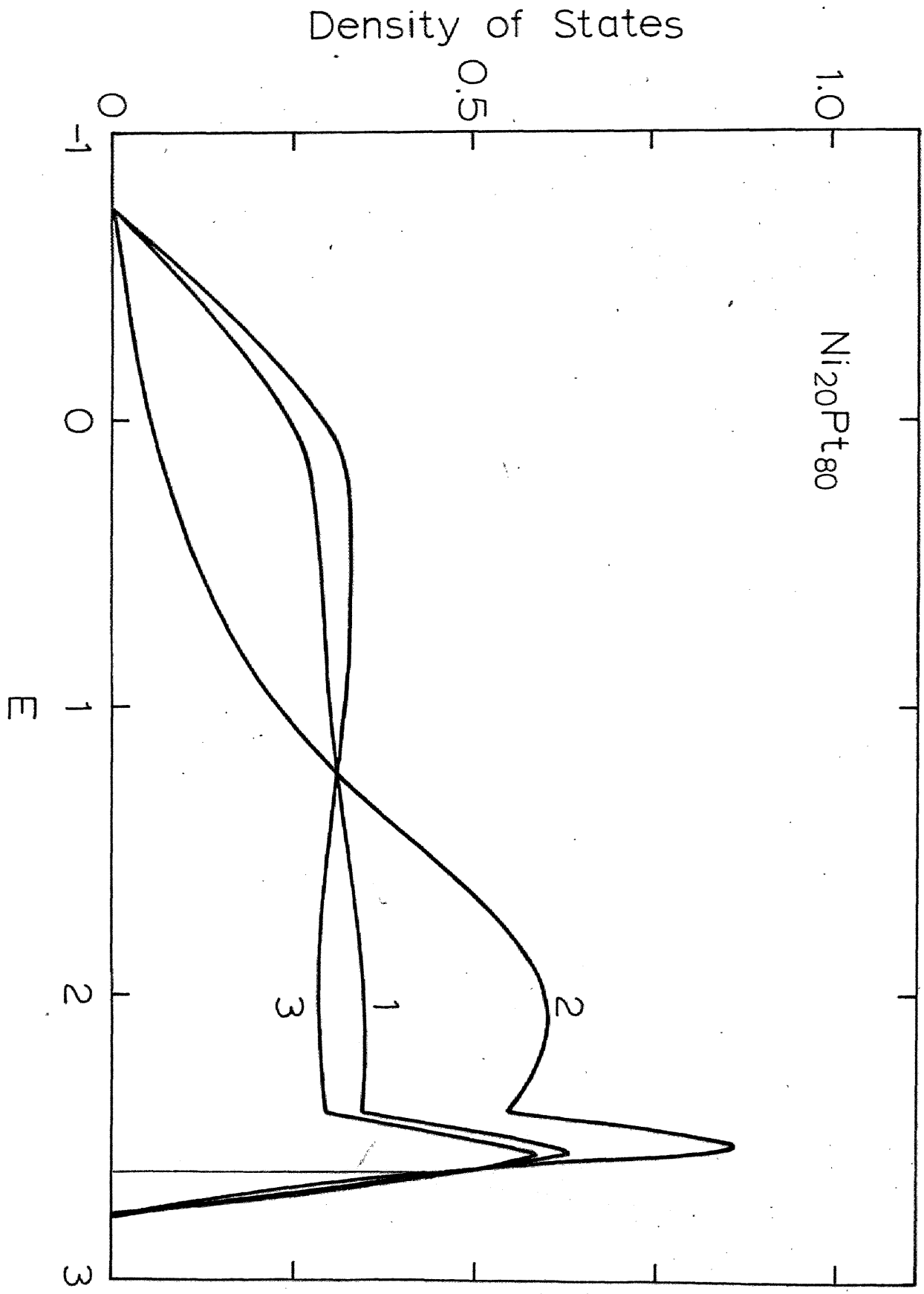

Fig. 50

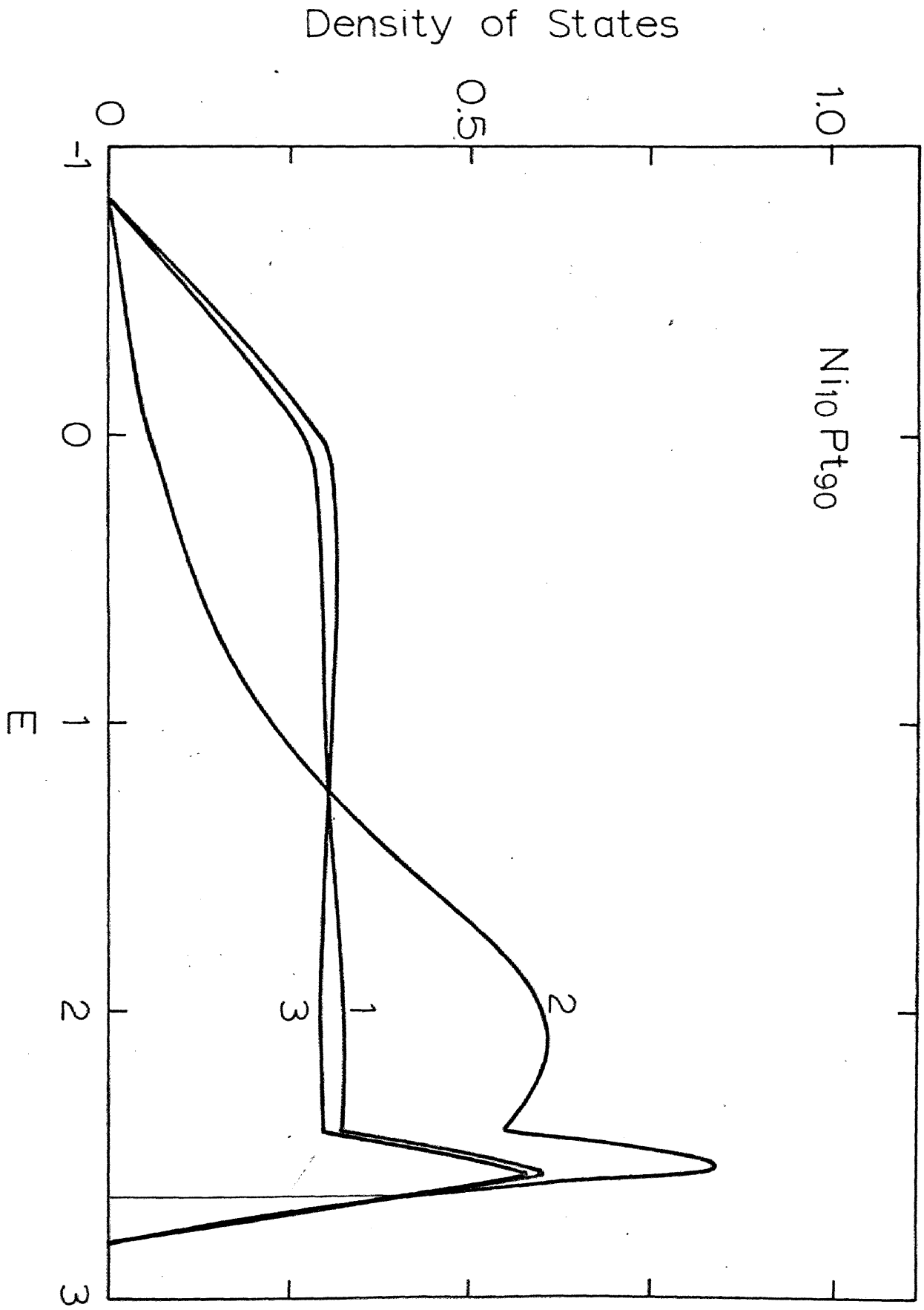

Fig. 51

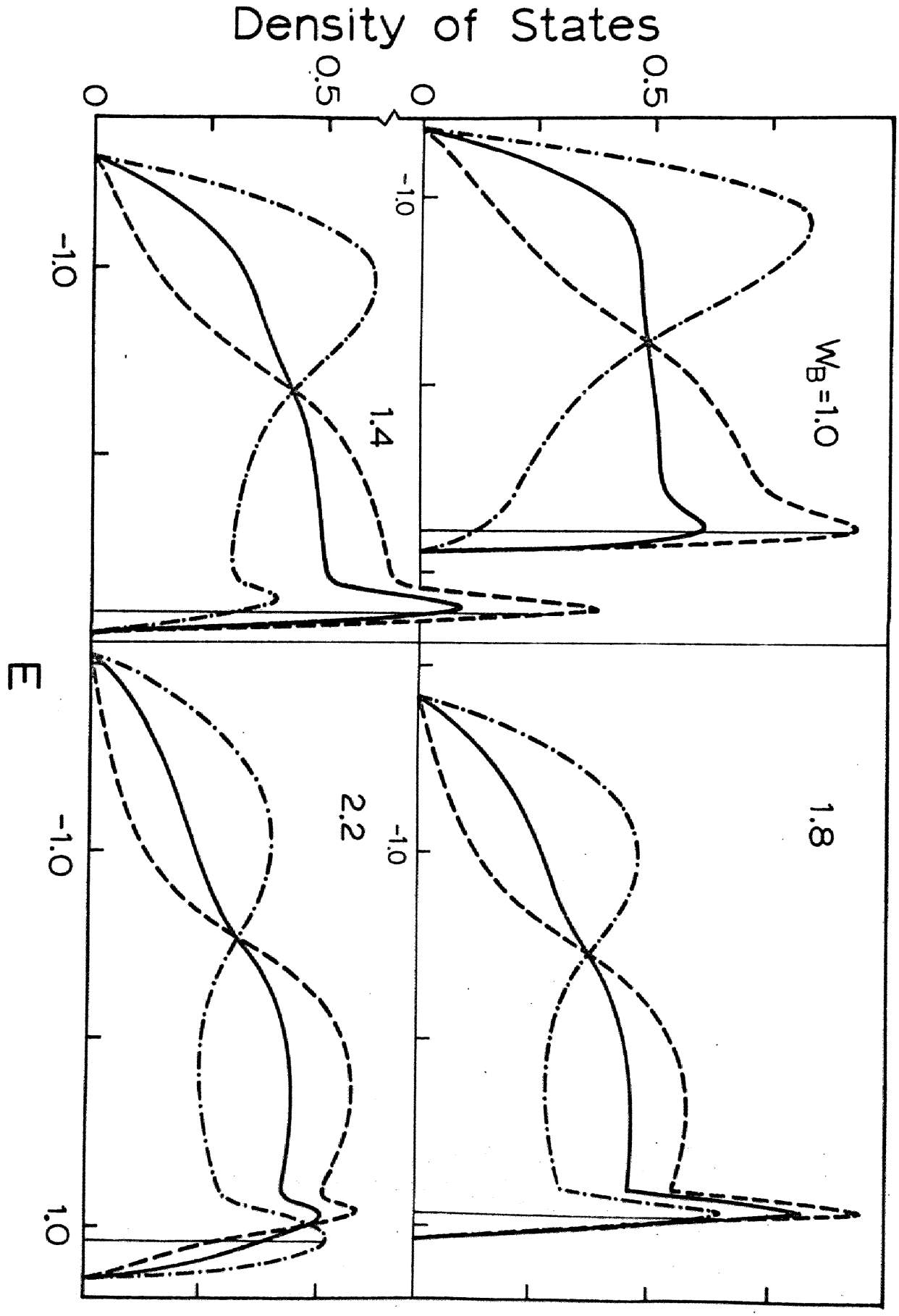

Fig. 52

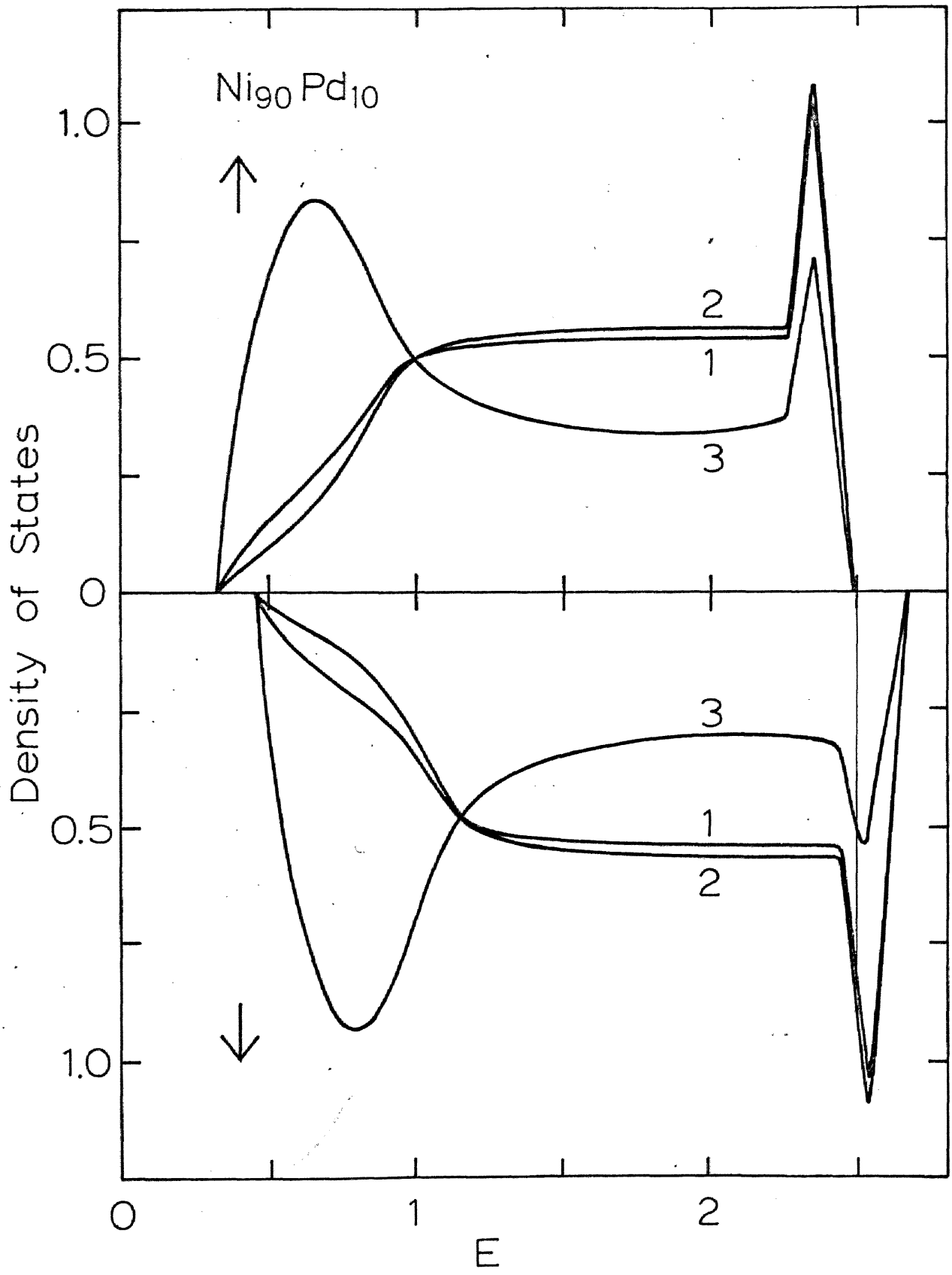

Fig. 53

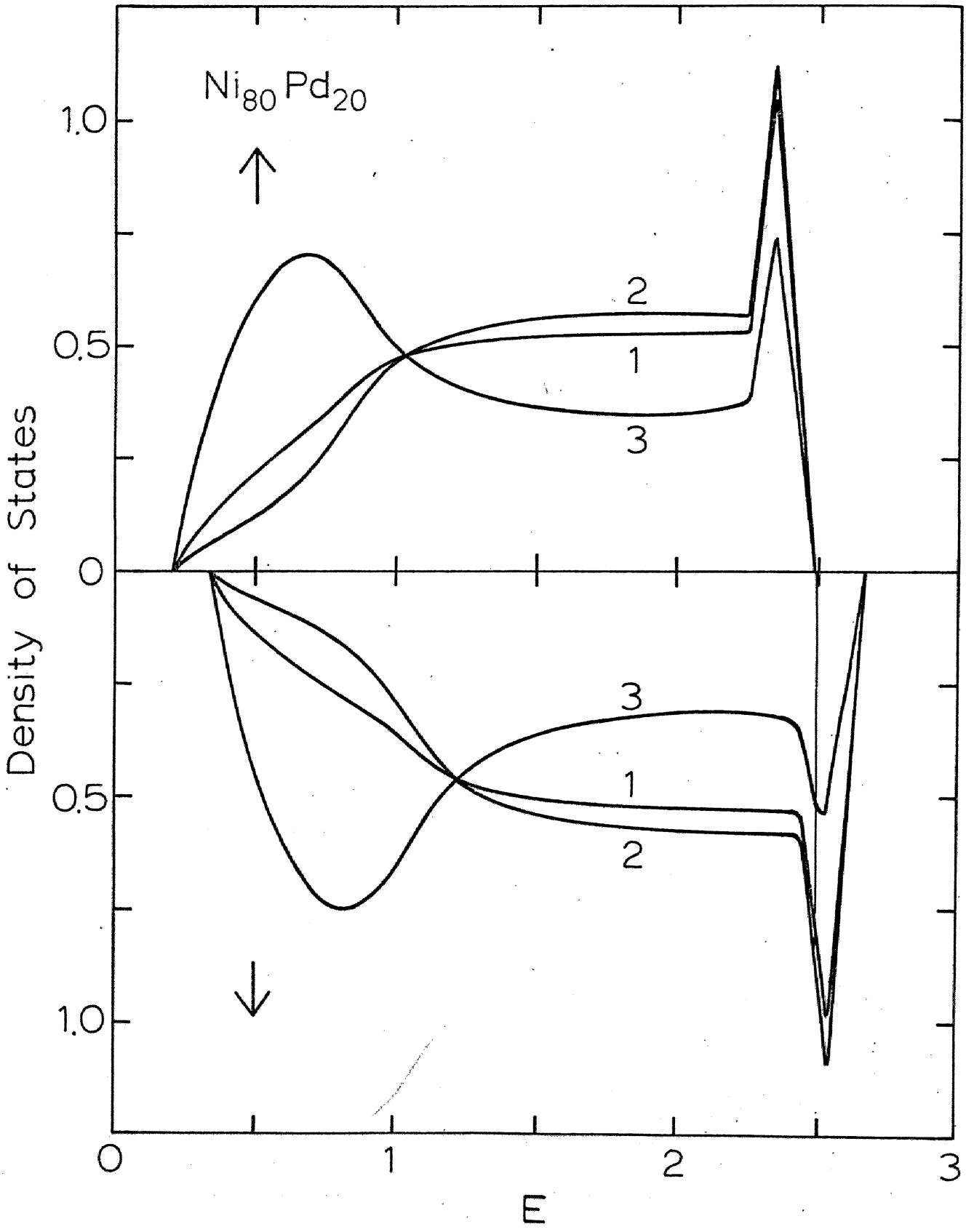

Fig. 54

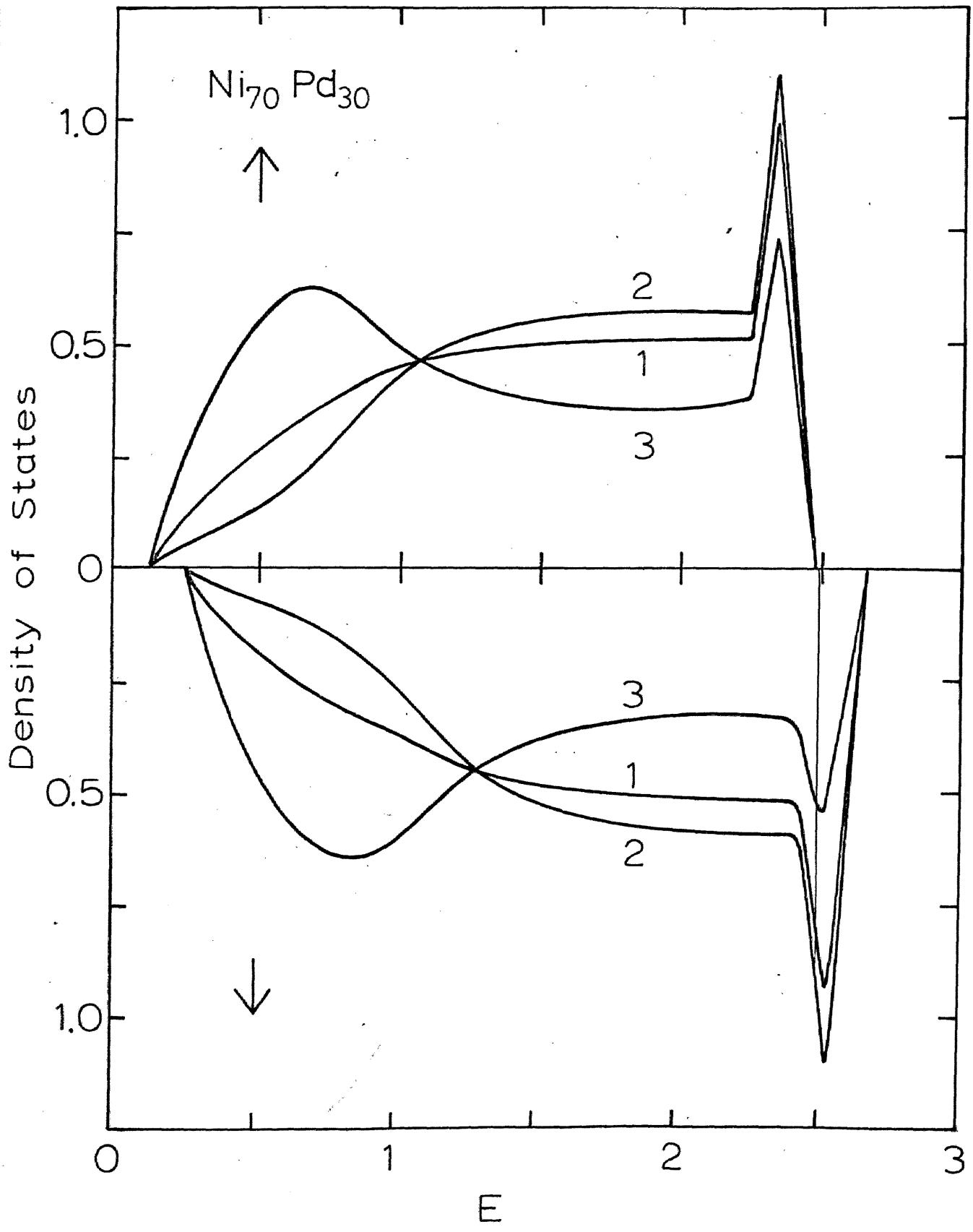

Fig. 55

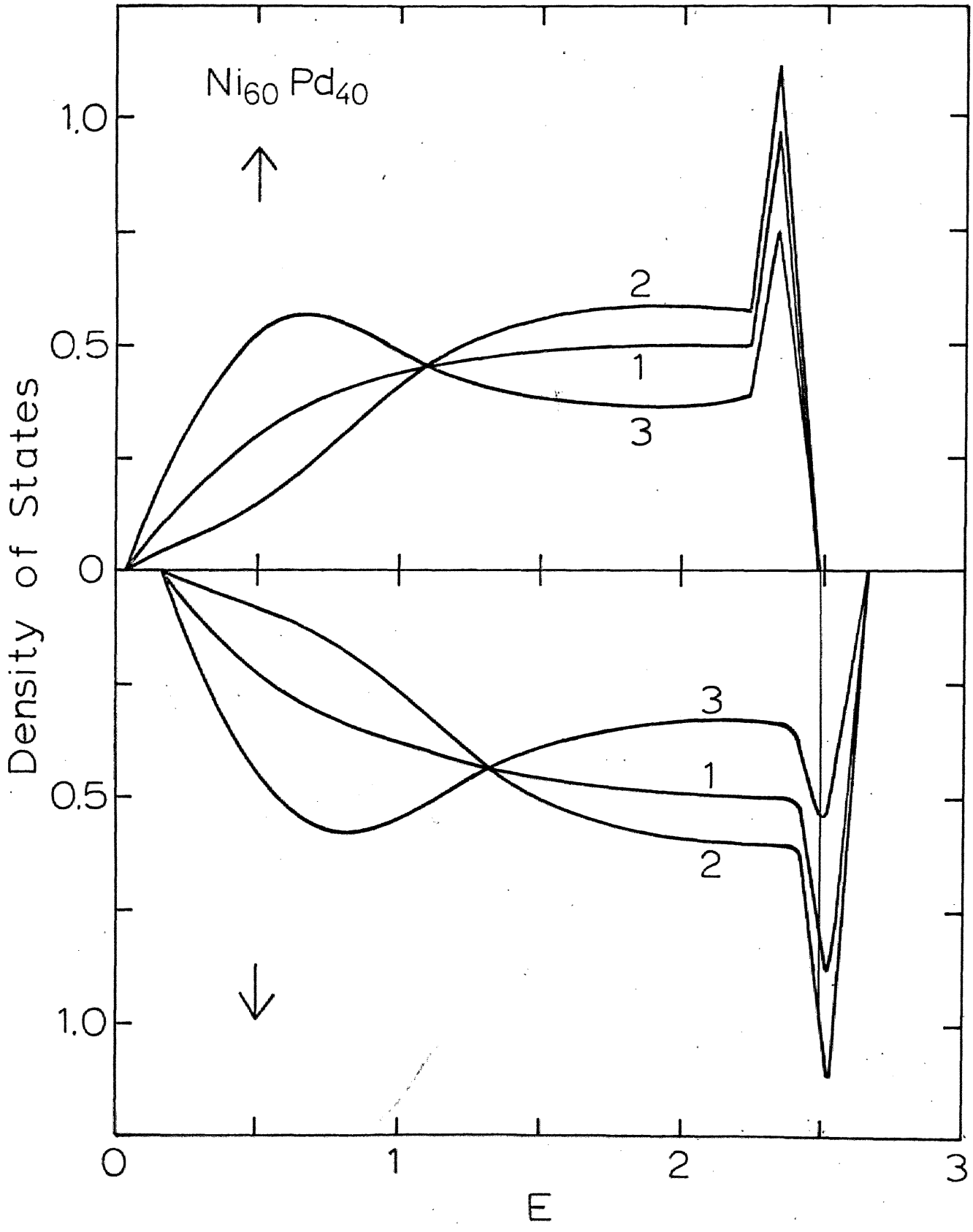

Fig. 56

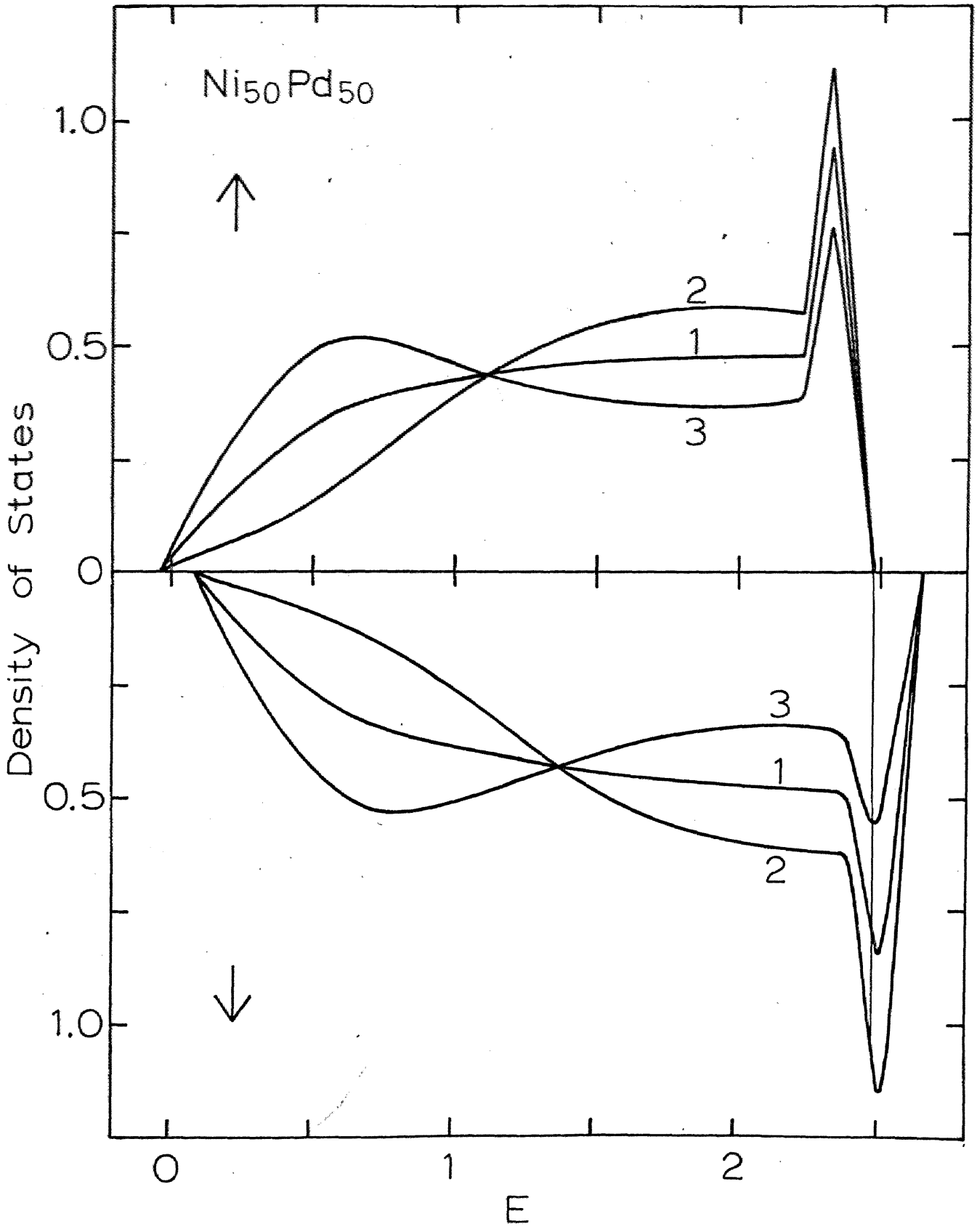

Fig. 57

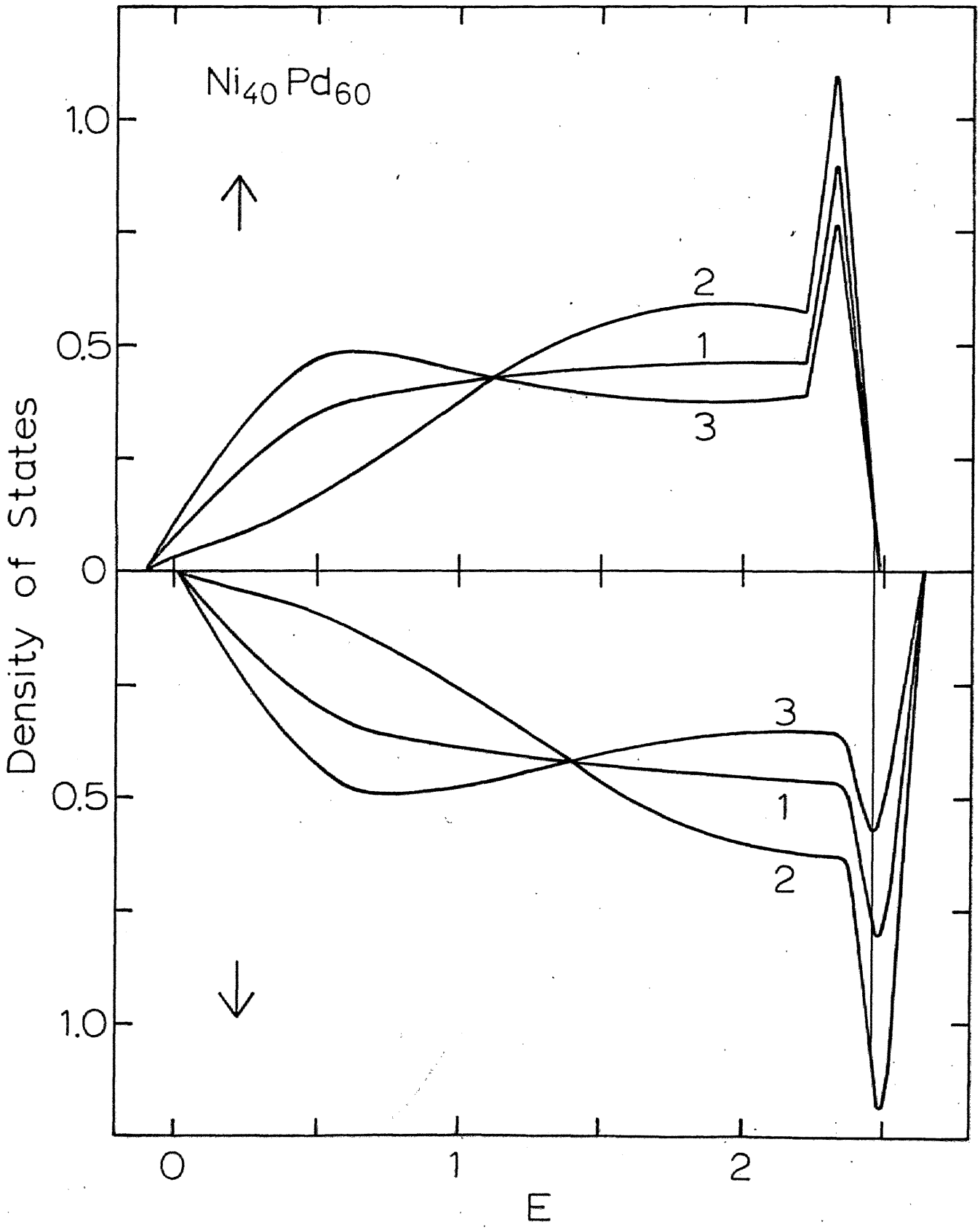

Fig. 58

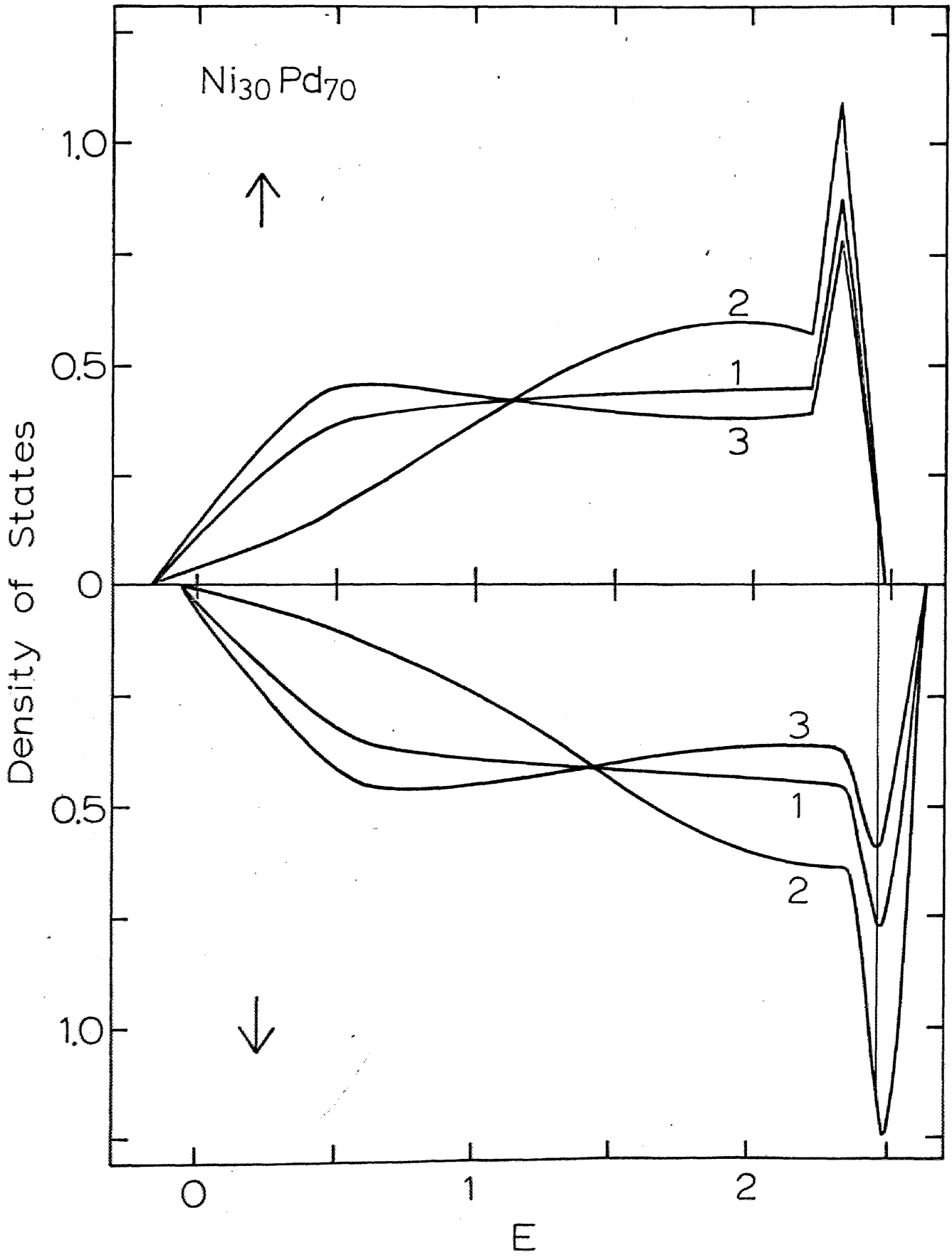

Fig. 59

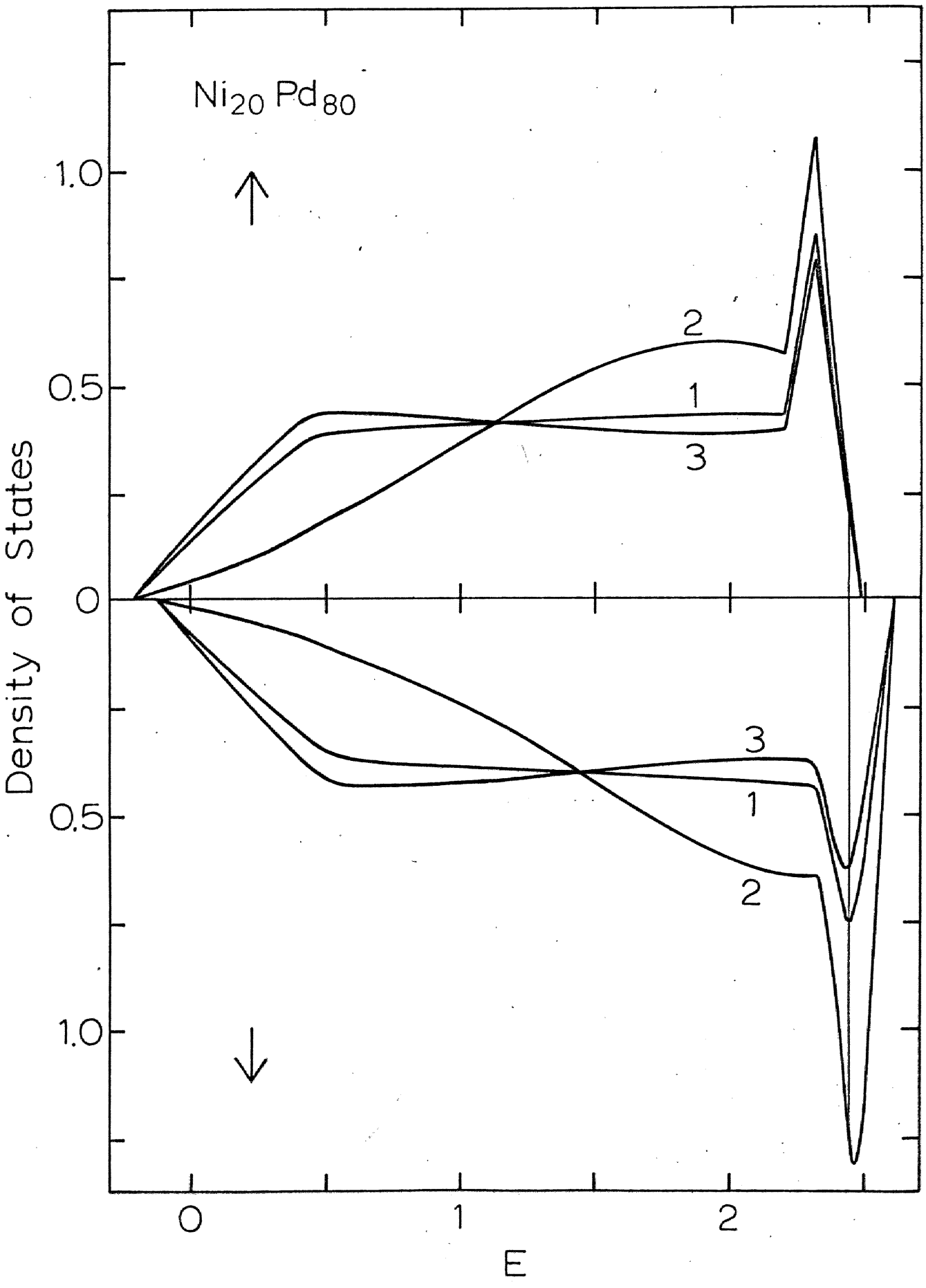

Fig. 60

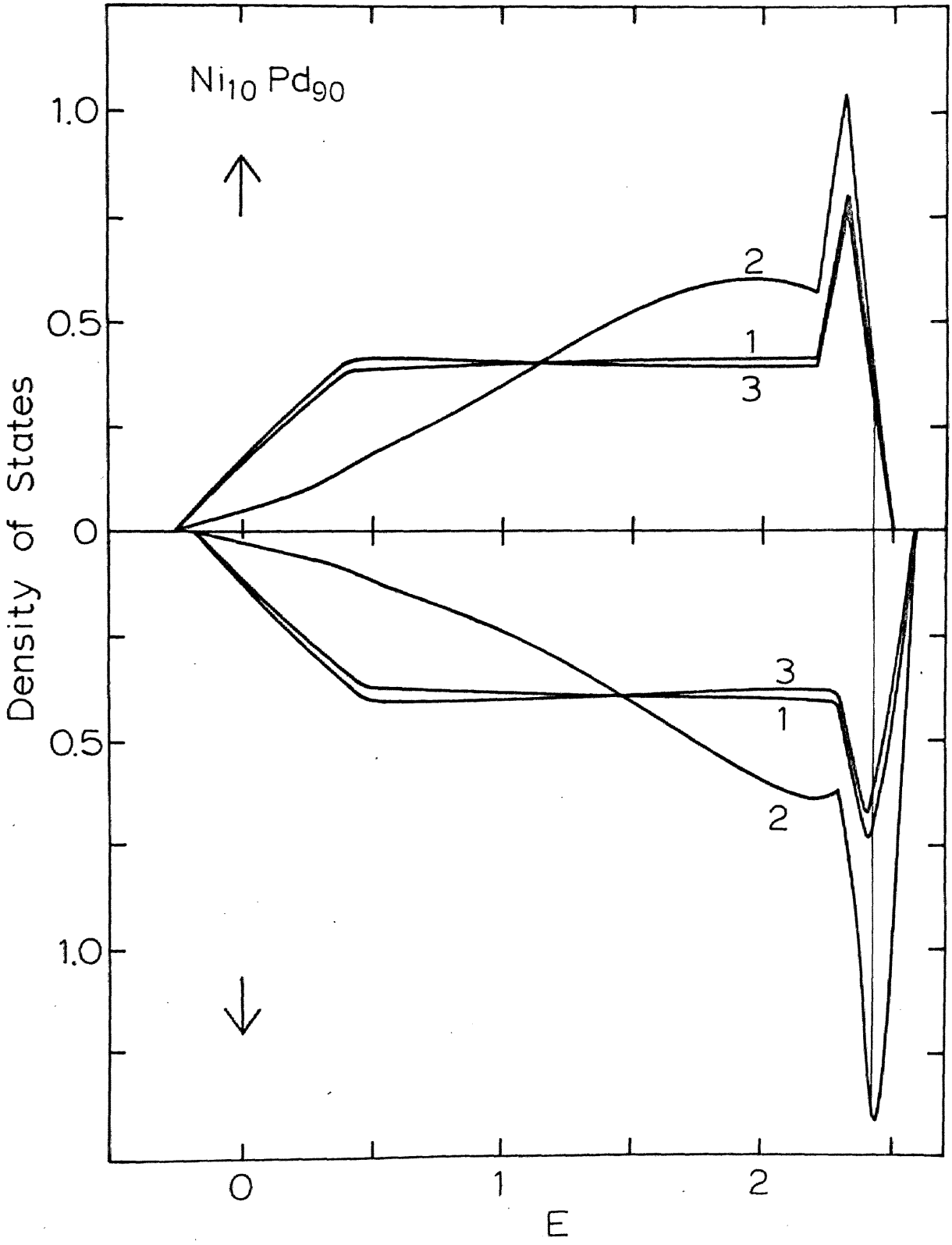

Fig. 61

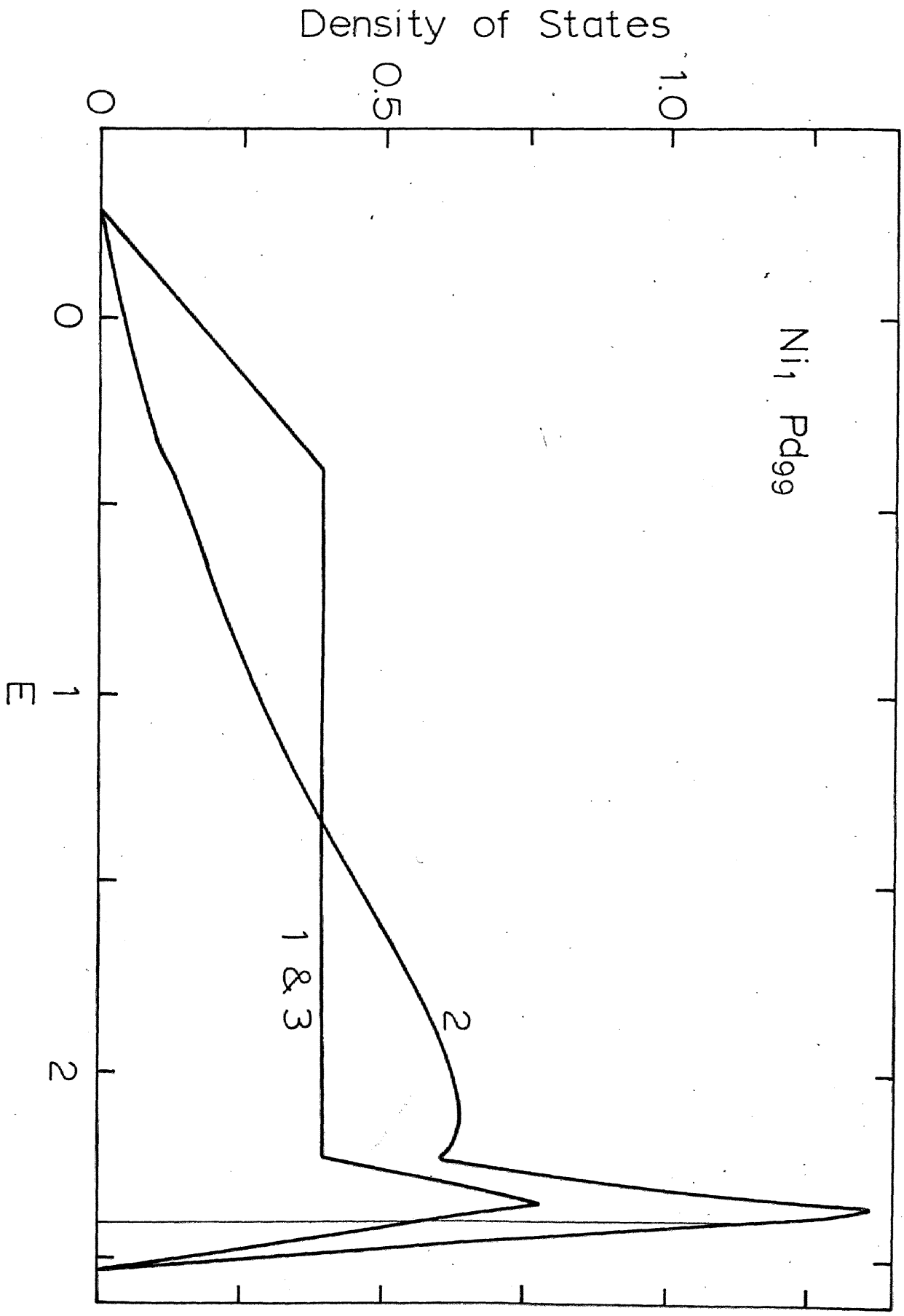

Fig. 62

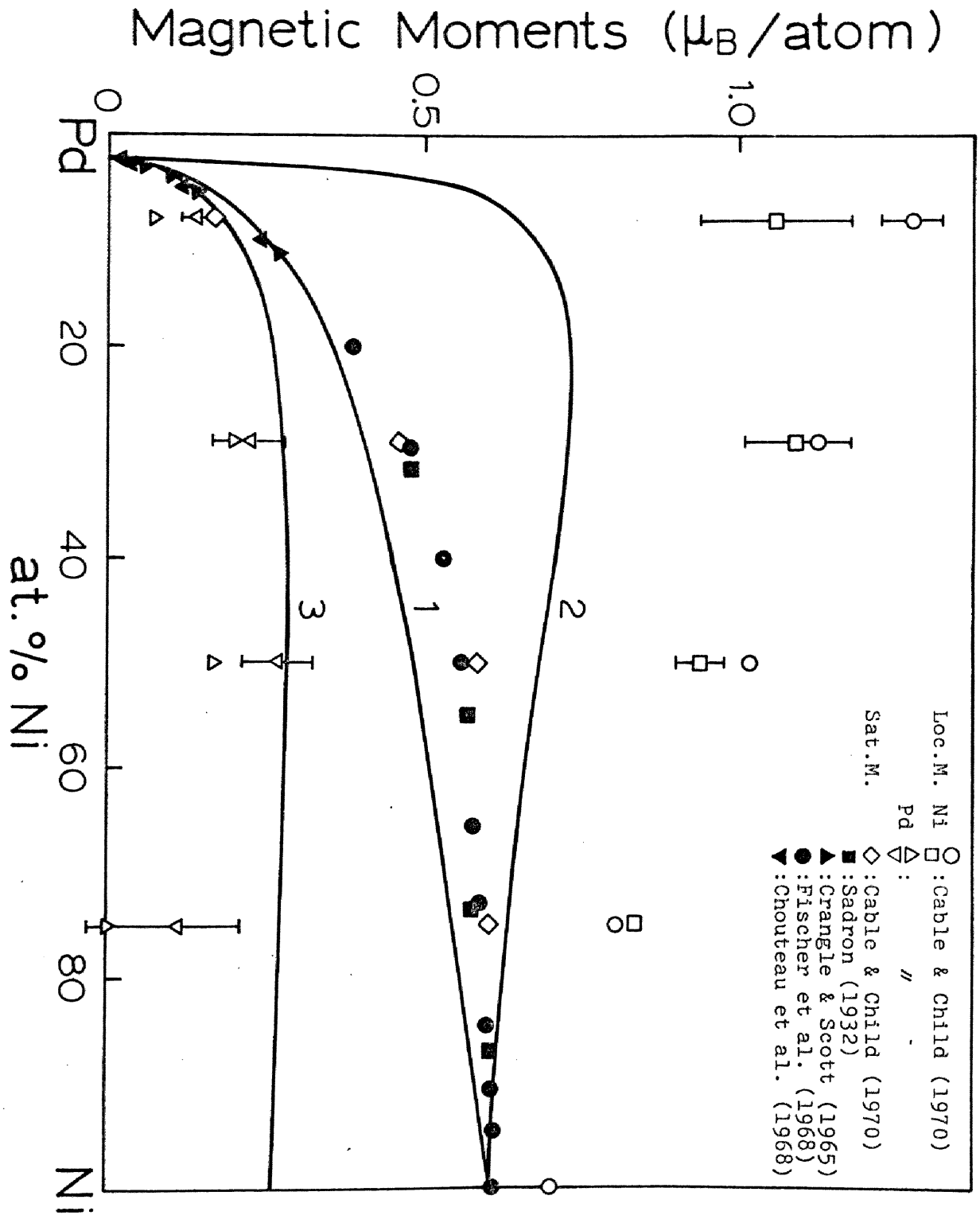
Magnetic Moments (μ_B/atom)
0
0.5
1.0
Pd
20
40
60
80
Ni
at.% Ni
1
2
3
Loc.M. Ni
:Cable & Child (1970)
Pd
:
〃
Sat.M.
:Cable & Child (1970)
:Sadron (1932)
:Crangle & Scott (1965)
:Fischer et al. (1968)
:Chouteau et al. (1968)

Fig. 63

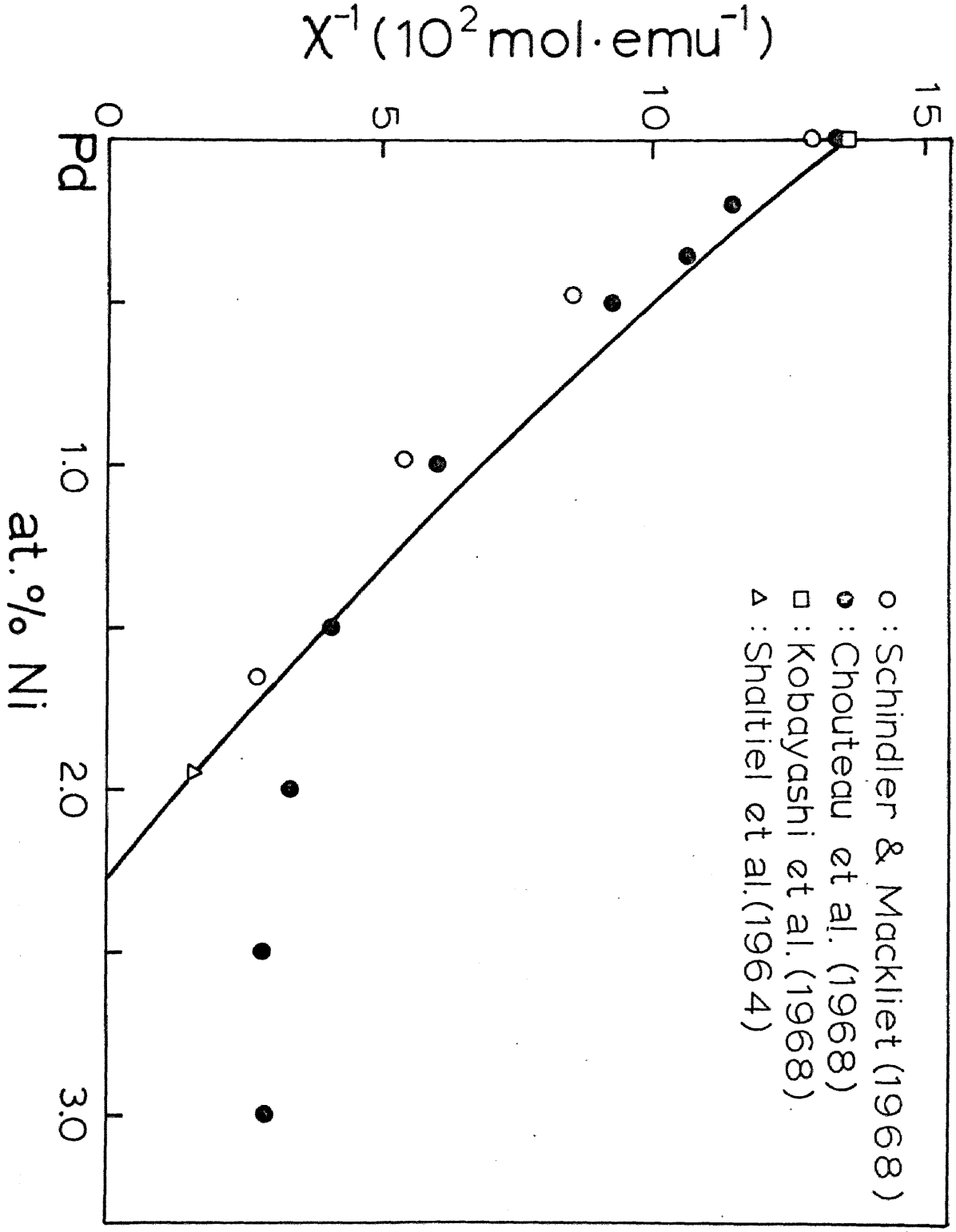
$\chi^{-1}(10^2 mol \cdot emu^{-1})$
0
5
10
15
Pd
1.0
2.0
3.0
at.% Ni
o : Schindler & Macklet (1968)
● : Chouteau et al. (1968)
□ : Kobayashi et al. (1968)
△ : Shaltiel et al. (1964)

Fig. 64

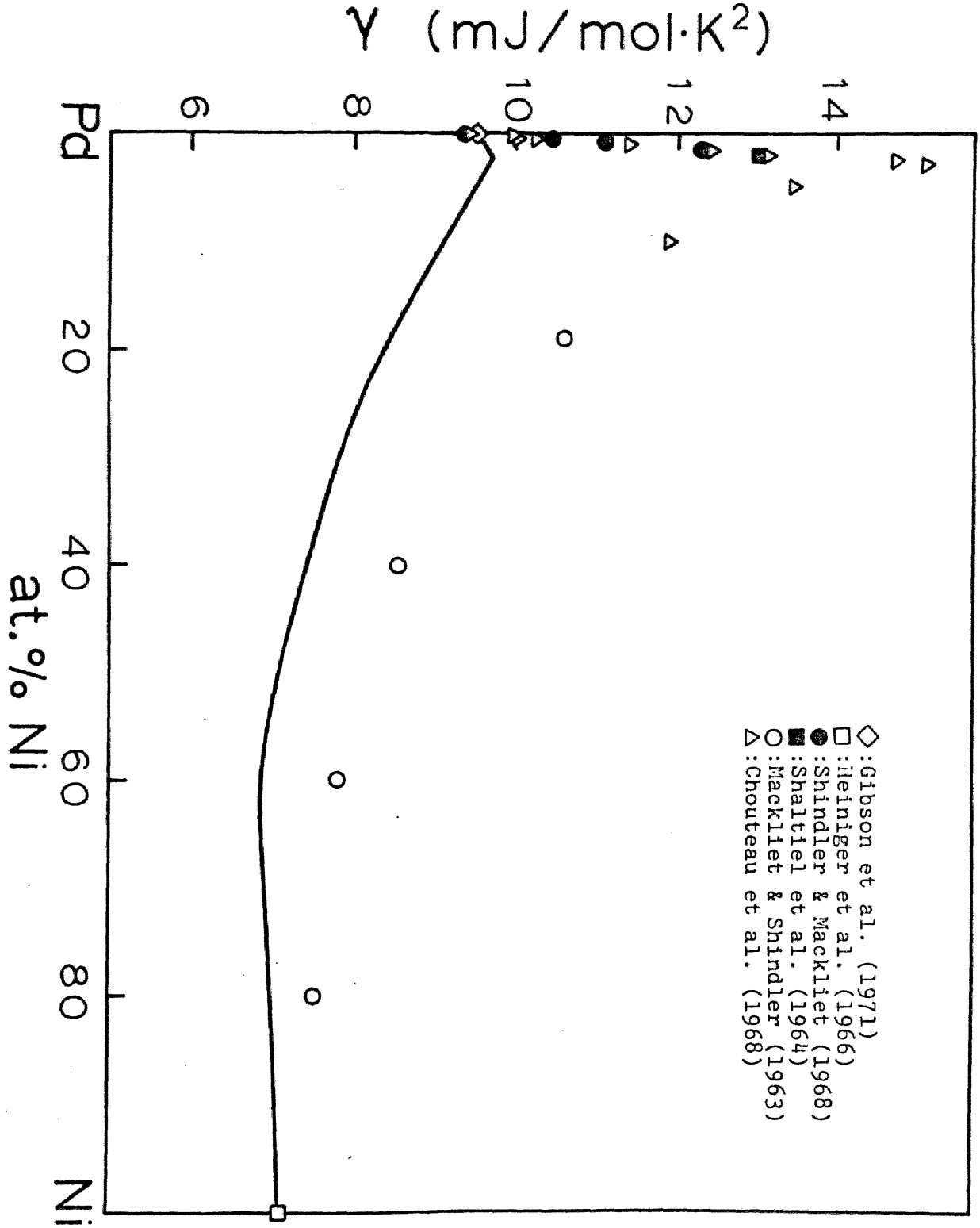
γ (mJ/mol·K²)
6
8
10
12
14
Pd
20
40
60
80
Ni
at.% Ni
◇:Gibson et al. (1971)
□:Heiniger et al. (1966)
●:Shindler & Macklet (1968)
■:Shaltiel et al. (1964)
○:Macklet & Shindler (1963)
△:Chouteau et al. (1968)

Fig. 65

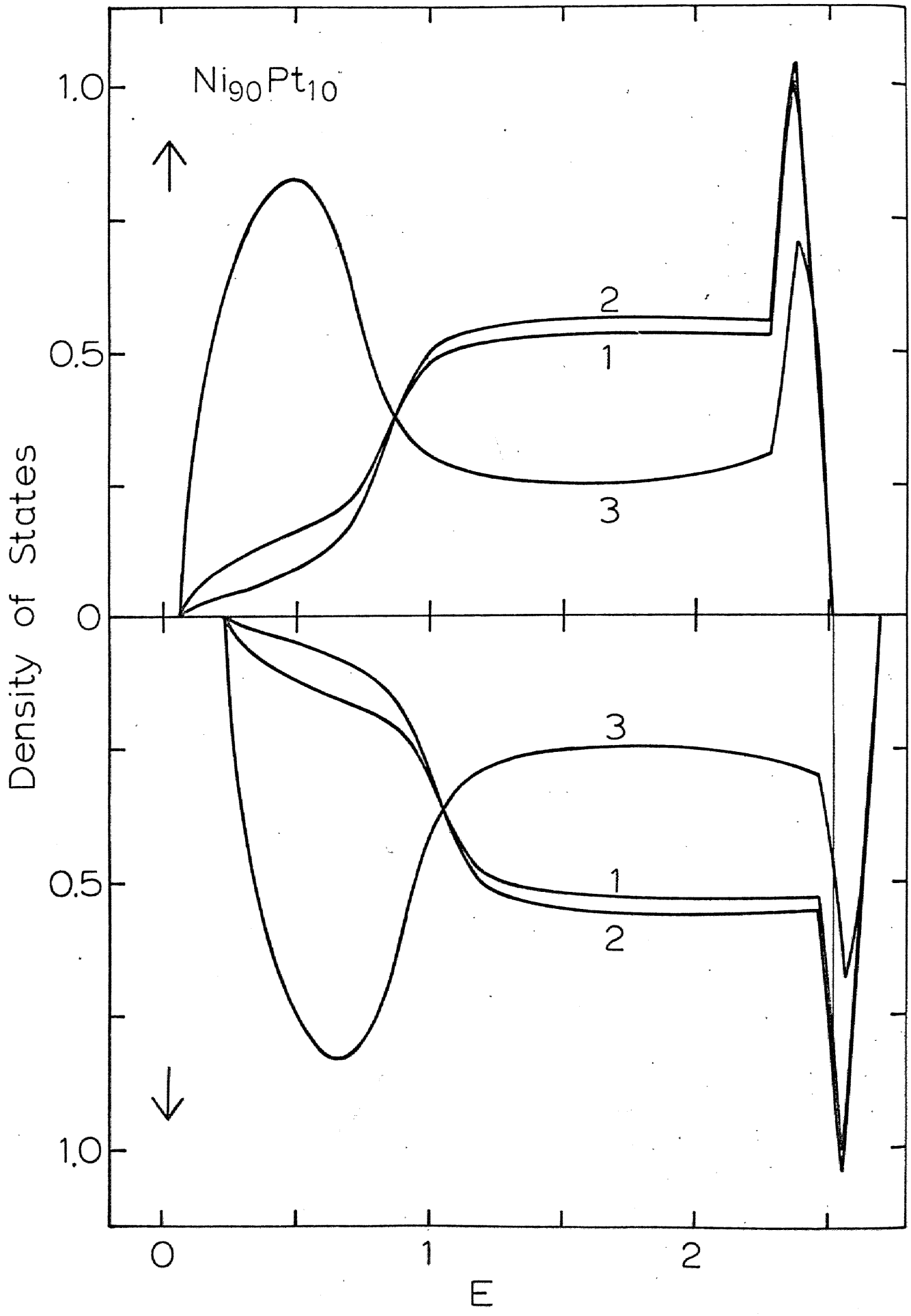

Fig. 66

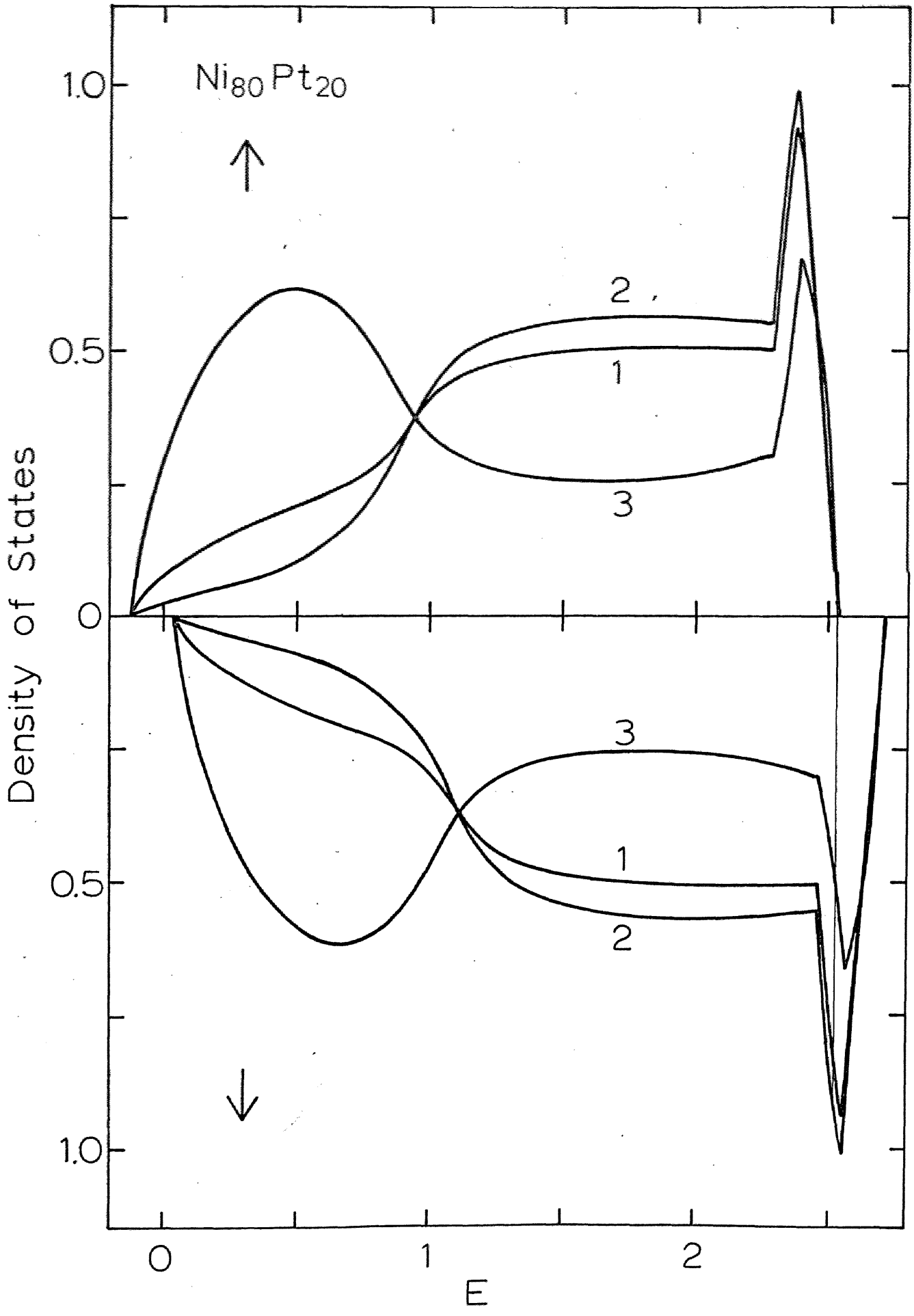

Fig. 67

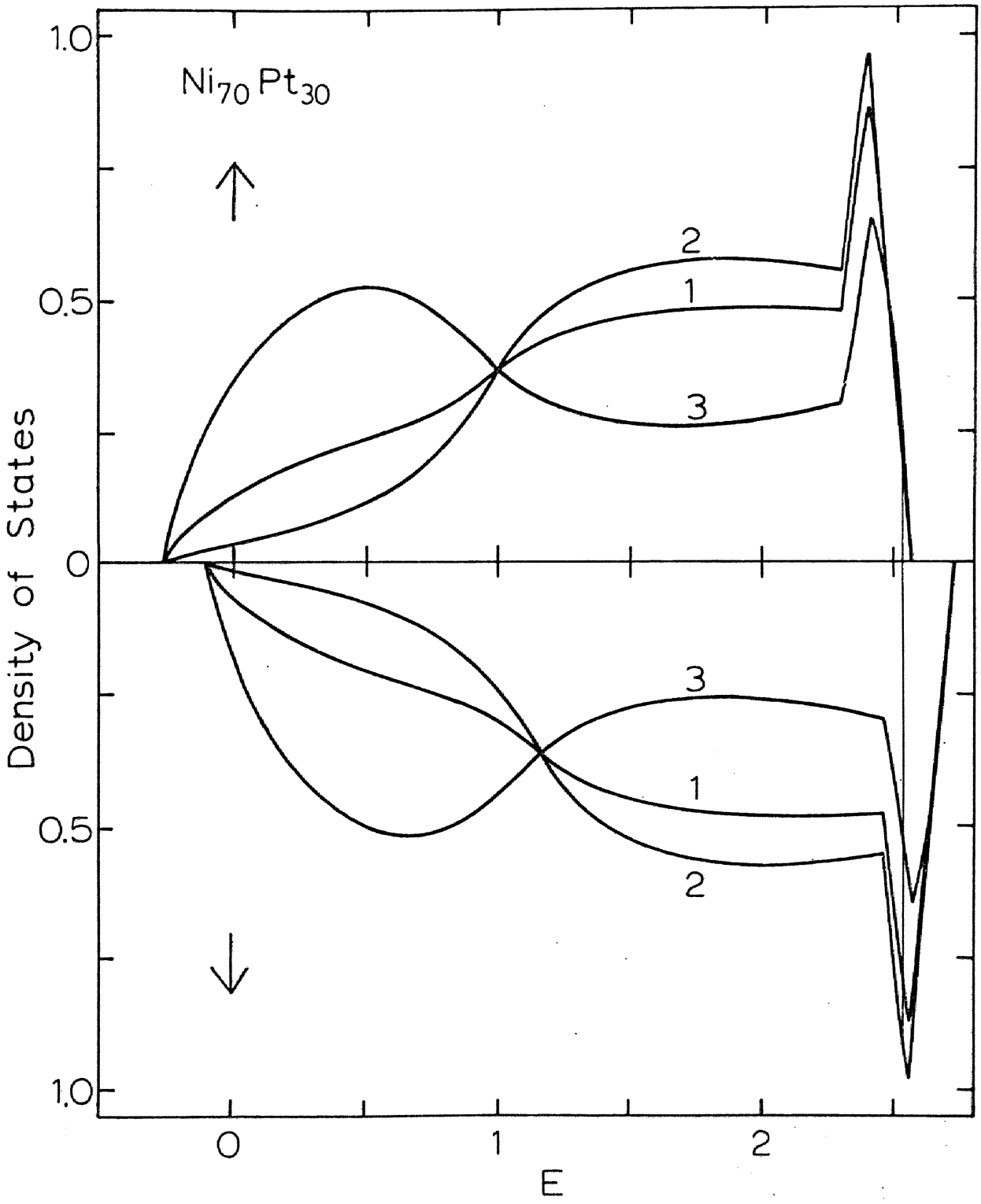

Fig. 68

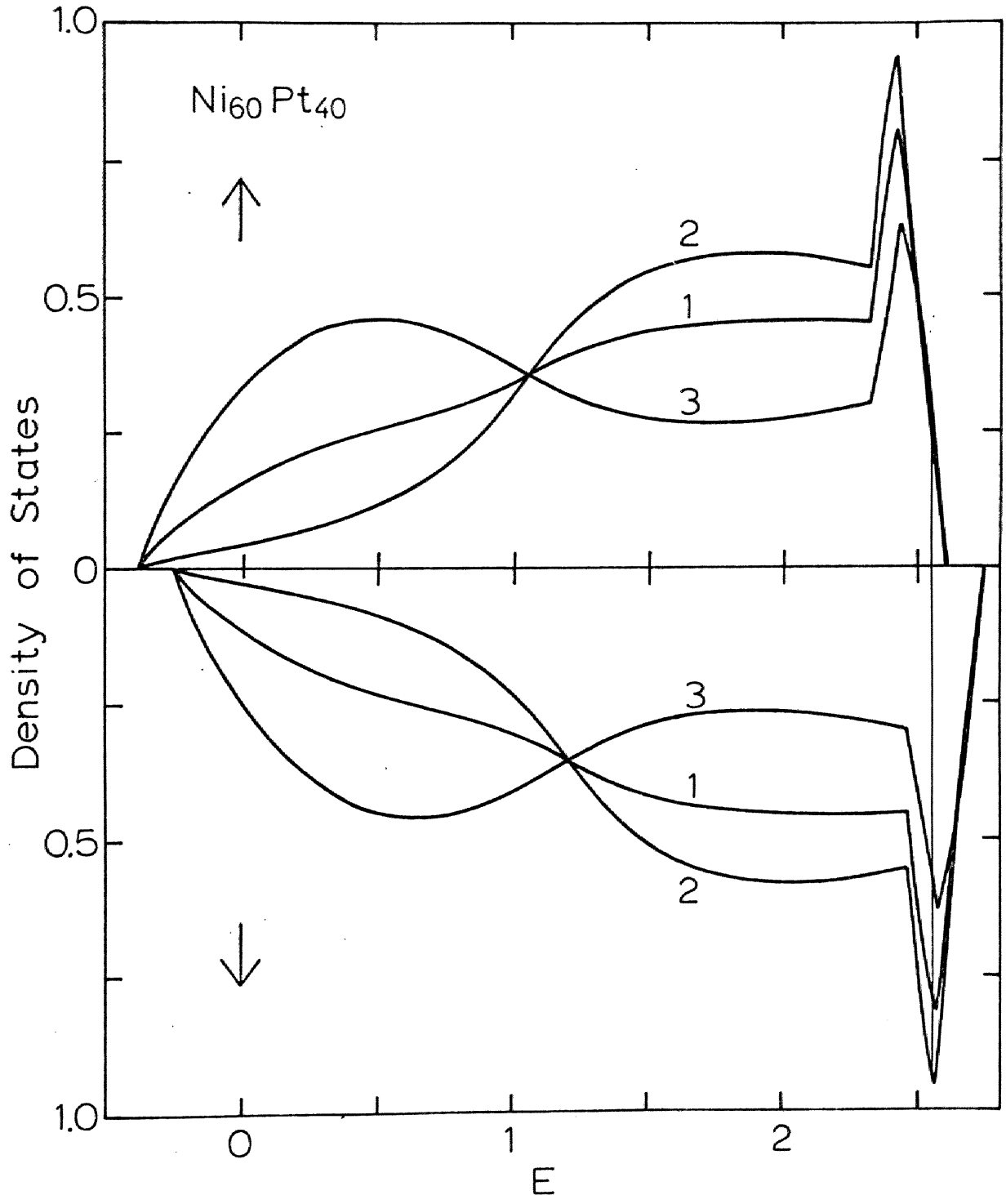

Fig. 69

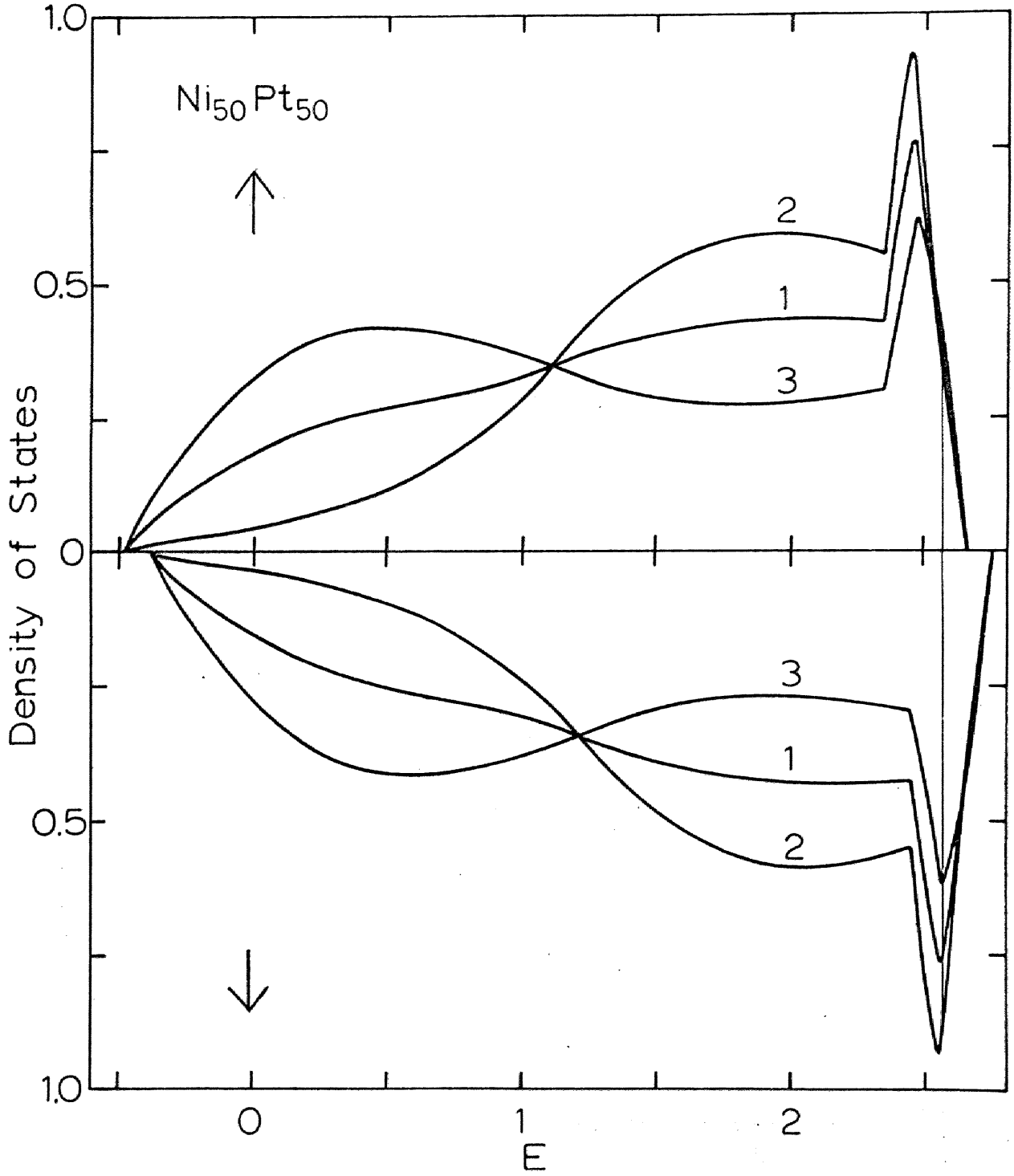

Fig. 70

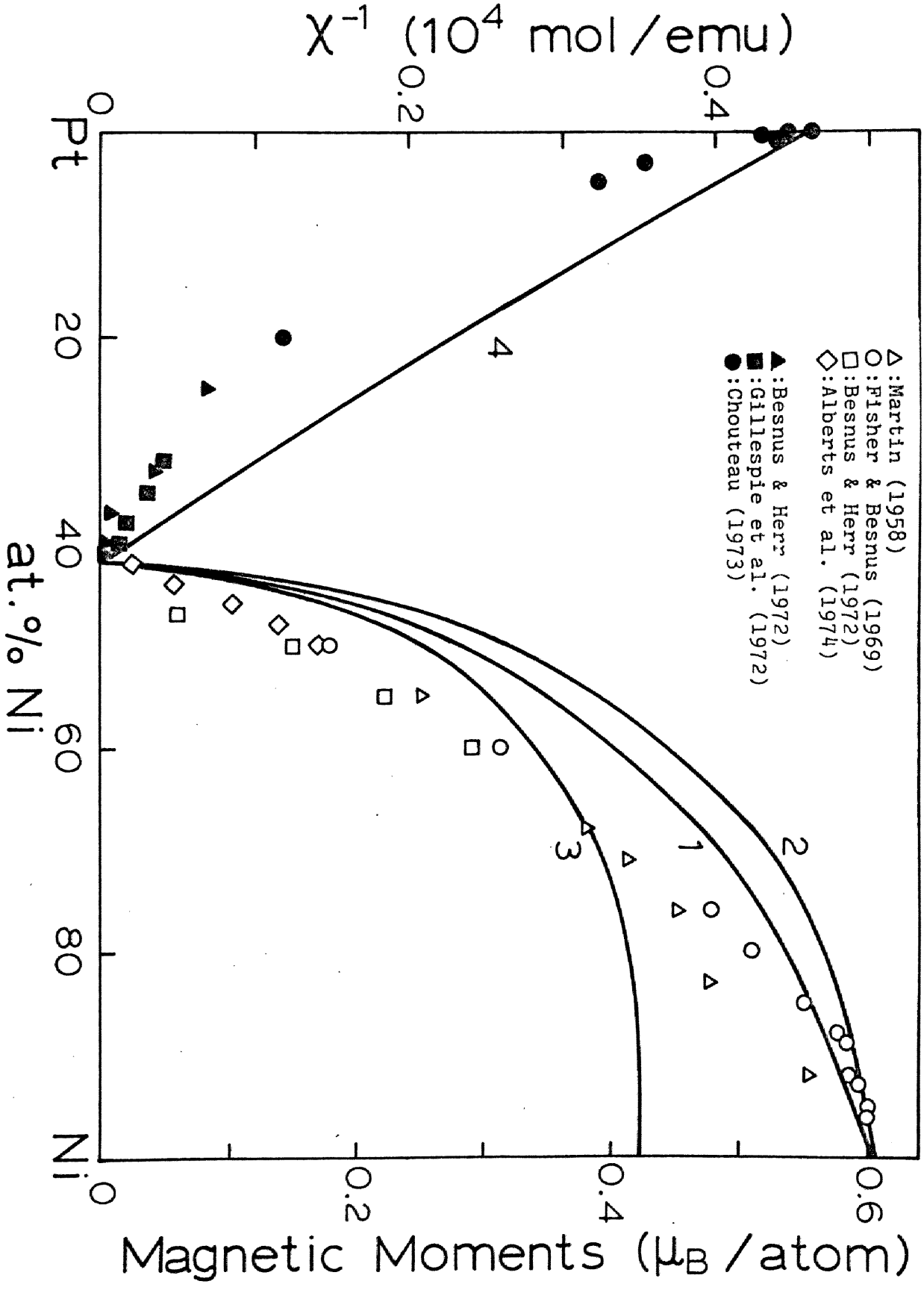
χ⁻¹ (10⁴ mol/emu)
0
0.2
0.4
Pt
20
40
60
80
Ni
at.% Ni
0
0.2
0.4
0.6
Magnetic Moments (μB/atom)
△:Martin (1958)
○:Fisher & Besnus (1969)
□:Besnus & Herr (1972)
◇:Alberts et al. (1974)
▲:Besnus & Herr (1972)
■:Gillespie et al. (1972)
●:Chouteau (1973)
1
2
3
4

Fig. 71

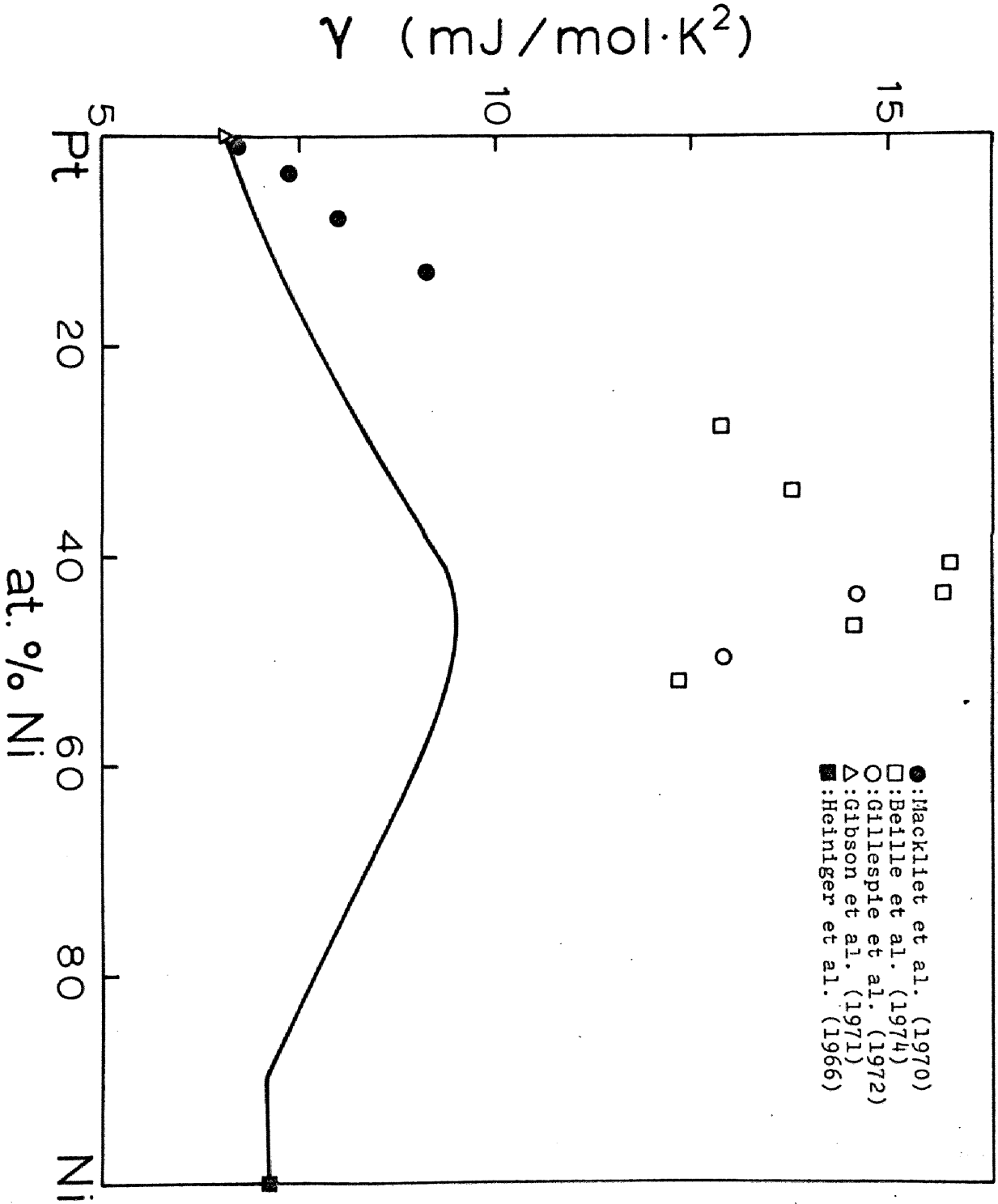
γ (mJ/mol·K²)
5
10
15
Pt
20
40
60
80
Ni
at. % Ni
●:Macklet et al. (1970)
□:Belle et al. (1974)
○:Gillespie et al. (1972)
△:Gibson et al. (1971)
■:Heiniger et al. (1966)

Fig. 72

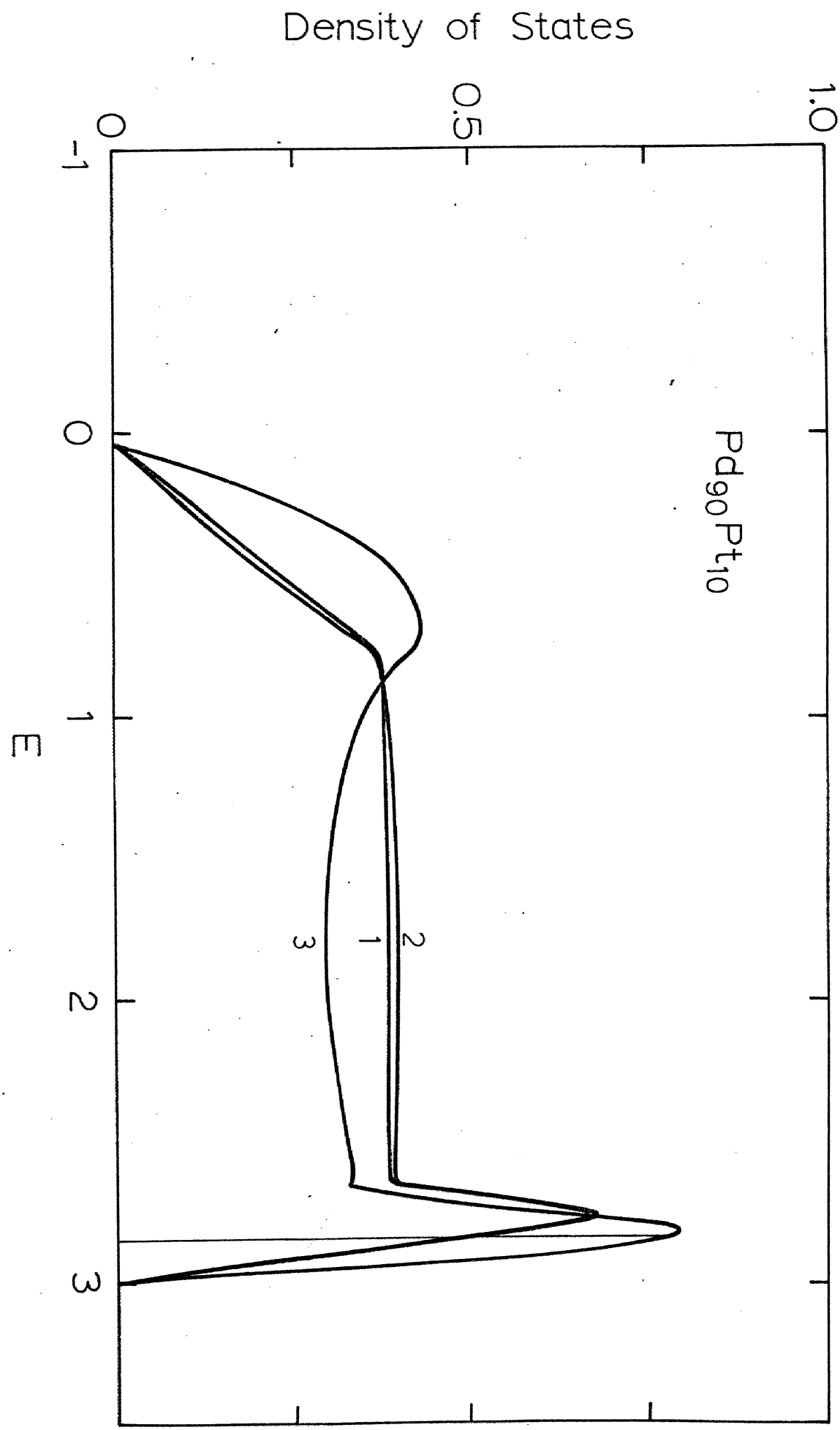

Fig. 73

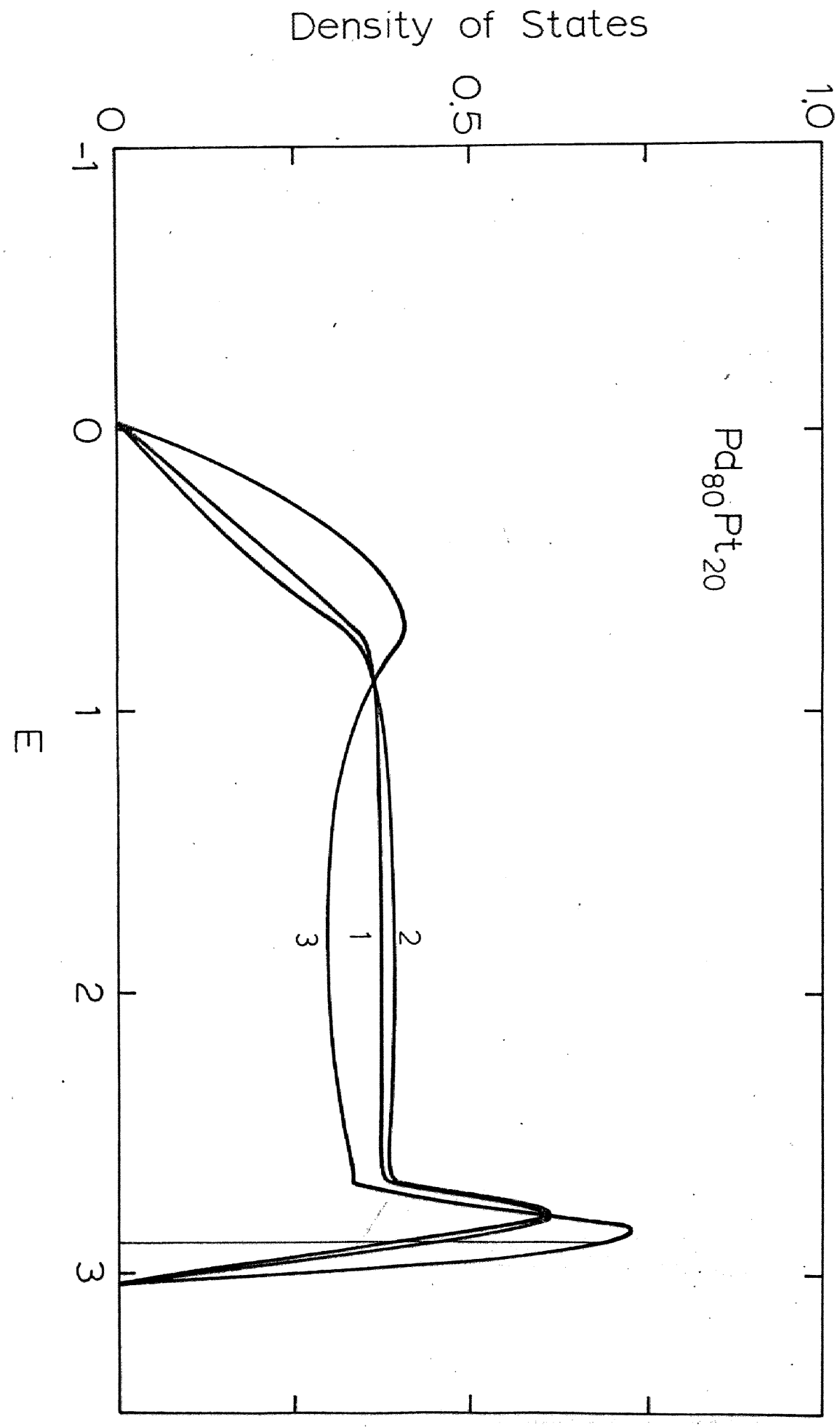

Fig. 74

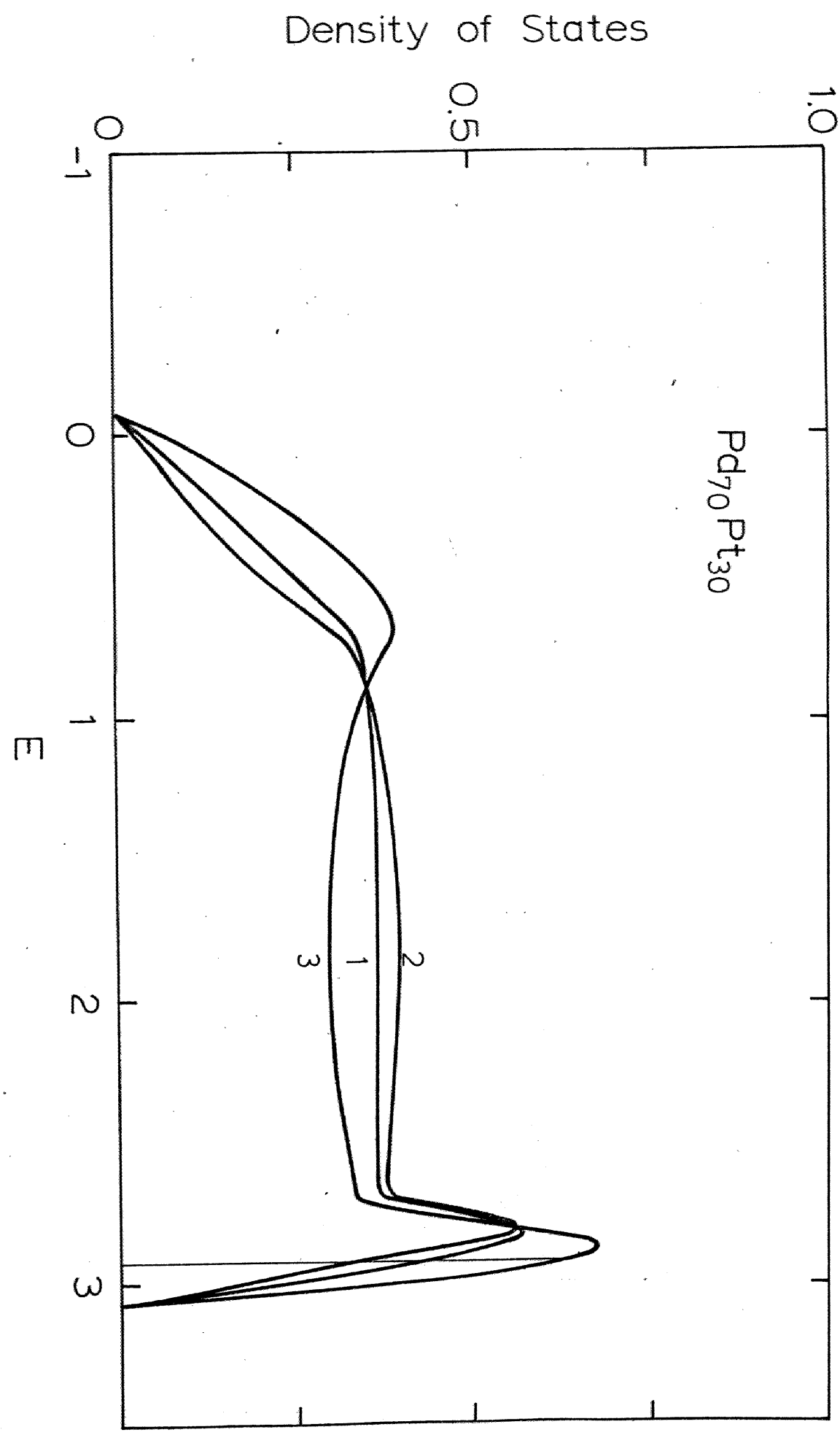

Fig. 75

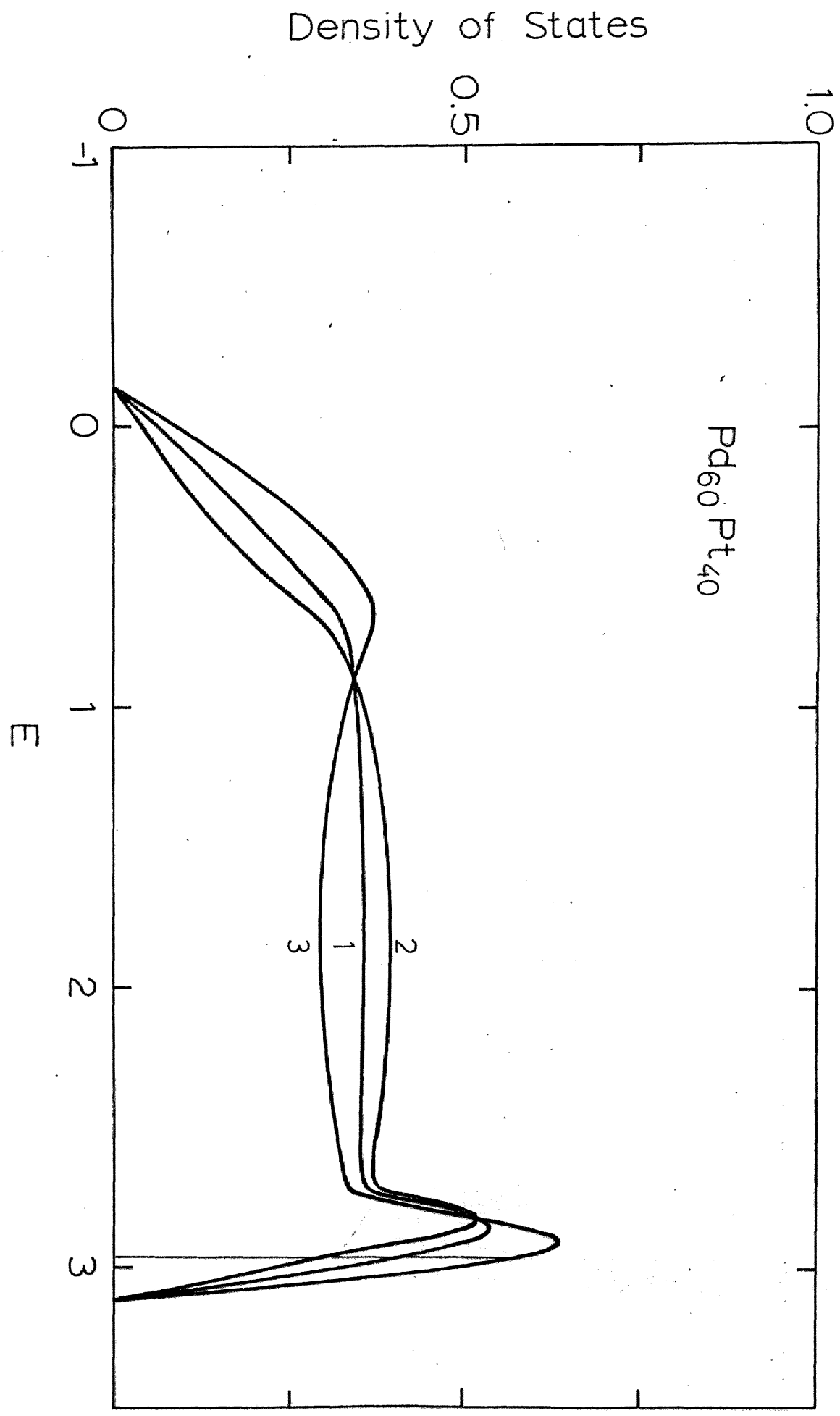

Fig. 76

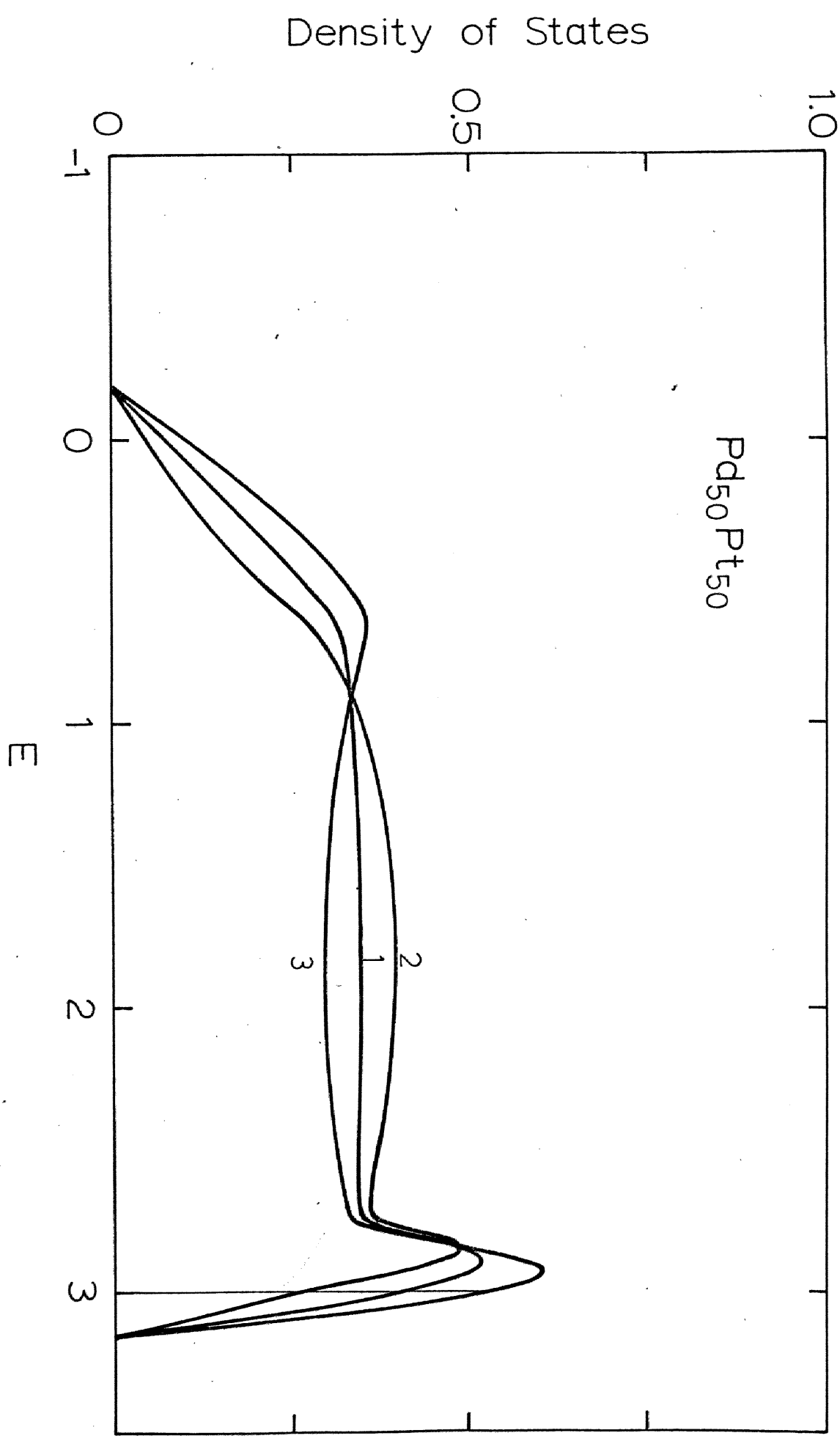

Fig. 77

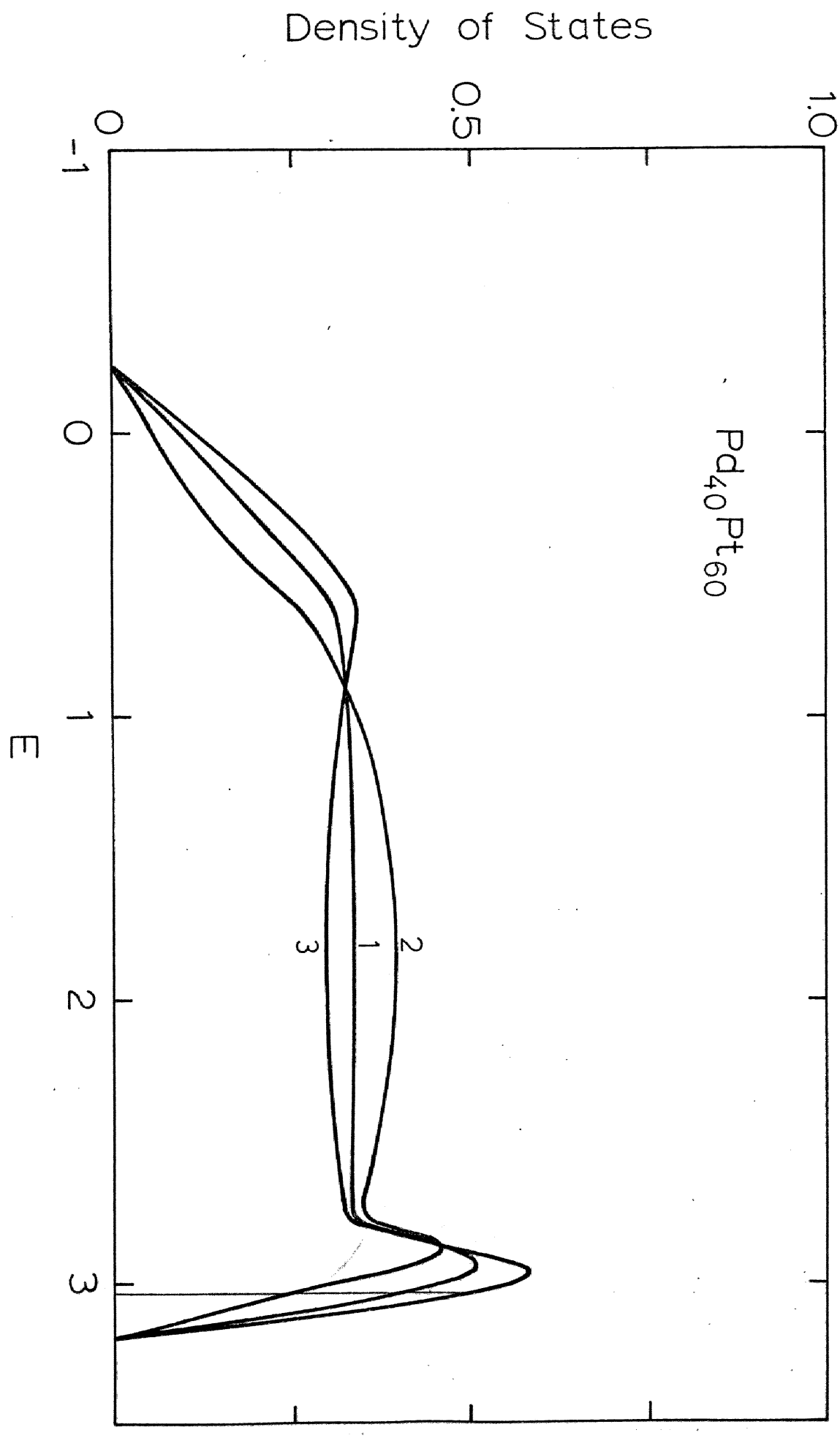

Fig. 78

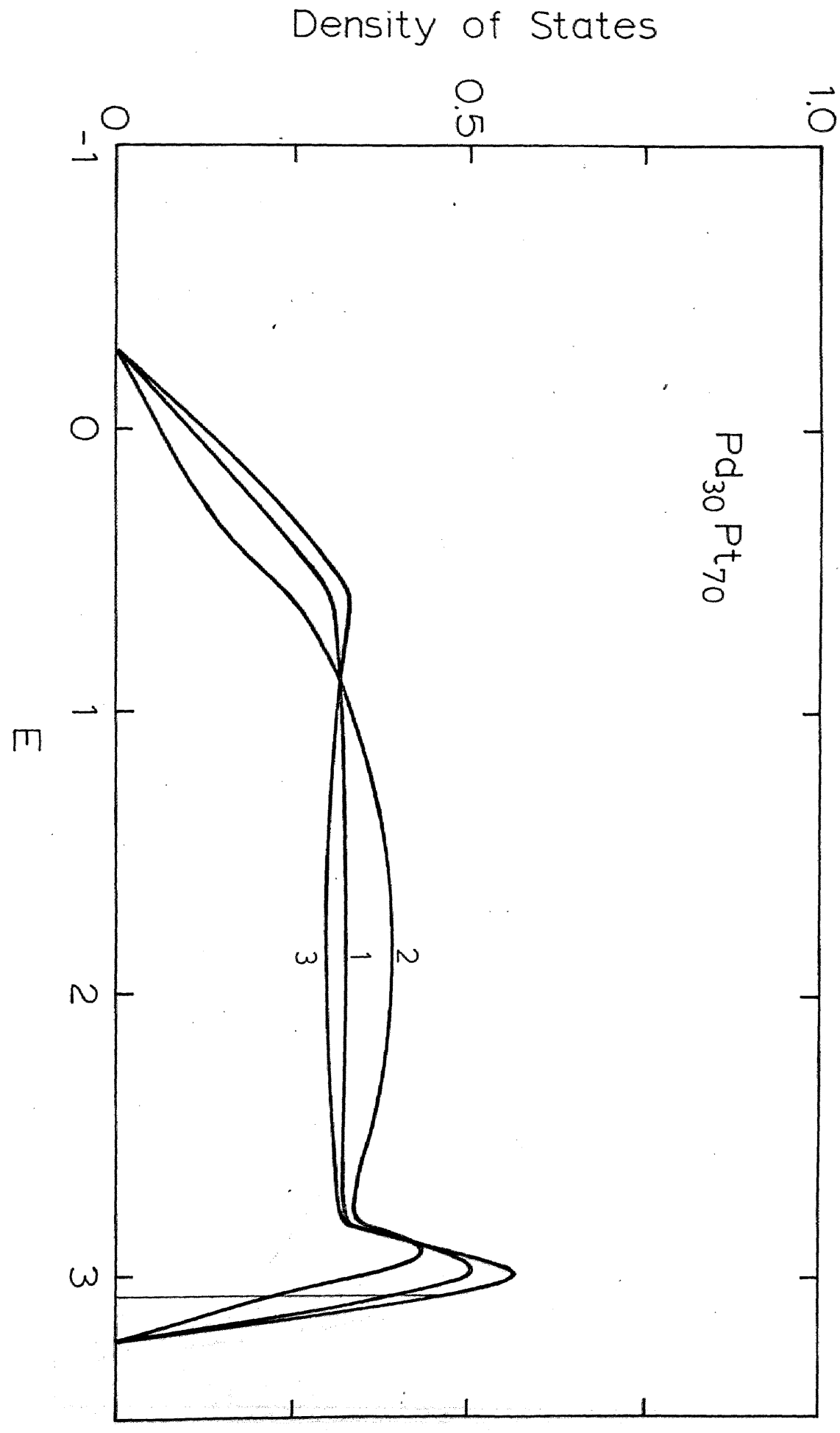

Fig. 79

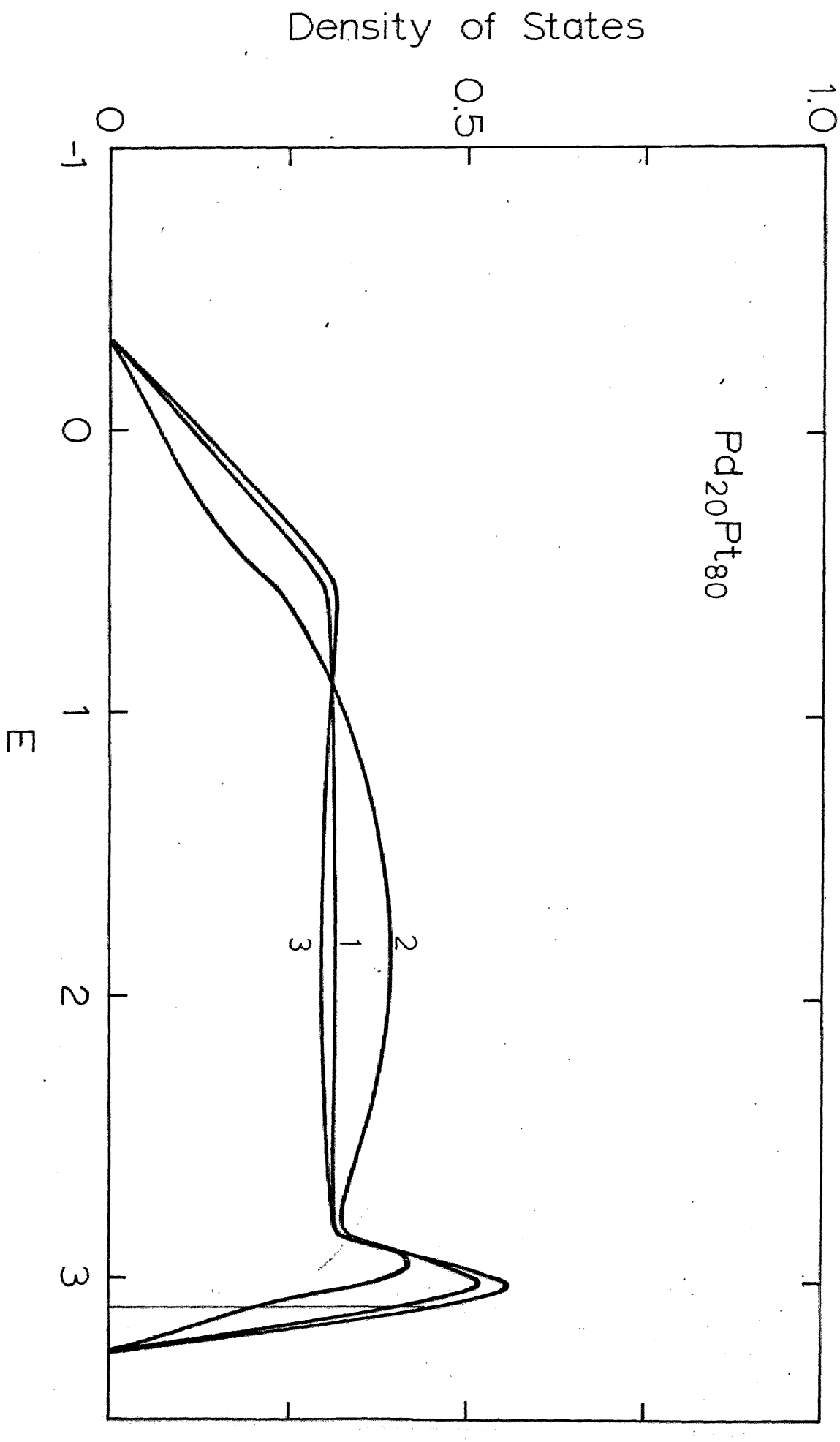

Fig. 80

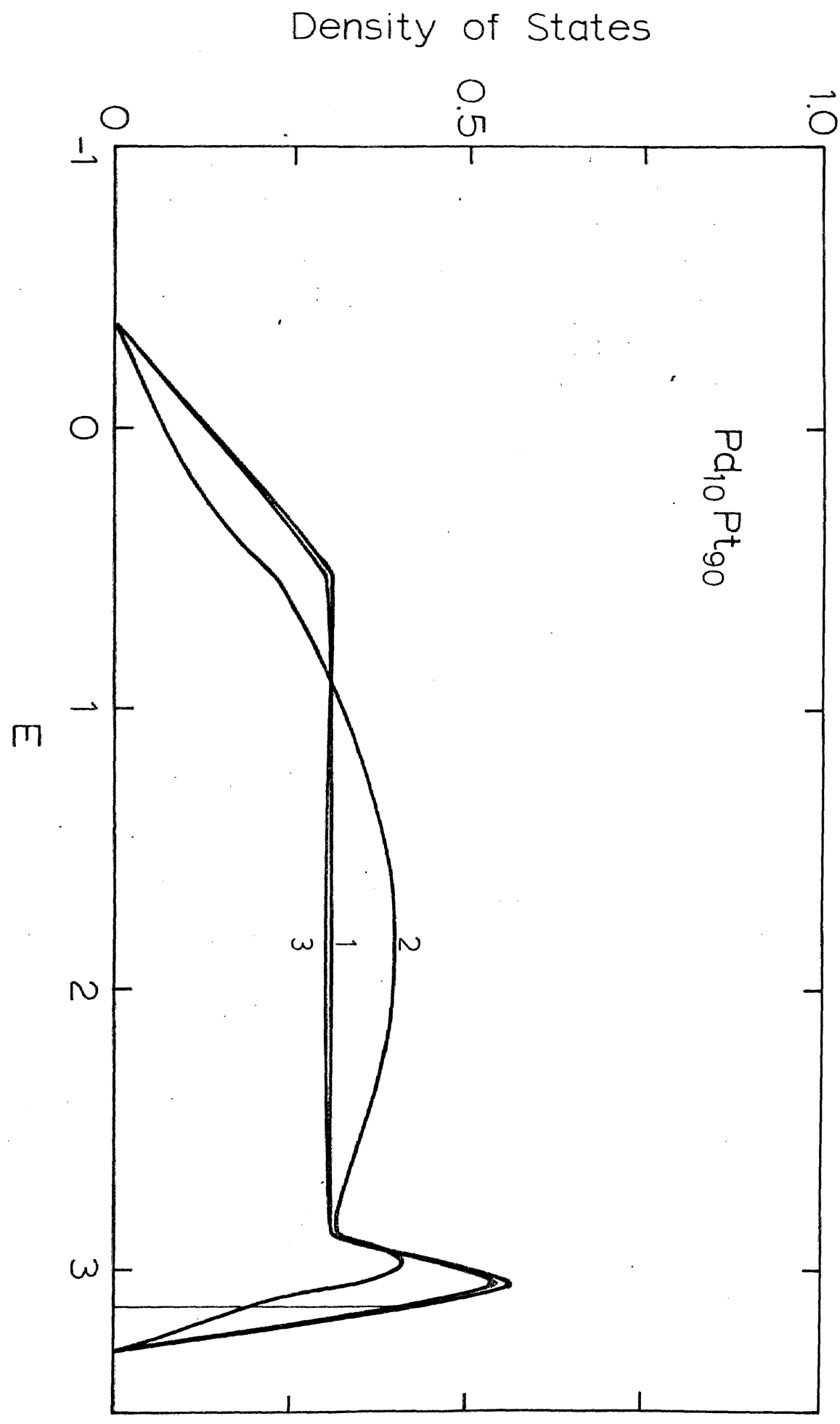

Fig. 81

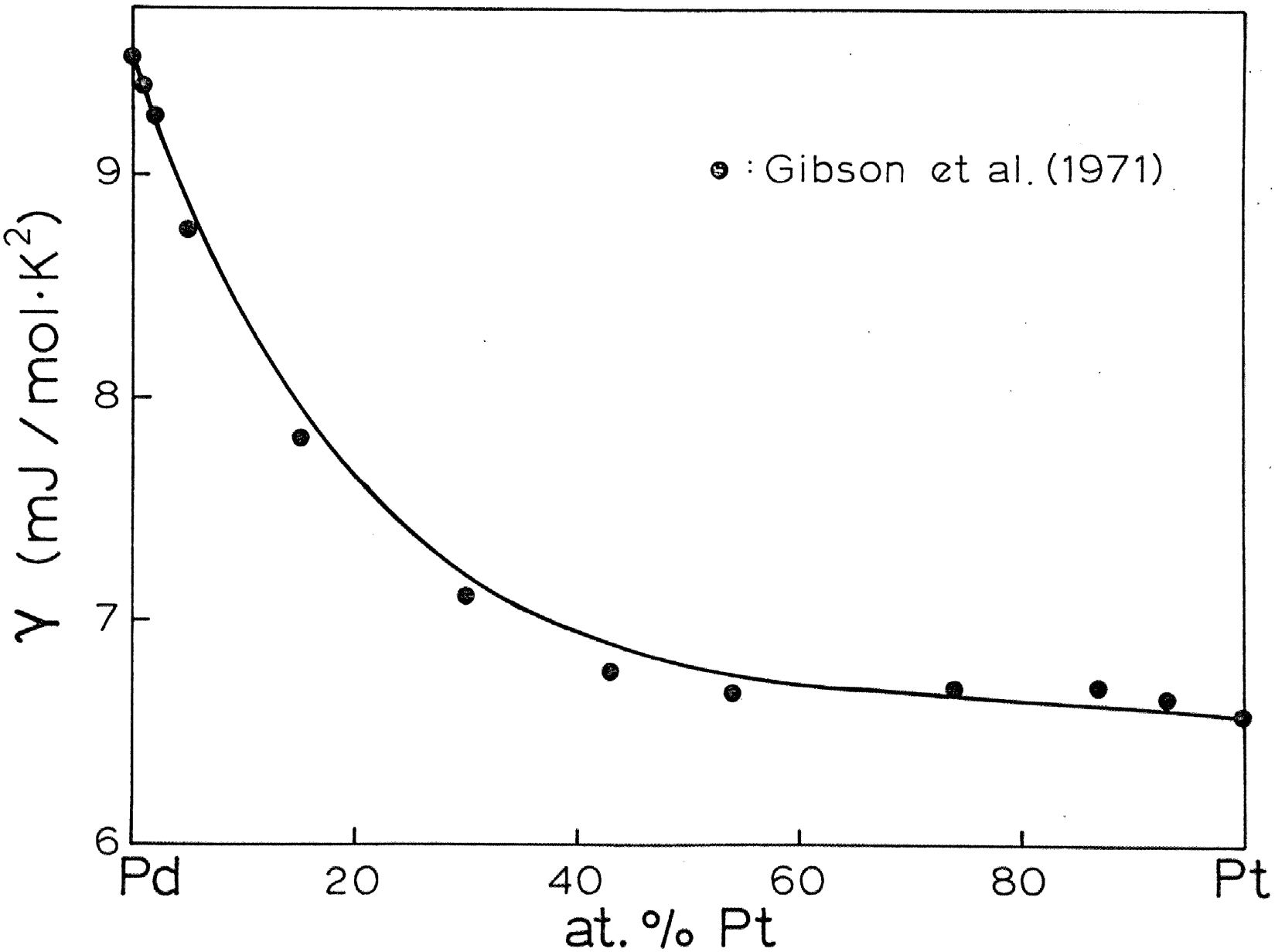

Fig. 82

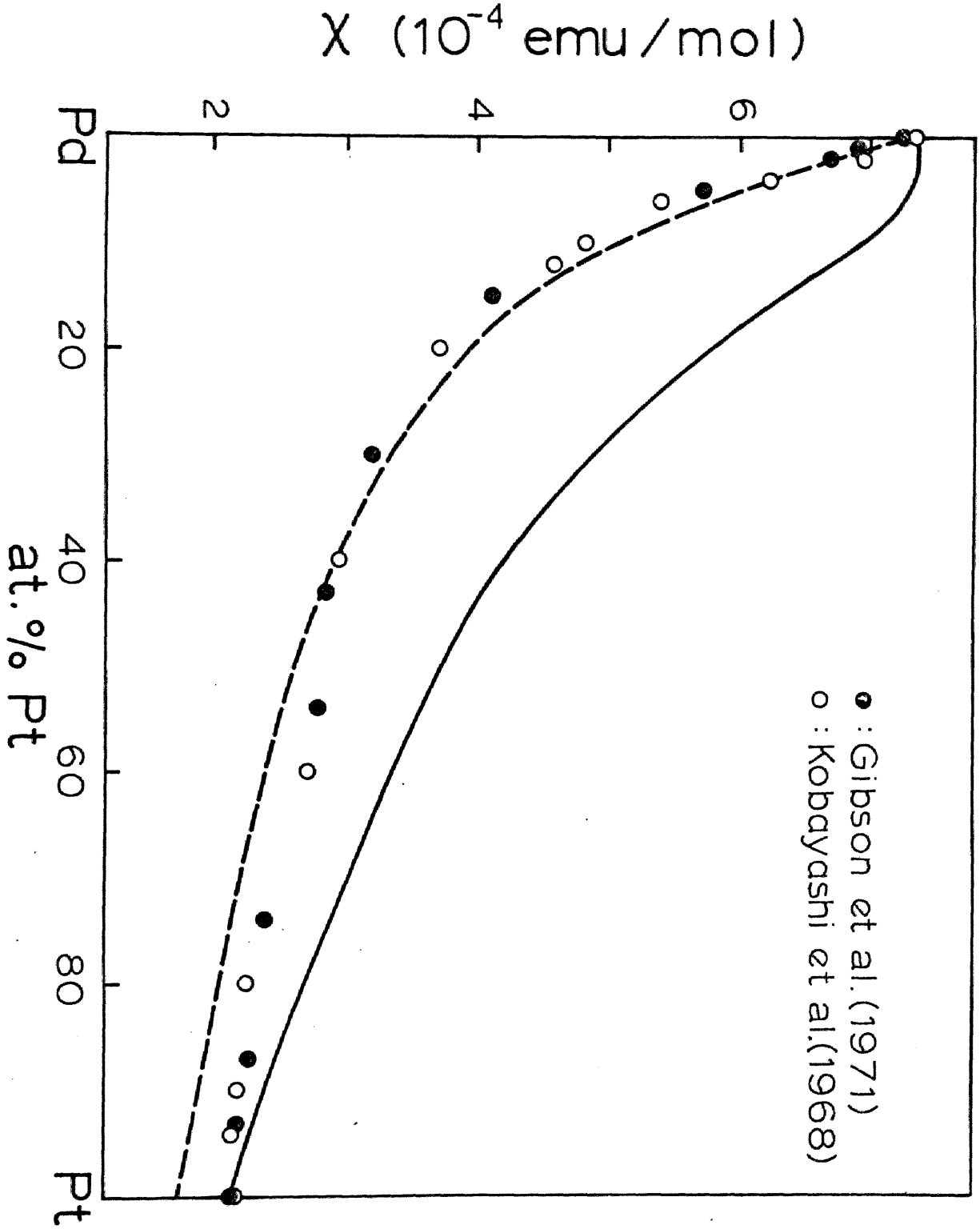
χ (10⁻⁴ emu/mol)
2
4
6
Pd
20
40
60
80
Pt
at.% Pt
● : Gibson et al.(1971)
○ : Kobayashi et al.(1968)

Fig. 83

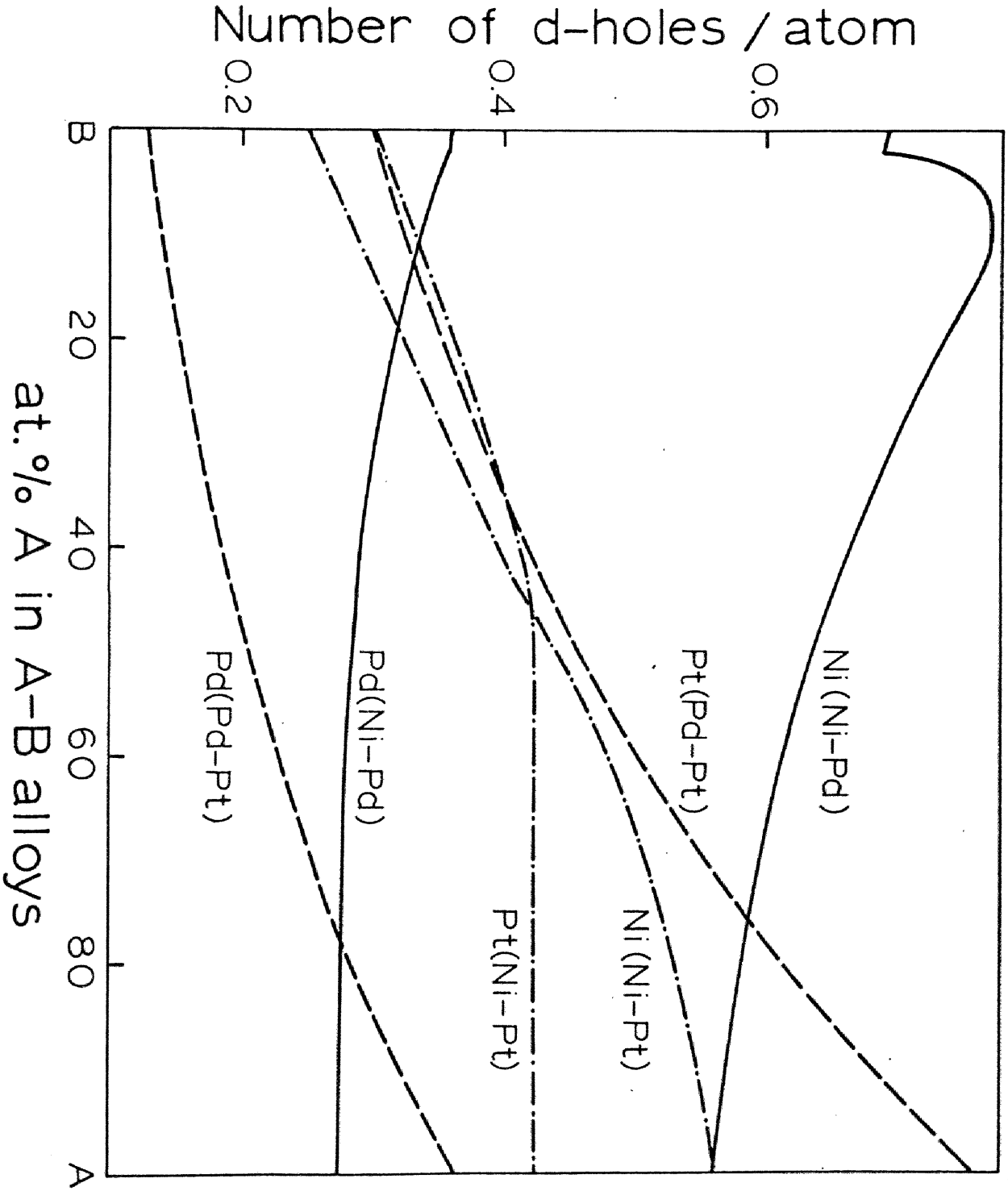
Number of d-holes / atom
0.2
0.4
0.6
B
20
40
60
80
A
at.% A in A-B alloys
Pd(Pd-Pt)
Pd(Ni-Pd)
Pt(Ni-Pt)
Pt(Pd-Pt)
Ni(Ni-Pt)
Ni(Ni-Pd)

Fig. 84

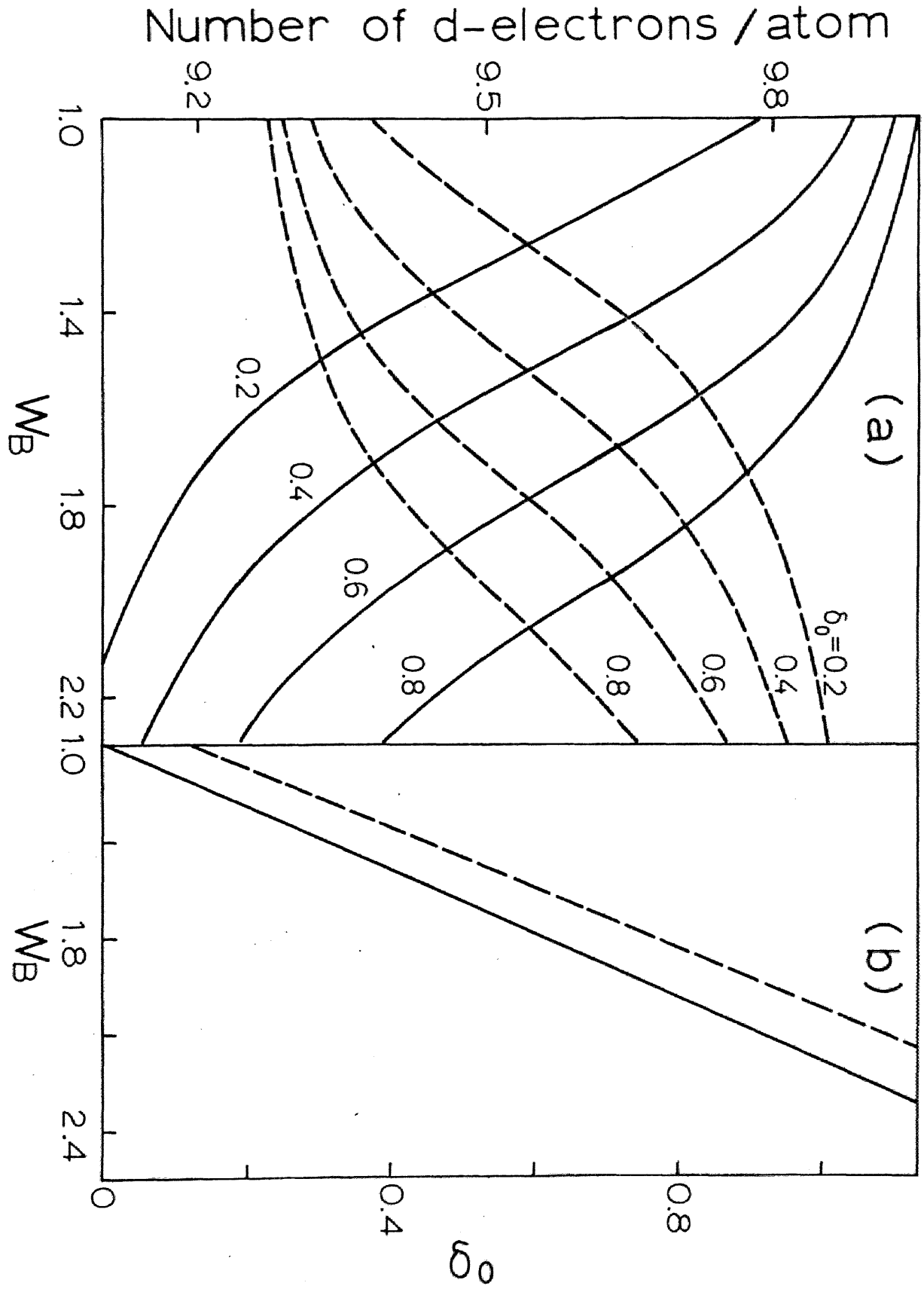
Number of d-electrons / atom
9.2
9.5
9.8
1.0
1.4
1.8
2.2
W_B
0.2
0.4
0.6
0.8
δ_0=0.2
0.4
0.6
0.8
(a)
1.0
1.8
2.4
W_B
(b)
0
0.4
0.8
δ_0

Fig. 85

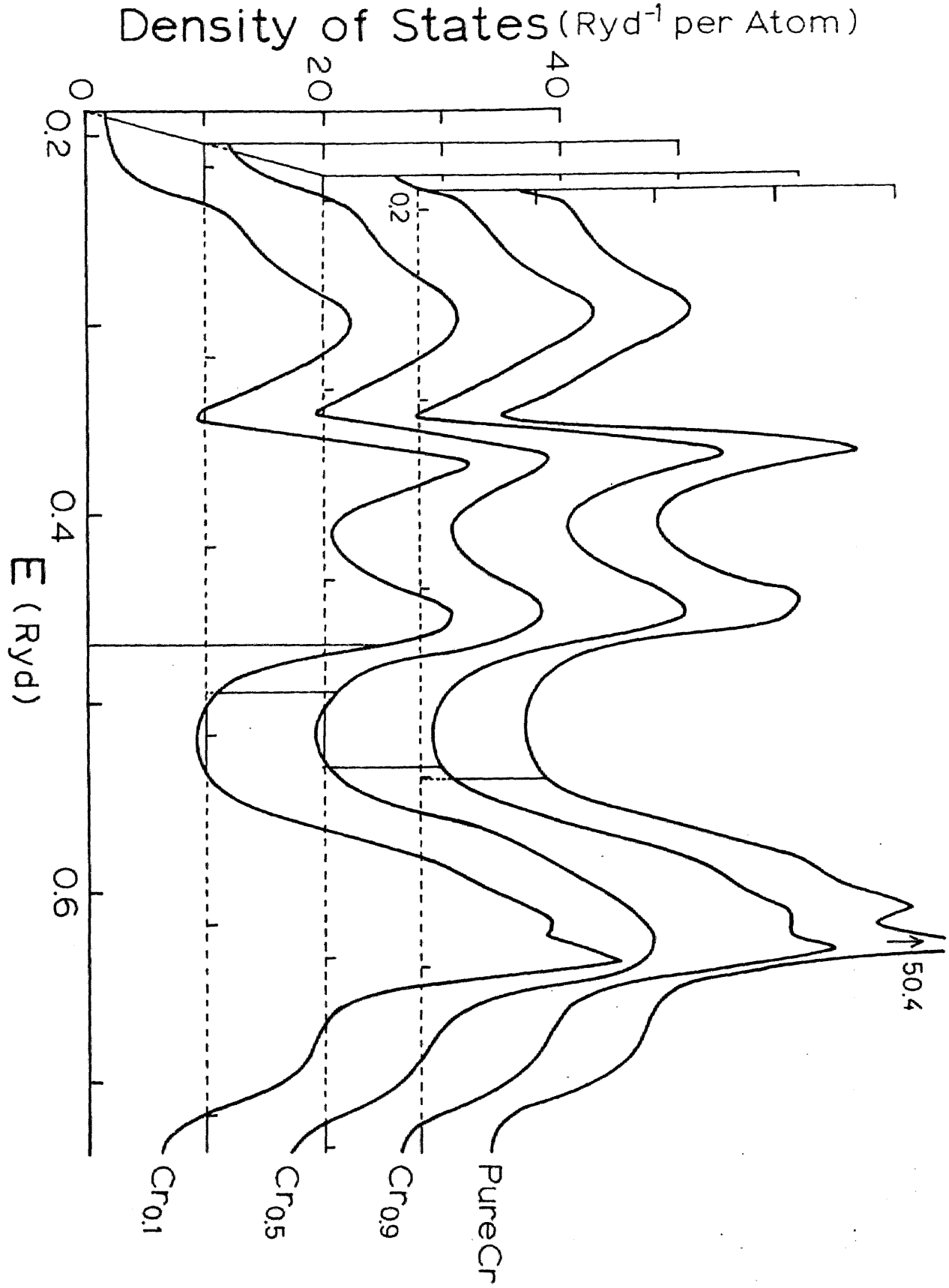
Density of States (Ryd^{-1} per Atom)
0
20
40
0.2
0.2
0.4
0.6
E (Ryd)
50.4
$Cr_{0.1}$
$Cr_{0.5}$
$Cr_{0.9}$
PureCr

Fig. 86

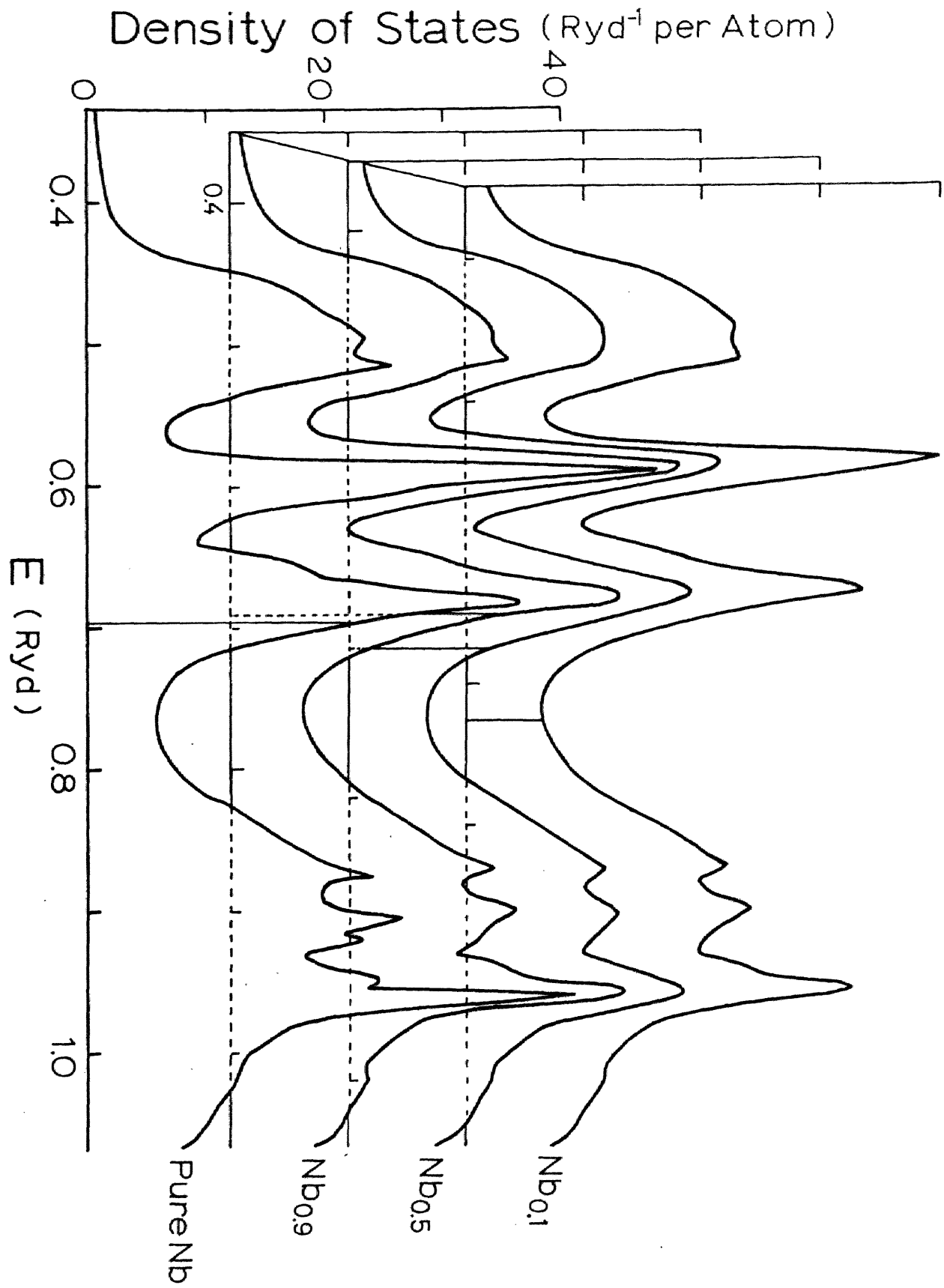
Density of States (Ryd⁻¹ per Atom)
0
20
40
0.4
0.4
0.6
0.8
1.0
E (Ryd)
Pure Nb
Nb0.9
Nb0.5
Nb0.1

Fig. 87

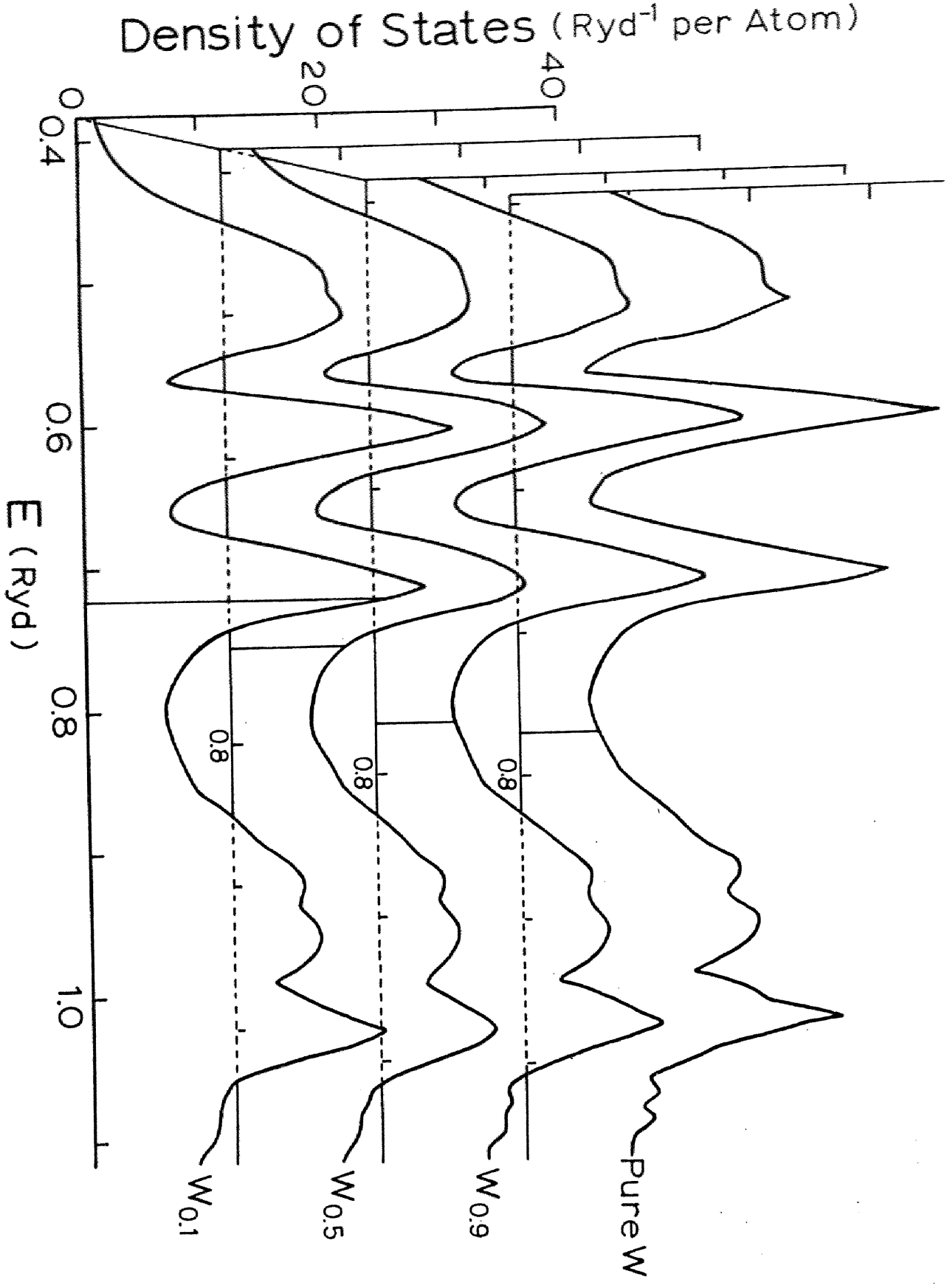
Density of States (Ryd^{-1} per Atom)
0
20
40
0.4
0.6
0.8
1.0
E (Ryd)
0.8
0.8
0.8
$W_{0.1}$
$W_{0.5}$
$W_{0.9}$
Pure W

Fig. 88

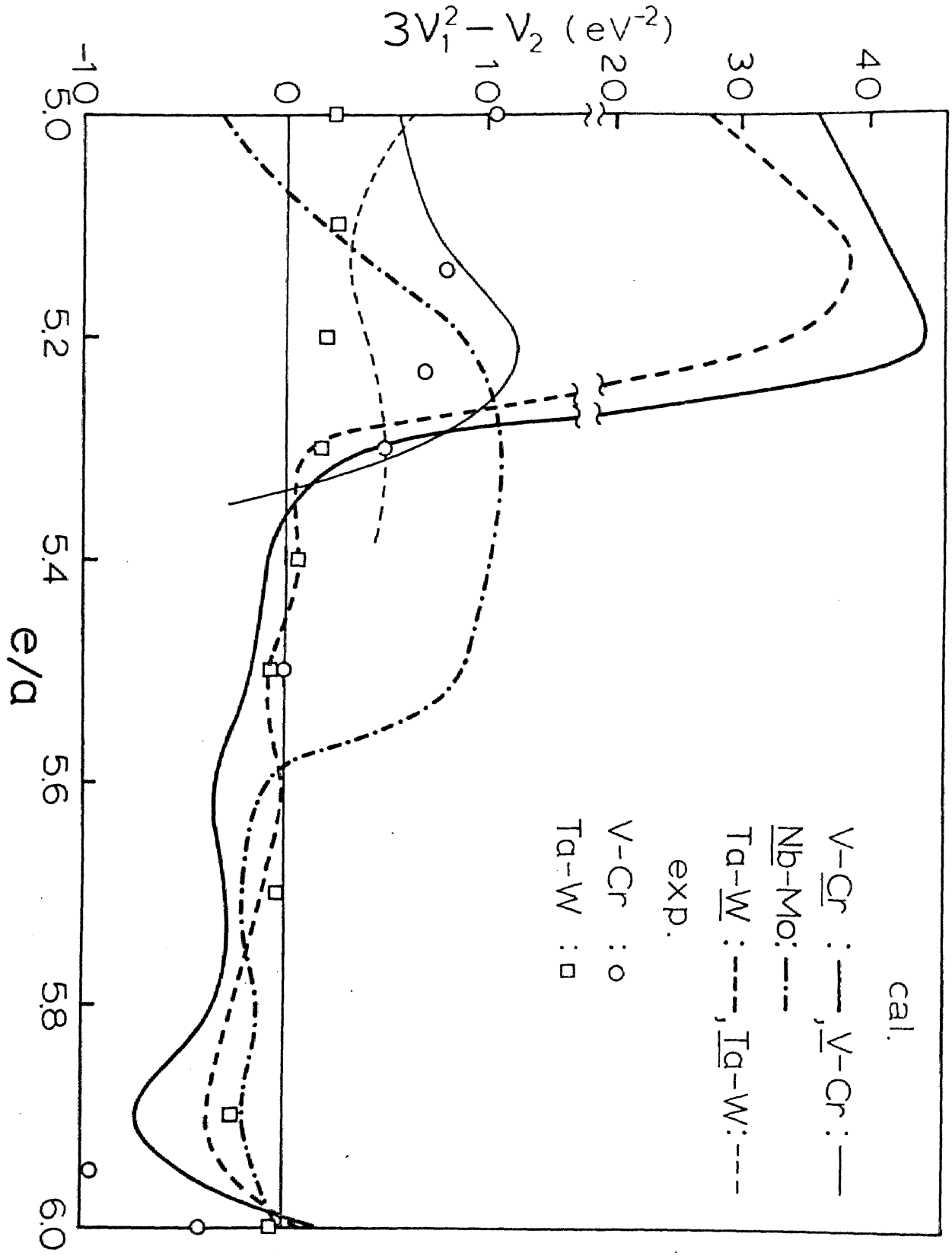
$3V_1^2 - V_2$ (eV^{-2})
-10
0
10
20
30
40
5.0
5.2
5.4
5.6
5.8
6.0
e/a
cal.
V-Cr : —, V-Cr : —
Nb-Mo: —·—
Ta-W : ---, Ta-W: ---
exp.
V-Cr : o
Ta-W : □

Fig. 89

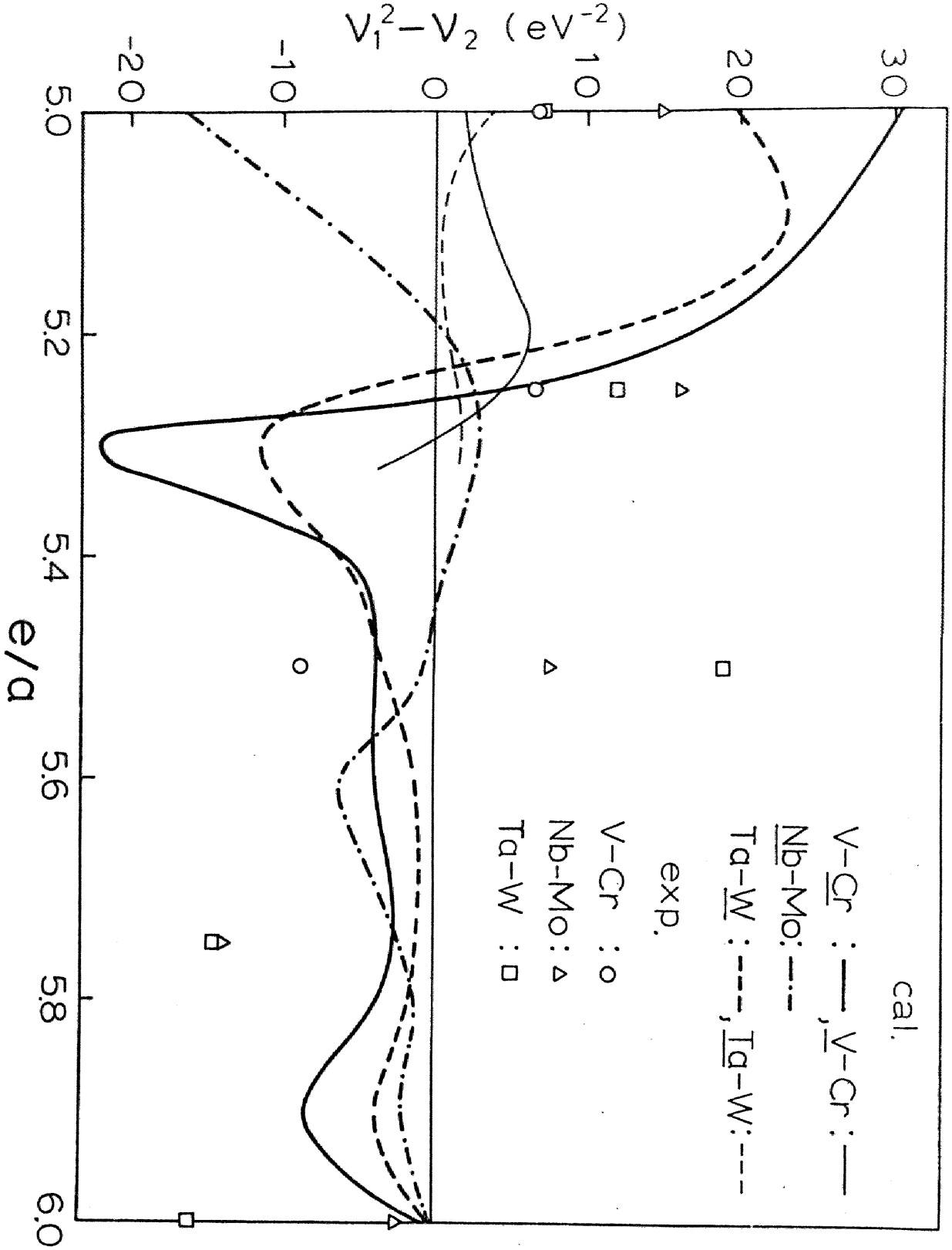
$V_1^2 - V_2$ (eV^{-2})
-20
-10
0
10
20
30
5.0
5.2
5.4
5.6
5.8
6.0
e/a
cal.
V-Cr : —, V-Cr : —
Nb-Mo: -·-
Ta-W : ---, Ta-W: ---
exp.
V-Cr : o
Nb-Mo: Δ
Ta-W : □

Fig. 90

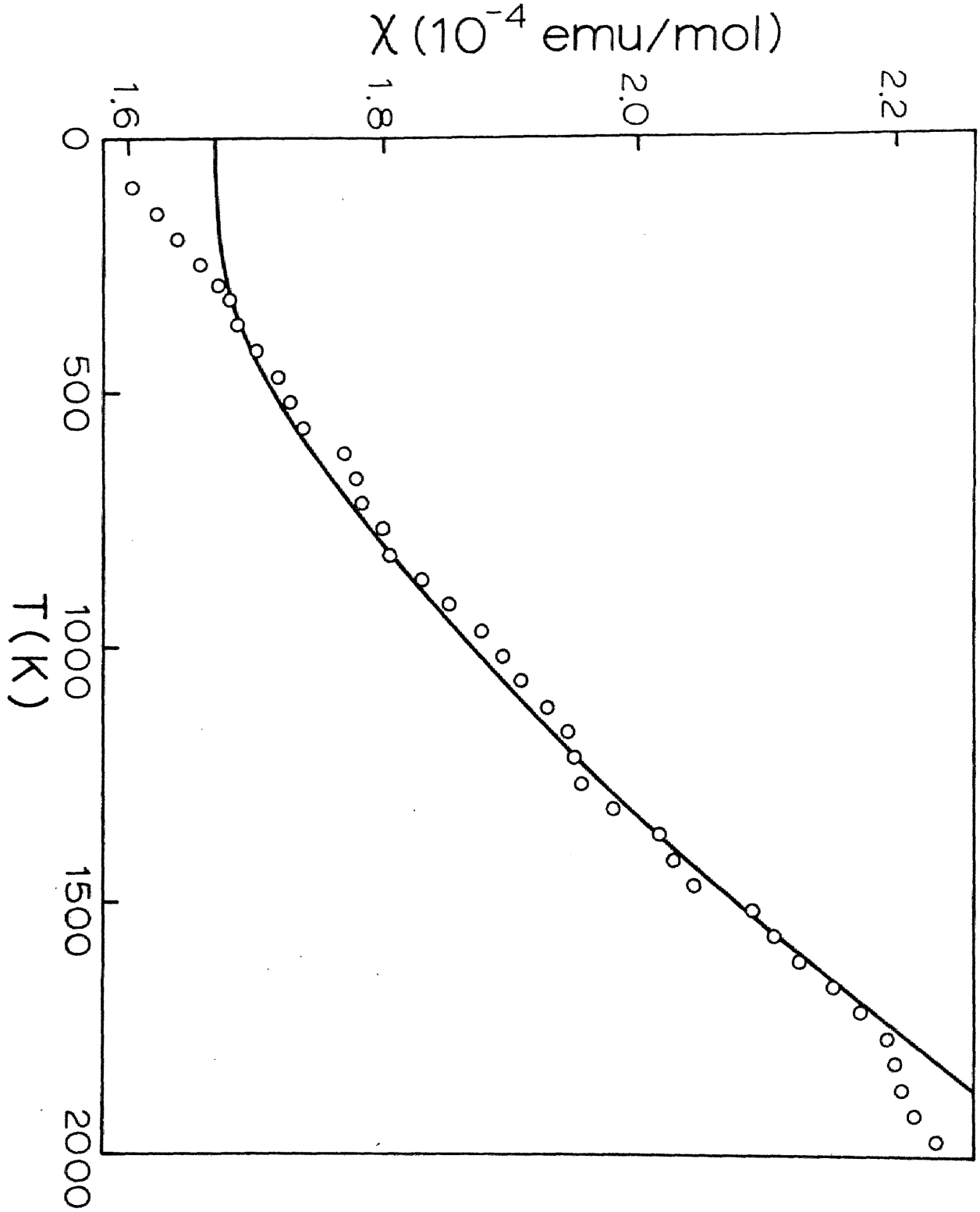

Fig. 91

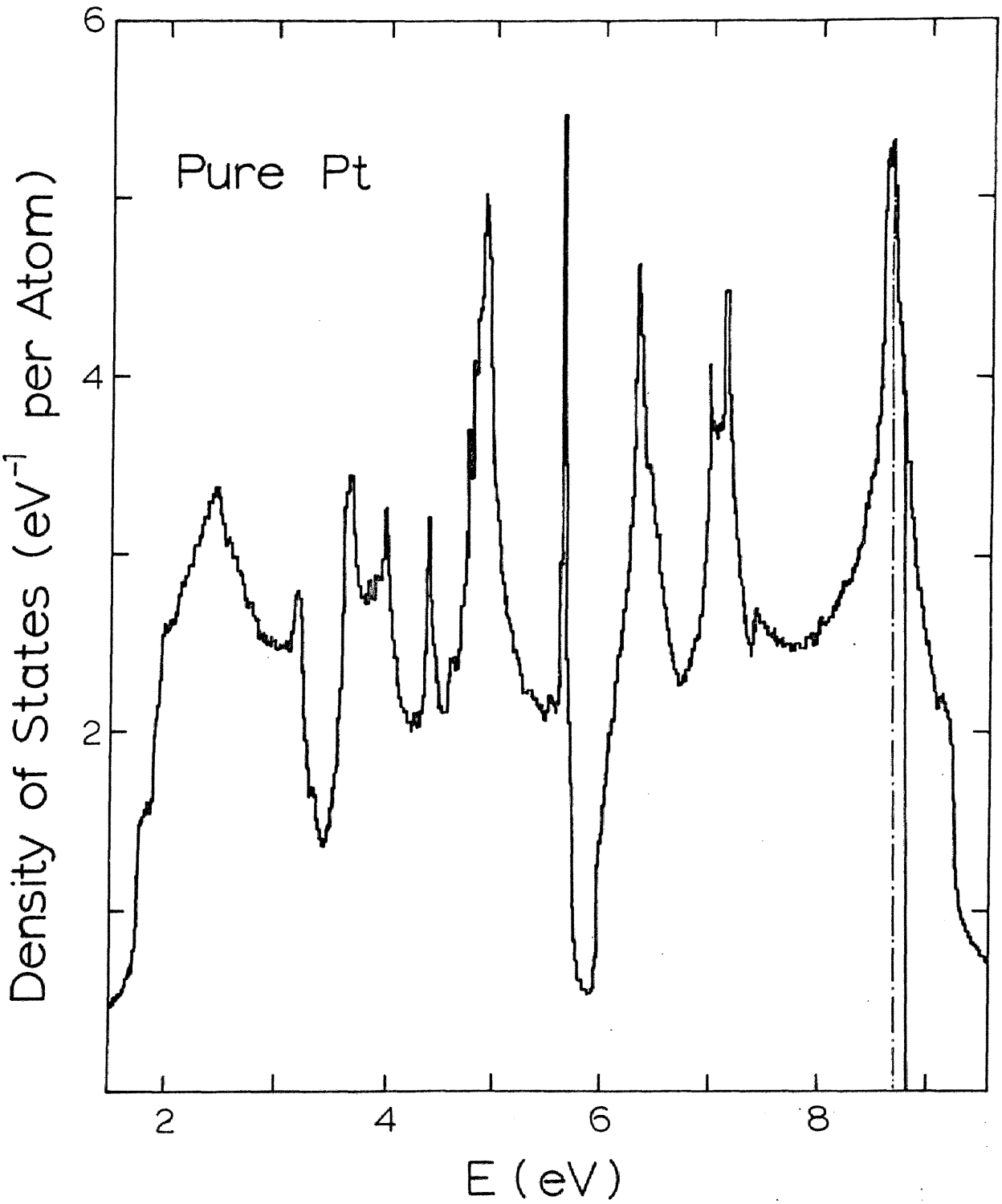

Fig. 92

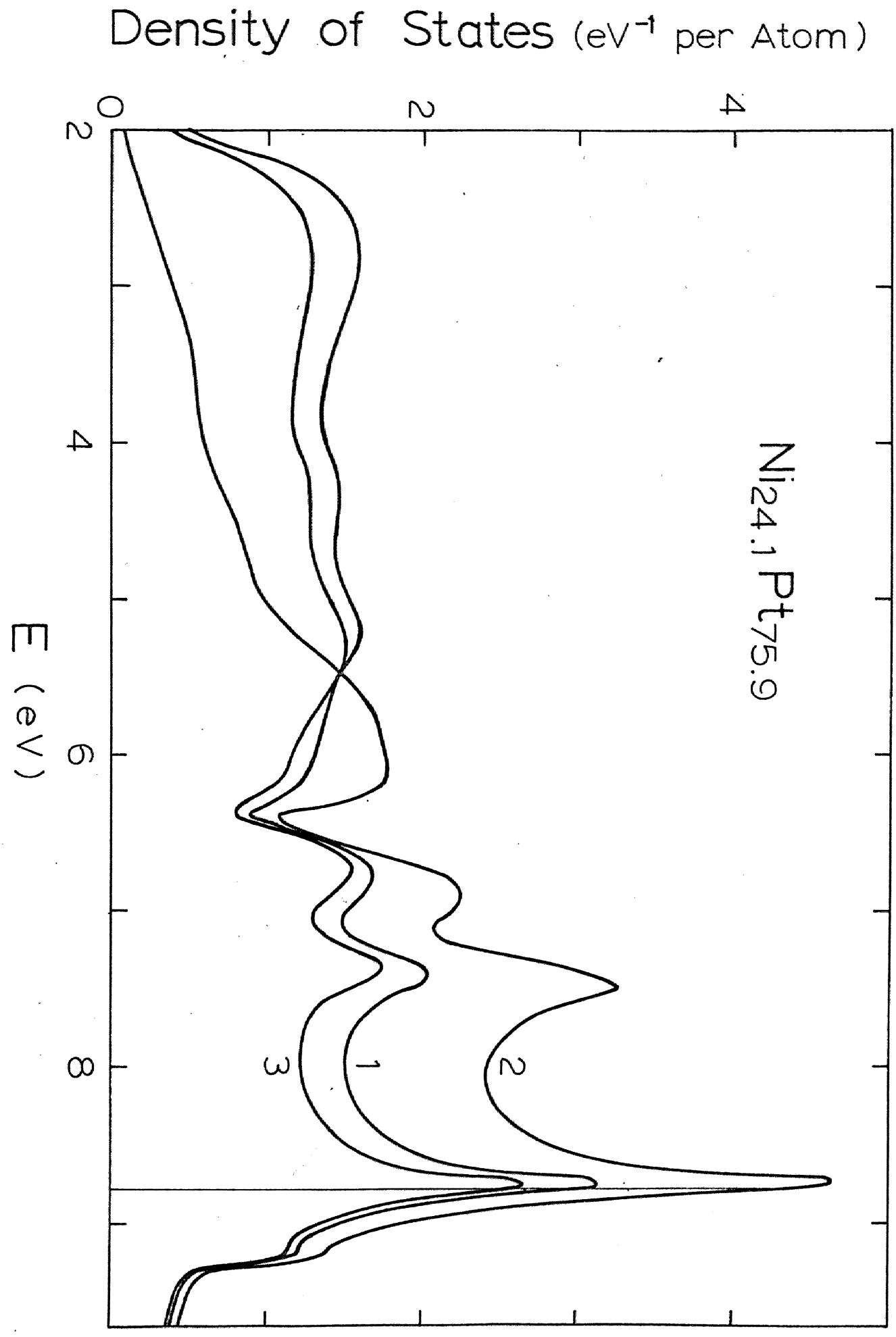

Fig. 93

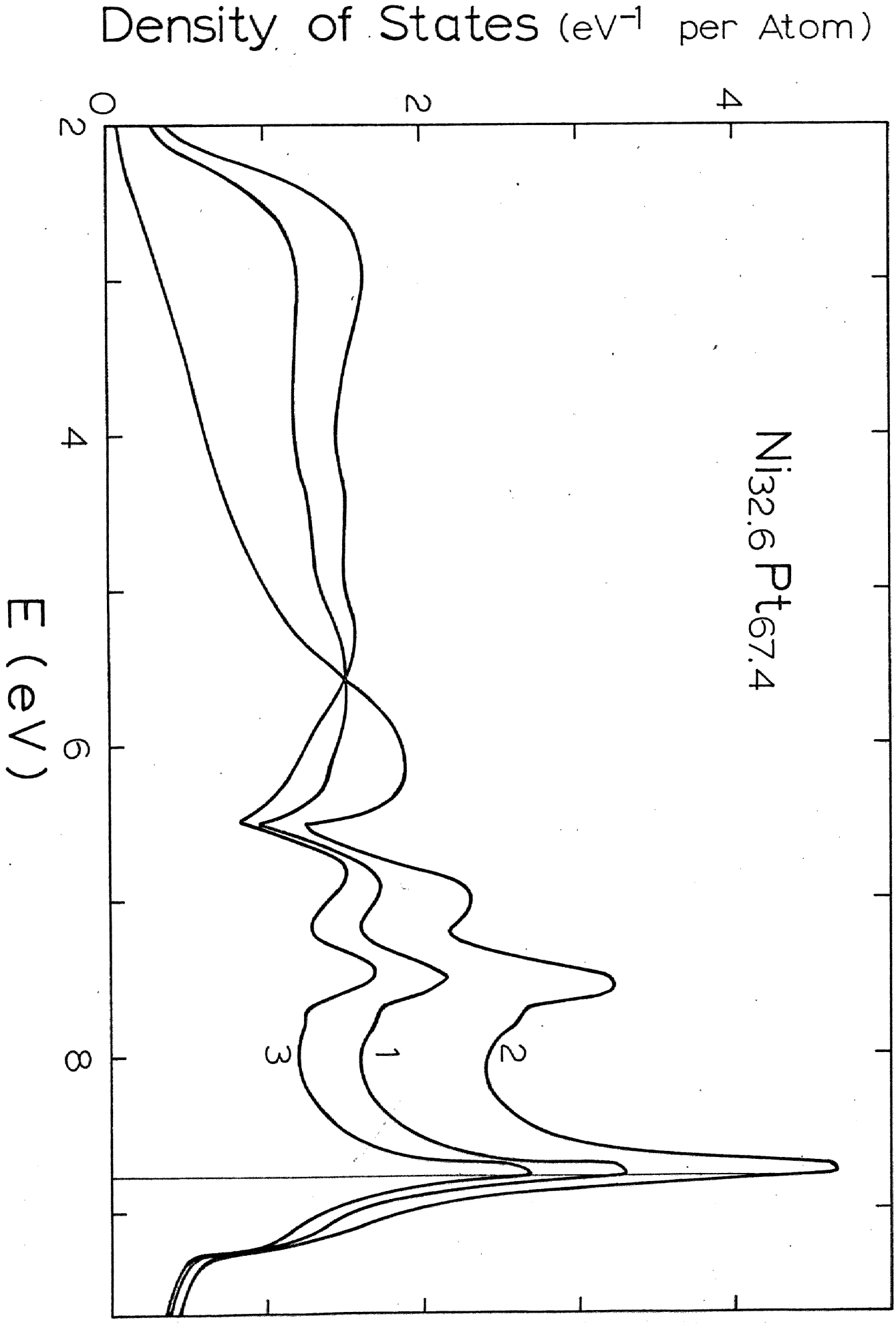

Fig. 94

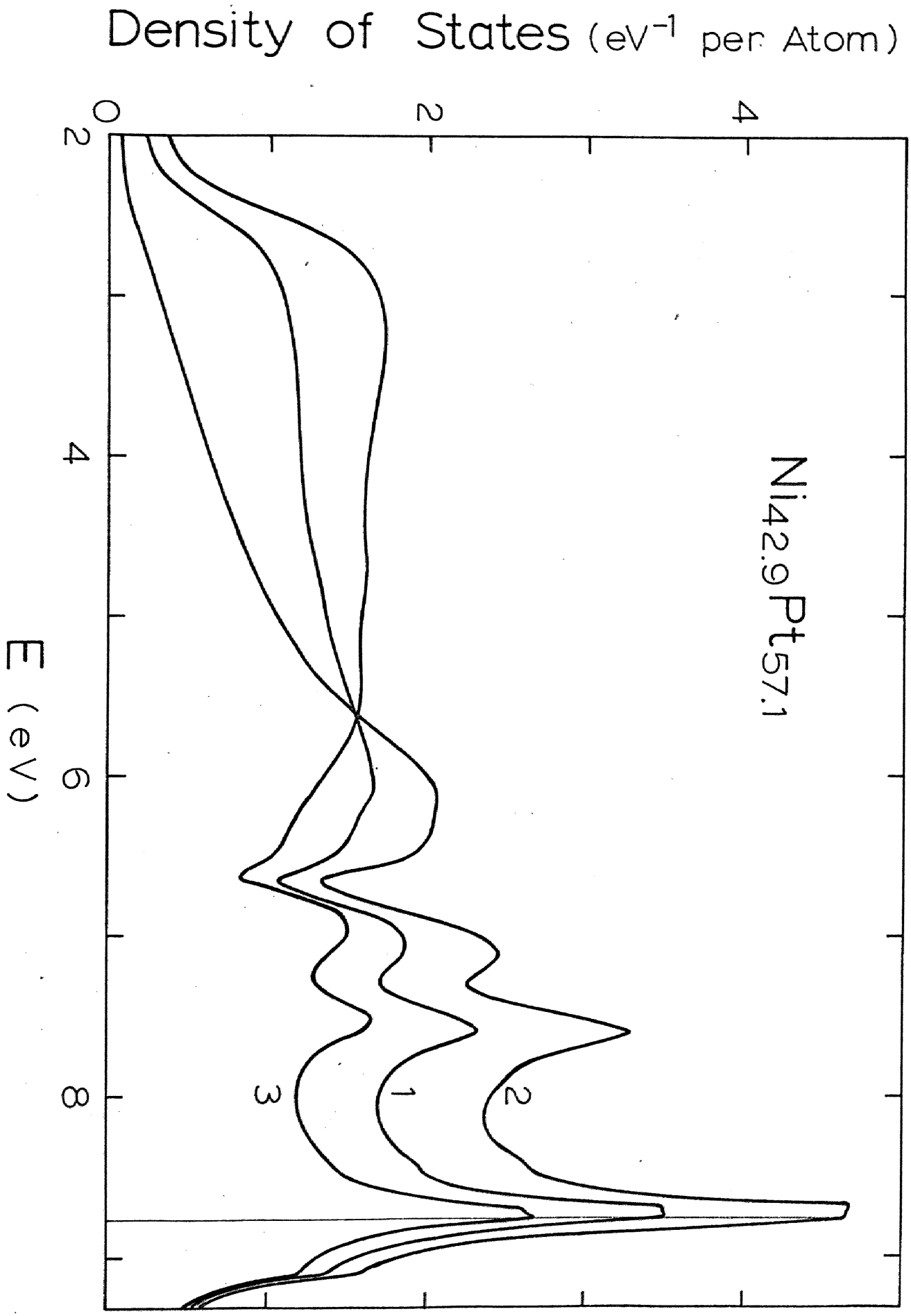

Fig. 95

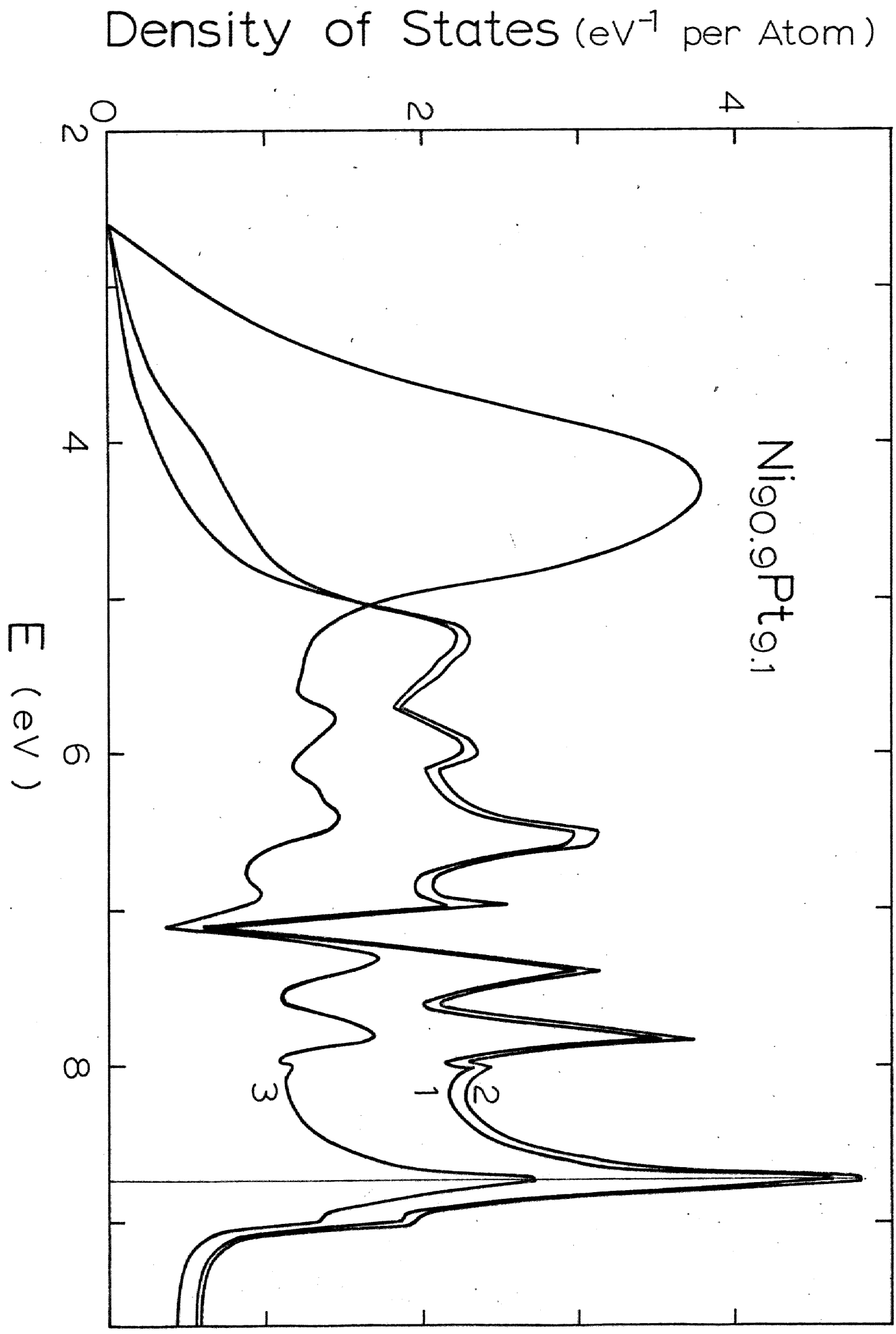

Fig. 96

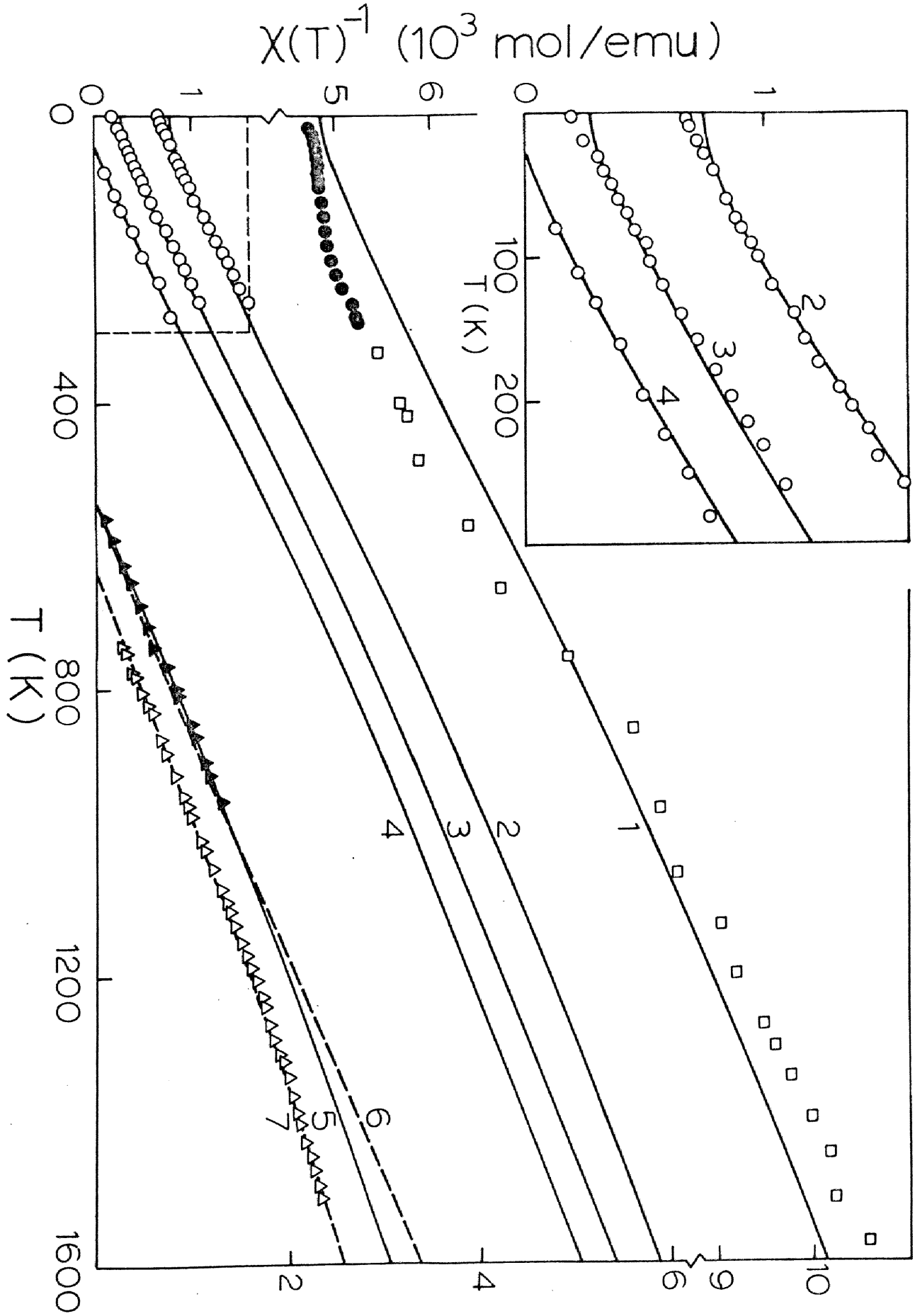

Fig. 97